The Roles of Erosion Rate and Rock Strength in the Evolution of Canyons along the Colorado River

by

Andrew Lee Darling

A Dissertation Presented in Partial Fulfillment
of the Requirements for the Degree
Doctor of Philosophy

Approved August 2016 by the
Graduate Supervisory Committee:

Kelin Whipple, Chair
Arjun Heimsath
Steven Semken
Ramón Arrowsmith
Duane DeVecchio

ARIZONA STATE UNIVERSITY

December 2016

ABSTRACT

For this dissertation, three separate papers explore the study areas of the western Grand Canyon, the Grand Staircase (as related to Grand Canyon) and Desolation Canyon on the Green River in Utah.

In western Grand Canyon, I use comparative geomorphology between the Grand Canyon and the Grand Wash Cliffs (GWC). We propose the onset of erosion of the GWC is caused by slip on the Grand Wash Fault that formed between 18 and 12 million years ago. Hillslope angle and channel steepness are higher in Grand Canyon than along the Grand Wash Cliffs despite similar rock types, climate and base level fall magnitude. These experimental controls allow inference that the Grand Canyon is younger and eroding at a faster rate than the Grand Wash Cliffs.

The Grand Staircase is the headwaters of some of the streams that flow into Grand Canyon. A space-for-time substitution of erosion rates, supported by landscape simulations, implies that the Grand Canyon is the result of an increase in base level fall rate, with the older, slower base level fall rate preserved in the Grand Staircase. Our data and analyses also support a younger, ~6-million-year estimate of the age of Grand Canyon that is likely related to the integration of the Colorado River from the Colorado Plateau to the Basin and Range. Complicated cliff-band erosion and its effect on cosmogenic erosion rates are also explored, guiding interpretation of isotopic data in landscapes with stratigraphic variation in quartz and rock strength.

Several hypotheses for the erosion of Desolation Canyon are tested and refuted, leaving one plausible conclusion. I infer that the Uinta Basin north of Desolation Canyon is eroding slowly and that its form represents a slow, stable base level fall rate. Downstream of Desolation Canyon, the Colorado River is inferred to have established itself in the exhumed region of Canyonlands and to have incised to near modern depths prior to the integration of the Green River and the production of relief in Desolation Canyon. Analysis of incision and erosion rates in the region suggests integration is relatively recent.

DEDICATION

To Ioana Elise Hociota

Our friend, a young woman whose passion for Grand Canyon may never be surpassed

ACKNOWLEDGMENTS

My scientific career began in earnest thanks to Rex Cole and Andres Aslan, who inspired my youthful mind to try new things and learn as much as possible. Their guidance lead to novel research before I even had a degree. Many days in the field brought their mentorship to an impactful level, and I owe them a great deal of gratitude. Karl Karlstrom and Laura Crossey took those seeds of inspiration and sky-rocketed them to new heights, expanding my thoughts through graduate school and introducing me to one of the most influential places in my life: Grand Canyon. Even after I left their direct tutelage, I looked to them for advice and support in science, in the field and in life for the following 6 years, and counting….

Getting a PhD has been a stressful and enjoyable marathon, possible only because of a fantastic advisor. I wish my repeated efforts to nominate him for advisor-ship awards were more successful. Kelin Whipple deserves many accolades for thoughtful scientific inspiration, yes, but probably more importantly, he deserves them for his balanced and kind approach to “life’s little hand-grenades”, the infinite possibilities of events that could pulverize an attempt to get a PhD into much wasted effort. Kelin, thank you for your invaluable and unwavering mentorship through the difficulties life has thrown at my wife and me in our graduate careers.

My career started to steer toward research in thinking and learning thanks to Steven Semken. This new tack in life helped to spawn my first job out of graduate school, where I have the freedom to research education or geology as I wish (and can get funded). My motivation for this broadened work was to better myself as a teacher and researcher, and I hope to contribute to teaching and learning as a professional practice.

Much of my excitement for getting a PhD at ASU came from my first meetings with Arjun Heimsath, who has been a key member of my committee, and has inspired much thought and enjoyment of the field of geomorphology.

Ramon Arrowsmith and Thomas Sharp have been helpful and insightful committee members, helping along not only this dissertation, but also with other courses and opportunities. This appreciation especially goes to NASA space grant with Tom’s support, which gave me the

opportunity to learn how to do education research and interact with hundreds of middle school students. I believe that experience will prove useful in my new interests in geoscience education research.

Special thanks to Duane DeVecchio for last-minute inclusion in the defense process and for help in the field for the work in Desolation Canyon.

The most influential experience in graduate school has been meeting and developing a relationship with my wife. At first, it was the ease and simplicity of an adventure-buddy who worked a few buildings away and started a PhD at the same time. Dr. Cameron Byerley has walked me through the toughest moments of graduate school. One might expect that the two of us writing our dissertations at the same time, and defending within weeks of each other, would be too stressful on a couple. We have found it to be cathartic to spend all of our days in a row for months, often within 5 feet of each other, writing away and chatting about how things are going and making faces at each other. I can't imagine how I would have held myself together throughout this project without my amazing wife, Cammie.

Fellow students Roman DiBiase, Byron Adams, Matt Rossi, and Matt Jungers as well as former post-doc Frances Cooper were the idols of the office. The always revered, more advanced graduate students shine the light on where to go through a career in science and life around and beyond graduate school. I hope I've been able to fill their shoes. I'd like to thank Marina Foster, Scott Robinson and Sayaka Araki as a great cohort to start PhD's with.

This research and my education have been made possible with grants and fellowships from the National Science Foundation, Science Foundation Arizona, and the ASU/NASA Space Grant Program.

TABLE OF CONTENTS

Page

LIST OF TABLES

LIST OF FIGURES

Figure Page

Figure Page

Figure Page

Figure Page

Figure Page

PREFACE

"You cannot see the Grand Canyon in one view,

as if it were a changeless spectacle from which a curtain might be lifted,

but to see it, you have to toil from month to month through its labyrinths."

John Wesley Powell

CHAPTER 1 INTRODUCTION

Motivation

The Colorado Plateau presents a landscape of diverse and fantastic topographic features that have developed primarily since the Miocene (Figure 1.1). The Colorado River system is the greatest driving force of erosion across the landscape, providing the means for gravitational potential energy to be unleashed in the numerous relatively steep sections of the river. This river and its canyons provide the boundary conditions and base level for eroding the hillslopes, cliffs and plateaus between rivers. John Wesley Powell and his expedition explored the deep canyons of the river system in 1869. Powell penned notes with (some) ideas that are still valid scientifically. Upon descending into the depths of the Inner Gorge of Grand Canyon, Powell lamented the black rocks of schist and granite and their tendency to host the worst rapids of the river. As will be explored in detail, the strength of rock is a measure for the resistance of rock to erosion that influences channel geometry (e.g. Grams and Schmidt, 1999; Pederson and Tressler, 2012; Bursztyn et al., 2015). As Powell pondered the river's irreverence for mountains, cutting through them instead of flowing around them, he questioned whether the rivers are antecedent to the geologic structures or that the rivers are superimposed on those structures. A century of research has expanded datasets and improved their logic, mostly disagreeing with Powell's antecedent interpretation for most of the canyons (Davis, 1901; Blackwelder, 1934; Longwell, 1946; Lucchitta, 1972; Young and Brennan, 1974), but the effects of tectonic activity on the Colorado Plateau are still relevant to the river system (Roy et al., 2004; Darling et al., 2012; Karlstrom et al., 2012; Crow et al., 2014; Darling and Whipple, 2015).

The earliest known major river system flowing west from the Colorado Rockies flowed west toward the Utah-Colorado border about 11 million years ago (11 Ma), but with no known path across the plateau (Aslan et al., 2010). Where did this river go? What has happened to the fluvial system as the landscape evolved? In order to grasp these questions, it is necessary to appreciate the scale and complexity of the Colorado Plateau itself, which is the result of protracted deposition and faulting in several non-discrete phases, resulting in a complex set of

rocks to erode. Fluvial evidence of the ancestral Colorado River is rare given the systematic removal of material since periods of deposition dominated through the Tertiary. The landscape that remains today is the integrated result of the geologic features and the erosional processes that have sculpted it. Through the history of the Colorado River, some 300,000 km^3 of rock have been transported from the plateau to the Gulf of California (Dorsey, 2010). Thus the erosional activity across this landscape is a complex smoke-screen that temporarily buries and permanently removes geologic features. Inherited geologic features, such as varied lithology or inactive faults, can have a strong control on the topographic expression of erosion. In undertaking the exploration of the canyons of the plateau, to explore the pace and pattern of erosion and try to reconstruct the history of landscape evolution, I have published one paper and prepared two more for submission to peer-reviewed journals, to comprise Chapters 2, 3, and 4. A fifth synthesis chapter highlights progress made here and future goals. The background material and citations are sometimes redundant, on account of preparation for publication as independent journal articles.

Brief Geologic Background of the Colorado Plateau

Cenozoic Tectonic Setting

A history of the tectonic and erosive modification of the Colorado Plateau logically begins at the last point this continental interior was under shallow seas: during the Late Cretaceous eustatic high-stand (Hancock and Kauffman, 1979). The Late Cretaceous seaway of the interior western US divided two sub-areal regions of North America, the craton to the east and the Sevier Orogenic belt to the west (Armstrong, 1968; Heller et al., 1986; Taylor et al., 2000). Sedimentation through the Cretaceous deposited kilometers of shale and sandstone. The sea eventually regressed, propagating terrestrial river deposits across the K/Pg boundary. Compression and faulting of the then nascent Laramide Orogeny apparently recorded an inboard transfer of deformation from the coastal margin of the Sevier fold-and-thrust belt and entrained the region of the seaway into continent-scale compression, which led to the central basement-cored block uplifts of the Rocky Mountains. Fault activity ranged from 75 - 35 Ma (Bird, 1998).

Several closed-interior basins between these block ranges record local depo-centers of Paleogene detritus eroded from these uplifted terrains (Figure 1.2, Dickinson et al., 1988).

Deformation after the Laramide Orogeny is considerably lower magnitude, in terms relief production and slip on faults through the Cenozoic, particularly within the Colorado Plateau proper. Younger faulting in the western interior US typically consists of extensional normal faulting after forces at the plate margin changed, likely related to the transition of motion along the sea-board from a convergent subduction zone to the strike-slip San Andreas fault system (e.g. Atwater and Stock, 1998). Structural features on the Colorado Plateau are limited such that the stratigraphy of the Colorado Plateau is often described as relatively simple, "layer-cake" stratigraphy. However, the geomorphic response to eroding variable rock types is not simple and requires an appreciation of the rock position, geometry, composition and strength, as will be explored in subsequent chapters on the Colorado River System.

Tertiary Rivers and Basins

The presumed source of fluvial sediment into Colorado Plateau Laramide basins was from nearby ranges (Figure 1.2, Dickinson, 1976); however, recent detrital zircon analysis enables more robust provenance studies to distinguish sediment sources (Gehrels et al., 2006). For instance, the zircon populations of the Uinta Basin of northern Utah are statistically indistinguishable from those of the McCoy Basin of Southern Arizona (Figure 1.2), which is used to infer a ~1000 km-scale drainage network sourced in southern California and Arizona, rather than in more proximal uplifts in Utah and Colorado (Figure 1.2, Davis et al., 2010; Dickinson et al., 2012). This deposition, ca. 50 Ma, is approximately coeval with the fluvial system of paleo-canyons of western Grand Canyon (Young and McKee, 1978; Young and Hartman, 2014) and the Rim Gravels of eastern Arizona (Potochnik, 1989; Dickinson et al., 2012). The Hualapai Plateau paleo-canyons contain up to several hundred meters of detritus from rock sources not present on the Colorado Plateau interior. Paleo-flow indicators reveal northeastward flow in the coarse conglomerate, which corroborates the possibility that these canyons are the conduit which brought some of the sediment of the Uinta Basin to Utah from Arizona and California during the

Eocene. Nearby basins show a range of potential Sevier volcanic arc input in detrital zircons, suggesting that the fluvial system extending from California and southern Arizona to Utah did not affect all basins (Dickinson et al., 2012).

Laramide tectonism in the Hualapai Plateau of the western Grand Canyon (Figure 1.2) produced compressional monoclines, which likely cut off the river system, leading to substantial shifts in drainage patterns (Young, 1979; Young and Crow, 2014). Young (1979) reports the presence of limestone on top of coarse gravel proximal to monoclines, inferred to represent abrupt ponding of once faster-moving water. Subsequent deposition is much younger (ca. 24 Ma,Young and Crow, 2014); indicating a hiatus in significant fluvial activity on the Hualapai Plateau. Post 24 Ma, relatively thin deposits of basalt and Peach Springs Tuff (18–19 Ma) are interbedded with locally sourced fluvial detritus and alluvial fanglomerate (Young and Brennan, 1974; Nielson et al., 1990; Wenrich et al., 1995), indicating that there were no large rivers in the area of the western Grand Canyon for tens of millions of years (Young and Crow, 2014; Darling and Whipple, 2015).

The generally termed Rim Gravels are deposits of coarse sediment that vary in age and occur along the Mogollon Rim. On the Hualapai Plateau, these gravels are named the Music Mountain Formation and occur in paleo-canyons mentioned previously (Late Cretaceous to middle Eocene, Young and Hartman, 2014). In central Arizona, the Mogollon Rim Formation ("rim gravels" as well) exhibits north-northeast flowing paleo-currents and source rocks from southern Arizona (Potochnik, 1989; Potochnik and Faulds, 1998). The 37-33 Ma deposits (Potochnik and Faulds, 1998) rest on an Eocene erosion surface that was tilted and down-dropped in the Neogene, but which preserves extensive planation across Paleozoic and Proterozoic rock types, indicating relatively little base level change in the area for an extended period of time (Potochnik, 1989). Eolianite rock of the Chuska Erg inter-fingers with and overlies Mogollon Rim Formation gravel, marking the boundary of an erg that may have extended to the Rio Grande Rift of New Mexico and far afield from the type section in the Chuska Mountains (Defiance Uplift, Figure 1.2, Cather et al., 2008). The Chuska Erg marks a significant milestone in Colorado Plateau geologic history as a well-dated (33.5-25 Ma) maximum extent of Paleogene deposition (Cather et al.,

2008). After this depositional period, the transition to an erosive regime has been spatially complex and episodic.

Sedimentation to Erosion, Transition through the Neogene

The transition from significant depositional facies such as the Chuska Erg, “rim gravels” and other early to mid-Cenozoic deposits is not uniform in time or space across the region, and the rocks of this time period are partly disrupted by gaps in the geologic record. However, it is clear that significant erosion of the Chuska Erg began soon after deposition (terminating 25 Ma), but was largely removed by the time of Lake Bidahochi (16 Ma) in the Little Colorado River Basin. Lake Bidahochi records a local, small-scale depositional basin with frequent volcanic eruptions in and around the lake until ~ 6 Ma (Dallegge et al., 2003). The timing of the end of deposition and the position of the lake upstream of Grand Canyon were used to support the hypothesis that Lake Bidahochi was a terminus of a proto-Colorado River, leading to a lake-spillover event posited to have begun the initial incision of Grand Canyon. This hypothesis has been refuted (Dallegge et al., 2003; Dickinson, 2013) on account of the shallow water depths suggested by depositional character and small volume of the sediment, which are inconsistent with a plausible proto-Colorado River or a filling and over-topping of a drainage divide posed to exist across the Kaibab uplift as a paleo-valley (Karlstrom et al., 2014). As explored in Chapter 4, it is possible that the proto-Colorado River potentially relevant to Lake Bidahochi was less than half its current size. This hypothetical, smaller, proto Colorado River would likely still be ruled out by the same argument as immediately above. The sink of the Colorado River prior to 6 Ma and its integration history both before and after this time are still an open question.

The earliest record of the Colorado River is a basaltic flow that filled a paleo-valley in western Colorado, preserving ca. 11 Ma gravel, hence providing datable material preserved by a resistant capstone (Aslan et al., 2010). Neogene to recent evidence for the pace and pattern of Colorado River activity is the result of numerous processes that provide an increasing amount of evidence more recent in time.

The erosive geomorphic processes on the Colorado Plateau include eolian (Reynolds et al., 2001) and fluvial systems (Howard and Dolan, 1981), which are punctuated by mass wasting (Huntoon, 1975; Huntoon, 1988).Volcanism (Wenrich et al., 1995; Crow et al., 2008) and travertine deposition at springs and paleo-springs (Crossey et al., 2009; Pederson et al., 2013a; Crow et al., 2014) preserve geologic evidence of fluvial systems. Process interactions have led to rich datasets for Quaternary fluvial incision, as the Colorado River erodes bedrock and leaves behind deposits that are sometimes covered with basaltic lava flows, which can be used to infer incision rates (Karlstrom et al., 2007). Travertine and landslide deposits periodically have preserved Colorado River-related deposits throughout the plateau (Pederson et al., 2013a; Crow et al., 2014). Isotopic dating of travertine deposits and cosmogenically derived isotopes in sediment further provide dates and rates for calibrating erosion processes and patterns (Wolkowinsky and Granger, 2004; Darling et al., 2012).

Climate Interactions with Erosion

Key aspects of Colorado Plateau erosion are driven by climate fluctuations in the region. The Rocky Mountains provide a primary high-elevation water source that has experienced repeated glaciation (Benedict, 1973; Chadwick et al., 1997). Geomorphic response downstream of the glacial outlets is a complex response between local base level, typically the Colorado River system, and local climate fluctuations that in turn influence vegetation, soil, sediment flux, and discharge. Sediment flux and discharge through the major rivers are in part controlled by the headwaters as well as local availability of sediment and runoff. Significant geomorphic response is expected as fluvial terraces form and become incised, including variations in channel slope due to variations in sediment flux and grain size (Bull, 1991). It has been axiomatic that climate variation leads to vegetation changes, which influence the ways sediment is produced on hillslopes and fed to streams. However, atmospheric circulation patterns, and storm tracks in particular may actually be more important than vegetation in controlling sediment flux to rivers (Antinao and McDonald, 2013a, b; Cyr et al., 2015). These key details add complexity to theoretical predictions that aggradation cycles do not match climate variations precisely due to

variations in tendency toward lateral or vertical erosion, driven by sediment flux and discharge variations (Hancock and Anderson, 2002). In other landscapes, it has been shown that climate variations have had far less impact on erosion rate than ecosystem transitions (Ivory et al., 2014), suggesting that proxies of sediment flux variation, like timing of terrace deposition, may not directly reflect glacial cycles from global proxies. The aforementioned studies focus on the Holocene transition in the southwestern United States and have broad implications for how climate cycles are expressed in the geomorphic record of the Colorado Plateau. While the data expressed in this dissertation do not directly address climate variations and landscape response, it is important to keep these ideas in mind.

Conceptual Framework of Canyon Incision

The fundamental concepts needed to think about canyon formation begin with the key terms of base level, incision and erosion, and the visual imagery, outlined in Figure 1.3, that relate these concepts to canyon formation. Base level refers to the lowest point which a river is flowing to. Typically, the ultimate base level of a river is the ocean, admitting that channels can erode slightly below the surface of the ocean. Streams typically follow a path to their base level that is steeper near the headwaters than at the terminus. Rivers that traverse this change in slope gradually, without any abrupt changes in slope, are termed “graded streams” as their longitudinal profiles are relatively smooth and concave up. For canyon cutting, the removal of bedrock below the channel, especially during high flow events that remove sediment, exposing the bed to attack by transported sediment, is referred to as incision. Incision produces a commensurate increase in potential energy as the channel bottom down-cuts and the surrounding hillsides are exposed to increasing relief and potential or failure. Weathering and hillslope erosion processes ranging from diffusive creep and dry ravel to mass rock failure are then able to attack the rocks along the walls of a canyon, widening it.

Incision of canyons drives erosion responses in the surrounding landscape. While incision deepens it, other erosive processes widen the canyon as discussed above. For landscapes as large as Grand Canyon, tributary stream networks expand the incision signal up

each channel (Figure 1.3), and more broadly control hillslope erosion beyond the primary incision by a trunk stream. Tributaries are more directly and fundamentally responsible for bedrock mass removal for large canyons, as tributaries number in the thousands for Grand Canyon and range many kilometers beyond the Colorado River corridor.

Some of the tributaries that broaden erosion of the landscapes are not entirely within a given canyon themselves, instead flowing from surrounding plateaus and mountains (Figures 1.2 and 1.3). On the Colorado Plateau and other regions, such tributaries often contain knickpoints that contribute to a definable boundary of canyon extent: the area above the knickpoints is outside the canyon, and below the knickpoints is within the canyon (Figures 1.2 and 1.3).

The accurate visualization of ongoing topographic change, as well as relative rates of that change described above, are key to understanding the progressive change from a low relief landscape to an incised canyon. Perhaps the most overlooked aspect of this erosion pattern is to discount or forget that the plateau and rim country are also eroding (Figure 1.3). As will be argued in each chapter, the spatial patterns of erosion, i.e., the comparison of rates within a canyon to outside a canyon, are important to the prior history of erosion of a landscape, and provides key clues as to the history of landscape evolution.

Outline of Chapters 2-5

The following chapters are focused on the study areas of western Grand Canyon (Chapter 2, published in Geosphere, 2015), the Grand Staircase (Chapter 3) and Desolation Canyon (Chapter 4), with all relevant figures and tables cited therein organized as self-contained papers. Citation of any part of this dissertation should be reserved for the pending publications and the existing published version of Chapter 2 (see below).

Chapter 2 Outline

Topographic analysis of the western Grand Canyon provides insights on the evolution of the landscape. The study was motivated by the publication of recent papers that variously cited evidence that the canyon may have been incised to near modern depths by 70 Ma (Wernicke, 2011; Flowers and Farley, 2012), or that incision began about 17 Ma (Polyak et al., 2008), or that

incision began only within the last 5 or 6 million years (e.g. Longwell, 1946; Lucchitta, 1972; Karlstrom et al., 2008; Karlstrom et al., 2014). This disparate range of potential ages seems too wide-ranging for all to be plausible hypotheses with regard to geomorphic processes that constantly sculpt and change the landscape. This research project began in order to understand fundamental erosion parameters and the history of incision events of the canyon. The key argument of this chapter is that the Grand Wash cliffs are an appropriate place to compare relative base level fall between a base level fall of known age (the Grand Wash fault was active 18-12 million years ago) and the incision of Grand Canyon. The streams in each area have primarily responded to their respective base level, so the resulting landscape is a response to local climate, rock types and the time since that incision began. The climate of the western Grand Canyon varies little over the few tens of kilometers considered and the headwaters of all catchments form at nearly the same elevation (that of the top of the Shivwits Plateau). The Grand Wash Cliffs and western Grand Canyon have been formed in the same Paleozoic strata. The magnitude of the base level fall change in both the Grand Wash Cliffs and the Grand Canyon is a net change of about 1 km, leaving the time from which erosion began (and rate of erosion) as the key remaining variables.

The Grand Wash Cliffs display lower hillslope angles and channel steepness than the Grand Canyon. Both hillslopes and channels are steep in proportion with erosion rate. Because the natural experimental setting controlled for independent factors, the most plausible conclusion is that the Grand Canyon is steeper than the Grand Wash Cliffs because it is eroding faster, indicating that its base level changed more recently than the slip along the Grand Wash Fault. The comparative analysis alone indicates that the canyon is likely younger than 12 Ma. The chapter outlines several other lines of discussion to support the inference that the geomorphology of the western Grand Canyon does not support the hypothesis that the canyon was incised in the Cretaceous Period, and our interpretation of evidence favors a ~6-Ma age over a 17-Ma age.

This chapter is published in the journal *Geosphere* with the following citation:
Darling, A., and Whipple, K., 2015, Geomorphic constraints on the age of the western Grand Canyon: *Geosphere*, v. 11, no. 4, p. 958-976.

Chapter 3 Outline

Analyses of topography, rock strength, and erosion rates in the Grand Staircase and Grand Canyon provide data that are compared to numerical simulations of similar landscapes. Scenarios where rock strength varies in horizontal strata provide distinctive differences in response of erosion rates to base level fall. Four scenarios are discussed in which base level rate is either constant or increases once stepwise. The primary control on erosion in these cases is the distribution of rock strength, which is modeled as strong over weak rock, weak over strong rock, or several couplets of weak and strong rock. The diagnostic power of the numerical simulations elaborated on in the chapter support the conclusion that Grand Staircase erosion rates are greater than rates of local base level fall. In this case, the resistant Claron Formation is undermined by weaker underlying Cretaceous rock units creating local high rates in the catchments that were sampled. For comparison of the Grand Staircase incision rates vs Grand Canyon incision rates, it is reasonable to think of the Grand Canyon as a whole (not just western Grand Canyon, as in Chapter 2) as the product of a relatively youthful increase in base level fall rate as inferred from incision rates and erosion rates from within Grand Canyon and on the Grand Staircase. This conclusion is based on the expected spatial erosion rate patterns predicted by the weak-over-strong model scenario.

Analysis of actual detrital cosmogenic sediment and simulated ^{10}Be sediment concentrations offer a framework for when and where cosmogenic estimates of erosion are expected to match real spatially averaged erosion rate, and where cosmogenic erosion rates should match base level fall rate despite possible high variation in quartz concentration and rock strength. Further, we show cases where cosmogenic erosion rates should *not* correspond to local base level fall rates. Each of these scenarios depends on the distribution of rock strength, and landscapes need to be considered on a case by case basis to determine if cosmogenic methods are appropriate and how such data can be interpreted. Our analyses provide a framework for discussing these complexities in other landscapes where rock and minerals vary significantly.

This chapter is intended with pending revision for submission to *Earth Surface Processes and Landforms.*

Chapter 4 Outline

Desolation Canyon on the Green River in Utah is an unusual landscape that is unlike the surrounding topographic features. The topographic analysis of the canyon indicates that channel steepness here exceeds that of nearby regions. This observation is set against four potential hypotheses that may have formed the canyon and the knickpoint that resides on the Green River therein. The most supported argument is that the canyon is the result of a top-down integration of the Green River through a gap in the Tavaputs Plateau that was exploited in the last few million years. This canyon is likely a more recent erosional feature than the Grand Canyon, indicating the Green River probably did not contribute to flow and sediment to the initial incision of the Grand Canyon.

To support this interpretation, we conducted seismic surveys of the two key rock units of the plateau, obtained cosmogenic erosion rates and evaluate existing incision rates in the literature. Our analysis indicates the two rock units are both weak, and show little apparent variation in channel steepness or erosion rate patterns that could affect a variation in rock strength. The cosmogenic erosion rate data show the erosion rate above the knickpoints of side-streams and the Green River itself is low, 41 +/- 7 (n=12) and the erosion rates within the canyon are high (220 +/- 26 m/Ma). This supports the interpretation that the canyon is a transient feature that is dynamically readjusting to a change in base level for the Green River. recent integration hypothesis generated from the topographic analysis.

This chapter is a possible candidate for submission to *Geology.*

Chapter 5 Outline

The final chapter is a synthesis of data and ideas explored in the previous chapters, highlighting key relationships to external studies and possible ways in which future research may be directed for both the Colorado Plateau and for geomorphology of complex-substrate landscapes in general. The mysteries of the Colorado River will provide extensive future debate and new methods will be applied, some of which will likely build from my work here.

References

Antinao, J. L., and McDonald, E., 2013a, An enhanced role for the Tropical Pacific on the humid Pleistocene–Holocene transition in southwestern North America: Quaternary Science Reviews, v. 78, p. 319-341.

-, 2013b, A reduced relevance of vegetation change for alluvial aggradation in arid zones: Geology, v. 41, no. 1, p. 11-14.

Armstrong, R. L., 1968, Sevier orogenic belt in Nevada and Utah: Geol. Soc. Amer. Bull., v. 79, p. 429-458.

Aslan, A., Karlstrom, K. E., Crossey, L. J., Kelley, S., Cole, R., Lazear, G., and Darling, A., 2010, Late Cenozoic evolution of the Colorado Rockies: Evidence for Neogene uplift and drainage integration: Field Guides, v. 18, p. 21-54.

Atwater, T., and Stock, J., 1998, Pacific-North America plate tectonics of the Neogene southwestern United States: an update: International Geology Review, v. 40, no. 5, p. 375-402.

Benedict, J. B., 1973, Chronology of cirque glaciation, Colorado front range: Quaternary Research, v. 3, no. 4, p. 584-599.

Bird, P., 1998, Kinematic history of the Laramide orogeny in latitudes 35o-49oN, western United States: Tectonics, v. 17, no. 5, p. 780-801.

Blackwelder, E., 1934, Origin of the Colorado River: Geological Society of America Bulletin, v. 45, no. 3, p. 551-566.

Bull, W. B., 1991, Geomorphic Responses to Climate Change, New York, Oxford University Press, 326 p.:

Bursztyn, N., Pederson, J., Tressler, C., Mackley, R., and Mitchell, K., 2015, Rock strength along a fluvial transect of the Colorado Plateau–quantifying a fundamental control on geomorphology: Earth and Planetary Science Letters, v. 429, p. 90-100.

Cather, S. M., Connell, S. D., Chamberlin, R. M., McIntosh, W. C., Jones, G. E., Potochnik, A. R., Lucas, S. G., and Johnson, P. S., 2008, The Chuska erg: Paleogeomorphic and paleoclimatic implications of an Oligocene sand sea on the Colorado Plateau: Geological Society of America Bulletin, v. 120, no. 1-2, p. 13-33.

Chadwick, O. A., Hall, R. D., and Phillips, F. M., 1997, Chronology of Pleistocene glacial advances in the central Rocky Mountains: Geological Society of America Bulletin, v. 109, no. 11, p. 1443-1452.

Crossey, L. J., Karlstrom, K. E., Springer, A. E., Newell, D., Hilton, D. R., and Fischer, T., 2009, Degassing of mantle-derived CO2 and He from springs in the southern Colorado Plateau region--Neotectonic connections and implications for groundwater systems: Geological Society of America Bulletin, v. 121, no. 7-8, p. 1034-1053.

Crow, R., Karlstrom, K., Darling, A., Crossey, L., Polyak, V., Granger, D., Asmerom, Y., and Schmandt, B., 2014, Steady incision of Grand Canyon at the million year timeframe: A case for mantle-driven differential uplift: Earth and Planetary Science Letters, v. 397, p. 159-173.

Crow, R., Karlstrom, K. E., McIntosh, W., Peters, L., and Dunbar, N., 2008, History of Quaternary volcanism and lava dams in western Grand Canyon based on lidar analysis, 40Ar/39Ar dating, and field studies: Implications for flow stratigraphy, timing of volcanic events, and lava dams: Geosphere, v. 4, no. 1, p. 183.

Cyr, A. J., Miller, D. M., and Mahan, S. A., 2015, Paleodischarge of the Mojave River, southwestern United States, investigated with single-pebble measurements of 10Be: Geosphere, v. 11, no. 4, p. 1158-1171.

Dallegge, T. A., Ort, M. H., and McIntosh, W. C., 2003, Mio-Pliocene chronostratigraphy, basin morphology and paleodrainage relations derived from the Bidahochi Formation, Hopi and Navajo Nations, northeastern Arizona: Mountain Geologist, v. 40, no. 3, p. 55-82.

Darling, A., and Whipple, K., 2015, Geomorphic constraints on the age of the western Grand Canyon: Geosphere, v. 11, no. 4, p. 958-976.

Darling, A. L., Karlstrom, K., Granger, D. E., Aslan, A., Kirby, E., Ouimet, W. B., Lazear, G. D., Coblentz, D. D., and Cole, R. D., 2012, New incision rates along the Colorado River system based on cosmogenic burial dating of terraces: implications for regional controls on Quaternary incision: Geosphere, v. 8, no. 5, p. 1020-1041.

Davis, S. J., Dickinson, W. R., Gehrels, G. E., Spencer, J. E., Lawton, T. F., and Carroll, A. R., 2010, The Paleogene California River: Evidence of Mojave-Uinta paleodrainage from U-Pb ages of detrital zircons: Geology, v. 38, no. 10, p. 931-934.

Davis, W. M., 1901, An excursion to the Grand Canyon of the Colorado, Cambridge, Massachusetts, Printed for the Museum, 201 p.:

Dickinson, W. R., 1976, Sedimentary basins developed during evolution of Mesozoic-Cenozoic arc-trench system in western North America: Canadian Journal of Earth Sciences, v. 13, no. 9, p. 1268-1287.

-, 2013, Rejection of the lake spillover model for initial incision of the Grand Canyon, and discussion of alternatives: Geosphere, v. 9, no. 1, p. 1-20.

Dickinson, W. R., Klute, M. A., Hayes, M. J., Janecke, S. U., Lundin, E. R., McKittrick, M. A., and Olivares, M. D., 1988, Paleogeographic and paleotectonic setting of Laramide sedimentary basins in the central Rocky Mountain region: Geological Society of America Bulletin, v. 100, no. 7, p. 1023-1039.

Dickinson, W. R., Lawton, T. F., Pecha, M., Davis, S. J., Gehrels, G. E., and Young, R. A., 2012, Provenance of the Paleogene Colton Formation (Uinta Basin) and Cretaceous–Paleogene provenance evolution in the Utah foreland: Evidence from U-Pb ages of detrital zircons, paleocurrent trends, and sandstone petrofacies: Geosphere, v. 8, no. 4, p. 854-880.

Flowers, R., and Farley, K., 2012, Apatite 4He/3He and (U-Th)/He evidence for an ancient Grand Canyon: Science, v. 338, no. 6114, p. 1616-1619.

Gehrels, G., Valencia, V., and Pullen, A., 2006, Detrital zircon geochronology by laser-ablation multicollector ICPMS at the Arizona LaserChron Center: Paleontological Society Papers, v. 12, p. 67.

Grams, P. E., and Schmidt, J. C., 1999, Geomorphology of the Green River in the eastern Uinta Mountains, Dinosaur National Monument, Colorado and Utah: Varieties of fluvial form, p. 81-111.

Hancock, G. S., and Anderson, R. S., 2002, Numerical modeling of fluvial strath-terrace formation in response to oscillating climate: Geological Society of America Bulletin, v. 114, no. 9, p. 1131-1142.

Hancock, J. M., and Kauffman, E., 1979, The great transgressions of the Late Cretaceous: Journal of the Geological Society, v. 136, no. 2, p. 175-186.

Heller, P. L., Bowdler, S. S., Chambers, H. P., Coogan, J. C., Hagen, E. S., Shuster, M. W., Winslow, N. S., and Lawton, T. F., 1986, Time of initial thrusting in the Sevier orogenic belt, Idaho-Wyoming and Utah: Geology, v. 14, p. 388-391.

Howard, A., and Dolan, R., 1981, Geomorphology of the Colorado River in the Grand Canyon: The Journal of Geology, p. 269-298.

Huntoon, P., 1988, Late Cenozoic gravity tectonic deformation related to the Paradox salts in the Canyonlands area of Utah: Salt deformation in the Paradox region, Utah: Utah Geological and Mineral Survey Bulletin, v. 122, p. 81-93.

Huntoon, P. W., 1975, The Surprise Valley landslide and widening of the Grand Canyon, Northern Arizona Society of Science and Art.

Ivory, S. J., McGlue, M. M., Ellis, G. S., Lézine, A.-M., Cohen, A. S., and Vincens, A., 2014, Vegetation controls on weathering intensity during the last deglacial transition in southeast Africa: PloS one, v. 9, no. 11, p. e112855.

Karlstrom, K., Coblentz, D., Dueker, K., Ouimet, W., Kirby, E., Van Wijk, J., Schmandt, B., Kelley, S., Lazear, G., and Crossey, L., 2012, Mantle-driven dynamic uplift of the Rocky Mountains and Colorado Plateau and its surface response: Toward a unified hypothesis: Lithosphere, v. 4, no. 1, p. 3-22.

Karlstrom, K. E., Crow, R., Crossey, L. J., Coblentz, D., and Van Wijk, J. W., 2008, Model for tectonically driven incision of the younger than 6 Ma Grand Canyon: Geology, v. 36, no. 11, p. 835.

Karlstrom, K. E., Crow, R. S., Peters, L., McIntosh, W., Raucci, J., Crossey, L. J., Umhoefer, P., and Dunbar, N., 2007, 40Ar/39Ar and field studies of Quaternary basalts in Grand Canyon and model for carving Grand Canyon: Quantifying the interaction of river incision and normal faulting across the western edge of the Colorado Plateau: Geological Society of America Bulletin, v. 119, no. 11-12, p. 1283-1312.

Karlstrom, K. E., Lee, J. P., Kelley, S. A., Crow, R. S., Crossey, L. J., Young, R. A., Lazear, G., Beard, L. S., Ricketts, J. W., and Fox, M., 2014, Formation of the Grand Canyon 5 to 6 million years ago through integration of older palaeocanyons: Nature Geoscience, v. 7, p. 239-244.

Longwell, C. R., 1946, How old is the Colorado River?: American Journal of Science, v. 244, no. 12, p. 817-835.

Lucchitta, I., 1972, Early history of the Colorado River in the Basin and Range Province: Geological Society of America Bulletin, v. 83, no. 7, p. 1933-1948.

Nielson, J. E., Lux, D. R., Dalrymple, G. B., and Glazner, A. F., 1990, Age of the Peach Springs Tuff: Journal of Geophysical Research, v. 95, p. 571-580.

Pederson, J., Burnside, N., Shipton, Z., and Rittenour, T., 2013, Rapid river incision across an inactive fault—Implications for patterns of erosion and deformation in the central Colorado Plateau: Lithosphere, v. 5, no. 5, p. 513-520.

Pederson, J. L., and Tressler, C., 2012, Colorado River long-profile metrics, knickzones and their meaning: Earth and Planetary Science Letters, v. 345, p. 171-179.

Polyak, V., Hill, C., and Asmerom, Y., 2008, Age and evolution of the Grand Canyon revealed by U-Pb dating of water table-type speleothems: Science, v. 319, no. 5868, p. 1377-1380.

Potochnik, A. R., 1989, Depositional style and tectonic implications of the Mogollon Rim Formation (Eocene), east-central Arizona: Globe, v. 1, no. 1, p. 0.

Potochnik, A. R., and Faulds, J. E., 1998, A tale of two rivers: Tertiary structural inversion and drainage reversal across the southern boundary of the Colorado Plateau: Geologic excursions in northern and central Arizona: Field trip guidebook: Flagstaff, Arizona, Northern Arizona University, p. 149-173.

Reynolds, R., Belnap, J., Reheis, M., Lamothe, P., and Luiszer, F., 2001, Aeolian dust in Colorado Plateau soils: nutrient inputs and recent change in source: Proceedings of the National Academy of Sciences, v. 98, no. 13, p. 7123-7127.

Roy, M., Kelley, S., Pazzaglia, F., Cather, S., and House, M., 2004, Middle Tertiary buoyancy modification and its relationship to rock exhumation, cooling, and subsequent extension at the eastern margin of the Colorado Plateau: Geology, v. 32, no. 10, p. 925.

Taylor, W. J., Bartley, J. M., Martin, M. W., Geissman, J. W., Walker, J. D., Armstrong, P. A., and Fryxell, J. E., 2000, Relations between hinterland and foreland shortening: Sevier orogeny, central North American Cordillera: Tectonics, v. 19, no. 6, p. 1124-1143.

Wenrich, K. J., Billingsley, G. H., and Blackerby, B. A., 1995, Spatial migration and compositional changes of Miocene-Quaternary magmatism in the western Grand Canyon: Journal of Geophysical Research, v. 100, no. B6, p. 10417-10410,10440.

Wernicke, B., 2011, The California River and its role in carving Grand Canyon: Geological Society of America Bulletin, v. 123, no. 7-8, p. 1288-1316.

Wolkowinsky, A. J., and Granger, D. E., 2004, Early Pleistocene incision of the San Juan River, Utah, dated with 26Al and 10Be: Geology, v. 32, no. 9, p. 749.

Young, R., 1979, Laramide deformation, erosion and plutonism along the southwestern margin of the Colorado Plateau: Tectonophysics, v. 61, no. 1, p. 25-47.

Young, R. A., and Brennan, W. J., 1974, Peach Springs Tuff: Its bearing on structural evolution of the Colorado Plateau and development of Cenozoic drainage in Mohave County, Arizona: Geological Society of America Bulletin, v. 85, no. 1, p. 83-90.

Young, R. A., and Crow, R., 2014, Paleogene Grand Canyon incompatible with Tertiary paleogeography and stratigraphy: Geosphere, v. 10, no. 4, p. 664-679.

Young, R. A., and Hartman, J. H., 2014, Paleogene rim gravel of Arizona: Age and significance of the Music Mountain Formation: Geosphere, v. 10, no. 5, p. 870-891.

Young, R. A., and McKee, E. H., 1978, Early and middle Cenozoic drainage and erosion in west-central Arizona: Geological Society of America Bulletin, v. 89, no. 12, p. 1745-1750.

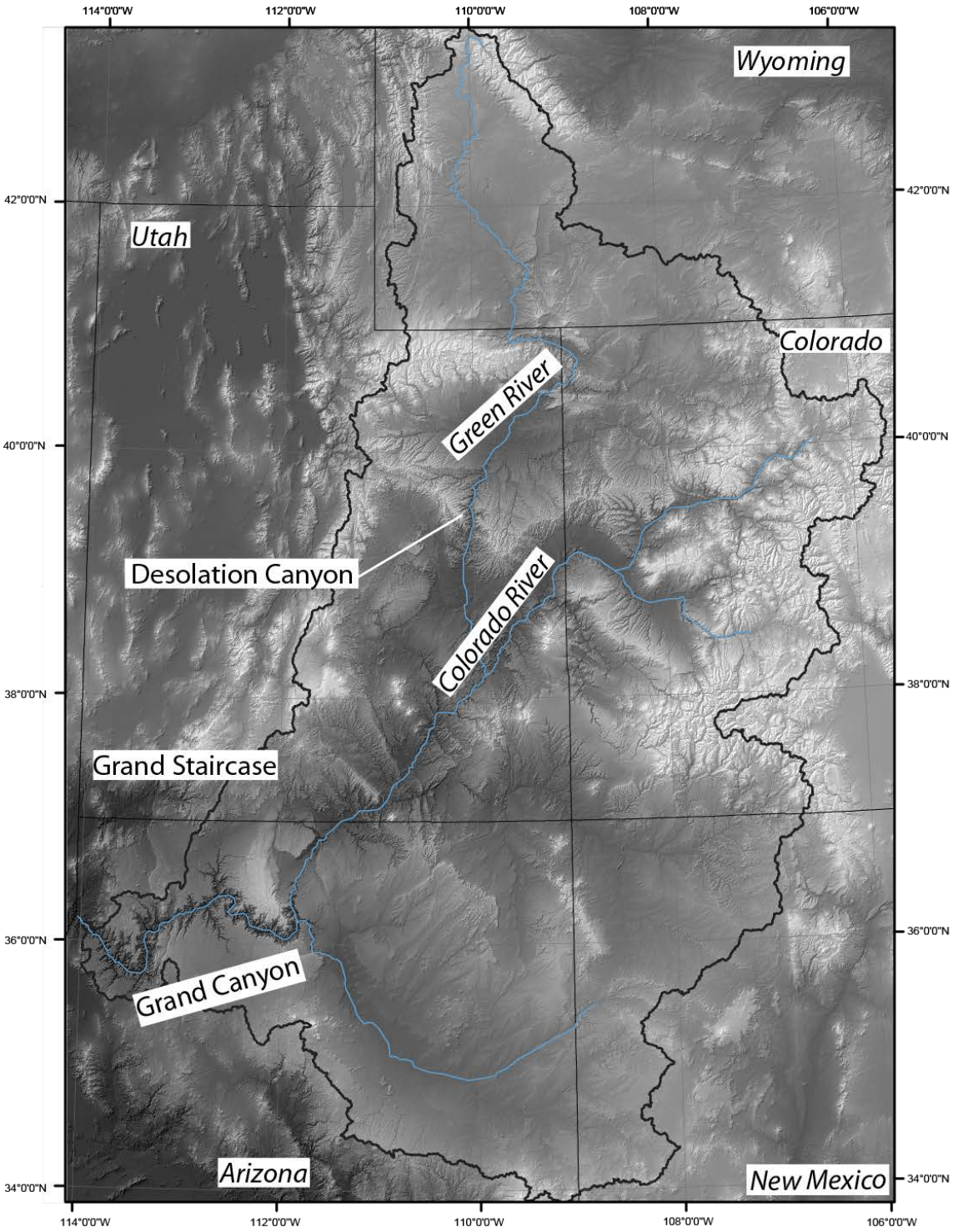

Figure 1.1 Digital Elevation model and hill-shade with the major tributaries of the Colorado River with field areas for each subsequent chapter. Western Grand Canyon (Ch. 2), Grand Staircase and Grand Canyon (Ch. 3) and Desolation Canyon (Ch. 4).

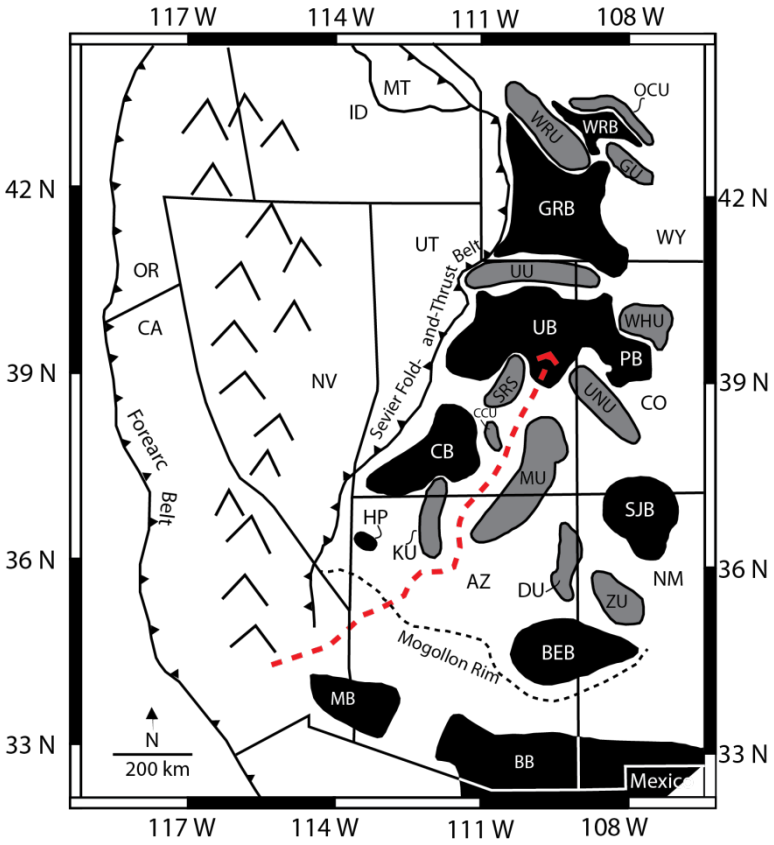

Figure 1.2 Map of regional uplifts and basins during the Paleogene. Inferred channels (red dash line) connecting sediment sources from the Mogollon Rim, thorugh Western Grand Canyon and to the Uinta Basin. From North to South, abbreviations are: Owl Creek Uplift (OCU), Wind River Basin (WRB), Wind River Uplift (WRU), Granite Mountain Uplift (GU), Green River Basin (GRB), Uinta Uplift (UU), Uinta Basin (UB), White River Uplift (WHU), Piceance Basin (PB), San Rafael Swell (SRS), Uncompahgre Uplift (UNU), Claron Basin (CB), Monument Upward (MU), Kaibab Plateau (KU), San Juan Basin (SJB), Hualapai Plateau (HP), Defiance Uplift (DU), Zuni Uplift (ZU), Baca-Eager Basin (BEB), McCoy Basin (MB), Bisbee Basin (BB).

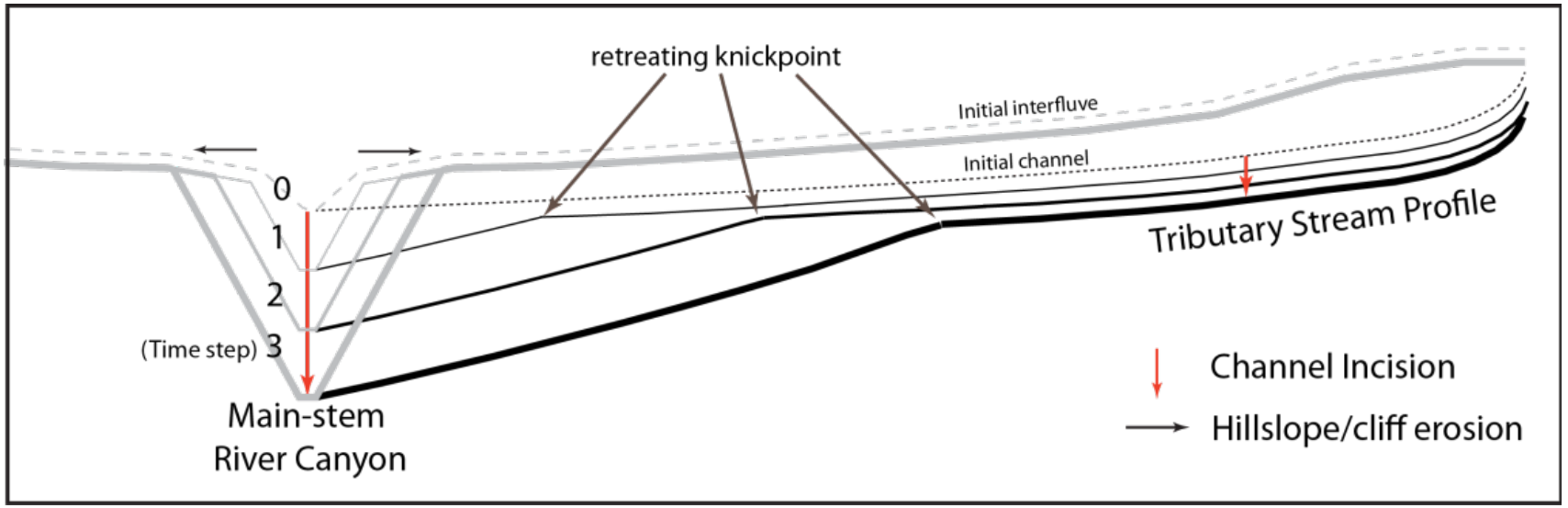

Figure 1.3 Conceptual diagram of development of topography of bedrock from a relatively low relief surface that is eroding slowly to a canyon incise and lowering base level of the tributaries.. Once canyon incision begins, it proceeds at a constant average rate that is higher than the surrounding plateau. Canyon walls retreat away from the river at a rate that controlled by the incision rate, cliff retreat processes and rock strength properties. In this diagram, topographic equilibrium is not reached. By the third time-step, the tributary incision response yields a knickpoint that separates the canyon incision rate from the preserved incision rate in the headwaters that is left over from before the canyon began to incise.

CHAPTER 2 GEOMORPHIC CONSTRAINTS ON THE AGE OF WESTERN GRAND CANYON

Abstract

Hypotheses for the age of western Grand Canyon (WGC) range from less than 6 Ma to more than 70 Ma. We study the relationships among topography, geology, and available erosion rates in space and time to place constraints on plausible canyon incision histories. Evidence suggests lateral retreat of the Shivwitz Plateau escarpment left a lithologically controlled bench on the Sanup Plateau, but the Hualapai Plateau is beveled indiscriminately across rock types of the Paleozoic stratigraphic section. A period of accelerated base level fall in the Tertiary is implicated by the canyon incised into the beveled Hualapai Plateau surface, consistent with higher erosion rates observed in canyons than on the surrounding plateau. Streams draining the Hualapai Plateau preserve relict headwater segments that were equilibrated with a slower base level-fall rate before canyon incision. These relict segments are now separated from Grand Canyon by knickpoints indicative of a transient landscape. Relief production since the beveling of the Hualapai Plateau is greater than 1 kilometer in WGC. Comparison of hillslope angle and channel steepness between the Grand Wash Cliffs and WGC provide a test to distinguish hypothesized ages of canyon incision. The data strongly suggest that carving of WGC is younger than relief production due to slip along the Grand Wash Fault since ~18-12 Ma. Thus the geomorphic data are only consistent with the late Tertiary, transient incision model of canyon incision beginning at integration <6 Ma.

Introduction

Motivation

The age of the Colorado River drainage system and timing of Grand Canyon incision have been debated since the pioneering studies of John Wesley Powell (1875). Although Powell interpreted the Colorado River as antecedent to Laramide structures and the uplift of the Colorado Plateau, since the turn of the 20th century most geologists have interpreted a mid-to

late-Tertiary age of integration of the superimposed Colorado River and carving of the Grand Canyon (Davis, 1901; Blackwelder, 1934; Longwell, 1946; Lucchitta, 1972; Young and Brennan, 1974), with much evidence pointing to a ~6 Ma river integration event (House et al., 2008), contemporaneous with a significant fraction of canyon incision (Pederson et al., 2002a; Pederson et al., 2006; Karlstrom et al., 2007; Karlstrom et al., 2008). Some recent evidence, however, has been suggested to support the carving of western Grand Canyon (WGC) by 70 Ma (Wernicke, 2011; Flowers and Farley, 2012), or perhaps since ~17 Ma (Polyak et al., 2008; Young, 2008) reinvigorating the debate over estimates of the canyon's age. Even the hypothesized 17 Ma precursor western Grand Canyon (WGC) cut by a moderate-sized pre-Colorado River drainage (Polyak et al., 2008; Young, 2008) is disputed (Karlstrom et al., 2008; Pearthree et al., 2008; Pederson et al., 2008) and the idea of WGC formation by 70 Ma is even more controversial. Wernicke (2011) and Flowers and Farley, (2012) argued on the basis of thermochronologic data that WGC had been cut to within a few hundred meters of its current depth by 70 Ma and maintained at the surface (not buried) since then. The interpretation of the thermochronologic data is not simple, however, and has been challenged (Fox and Shuster, 2014; Karlstrom et al., 2014). In addition, Young and Crow (2014) have re-iterated, clarified, and augmented geologic and qualitative geomorphic evidence of the Tertiary cutting and infilling of smaller paleo-canyons, that is incompatible with the formation and maintenance of a deep canyon in the WGC area prior to ~19 Ma. Further, the Muddy Creek Formation of the Grand Wash Trough has long been interpreted to prohibit the existence of a large river at the terminus of WGC (Longwell, 1946; Lucchitta, 1966; Pederson, 2008; Ingersoll et al., 2013). Beyond sorting out the local geologic history, resolving this debate presents an opportunity for refining our understanding of both thermochronologic and geomorphic records of river incision and relief production. In this paper, we analyze constraints on the timing of the incision of WGC from landscape morphology and existing incision-rate estimates.

Classic interpretation of a young WGC is consistent with the steep-walled, narrow, high-relief inner gorge morphology, which is immediately apparent on topographic maps and photos (Figs. 2.1 and 2.2). The range of circumstances that could produce and maintain such a

landscape, however, has not been thoroughly explored. Moreover, given the broad attention this controversy has garnered, and given the apparent challenge of the “old canyon” evidence to this classical interpretation of a “youthful” landscape” (e.g., Davis, 1901), an independent, quantitative assessment of the geomorphic constraints on the antiquity of the WGC is needed. Three main hypotheses for the age of WGC (> 70Ma, <17Ma, and largely < 6 Ma) are the focus of debate, and each must be consistent with the known paleo-canyons preserved on the Hualapai Plateau (Young, 1979; Young, 2008; Young and Crow, 2014). Each hypothesis constitutes a set of testable predictions for both landscape morphology and the spatio-temporal pattern of erosion. We analyze details of landscape morphology and available constraints on erosion rates to test the viability of each hypothesis on geomorphic grounds.

Landscape morphology alone is not diagnostic of the cause (or mode) of canyon formation. Narrow, steep-walled canyons incised into low-relief plateau surfaces can form in response to either (1) an acceleration in mainstem river incision (as implied in the 17 Ma and 6 Ma models) or (2) ~steady incision into a sub-horizontal stratigraphic succession with weak, easily eroded rocks or sediments overlying a notably stronger, erosionally resistant package of rocks (which could be consistent with the 70 Ma model). In the latter case, the low-relief erosion surface surrounding the canyon forms as weak rocks are eroded along the basal contact between weak and with underlying strong rocks (the surrounding bench post-dates rather than pre-dates canyon incision) and canyon formation need not reflect an increase in the rate of relative base level fall (Fig. 2.3). Both scenarios involve relief production resulting from more rapid erosion within the canyon than on the surrounding low-relief bench: in one case the erosion rate within the canyon increases in response to base level fall; in the other case the erosion rate in the surrounding landscape decreases in response to the formation of a lithologically controlled erosional bench. Consequently, the cause and timing of canyon formation must be considered separately. Fortunately, for either mode of canyon formation (accelerated incision vs. incision into stronger rocks), there are clear differences in the expected evolution of both canyon side walls and tributary valley profiles that will be diagnostic of whether incision of the main-stem valley has

persisted to recent times, or whether the landscape has experienced a significant period of reduced rate of base level fall after canyon formation (as required by the 70 Ma hypothesis).

Approach and Scope

We do not address the incision history of all of Grand Canyon but rather focus on Western Grand Canyon (WGC), west of the Hurricane fault (Fig. 2.1). In our study area we determine (1) if WGC is more consistent with an increase in incision rate or simply a lithologic control on landscape morphology, (2) how much relief production is recorded by landscape morphology; (3) the range of plausible incision ages. The first two goals encompass determining the cause of canyon formation and the amount of relief production involved. Both are accomplished through an analysis of 2-D landform morphology (topographic cross sections, analysis of modern tributary river profiles, and reconstruction of pre-incision river profiles) and a qualitative evaluation of the correlation between rock strength and landscape morphology. As shown below, details of tributary canyon morphology can be used to differentiate between models allowing sustained river incision to present (e.g., the 17 Ma and 6 Ma models) and models requiring negligible incision following initial canyon cutting (the 70 Ma model). Constraining the age of the canyon is independently accomplished through (a) a quantitative comparison between canyon walls in the WGC and the escarpment along the Grand Wash Fault (GWF, most active 18-12 Ma), and (b) a compilation of incision rates over a range of timescales in tributaries and on the surrounding plateau. Given the common climate, lithology, and base level, our comparative morphological analysis can readily gauge the relative timing of incision of WGC and its tributaries and relief production related to slip on the Grand Wash Fault (GWF).

Background and Methods of River Profile Analysis

We employ river profile analysis and evaluate the relations between landscape morphology and geology to achieve our goals. USGS 30 m resolution digital elevation models (DEMs) are used for all topographic analyses. Pioneered and advanced by Hack (1957, 1975), analysis of river profiles can provide significant insight into the history of relative base level fall in a region. As the methods and foundational conceptual background are not as well-known as

more standard analyses of river incision rates from dated terraces, mean catchment hillslope gradients or topographic relief, we include here a brief primer tailored to aspects of river profile evolution that have diagnostic power for the questions outlined above. More detailed reviews of river profile evolution patterns and methods of profile analysis have been published recently by Wobus et al. (2006), Kirby and Whipple, (2012), Whittaker (2012), and Lague (2014).

River channels tend toward smooth concave-up river profiles that are well described by Flint's Law (Hack, 1957; Flint, 1974):

$$S = k_s A^{-\theta}, \qquad (1)$$

where S is local channel gradient, A is upstream area (a proxy for water and sediment discharge), k_s is the channel steepness index, and θ is the concavity index (usually between 0.4 and 0.6) (Tucker and Whipple, 2002). The most common deviations from this expected equilibrium form are either (1) channels broken into segments marked by slope-break knickpoints that separate reaches of distinct steepness but similar concavity, or (2) channels with smooth profiles but generally high concavity (θ > 0.6). Segmented channel profiles marked by slope-break knickpoints are expected to form in response to temporal changes in river incision rate or spatial patterns in rock uplift rate, substrate properties, or climatic conditions (e.g., Kirby and Whipple, 2012; Whittaker, 2012; Lague, 2013). Since the concavity index of discrete segments varies little, and because channel steepness and concavity determined from river profiles are strongly correlated, a normalized channel steepness index, k_{sn}, is used to quantify the relative steepness of channels (e.g. Wobus et al., 2006):

$$S = k_{sn} A^{-\theta_{ref}}, \qquad (2)$$

where θ_{ref} is a reference concavity often assumed to be around 0.5 (here we use 0.45 for computing regional maps of k_{sn} patterns, in keeping with most published estimates of k_{sn}). Typically, as here, the assigned θ_{ref} represents local determinations of the concavity of well-adjusted channel segments. High values of k_{sn} are associated with rapid incision rates, hard rocks, low erosivity climates (few large floods), and coarse bed material (e.g., Kirby and Whipple, 2012). Convex-up knickpoints are thus associated with either a temporal increase in the rate of

relative base level fall or a downstream increase in rock strength as might be caused by incision into sub-horizontal stratigraphy with higher average strength in lower rock layers.

We include a complementary analysis useful for visualizing perturbations to the long profile known as the integral method (Fig. 2.4C, Harkins et al., 2007; Perron and Royden, 2013). The integration of equation two yields elevation *(z)* as a function of distance along profile *(x)*,

$$z(x) = k_s \int_0^x A(x')^{-\theta} dx' \equiv k_s \chi(x), \qquad (3)$$

where *χ(x)* is determined directly from numerical integration of drainage area data. Any segments along the channel profile that are well described by theta_ref will be straight lines on a chi plot (Fig. 2.4C), with slope equal to *ksn*.

Figure 2.5 illustrates how canyon side walls and tributary channel profiles can be expected to evolve as a function of different base level histories following the onset of canyon incision, assuming for simplicity no strong lithologic control on channel steepness below the canyon rim (the canyon rim itself may be either lithologically controlled or reflect an acceleration in mainstem incision rate in either case (Fig. 2.3) – as noted above, canyon morphology is not diagnostic of the underlying cause of canyon formation): (1) on-going, roughly steady incision (plausibly consistent with both 17 and 6 Ma models), and (2) early incision followed by a substantial reduction or even cessation of incision (consistent with the 70 Ma model). On-going incision (scenario 1) maintains steep hillslopes and channels, with morphology set by incision rate, climate, and rock strength. Lithologic effects could be over-printed on this pattern, potentially inducing segmented profiles below the canyon rim with higher ksn through stronger rock layers. Substantial reduction or cessation of incision (scenario 2) triggers a progressive relaxation of initially steep canyon walls and tributaries even as slope-break knickpoints defining the canyon rim continue to migrate upstream. A sustained period of post-incision base level stability (or significantly reduced base level fall rate) is expected to manifest in tributary channel profiles as a distinct flattening of downstream reaches that can be anticipated to be most pronounced in larger tributaries (see Gasparini and Whipple, 2014), to be mimicked in the morphology of surrounding hillslopes, and to not coincide with lithologic layering. Thus scenarios involving recently active, quasi-steady incision can be readily distinguished from those with base level stability over 10^6-10^8

year timescales after canyon formation (e.g., the 70 Ma model) even in the presence of variable rock strength.

Figure 2.5 also illustrates how reconstruction of pre-incision river profiles (profiles prior to either mainstem incision into harder rocks or at an accelerated rate) can be used to quantify the amount of relief production, and, if erosional lowering of the surrounding landscape can be quantified, the total amount of main-stem river incision during the period of relief production. The method involved has been used successfully by Schoenbohm et al., (2004) Harkins et al., (2007), and DiBiase et al., (2014) and is illustrated in Figure 2.4 for the example of Jeff Canyon on the South Rim of WGC (Fig. 2.1). In our analysis, profile reconstruction and projection differ by an estimate of erosional lowering of the channel profile upstream of the slope-break knickpoint over the period of interest (Fig. 2.4). Projection begins with locating the major slope-break knickpoint(s) on the long-profile. Upstream of many knickpoints, subtly over-steepened zones truncate well-graded upstream stretches and are readily recognized on profiles and slope-area diagrams (Fig.2.4). Such oversteepened reaches are thought to result from stream flow acceleration and increased erosion rate that propagates upstream, sometimes 10's km's, over time (e.g. Haviv et al., 2006) and are not representative of pre-incision river profiles. The upstream limit of these oversteepened reaches is selected as the anchor point for profile projections. The average channel-steepness and concavity of well-graded sections upstream of the anchor point are found by regression following the methods outlined in Wobus et al., (2006) and Kirby and Whipple (2012). Slope-area data are smoothed using a 250 m window along the profile and a 40' contour interval consistent with USGS elevation source data. Assuming that drainage area and channel network geometry have remained invariant over the time period of interest, and that upstream reaches are reflective of channel form prior to canyon formation, the best-fit channel steepness and concavity upstream of anchor points are used in equation (1) to model the existing upstream profile and project the downstream profile as a function of drainage area. The projection from modern stream data is used as a baseline to which incision estimates can be added, allow reconstruction the paleo-stream profile (Fig. 2.4).

Uncertainty in the profile reconstruction includes restoration of the profile based on incision rate estimates and the projection uncertainty. Projection uncertainties are: (1) any unrecognized modification of channel slope above the knickpoint such that the upper channel segment is not reflective of pre-incision conditions, (2) possible changes in drainage area or network geometry, (3) uncertainty in the channel concavity, and (4) uncertainty in the channel steepness index. Error sources (1) and (2) cannot be accurately quantified and may be responsible for outliers. Error sources (3) and (4) are constrained by regression analyses and used to represent the range of uncertainties in profile reconstructions (Fig. 2.4). Anchor points are at the downstream end of the slope-area data used in the regression. Projection uncertainty is quantified by fixing θ_{ref} to the regional mean and using the associated channel steepness uncertainty. Particular streams require slightly different concavity index (either 0.4, 0.45, or 0.5), determined by comparing the projection and actual profile *upstream* of the anchor point. If the projection does not bracket the headwater, a different θ_{ref} and K_{sn} may be used (see Table 2 for θ_{ref} and k_{sn} of each projection). The projection is calculated from the mean and 2-sigma standard deviation (95% confidence interval) of the regressed, channel steepness index, k_{sn}. The projection and reconstruction terminate at the confluence with the Colorado River. The difference in elevation between the Colorado River at this point and the projected elevation is reported as the height of the projection, an estimate of relief production. The associated *reconstructed* height above the river is the projected height plus the restored incision of the upper tributary segment since initiation of canyon cutting (Fig. 2.4). Without the reconstruction, incision estimates from the projection are minimum estimates. We use pre-dam Colorado River surface elevations (USGS 1:24,000 scale maps) when calculating heights for tributaries that enter the Lake Mead reservoir.

River Canyon Formation: Lithology or Base level

Western Grand Canyon is a deep, narrow, steep-walled gorge inset into a broad low relief plateau with tributaries that head on the low-relief surface but are deeply incised below abrupt slope-break knickpoints near the main canyon (Figs. 2.1-2. 6). This morphology implies 3 possibilities: (1) recent acceleration of incision, (2) re-entrenchment of a previously buried,

ancient canyon, or (3) stripping of weak rocks to form a low relief surface cut on a hard, lithologically controlled bench surrounding the canyon. The first two scenarios could produce identical morphologies and would have to be distinguished based on geologic evidence for base level rise and regional aggradation. As neither the geology nor the thermochronology support (2) for WGC, we do not consider this scenario further except in discussion of the partially re-exhumed Laramide-age paleo-canyons on the eastern Hualapai Plateau (Young and Brennan, 1974; Young and McKee, 1978; Elston and Young, 1991b; Young and Crow, 2014). The third scenario has been discussed in terms of the evolution of Grand Canyon and river knickpoints (Cook et al., 2009; Pederson and Tressler, 2012) and can produce identical landforms as the other scenarios, though cases with steadily falling versus stable base level conditions following initial canyon cutting would have different expressions in tributary channel profiles and spatial incision rate patterns (Figs. 2.3 and 2.5).

Hillslope profiles in the Grand Canyon and surrounding Colorado Plateau are replete with classic examples of lithologic control on landform morphology with alternating strong cliff-forming and weak slope-forming rock layers (Selby, 1993). Indeed, the topographic expression of different rock layers is a great aid in geologic mapping in the region. These familiar hillslope expressions of variable rock strength have been recently corroborated with direct laboratory measurement of rock tensile and compressive strength and associated with variations in river slope and channel width (Pederson and Tressler, 2012). Ironically, the simple geology of only moderately deformed sub-horizontal sedimentary rocks greatly complicates the geomorphology, making it difficult in much of the Grand Canyon to differentiate between lithologic and base level controls on canyon morphology. Indeed, in WGC, the Sanup Plateau north of the Colorado River is often informally referred to as part of the “Esplanade surface” as it coincides with the top of the resistant Esplanade sandstone (Fig. 2.7). The Sanup Plateau appears to be a lithologically controlled bench associated with the erosional retreat of the Shivwitz escarpment along the contact between the easily eroded Hermit Shale and the resistant Esplanade Sandstone (Figure 2.7, Lucchitta, 1966; Young and Crow, 2014). This configuration and the prevalence of cliff-forming limestones of the Redwall, Temple Butte, and Muav Formations and Proterozoic basement exposed in

canyon walls is suggestive of, but not diagnostic of, lithologic control of the narrow, steep-walled WGC. It remains plausible that the morphology of WGC records accelerated river incision rate that is coincidental with incision below the level of the Esplanade Sandstone on the Sanup Plateau. Fortunately, Laramide-age deformation in the area of WGC created a setting that allows us to resolve this conundrum.

From geology, geomorphology, and Cenozoic stratigraphy of the Haulapai Plateau on the south side of the Colorado River (Figs. 2.1 and 2.7), inspection reveals that it is not a lithologically controlled bench but rather a product of a long period of erosion under a relatively stable base level. The critical observation is that the Hualapai Plateau is beveled indiscriminately across rock types ranging from Supai Group shales to Muav Fm. limestones, consistent with arguments put forward previously by Young (1999; 2001) and Young and Crow (2014) that this is an ancient and long-lived low-relief surface (Figs. 2.7 and 2.8). Importantly, the Haulapai Plateau is a low-relief erosional surface beveled to the same elevation as the Sanup Plateau – the two plateaus are part of a common surface incised by the Colorado and its tributaries, suggesting a common paleo-base level control overprinted by lithologically controlled retreat of the Shivwitz Plateau escarpment to the north. Thus, we infer that the morphology of WGC reflects a period of accelerated incision into a pre-existing low-relief landscape as outlined in more detail below.

First, tributary channel profiles have all the hallmarks of a disequilibrium landscape: deeply incised, steep-walled canyons in the vicinity of the main-stem that are marked by significant slope-break knickpoints where they cross the canyon rim (Figs. 2.1, 2.5, 2.6, and 2.7). Of course either an acceleration of incision rate or a lithologically induced pattern of differential erosion could be the driver behind the transient evolution of landscape morphology implied by this topography (Fig. 2.3). Downstream of major knickpoints some tributaries show strong lithologic control of channel steepness while others do not (Fig. 2.6). Smaller tributaries and those lacking a significant source of gravel in headwater reaches appear detachment-limited (e.g. Johnson et al., 2009) and have segmented channel profiles with *ksn* >400 $m^{0.9}$ through the Paleozoic limestones (Redwall, Temple Butte and Muav Formations), moderate ksn (~160 $m^{0.9}$) through the Bright Angel Shale, steepening somewhat where cutting through basement rocks. Larger tributaries and

those with significant headwater gravel sources (such as most of the streams draining the Shivwitz and Sanup plateaus) appear transport-limited, showing no lithologic control on channel profiles (e.g. Johnson et al., 2009) that have the same steepness as segments in the Bright Angel Shale on both sides of the canyon (Fig. 2.6). Additional complexities reflect young travertine dams in some tributaries (e.g., near the outlet of Jeff and Quartermaster canyons, and at 800m elevation in Meriwhitica, Figs. 2.4 and 2.6). Variable elevation ranges of the prominent high ksn segments well expressed on Figure 2.6 are inconsistent with temporal changes in the rate of base level fall following the initiation of canyon cutting (e.g., Wobus et al., 2006; Kirby and Whipple, 2012) and in fact coincide with outcrop patterns of the sequence of Paleozoic limestones. However, the lack of similar lithologic control on profiles of channels draining the Shivwitz and Sanup Plateaus suggests canyon formation and the prominent slope-break knickpoints that define the canyon rim cannot be attributed to lithology. Indeed, the surrounding low-relief surface (Hualapai and Sanup Plateaus) extends from the "Esplanade" surface (atop this sandstone) to cut across the limestones of the Muav, Temple Butte, and Redwall Formations, and the shales and sandstones of the Lower Supai Group and Esplanade Sandstone (Figs. 2.7 and 2.8). Far from forming lithologically controlled benches, the resistant Paleozoic limestones are beveled to the same level as the much weaker units of the lower Supai Group. Long-term stability of erosional base level at the elevation of the Hualapai Plateau (ca. 1400 m elevation at present) is required for such effective erosional beveling of erosionally resistant cliff-forming limestones (e.g. Baldwin et al., 2003). These morphological observations are consistent with interpretation of landscape evolution based on the nature, distribution, provenance, and paleo-flow directions of Tertiary sediments preserved on the Hualapai Plateau (e.g. Young and Brennan, 1974; Young and McKee, 1978; Elston and Young, 1991b; Young and Crow, 2014). The morphological observations summarized above, however, speak only to the cause of canyon formation (accelerated incision dominating over lithologic controls), not to its timing.

Amount of River Incision and Relief Production

The amount of river incision is the relative change in elevation of the main-stem river. Relief

production associated with canyon cutting differs from total river incision: it is the difference between river incision above a knickpoint and river incision below that knickpoint (Fig. 2.5). Relief production can be measured as the difference in elevation of a projected stream and the modern stream (the projected stream height, Table 2). A simple measure of the vertical drop from canyon rim to river level will over-estimate relief production because the rim is higher elevation than the upper streams incised into the low-relief plateau. Determining the paleo-elevation of the main-stem river involves two steps. First, relief production is measured from the elevation projected from relict upper channel segments above oversteepened zones down to the tributary confluence with the main-stem river (Fig. 2.5). Second, estimates of the lowering rate of the surrounding low-relief landscape can be multiplied by proposed or dated surface age to restore the lowering of relict channels over the time period of interest (Figs. 2.4 and 2.5). The sum of these provides an estimate of total river incision, such as might be recorded by thermochronometers.

Figure 2.9 summarizes the results of the profile projections, i.e. relief production. Thirty-eight streams were analyzed to determine if projections to paleo-base level could be made. We attempt profile projections only where we have grounds to believe the headwater reach of the profile reflects pre-incision channel morphology plausibly graded to paleo-base level. Thus channels that clearly express lithologic controls above the slope-break knickpoints that define the canyon rim are excluded. Conversely, streams that flow on the Tertiary angular unconformity and/or Tertiary sedimentary deposits are ideal (Figs. 2.6 and 2.7). Moreover, if these headwater stream segments preserve relict conditions they should all have similar slope-area relationships. We identify 12 streams most suitable for analysis. In Table 1, these 12 representative streams (red circles, Fig.2. 1) have a mean concavity of 0.44 +/- 0.02 and mean channel steepness of 27.5 +/-9.6, a narrow range of channel profile morphology. Our analysis of surrounding streams yielded 1 stream, “Bat Cave”, which matches slope-area metrics and may represent the same paleo-surface but is not associated with independent geologic evidence of a stable base level. These 13 projectable streams yielded an estimate of relief production in WGC of 1047 +/-25 m. As expected, this is a minimum relative to the simple estimate of the elevation difference between the Colorado River (~350m) and the lip of the Hualapai Plateau (>1400m).

Of the 26 other streams (Table 2), headwater reaches of 10 were too short to allow reliable projection. The remaining 16 either showed evidence of lithologic complications (13 of 16) or were associated with drainages that traverse the modern Grand Wash Trough, a now sub-areal region that was paleo-lake Hualapai up until ~6 million years ago (Lucchitta, 1979; Faulds et al., 2001) and given the certainty of drainage network disruptions could not be projected with confidence.

The lithologic complications above partly reflect the retreating Shivwitz Plateau escarpment (Fig. 2.8) which significantly complicates interpretation of longitudinal profiles of drainages on the north side of the Colorado River. The hard (Kaibab and Toroweap) over soft (Hermit) lithology of the Shivwitz escarpment implies that pre-incision channel profiles likely had lithologically controlled knickpoints perched above the base level of the Sanup and Haulapai Plateaus the streams were graded to. Indeed, projection of the thirteen streams thought to represent the pre-incision topography is contingent on the assumption that the Shivwits escarpment was already north of these streams when their headwater reaches equilibrated to their current form. The Tertiary sediments and beveled unconformity on the Hualapai Plateau support this assumption directly in the immediate area of most of these streams. However, those streams that now exist in the area between the modern Shivwitz escarpment and the Tertiary sediments on the south rim are likely to have evolved from steep reaches draining off the retreating Shivwits escarpment. Such streams would experience a complex history not conducive to simple profile projection and reconstruction.

In summary, although only 13 streams could be reliably projected and all but one rise on the Hualapai Plateau, this drainage-projection analysis makes it clear that carving of the WGC into the preserved older, low relief landscape of the Haulapai and Sanup plateaus involved ~1000 m of relief production since incision rate increased during formation of western Grand Canyon. We infer >700m of incision from elevation of the base of the Tertiary sediments (~1120m). Considering the ~400 m thickness of the Tertiary sediments (Young and Crow, 2014) gives about 1100 m, compared to our 1050 m for total relief production. Flowers and Farley (2012) and Wernicke (2011) interpret low-temperature thermochronometric data from river-level samples as

requiring “70-80% of canyon incision” since 70Ma. Although not more than 70 m of incision is recorded directly by the interaction of the river and basaltic lava flows in the last 0.625 Myr (Karlstrom et al., 2007) and less than 300m is inferred from ground water table elevation inferred from speleothems since 3.87 Ma (Polyak et al., 2008), our result of ~1000m of relief production in the late Tertiary suggests the understanding and interpretation of thermochronometric data in (Flowers and Farley, 2012) is incomplete, as recently independently suggested by Fox and Shuster (2014) on the basis of models of thermal evolution and kinetics of damage annealing and helium diffusion.

Plateau Lowering Rate

We derive estimates of the lowering rate of the plateau from volcanic deposits (Young and Brennan, 1974; Wenrich et al., 1995) with incision amounts estimated as the relief between tops of hills capped by dated basalts to closest channel bottoms. Height measured from the tops of flows to channel bottoms results in rates that are local maxima. Ages range from 15 to 19 Ma, yielding a minimum lowering rate on the low-relief surface of 2-11 m/Ma, with a mean of ~6 m/Ma (Table 3). The amount that incision estimates differ from relief production requires an estimate of the time of incision onset.

Incision magnitude vs relief production

The three competing hypotheses for the incision of western Grand Canyon suggest incision starting at ~6 Ma or ~17 Ma, or virtually complete by 70 Ma. A succession of sedimentary deposits from early Tertiary until ~19 Ma records net moderate aggradation (up to ~400m in infilled paleo-canyons) on the Hualapai Plateau over that interval (Young and Brennan, 1974; Young and McKee, 1978; Young, 1979; Elston and Young, 1991a; Young and Spamer, 2001; Young, 2008; Young and Crow, 2014). The plateau lowering rate estimate (~6 m/Ma) is a measure of the average rate of lowering since the ~19 Ma cessation of aggradation. It is important to acknowledge that slow headwaters erosion is not zero so total incision during canyon cutting will exceed the relief production estimates presented above. In addition, the background erosion rate of the plateau surface is the only direct constraint on the paleo, pre-canyon erosion

rates in the region. At 6 m/Ma, total Colorado River incision would be 36 m greater than relief production if canyon incision began 6 Ma, and 100 m greater if canyon incision began 17 Ma. The latter estimate is a maximum given the record of aggradation on the plateau prior to ~19 Ma. Thus our estimate of total incision since the onset of canyon formation ranges between 1000 and 1200 meters.

Age of Canyon Incision

Here we develop geomorphologic constraints on the timescale over which incision of the Colorado River and its tributaries into the low relief surface defined by the Hualapai and Sanup Plateaus in Western Grand Canyon occurred. We take two approaches to this analysis. The first is based on a comparative analysis of landscape morphology in the WGC and nearby Grand Wash Trough (GWT). The second is based on measurements and estimates of erosion rates over a range of timescales within and around the WGC.

Morphological Analysis

As discussed earlier, details of tributary river profile forms can be diagnostic – at least in general terms – of the history of base level fall. Similar examples of this type of analysis are discussed in Whittaker (2012), Kirby and Whipple (Kirby and Whipple, 2012), Gallen et al. (2013). Comparison of all tributaries to WGC (Figs. 2.4-2.7; Appendix A), with expectation from theory, strongly suggest that there is no indication of the morphology expected to result from a stable base level maintained for millions to 10s of millions of years after canyon incision (see Fig. 2.5B). Tributary profiles are rather suggestive of relatively steady incision over the duration of canyon formation and persisting to present (Fig. 2.5A), with variable degrees of lithologic control on below-rim channel steepness (Fig. 2.6), as recorded by lava flow remnants (Crow et al., 2008) and speleothems (Polyak et al., 2008).

The above interpretation of WGC tributary profile morphology is powerfully re-enforced by a morphological comparison of the WGC landscape with the landscape of the Grand Wash Cliffs. The history of the Grand Wash Fault (GWF) provides a well-known timing of relief production in a setting where both climate and rock strength are nearly identical to the WGC. Slip along the GWF

is well documented to begin about 18 Ma, with most of its 5.5 km of offset accumulated by 12 Ma (Lucchitta, 1966; Lucchitta, 1972; Lucchitta, 1979; Bohannon, 1984; Bohannon et al., 1993; Karlstrom et al., 2010; Quigley et al., 2010; Umhoefer et al., 2010). Ensuing slip along the GWF is dramatically less, ca. 300 m, from 12 Ma to 6 Ma. It is possible there has been limited post-6 Ma slip on the GWF. While the history of the GWF is not fully known and is itself complicated, relief production is no older than 18 Ma and both hillslope and channel morphologies may reflect rejuvenation by younger episodes of slip and by base level fall associated with the ~6 Ma breaching of Lake Hualapai and the subsequent incision though the Hualapai Limestone and associated basin fill sediments.

We use topographic metrics to determine directly whether incision in the WGC is older, younger, or similar in age to incision of the tributaries of the GWT in response to faulting on the GWF and base level fall associated with post ~6 Ma incision. Tributaries to the GWT exhibit subtle knickpoints at the edge of the Sanup Plateau, suggesting a period of slow incision or stable base level but have nearly identical channel steepness and concavity to north-side tributaries in the WGC (Figs. 2.7 and 2.8). The ~160 $m^{0.9}$ mean steepness index is identical to channel segments not exhibiting lithologic control and strong over-steepening where cut on resistant Paleozoic limestones or basement rocks, suggesting a very similar timing and rate of base level fall, but under transport-limited conditions (e.g. Johnson et al., 2009). Like channel steepness, hillslope gradients are a function of erosion rate, rock strength, and climate. Figure 2.11 shows a composite hill-shade and slope map of the GWT and WGC. In the WGC, hillslopes are clearly steep all the way from the rim of the Hualapai and Sanup Plateaus down to the Colorado River, particularly where Paleozoic limestones and basement rocks crop out (Fig. 2.7). Canyon walls have not retreated laterally from river's edge. The escarpment of the GWC on the other hand has in places retreated 2-3 kilometers from the trace of the GWF and is less steep and more subdued. Topographic profile (Fig. 2.12) emphasize this difference. Average slopes of inter-fluvial ridges near 270-mile, Quartermaster and Horse Flat canyons are 0.76, 0.44 0.49, respectively. Similar ridges along Pearce, Pigeon and Squaw canyons of the GWT, show average hillslope gradients of 0.14, 0.21 and 0.17, respectively. The topographic comparisons of WGC to

the GWC show that the two regions have had significantly different base level fall histories. Twelve million years of minimal fault activity has resulted in several kilometers of retreat of the Grand Wash Cliffs and considerable relaxation of hillslope gradients. Morphologic analysis strongly suggests relief production in WGC is younger than along the GWC where the bulk of relief production occurred from 18-12 Ma. The hypothesis that the narrow, steep-walled WGC is ≥70 Myr old is quite simply untenable.

Erosion Rate Constraints

The hypotheses about the timing of WGC incision require different rates of tributary incision and cliff retreat in order to produce and maintain the observed landscape morphology for the duration of the different hypothesized incision histories. We use several methods to determine average incision rates on the Colorado River in WGC. Separation Hill basalt (1500m high and 19 Ma, Wenrich et al., 1995) yields an average incision rate of 60 m/Ma over the last 19 million years. Quaternary basalt flows along the Colorado River overlie river gravel yielding similar rates on the order of 70 m/Ma (Karlstrom et al., 2008) over the last 0.625 Myr. Recently determined cosmogenic erosion rates in WGC yield rates of 61 +/- 18 m/Ma (Nichols et al., 2011) averaged over the last ~10 k years. Given the broad range of timescales of these data, it is possible significant rate fluctuations exist between data points but the available evidence implies that the incision rate since ~0.7 Ma is roughly equal to the average incision rate since 19 Ma.

The old canyon model suggests 70-80% of Colorado River incision in 70 million years (Flowers and Farley, 2012). Using our estimate of incision magnitude of 1100 m, then the 70 Ma model suggests at most 400 m of incision since 70 Ma. Basalt flows in WGC are up to ~70 m above the COR, so the remaining 330 m of “allowable” incision in the model imply an average incision rate of 4 m/Ma prior to the time of WGC basaltic volcanism in the gorge to be consistent with the 70 Ma hypothesis. This rate is consistent with erosion on the flat plateau, but all independent measures of canyon incision rate are consistently and substantially higher than rates determined from the hypothesis that a canyon of near-modern depth existed by 70 Ma.

The 17-Ma-canyon hypothesis implies that average incision has occurred at ~60 m/Ma

(1000 m/17 Ma), implying incision slightly slower on average than estimates in the last 0.7 Myr. The 6-Ma-canyon hypothesis, on the other hand, implies that 1000 m of incision has occurred at an average rate of 167 m/Ma (~200 with correct significant figures) over the last 6 Myr. Although this appears to be a mis-match with independent constraints (faster than both the average since ~17 Ma and rates recorded in the last 0.7 Myr and 0.01 Myr), the difference is consistent with expected evolution of WGC following initiation of incision. Integration of the Colorado River across the GWC would trigger a period of rapid incision that would decrease with time as a knickpoint swept upstream (Pederson et al., 2002a; Cook et al., 2009). Available constraints on incision rate history allows a few million years over which incision may have been faster than ~160 m/Ma and then slowed to ~70 m/Myr. Alternatively, this difference in rates could indicate that part of the incision of WGC occurred between ~17 and ~6 Ma by a moderate sized local stream in response to slip on the GWF (Polyak et al., 2008; Young, 2008; Young and Crow, 2014) followed by a further acceleration of incision in response to integration of the Colorado River across the Grand Wash Cliffs at ~6 Ma.

Conclusions

The first order observation that the Hualapai Plateau cuts a surface across numerous rock types is a strong indication that it is a long-timescale erosional bench regardless of contrasting lithologic strength. Paleo-base level of the region is therefore directly associated with this preserved landscape. Regional erosion reached the level of the Hualapai Plateau >60 Ma from regional thermochronology (Flowers et al., 2008). This is likely the time that setup the major landscape features of a paleo-Shivwits Plateau that extended further south than today and the Hualapai Plateau. Minor incision of paleo-canyons and the beveling of the drainage divides and local planation with broad local sedimentation was ongoing between >50 and 18 Ma, (Young and Brennan, 1974; Young and McKee, 1978; Young, 1979; Elston and Young, 1991a; Wenrich et al., 1995; Young and Spamer, 2001; Young, 2008; Young and Crow, 2014). The fluvial geomorphic data from headwater portions of Hualapai Plateau streams is interpreted to be consistent with preservation of a stable base level prior to incision. Channel projections throughout the Hualapai

and Sanup plateaus yield estimates of relief production magnitude near 1000 meters throughout western Grand Canyon.

Our data are most consistent with the 6 Ma model for the timing of canyon cutting. The 70 Ma model requires erosion at an improbably low ~4 m/Ma for tens of millions of years while supporting significant amounts of relief. The 17 Ma model is plausible based on existing incision rates and is compatible with Tertiary deposits on the Hualapai Plateau. However, landscape morphology indicates the erosion of the walls of the WGC started considerably more recently than the erosion of the Grand Wash Cliffs 18-12 million years ago. Therefore, the geomorphology and incision rates are consistent with a transient increase in incision rate directly after integration of the Colorado River around 6 million years ago and slowing down to match a longer-term average rate by the Quaternary.

References

Baldwin, J. A., Whipple, K. X., and Tucker, G. E., 2003, Implications of the shear stress river incision model for the timescale of postorogenic decay of topography: Journal of Geophysical Research-Solid Earth, v. 108, no. B3, p. art. no.-2158.

Blackwelder, E., 1934, Origin of the Colorado River: Geological Society of America Bulletin, v. 45, no. 3, p. 551-566.

Bohannon, R. G., 1984, Nonmarine sedimentary rocks of Tertiary age in the Lake Mead region, southeastern Nevada and northwestern Arizona: U.S. Geological Survey Professional Paper, v. 1259, p. 72.

Bohannon, R. G., Grow, J. A., Miller, J. J., and BLANK, R. H., 1993, Seismic stratigraphy and tectonic development of Virgin River depression and associated basins, southeastern Nevada and northwestern Arizona: Geological Society of America Bulletin, v. 105, no. 4, p. 501-520.

Cook, K. L., Whipple, K. X., Heimsath, A. M., and Hanks, T. C., 2009, Rapid incision of the Colorado River in Glen Canyon–insights from channel profiles, local incision rates, and modeling of lithologic controls: Earth Surface Processes and Landforms, v. 34, no. 7, p. 994-1010.

Crow, R., Karlstrom, K., Darling, A., Crossey, L., Polyak, V., Granger, D., Asmerom, Y., and Schmandt, B., 2014, Steady incision of Grand Canyon at the million-year timeframe: A case for mantle-driven differential uplift: Earth and Planetary Science Letters, v. 397, p. 159-173.

Crow, R., Karlstrom, K. E., McIntosh, W., Peters, L., and Dunbar, N., 2008, History of Quaternary volcanism and lava dams in western Grand Canyon based on lidar analysis, 40Ar/39Ar dating, and field studies: Implications for flow stratigraphy, timing of volcanic events, and lava dams: Geosphere, v. 4, no. 1, p. 183.

Davis, W. M., 1901, An excursion to the Grand Canyon of the Colorado, Cambridge, Massachusetts, Printed for the Museum, 201 p.:

DiBiase, R. A., Whipple, K. X., Lamb, M. P., and Heimsath, A. M., 2014, The role of waterfalls and knickzones in controlling the style and pace of landscape adjustment in the western San Gabriel Mountains, California: Geological Society of America Bulletin, p. B31113. 31111.

Elston, D. P., and Young, R. A., 1991a, Cretaceous-Eocene (Laramide) Landscape Development and Oligocene-Pliocene Drainage Reorganization of Transition Zone and Colorado Plateau, Arizona: Journal of Geophysical Research-Solid Earth and Planets, v. 96, no. B7, p. 12389-12406.

Elston, D. P., and Young, R. A., 1991b, Cretaceous-Eocene (Laramide) landscape development and Oligocene-Pliocene drainage reorganization of transition zone and Colorado Plateau, Arizona: Journal of Geophysical Research: Solid Earth (1978–2012), v. 96, no. B7, p. 12389-12406.

Faulds, J. E., Price, L. M., and Wallace, M. A., 2001, Pre–Colorado River paleogeography and extension along the Colorado Plateau–Basin and Range boundary, northwestern Arizona: Colorado River: Origin and Evolution. Monograph, v. 12, p. 93-99.

Flint, J. J., 1974, Stream gradient as a function of order, magnitude, and discharge: Water Resources Research, v. 10, p. 969-973.

Flowers, R., and Farley, K., 2012, Apatite 4He/3He and (U-Th)/He evidence for an ancient Grand Canyon: Science, v. 338, no. 6114, p. 1616-1619.

Flowers, R. M., Wernicke, B. P., and Farley, K. A., 2008, Unroofing, incision, and uplift history of the southwestern Colorado Plateau from apatite (U-Th)/He thermochronometry: Geological Society of America Bulletin, v. 120, no. 5-6, p. 571-587.

Fox, M., and Shuster, D., 2014, The influence of burial heating on the (U-Th)/He system in apatite: Grand Canyon case study: Earth and Planetary Science Letters, v. 397, p. 174-183.

Gallen, S. F., Wegmann, K. W., and Bohnenstiehl, D., 2013, Miocene rejuvenation of topographic relief in the southern Appalachians: GSA Today, v. 23, no. 2, p. 4-10.

Hack, J. T., 1957, Studies of longitudinal stream profiles in Virginia and Maryland: U.S. Geological Survey Professional Paper, v. 294-B, p. 97.

-, 1975, Dynamic equilibrium and landscape evolution, in Melhorn, W. N., and Flemal, R. C., eds., Theories of Landform Development: New York, Allen & Unwin, p. 87-102.

Harkins, N., Kirby, E., Heimsath, A., Robinson, R., and Reiser, U., 2007, Transient fluvial incision in the headwaters of the Yellow River, northeastern Tibet, China: Journal of Geophysical Research, v. 112, no. F3.

Haviv, I., Enzel, Y., Whipple, K. X., Zilberman, E., Stone, J., Matmon, A., and Fifield, L. K., 2006, Amplified erosion above waterfalls and oversteepened bedrock reaches: Journal of Geophysical Research, v. 111, no. F4.

House, P. K., Pearthree, P. A., and Perkins, M. E., 2008, Stratigraphic evidence for the role of lake spillover in the inception of the lower Colorado River in southern Nevada and western Arizona: Geological Society of America Special Papers, v. 439, p. 335-353.

Ingersoll, R. V., Grove, M., Jacobson, C. E., Kimbrough, D. L., and Hoyt, J. F., 2013, Detrital zircons indicate no drainage link between southern California rivers and the Colorado Plateau from mid-Cretaceous through Pliocene: Geology, v. 41, no. 3, p. 311-314.

Johnson, J. P., Whipple, K. X., Sklar, L. S., and Hanks, T. C., 2009, Transport slopes, sediment cover, and bedrock channel incision in the Henry Mountains, Utah: Journal of Geophysical Research: Earth Surface (2003–2012), v. 114, no. F2.

Karlstrom, K. E., Crow, R., Crossey, L. J., Coblentz, D., and Van Wijk, J. W., 2008, Model for tectonically driven incision of the younger than 6 Ma Grand Canyon: Geology, v. 36, no. 11, p. 835.

Karlstrom, K. E., Crow, R. S., Peters, L., McIntosh, W., Raucci, J., Crossey, L. J., Umhoefer, P., and Dunbar, N., 2007, 40Ar/39Ar and field studies of Quaternary basalts in Grand Canyon and model for carving Grand Canyon: Quantifying the interaction of river incision and normal faulting across the western edge of the Colorado Plateau: Geological Society of America Bulletin, v. 119, no. 11-12, p. 1283-1312.

Karlstrom, K. E., Heizler, M., and Quigley, M. C., 2010, Structure and 40Ar/39Ar K-feldspar thermal history of the Gold Butte block: Reevaluation of the tilted crustal section model: Geological Society of America Special Papers, v. 463, p. 331-352.

Karlstrom, K. E., Lee, J. P., Kelley, S. A., Crow, R. S., Crossey, L. J., Young, R. A., Lazear, G., Beard, L. S., Ricketts, J. W., and Fox, M., 2014, Formation of the Grand Canyon 5 to 6 million years ago through integration of older palaeocanyons: Nature Geoscience, v. 7, p. 239-244.

Kirby, E., and Whipple, K. X., 2012, Expression of active tectonics in erosional landscapes: Journal of Structural Geology, v. 44, p. 54-75.

Lague, D., 2014, The stream power river incision model: evidence, theory and beyond: Earth Surface Processes and Landforms, v. 39, no. 1, p. 38-61.

Longwell, C. R., 1946, How old is the Colorado River?: American Journal of Science, v. 244, no. 12, p. 817-835.

Lucchitta, I., 1966, Cenozoic geology of the upper Lake Mead area adjacent to the Grand Wash Cliffs: Arizona [Ph. D. thesis]: Pennsylvania State University, University Park.

Lucchitta, I., 1972, Early history of the Colorado River in the Basin and Range Province: Geological Society of America Bulletin, v. 83, no. 7, p. 1933-1948.

Lucchitta, I., 1979, Late Cenozoic uplift of the southwestern Colorado Plateau and adjacent lower Colorado River region: Tectonophysics, v. 61, no. 1, p. 63-95.

Nichols, K. K., Webb, R. H., Bierman, P. R., and Rood, D. H., 2011, Measurements of cosmogenic 10 Be reveal rapid response of Grand Canyon tributary hillslopes to Colorado River incision: Geological Society of America - Abstracts with Programs, v. 43, p. 274.

Pearthree, P. A., Spencer, J. E., Faulds, J. E., and House, P. K., 2008, Comment on "Age and evolution of the Grand Canyon revealed by U-Pb dating of water table-type speleothems": Science, v. 321, no. 5896, p. 1634.

Pederson, J., Karlstrom, K., Sharp, W., and McIntosh, W., 2002, Differential incision of the Grand Canyon related to Quaternary faulting - Constraints from U-series and Ar/Ar dating: Geology, v. 30, no. 8, p. 739-742.

Pederson, J., Young, R., Lucchitta, I., Beard, L. S., and Billingsley, G., 2008, Comment on "Age and evolution of the Grand Canyon revealed by U-Pb dating of water table-type speleothems": Science, v. 321, no. 5896, p. 1634; author reply 1634.

Pederson, J. L., 2008, The mystery of the pre-Grand Canyon Colorado River-results from the Muddy Creek formation: GSA Today, v. 18, no. 3, p. 4.

Pederson, J. L., Anders, M. D., Rittenhour, T. M., Sharp, W. D., Gosse, J. C., and Karlstrom, K. E., 2006, Using fill terraces to understand incision rates and evolution of the Colorado River in eastern Grand Canyon, Arizona: Journal of Geophysical Research, v. 111, no. F2.

Pederson, J. L., and Tressler, C., 2012, Colorado River long-profile metrics, knickzones and their meaning: Earth and Planetary Science Letters, v. 345, p. 171-179.

Perron, J. T., and Royden, L., 2013, An integral approach to bedrock river profile analysis: Earth Surface Processes and Landforms, v. 38, no. 6, p. 570-576.

Polyak, V., Hill, C., and Asmerom, Y., 2008, Age and evolution of the Grand Canyon revealed by U-Pb dating of water table-type speleothems: Science, v. 319, no. 5868, p. 1377-1380.

Powell, J. W., 1875, Exploration of the Colorado River of the West and its Tributaries.

Quigley, M. C., Karlstrom, K. E., Kelley, S., and Heizler, M., 2010, Timing and mechanisms of basement uplift and exhumation in the Colorado Plateau-Basin and Range transition zone, Virgin Mountain anticline, Nevada-Arizona: Geological Society of America Special Papers, v. 463, p. 311-329.

Schoenbohm, L., Whipple, K., Burchfiel, B., and Chen, L., 2004, Geomorphic constraints on surface uplift, exhumation, and plateau growth in the Red River region, Yunnan Province, China: Geological Society of America Bulletin, v. 116, no. 7-8, p. 895-909.

Selby, M. J., 1993, Hillslope Materials and Processes, Oxford, Oxford University Press.

Tucker, G. E., and Whipple, K., 2002, Topographic outcomes predicted by stream erosion models: Sensitivity analysis and intermodel comparison: Journal of Geophysical Research, v. 107, no. B9.

Umhoefer, P. J., Duebendorfer, E. M., Blythe, N., Swaney, Z. A., Beard, L. S., and McIntosh, W. C., 2010, Development of Gregg Basin and the southwestern Grand Wash Trough during late-stage faulting in eastern Lake Mead, Arizona: Geological Society of America Special Papers, v. 463, p. 221-241.

Wenrich, K. J., Billingsley, G. H., and Blackerby, B. A., 1995, Spatial migration and compositional changes of Miocene-Quaternary magmatism in the western Grand Canyon: Journal of Geophysical Research, v. 100, no. B6, p. 10417-10410,10440.

Wernicke, B., 2011, The California River and its role in carving Grand Canyon: Geological Society of America Bulletin, v. 123, no. 7-8, p. 1288-1316.

Whittaker, A. C., 2012, How do landscapes record tectonics and climate?: Lithosphere, v. 4, no. 2, p. 160-164.

Wobus, C. W., Whipple, K. W., Kirby, E., and Snyder, N. P., 2006, Tectonics from topography: Proceedures, promise, and pitfalls, in Willett, S. D., Hovius, N., Brandon, M., and Fisher, D. M., eds., Climate, Tectonics and Landscape Evolution: Geological Society of America Special Paper, Volume 398, Penrose Conference Series, p. 55-74.

Young, R., 1979, Laramide deformation, erosion and plutonism along the southwestern margin of the Colorado Plateau: Tectonophysics, v. 61, no. 1, p. 25-47.

Young, R. A., 1999, Nomenclature and Ages of Late Cretaceous-Tertiary Strata in the Hualapai Plateau Region, Northwest Arizona, US Government Printing Office.

Young, R. A., 2008, Pre-Colorado River drainage in western Grand Canyon: potential influence on Miocene stratigraphy in Grand Wash trough, in Reheis, M. C., Hershley, R., and Miller, D. M., eds., Special Paper - Geological Society of America, Volume 439, p. 319.

Young, R. A., and Brennan, W. J., 1974, Peach Springs Tuff: Its bearing on structural evolution of the Colorado Plateau and development of Cenozoic drainage in Mohave County, Arizona: Geological Society of America Bulletin, v. 85, no. 1, p. 83-90.

Young, R. A., and Crow, R., 2014, Paleogene Grand Canyon incompatible with Tertiary paleogeography and stratigraphy: Geosphere, v. 10, no. 4, p. 664-679.

Young, R. A., and McKee, E. H., 1978, Early and middle Cenozoic drainage and erosion in west-central Arizona: Geological Society of America Bulletin, v. 89, no. 12, p. 1745-1750.Young, R. A., and Spamer, E. E., 2001, Colorado River: Origin and Evolution: Proceedings of a Symposium Held at Grand Canyon National Park in June, 2000, Grand Canyon Assn, v. 12.

Figures

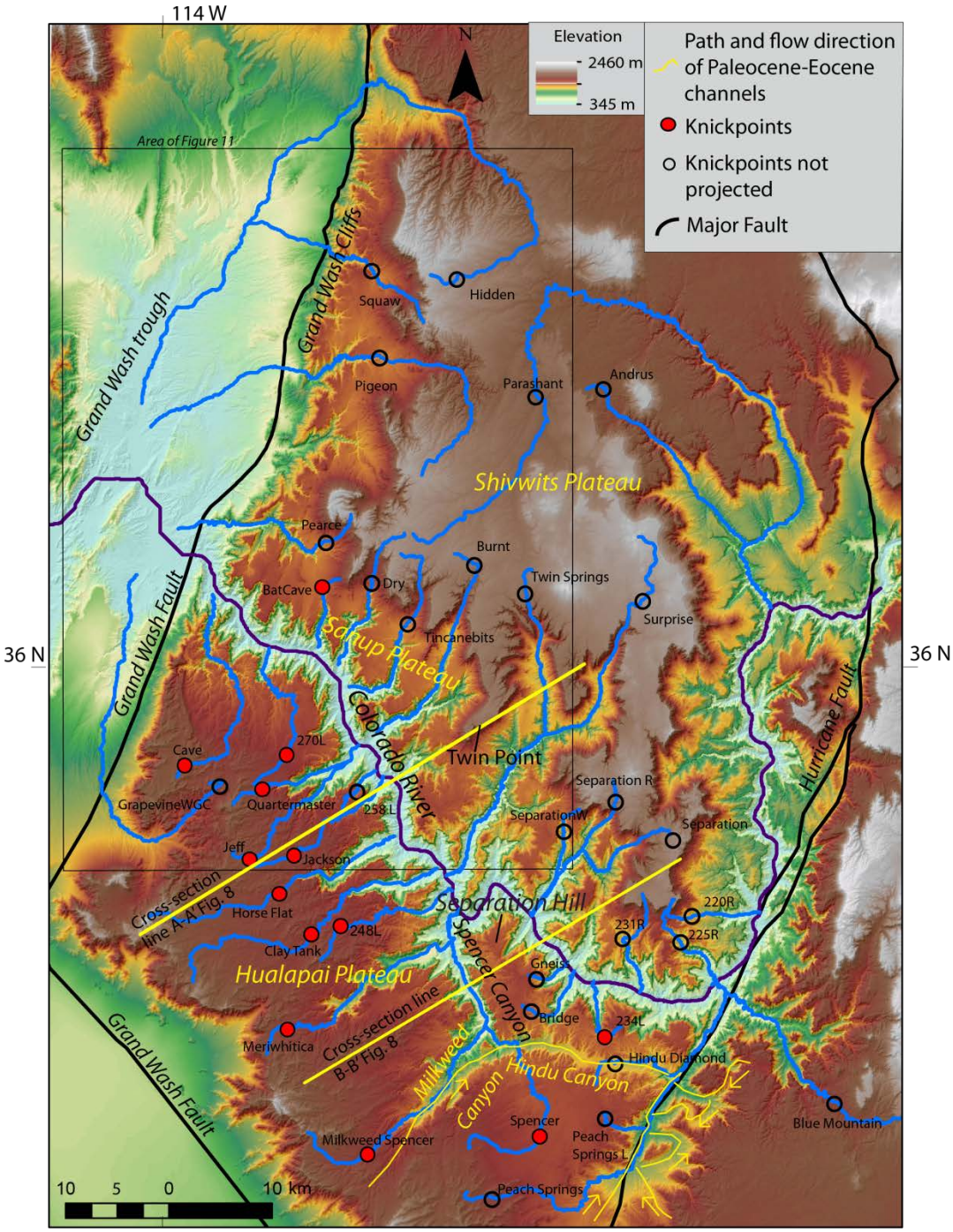

Figure 2.1. Western Grand Canyon study area, defined by the area downstream of Hurricane fault and upstream of Grand Wash Trough. Elevation colored over hill-shade with analyzed tributary rivers shown in blue. Major faults, major tributary knickpoints, early Tertiary paleo-channels, and topographic section lines are indicated. Box shows extent of Fig. 2.11.

Figure 2.2. Photographs taken from Twin Point overlook. A) View to the southeast, showing the Shivwitz Plateau escarpment above the Sanup Plateau (Photo credit: Rich Rudow). B) View to the south, showing the Sanup Plateau in the foreground and the Hualapai Plateau

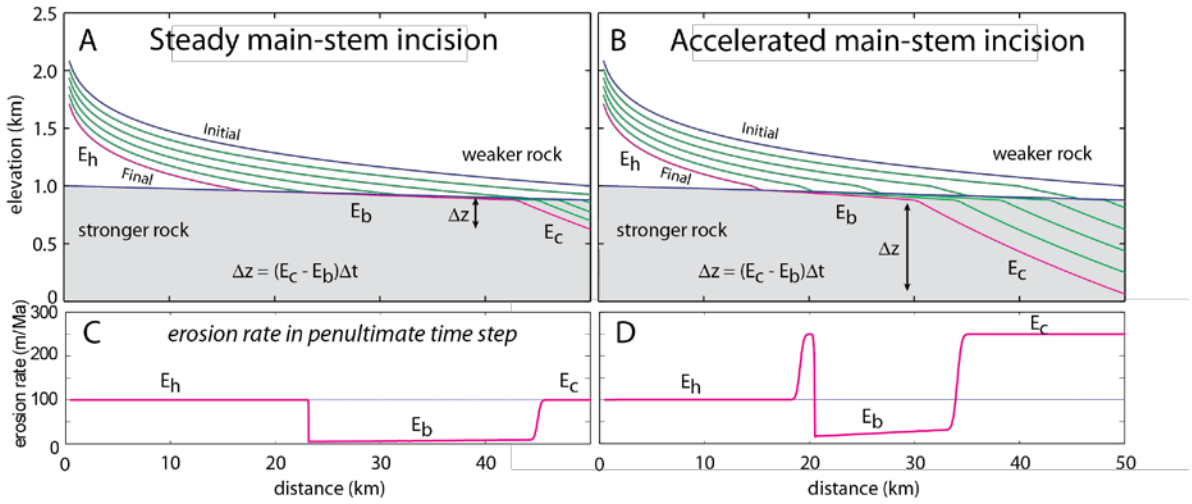

Figure 2.3. Illustration of canyon formation (local-relief increase Dz) associated with exposure of a sub-horizontal layer of stronger rock (grey) under both (A) steady mainstem incision (100 m/Ma) and (B) following an increase in mainstem incision (stream power model simulation: blue – initial profile for steady state incision in weak rocks; green – intermediate time steps; magenta – final time step of simulation). Model illustrates tributary response to incision of mainstem (right edge). In both cases relief is set by the difference between erosion rate in the canyon (Ec) and on the surrounding lithologically controlled bench (Eb), times the time since exposure of the harder rock layer or acceleration of incision (Dt). (C) and (D) show that the most easily measured diagnostic difference is the relation between Ec and the erosion rate in headwater catchments (Eh) still incising the overlying weaker rock and largely insulated from changes downstream (see text). Note that the slight steepening just above the main knickpoint in (B) and associated spike in erosion rate in (D) reflects the fact that in the simulation the acceleration of incision precedes exposure of the stronger rock -- the main knickpoint is lithologic in nature in both cases.

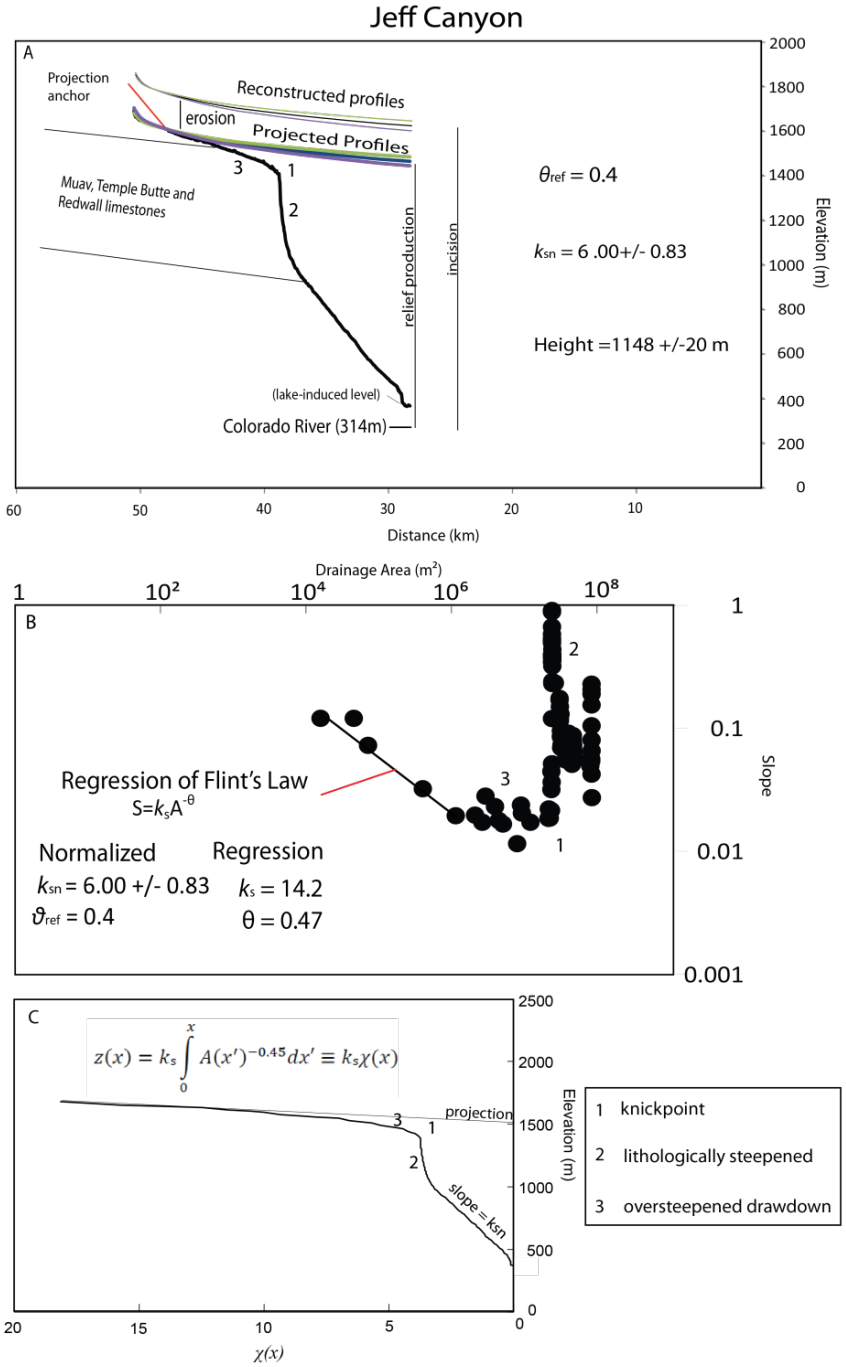

Figure 2.4. River profile reconstruction method illustrated for Jeff Canyon (see Fig. 2.1 for location). Panel A shows channel profile and reconstructed pre-incision channel profile projections, with uncertainty bounds. Note that Theta_ref is 0.4, 0.45 or 0.5. Panel B shows log slope-log area diagram illustrating the dramatic slope-break knickpoint and the regression used to characterize the relict upstream channel segment. Note the single slope-break knickpoint and that the channel remains steep all the way to the confluence. Panel C shows elevation vs chi. Slope of the line is k_{sn}. Highest k_{sn} is closely associated with thick limestone packages.

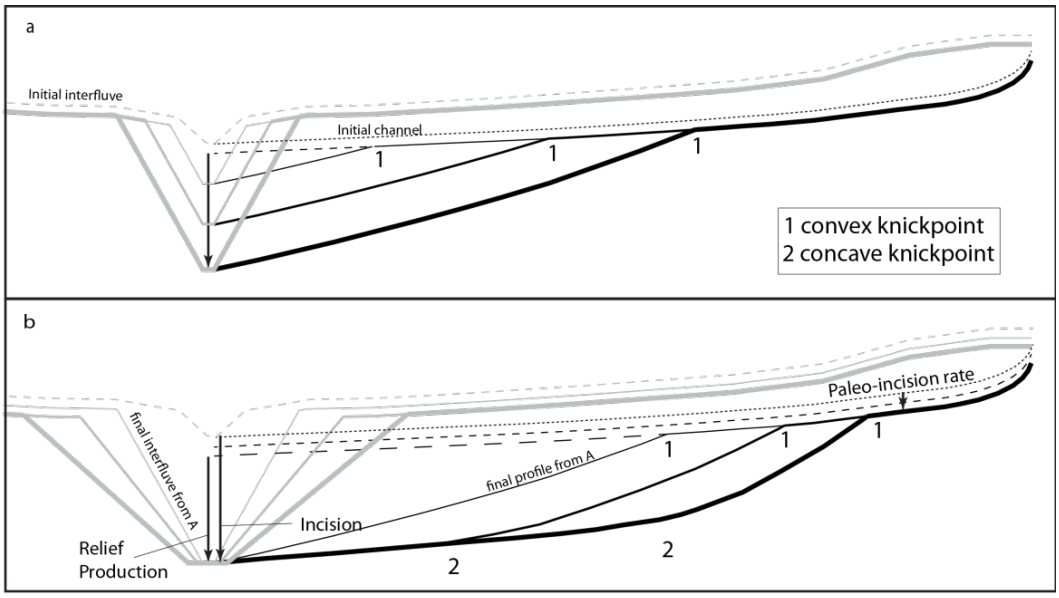

Figure 2.5. Schematic illustration of landscape evolution associated with canyon formation. Upper panel (scenario 1) shows landform evolution during active (assumed steady for simplicity) incision. Lower panel (scenario 2) shows evolution after cessation of incision. River profiles are in black, canyon side walls and interfluves are in grey. Later time steps shown in thicker lines (each panel shows 4 time steps). Initial condition shown as dashed grey line (interfluve) and dotted black line (channel). First time-step in lower panel is the final time-step from the upper panel. For clarity only initial and final time-steps are shown for the interfluve, channel, and reconstructed channel projection associated with the low relief erosion surface. Arrows show net observed relief production. Total incision is larger as this includes the slow lowering of the surrounding low relief landscape (distance between final dashed channel reconstruction and the initial channel profile shown as a dotted line).

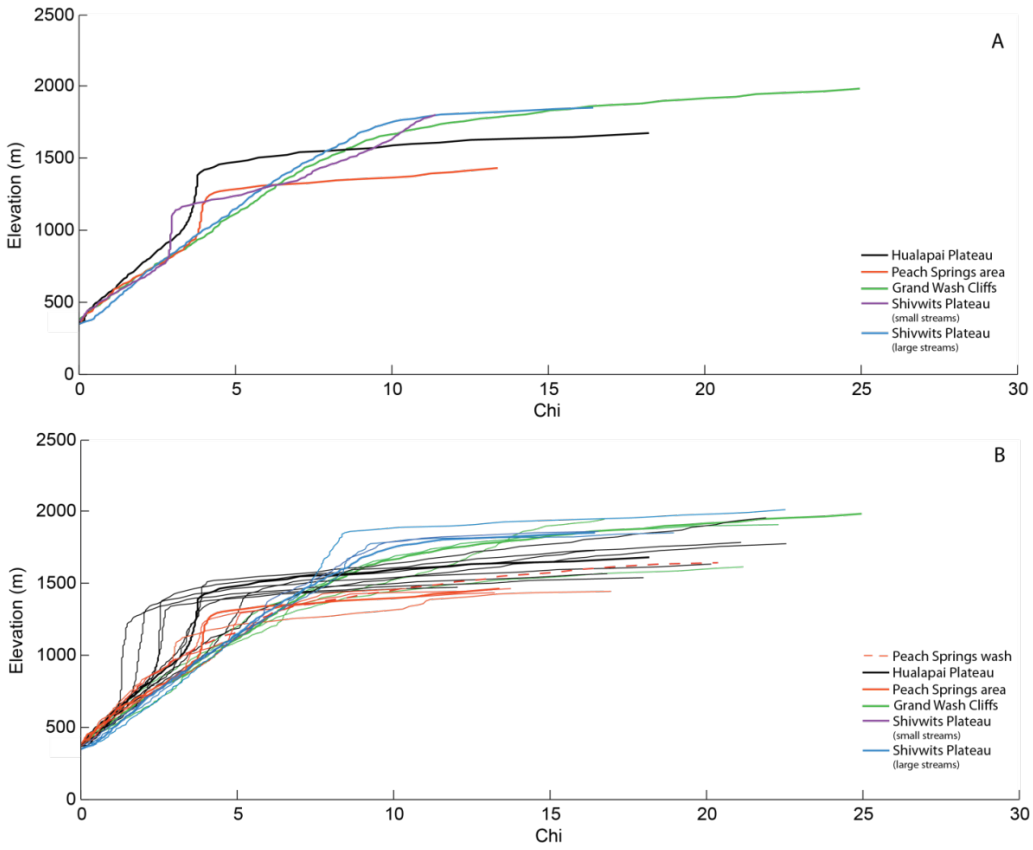

Figure 2.6. Chi vs elevation determined from drainage area data for a) exemplary channels and the representative sample of most streams b). All streams analyzed are included in Appendix A. Linear sections are associated with regions well represented by theta_ref and the slope of the line is ksn. All streams show 2 dominant regions of ksn, one within the canyon (at low elevations) and one above the canyon. Streams 234L and Jeff canyons contain upward perturbations, reflecting anomalously high k_{sn} that are associated with thick sections of erosion-resistant limestone bedrock below the rim of the canyon.

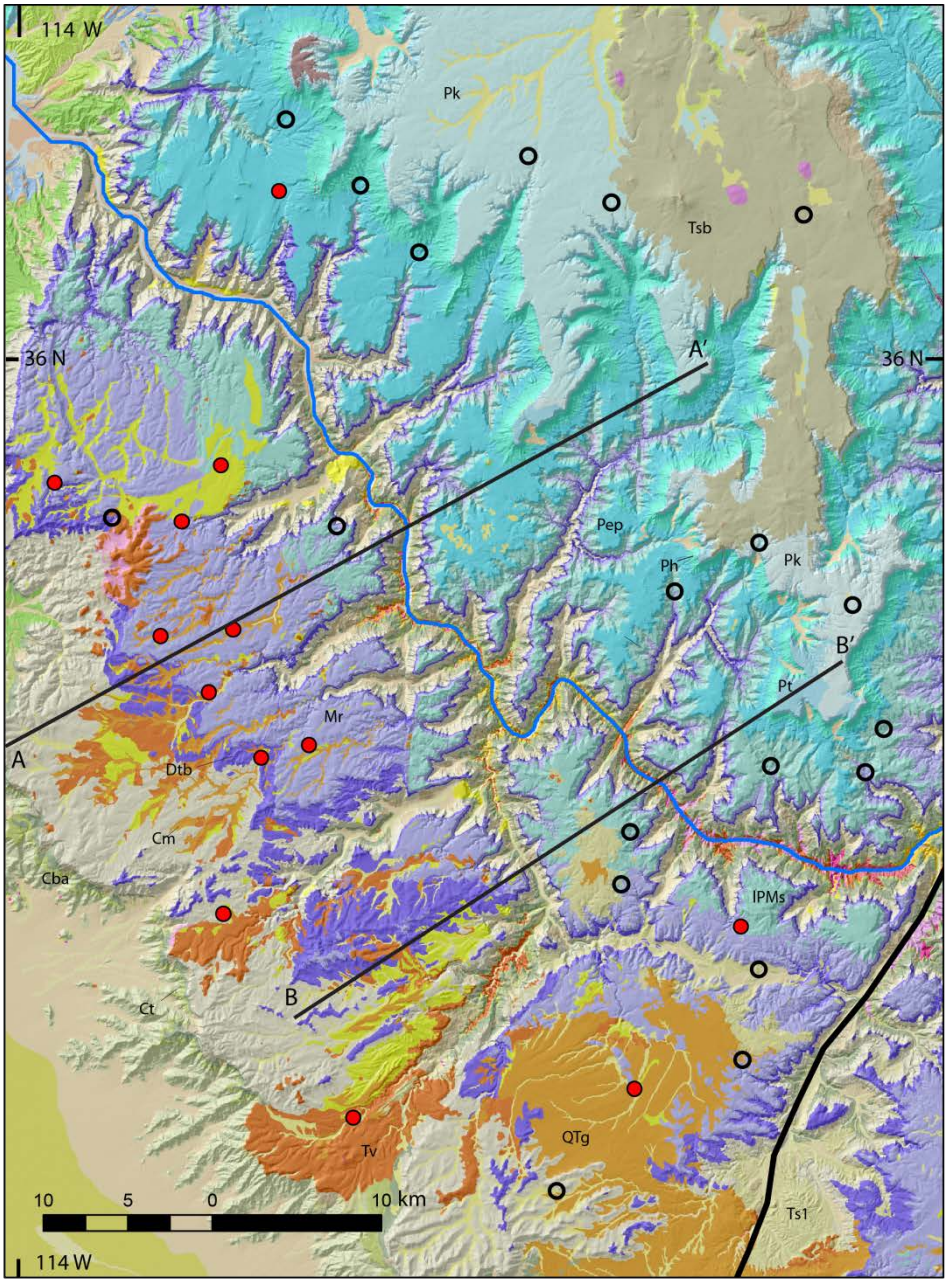

Figure 2.7. Geologic map of Hualapai Plateau and surrounding area. Cross-section lines for Fig. 2.8 shown. Map units: (Ct – Tapeats Fm, Cba – Bright Angel Fm, Cm – Muav Fm, Dtb – Temple Butte Fm, Mr – Redwall Ls, IPMs – lower Supai group, Pep – Esplanade Ss, Ph – Hermit Fm, Pt – Toroweap Fm, Pc – Coconino Fm, Pk – Kaibab Fm, Ts1 – tertiary sediments, i.e. Music Mountain Fm., Buck and Doe Cong., Tsb – Tertiary basalt, QTg – Quaternary/Tertiary local gravel).

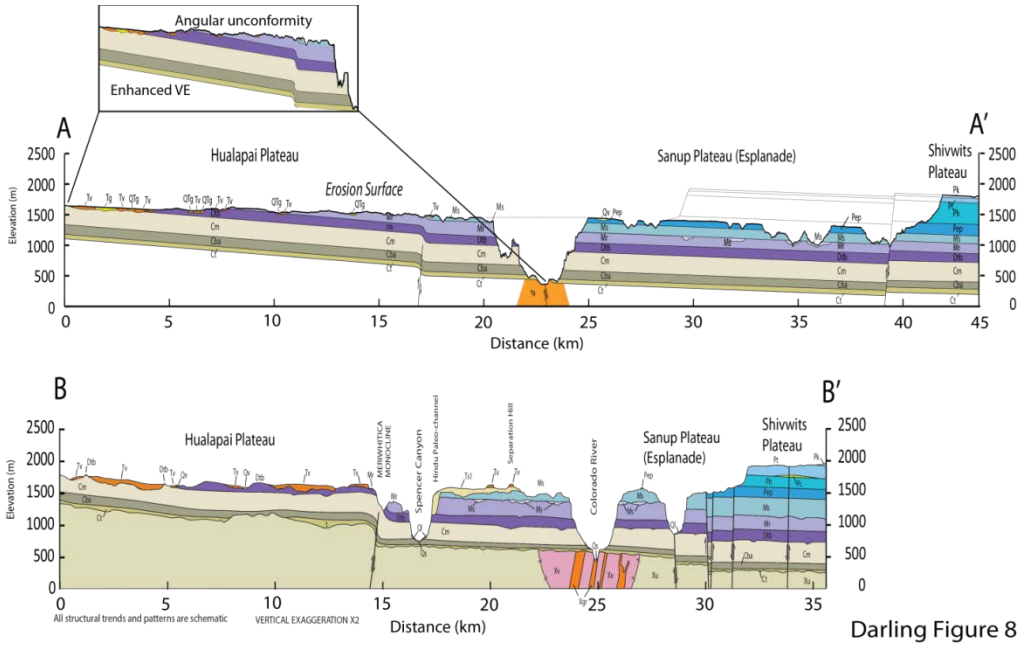

Figure 2.8. Geologic cross-section is modified from section B-B' in Billingsley et al. (2006) USGS SIM 2900 map, used and modified by permission. Modifications relate to projecting nearby outcrops of late Tertiary sediments and volcanics into the section and illustrating the location, incision depth, and depth of fill associated with the Hindu paleo channel. Red dots are knickpoints as in Figs. 2.1 and 2.9. (Ct – Tapeats Fm, Cba – Bright Angel Fm, Cm – Muav Fm, Dtb – Temple Butte Fm, Mr – Redwall Ls, IPMs – lower Supai group, Pep – Esplanade Ss, Ph – Hermit Fm, Pt – Toroweap Fm, Pc – Coconino Fm, Pk – Kaibab Fm, Ts1 – tertiary sediments, i.e. Music Mountain Fm., Buck and Doe Cong., Tsb – Tertiary basalt, QTg – Quaternary/Tertiary local gravel).

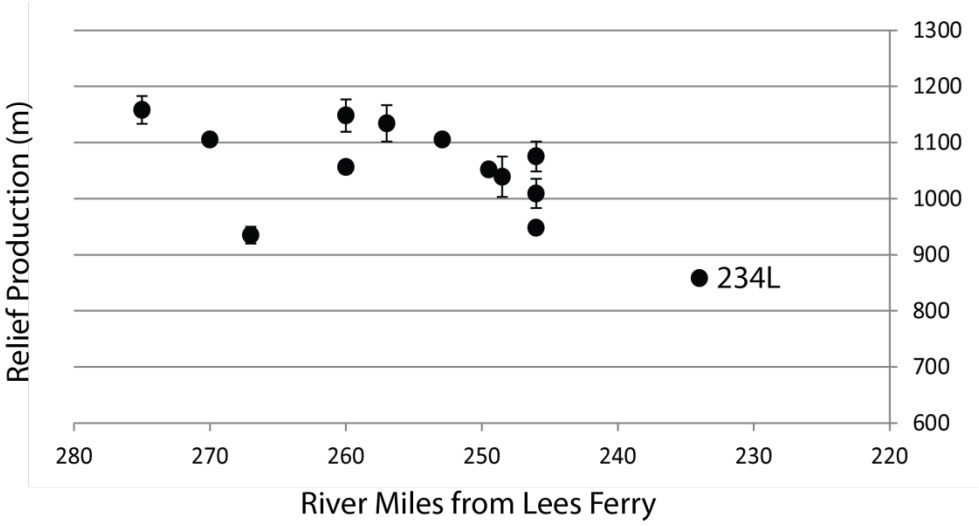

Figure 2.9. Reconstruction of the height of the pre-incision surface above the Colorado River from downstream projections of relict channel profiles upstream of abrupt slope-break knickpoints that surround WGC, following the method illustrated in Fig. 2.5 and showing uncertainties associated with characterization of upstream channel form (concavity and steepness indices). Outliers are discussed in the text.

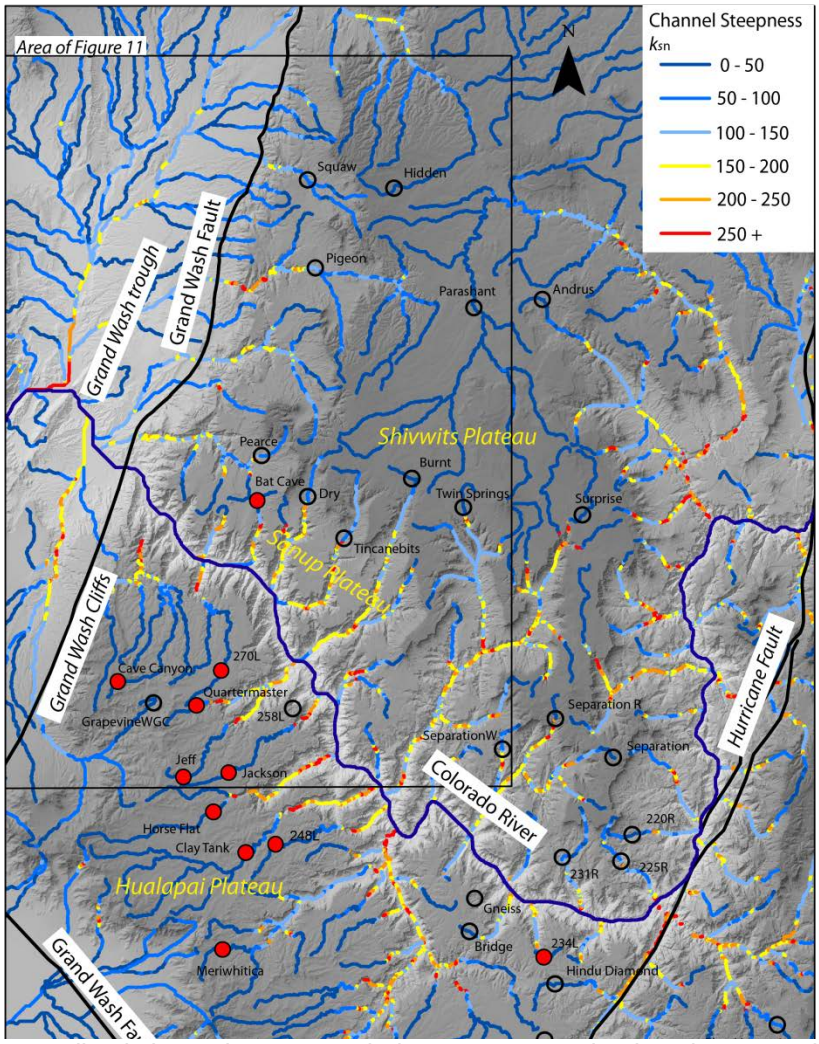

Figure 2.10. Normalized channel steepness index over greyscale elevation map with hillshading. Profile projection anchor points marked as red dots. Major slope-break knickpoints (defined as largest visual topographic expression) on tributary rivers indicated by cool to warm color transitions in channel steepness data. Tributaries to WGC show similar mean channel steepness indices and exhibit the profile geometries illustrated in Figs. 2.4 and 2.5. Streams draining the Grand Wash Cliffs show more subdued knickpoints and generally lower channel steepness, but with a tendency to towards increased ksn in their lower reaches

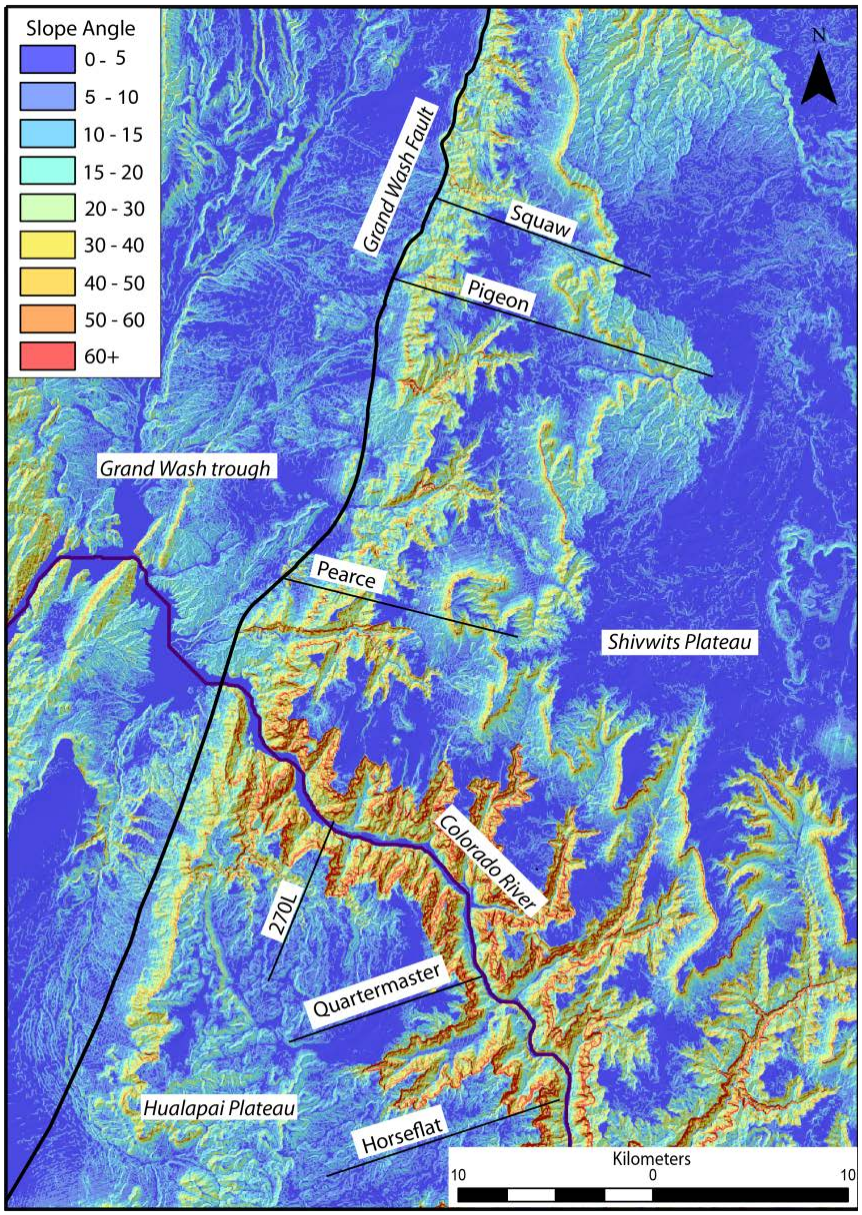

Figure 2.11. Slope map of WGC and GWC areas (30m resolution, location shown on Fig. 2.1). Although incised through the same rocks and experiencing the same climate, the topographic expression of the GWCs and associated tributary canyons and side slopes is far more subdued than that of the WGC, indicating either notably slower erosion rates, a longer period of topographic relaxation since relief production (known to date to 18-12 Ma for the GWC), or both.

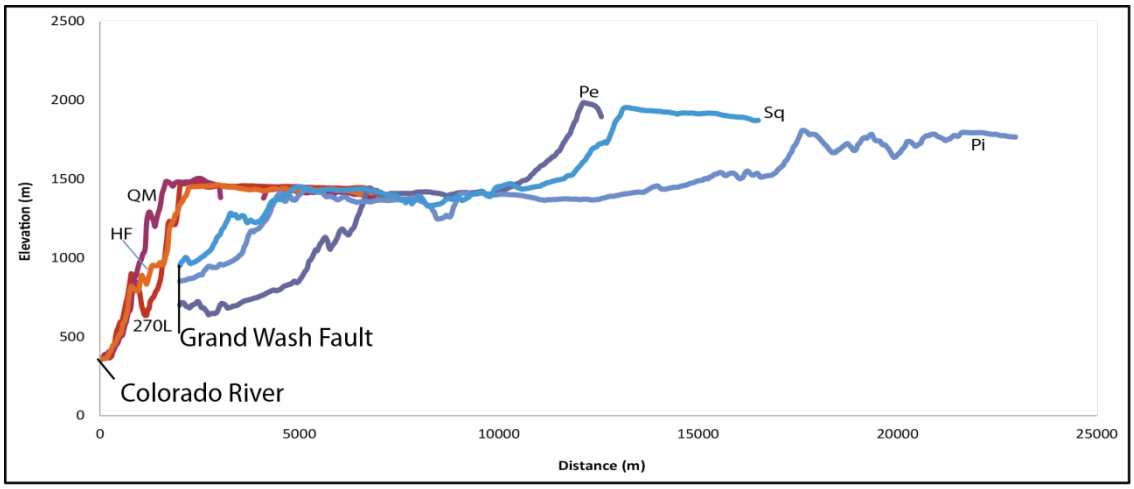

Figure 2.12. Comparative inter-fluvial topographic profiles in WGC and along the GWC. Topographic section line locations are shown in figures 2.1 and 2.10. Profiles in the WGC are shown in reds and oranges and those along the GWC in blues. Profiles are represented at actual elevations, but only shown above the COR in WGC or above the GWF along the GWC. Interfluves in the WGC show no indication of significant retreat or relaxation from threshold slopes since canyon formation. Interfluves along the GWC document both significant retreat and significant relaxation since relief production associated with normal faulting along the GWF. Profiles named after nearby canyons: QM – Quartermaster, HF – Horse Flat, Pe -Pearce Canyon, Sq – Squaw, Pi Pigeon Canyon

Tables

Table 2.1. Summary of Topographic Analysis of western Grand Canyon Tributary Streams

TABLE 1. SUMMARY OF TOPOGRAPHIC ANALYSIS OF WESTERN GRAND CANYON TRIBUTARY STREAMS

Stream name	Related to Hualapai Plateau surface?	Projection represents	Rim	RM	k_s	θ	k_{sn} ($\theta = 0.45$)
220R	no	High concavity/k_s	North	220	560.0	0.73	27.1
225R	no	High concavity/k_s	North	225	236.0	0.53	90.9
231R	no	High concavity/k_s	North	231	58000000.0	1.4	95.2
234L	yes	Esplanade, Hualapai Plateau	South	234	56.0	0.53	15.8
248L	yes	Esplanade, Hualapai Plateau	South	248.5	14.2	0.45	11.9
258L	yes	Insufficient S-A data	South	258			
270L	yes	Esplanade, Hualapai Plateau	South	270	7.0	0.42	10.3
Andrus	no	Shivwits	North	199	59.5	0.54	12.5
Bat Cave	no	Esplanade, Hualapai Plateau	North	267	26.2	0.47	17.2
Blue Mountain	no	High k_{sn}	South	226	10.4	0.35	53.9
Bridge	yes	Insufficient S-A data	South	235			
Burnt	no	Shivwits	North	260	7.5	0.43	7.7
Cave	yes	Esplanade, Hualapai Plateau	South	275	17.1	0.46	12.4
Clay Tank	yes	Esplanade, Hualapai Plateau	South	250	5.6	0.36	17.4
Dry	no	High concavity/k_s	North	265	514.0	0.56	81.3
Gneiss	yes	Insufficient S-A data	South	236			
Grapevine WGC	no	Insufficient S-A data	South	281			
Hidden	no	Shivwits, GWT	North	286	3.6	0.34	15.7
Hindu Diamond	yes	Poor S-A relationship	South	226			
Horse Flat	yes	Esplanade, Hualapai Plateau	South	253	45.0	0.49	25.7
Jackson	yes	Esplanade, Hualapai Plateau	South	257	3.0	0.36	9.6
Jeff	yes	Esplanade, Hualapai Plateau	South	260	16.3	0.47	8.4
Meriwhitica	yes	Esplanade, Hualapai Plateau	South	246	2.2	0.32	11.0
Milkweed Spencer	yes	Esplanade, Hualapai Plateau	South	246	12.9	0.40	24.1
Parashant	no	Shivwits	North	199	2.1	0.36	10.3
Peach Springs	yes	Poor S-A relationship	South	226			
Peach SpringsL	yes	Insufficient S-A data	South	226			
Pearce	no	GWT	North	281	1820.0	0.68	59.6
Pigeon	no	GWT	North	286	98100.0	0.96	94.3
Quartermaster	yes	Esplanade, Hualapai Plateau	South	260	119.0	0.57	20.9
Separation	no	Insufficient S-A data	North	240			
Separation W	no	High concavity/k_s	North	240	12200.0	1.10	63.3
Separation R	no	Shivwits	North	240	14.1	0.38	6.2
Spencer	yes	Esplanade, Hualapai Plateau	South	246	31.5	0.50	11.6
Squaw	no	GWT	North	286	274.0	0.55	55.8
Surprise	no	Shivwits	North	249	161.0	0.65	10.0
Tincanebits	no	High concavity/k_s	North	264	3220.0	0.80	106.0
Twin Springs–Surprise	no	Insufficient S-A data	North	249			

Note: WGC—Western Grand Canyon; GWT—Grand Wash trough; Esplanade—Esplanade surface; Shivwits—Shivwits Plateau surface; S-A—slope-area; RM—river mile; k_s—channel steepness index; k_{sn}—normalized channel steepness index; Θ—concavity index; L—left; R—right; W—west.

Table 2.2. Summary of Tributary Projections, Western Grand Canyon

TABLE 2. SUMMARY OF TRIBUTARY PROJECTIONS, WESTERN GRAND CANYON

Stream name	Rim	Anchor Elevation (m above sea level)	Easting	Northing	Analyzed Θ_{ref} 0.5 k_{sn} ($m^{0.5}$)	(±)	0.45 k_{sn} ($m^{0.5}$)	(±)	0.4 k_{sn} ($m^{0.5}$)	(±)	Projected Θ_{ref}	Projected elevation (m above sea level)	Maximum	Minimum	Relief production Projection height (m)	Maximum	Minimum	(±)	Incision magnitude using assumed rate 6 m/m.y.: 19 Ma	6 m/m.y.: 6 Ma	114	36
Milkweed Spencer	South	1494	251939	3944233	48.6	1.9	24.1	0.7	11.40	0.30	0.45	1295	1262	1254	948	954	942	9	1062	984		
Spencer	South	1443	268587	3945967	27.8	3.8	11.6	1.5	5.11	0.94	0.40	1356	1374	1340	1009	1027	993	26	1123	1045		
248L	South	1500	249329	3966343	24.7	2.2	11.5	0.5	5.99	0.26	0.40	1374	1378	1370	1031	1035	1027	6	1145	1067		
Quartermaster	South	1512	241767	3979567	38.4	1.1	20.9	1.1	10.10	0.84	0.45	1369	1377	1362	1056	1063	1048	11	1170	1092		
Clay Tank	South	1496	246477	3965557	44.4	1.7	17.4	1.0	8.47	0.42	0.40	1391	1396	1386	1050	1054	1045	7	1164	1086		
Meriwhitica	South	1551	244229	3956323	27.3	2.2	11.0	1.6	5.90	1.20	0.40	1423	1093	1059	1075	1093	1058	27	1189	1111		
Horse Flat	South	1531	243387	3969457	52.3	1.1	25.7	0.3	11.00	0.95	0.50	1432	1437	1428	1105	1110	1101	7	1219	1141		
270L	South	1481	244109	3982903	20.3	1.3	10.3	0.4	5.01	1.12	0.45	1397	1401	1394	1105	1109	1102	6	1219	1141		
Jackson	South	1539	244827	3973147	18.7	1.9	9.6	0.7	3.94	3.68	0.40	1453	1473	1429	1134	1155	1111	33	1248	1170		
Cave Canyon	South	1612	234267	3981877	23.8	2.7	12.4	1.2	5.77	2.83	0.45	1441	1457	1425	1158	1175	1142	25	1272	1194		
Jeff	South	1605	240537	3972787	14.3	2.8	8.4	1.3	6.00	1.25	0.40	1462	1481	1442	1148	1167	1128	29	1262	1184		
234L	South	1351	274889	3955573	31.1	2.4	15.8	0.9	7.99	1.61	0.45	1245	1251	1239	858	864	852	9	972	894		
Bat Cave	North	1350	247559	3999133	33.0	2.4	17.2	1.3	8.94	0.73	0.45	1236	1245	1227	935	944	923	15	1049	971		

Note: k_{sn}—normalized channel steepness index; Θ_{ref}—reference concavity; 0.5, 0.45, and 0.4 are concavity indexes.

Table 2.3. Erosion Rates Summary for the Hualapai Plateau Surface

TABLE 3. EROSION RATES SUMMARY FOR THE HUALAPAI PLATEAU SURFACE

Sample	Location or unit	Age (Ma)	E1*	E2*	H1† (m)	H2† (m)	Erosion rate (m/m.y.)	Minimum or maximum rate	Latitude	Longitude	Publication	Comment
14-B86	Grapevine Canyon	15.3	1640	1495	145		9.48	maximum	35.9147	113.9000	Wenrich et al. (1995)	Height above west side of hill
UAKA 88-51	Grapevine Canyon near Buck and Doe Road	15.25	1655	1551	104		6.82		35.9150	113.8908	Wenrich et al. (1995)	Height above east side of hill
8-B86	Separation Hill basalt	19	1495	1400	95		5.00		35.7867	113.5972	Wenrich et al. (1995)	Height above surrounding plateau
12-B86	Grand Pipe Neck basalt	17.4	1420	1350	70		4.02		36.1133	113.8860	Wenrich et al. (1995)	Neck is inset into a valley
PED 27 -63	Peach Spring Tuff, Upper Milkweed Canyon	18.3	1536	1340	196		10.71	maximum	35.6366	113.7034	Young and Brennan (1974)	
PED 27 -63	Plain Tank Flat	18.3	1430	1390	40		2.19		35.6697	113.5680	Young and Brennan (1974)	
14-B86	Grapevine Canyon	15.3	1640	1600		40	2.61	minimum	35.9147	113.9000	Wenrich et al. (1995)	Height above south side of hill
UAKA 88-51	Grapevine Canyon near Buck and Doe Road	15.25	1655	1600		55	3.61		35.9150	113.8908	Wenrich et al. (1995)	Height above north side of hill
8-B86	Separation Hill basalt	19	1495	1440		55	2.89		35.7867	113.5972	Wenrich et al. (1995)	Height above surrounding plateau

Note: NAD83 (North American Datum of 1983) points mark area of incision points, in the area of original sample locations. Dating method for all samples was K/Ar.
*E1—Sample or deposit elevation; E2—Landscape elevation (channel or interfluve).
†H1—Height above nearest stream (above any major knickpoints). H2—Height above nearest interfluve.

CHAPTER 3 EFFECTS OF STRATIGRAPHIC VARIATION IN ROCK STRENGTH ON EROSION RATE PATTERNS: LANDSCAPE EVOLUTION IN THE GRAND CANYON AND GRAND STAIRCASE

Andy Darling, Kelin Whipple, Brian Clarke, Adam Forte, Paul Bierman

Abstract

Rock strength variation is known to affect the topographic expression of erosion. On the Colorado Plateau, canyons incised by the Colorado River system often encounter stronger rocks at greater depths, potentially complicating interpretation of base level history normally studied in landscapes with more uniform rock strength. Using numerical models to predict erosion rate patterns, we determine the diagnostic differences in erosion rate between scenarios of weak-over-strong rock with steady base level and with increased base level fall. As the river encounters the strong underlying layer, knickpoints are produced that move upstream as a kinematic wave that moves (horizontally) more slowly than the kinematic wave of erosion in the headwaters. This produces erosion rates in the canyon that depend on the canyon base level fall rate and headwaters that are still responding to boundary conditions imposed before the rock strength contrast or base level rate increase occurred, preserving a relict landscape. In the opposite scenario, strong-over-weak rock yields localized high erosion rates along the contact caused by competing long profile adjustment to different erosional efficiencies, leading to erosion of the weak rock that undermines the strong rock and produces locally high erosion rates. Incision and cosmogenic erosion rates in the Grand Canyon (~150 m/Ma) are higher than incision rates in the Grand Staircase (~75 m/Ma). Cosmogenic erosion rates in the Grand Staircase, on the other hand, are higher than either (200+ m/Ma) and are likely the combined effect of enhanced real erosion by undermining of strong rock by the erosion of underlying weak rock and enhanced ^{10}Be erosion rate attributable to localized quartz sourcing from the rapidly eroding cliffs. Further, erosion rates determined in simulated scenarios like the Grand Canyon typically do not deviate from base level fall significantly when several rock layers are supplying the sampled stream. The Grand Canyon and Grand Staircase are therefore interpreted as co-evolved landscapes that

result from an increase in base level fall rate in the last few million years that is acting on strata of varied rock strength, providing complex but predictable erosion rate patterns and cosmogenic inventories.

Introduction and Motivation

Recent studies in canyons on the Colorado Plateau have raised important questions about the incision history of the Colorado River and its tributaries; an abundance of new data has driven conflicting interpretations about temporal evolution of topography (Wolkowinsky and Granger, 2004; Flowers et al., 2008; Polyak et al., 2008; Cook et al., 2009; Darling et al., 2012; Flowers and Farley, 2012; Karlstrom et al., 2012; Marchetti et al., 2012; Pederson and Tressler, 2012; Donahue et al., 2013; Pederson et al., 2013a; Pederson et al., 2013b; Aslan et al., 2014; Crow et al., 2014; Karlstrom et al., 2014; Bursztyn et al., 2015; Crossey et al., 2015; Darling and Whipple, 2015). The Colorado River system drains the western slope of the Rocky Mountains and has removed on the order of 300,000 km^3 of rock (Dorsey, 2010) since its integration beginning in the Miocene (Figure 3.1). Evolving hypotheses about the river system's development over the last 11 million years (Aslan et al., 2010) address evolution of the Colorado River System into a well-connected and highly erosive river system deeply incised into predominantly flat-lying sedimentary strata. Incision history is interpreted directly and indirectly via geochronometers (e.g. Darling et al., 2012; Crow et al., 2014) and thermochronometers (e.g. Flowers and Farley, 2012; Karlstrom et al., 2014). Despite the abundance of new data from a decade of intense study, no consensus has emerged for key questions about the antiquity of the topographic features like Grand Canyon (Polyak et al., 2008; Flowers and Farley, 2012; Karlstrom et al., 2014; Darling and Whipple, 2015) and the relative importance of tectonic uplift and isostatic rebound (Roy et al., 2004; Roy et al., 2009; Darling et al., 2012; Karlstrom et al., 2012; Pederson et al., 2013b; Crow et al., 2014). A critical unanswered question that complicates interpretations is how strongly the variation in rock strength exposed along the Colorado River and its tributaries has influenced the spatio-temporal patterns of river incision, the resulting landforms, and our ability to accurately

determine river incision history (Grams and Schmidt, 1999; Pederson and Tressler, 2012; Pederson et al., 2013b; Bursztyn et al., 2015; Darling and Whipple, 2015).

Landscape evolution reflects the competition between the uplift of rock relative to base level and climatically and lithologically mediated erosion that is expressed in fluvial networks (Ahnert, 1970; Whipple et al., 1999a; Kirby and Whipple, 2012). Where rock strength does not vary significantly in a study area, a record of tectonic or climatic conditions can be extracted from topography (e.g. Whittaker et al., 2007; DiBiase et al., 2010; Rossi, 2014; Rossi et al., In Review). In most landscapes, however, the erodibility of bedrock varies both spatially and temporally as patterns and depths of rock exposure evolve. On the Colorado Plateau, relatively simple stratigraphy produces significant variation in erosion process in the landscape as cliffs form and scarps retreat, contributing to spatial variation in erosion rate and topographic form (Koons, 1955; Ward et al., 2011). The pace and pattern of erosion in variable rock type is key to understanding how base level history, climate, and tectonics are recorded in landscapes that do not host uniform rock types. This study analyzes how changes in rock strength affect erosion rate patterns and how erosion rate patterns impact techniques for determining erosion rates from detrital cosmogenic nuclides and incision rates from dated surficial markers like river terraces. Exploring relationships among rock strength, topography, and erosion rates yields implications for base level fall history of the Colorado River related to the topographic characteristics of several national parks and monuments.

Approach

In order to develop an understanding of the history of base level on the Colorado Plateau, evaluation of the effects of rock strength patterns on topography is needed (Dietrich and Smith, 1983; Grams and Schmidt, 1999; Roberson and Pederson, 2001; Pederson and Tressler, 2012; Bursztyn et al., 2015). Numerical simulation of erosion through horizontally bedded strata with contrasts in rock strength produces significant variation in topography and erosion rate as erosion progresses (Forte et al., 2016). To improve understanding of the incision and erosion rate patterns of the Colorado River System we compare new and existing erosion-rate data to the

theoretical framework surrounding landscape evolution (e.g. Whipple and Tucker, 1999; Whipple, 2001a; Tucker and Whipple, 2002) with explicit discussion of rock strength in flat-lying stratigraphy and its effect on erosion rate patterns (cf. Darling and Whipple, 2015; Forte et al., 2016). This study builds on key research incorporating rock strength into fluvial incision studies in other landscapes (Stock and Montgomery, 1999; Duvall et al., 2004; Korup and Schlunegger, 2009) by advancing landcape evolution simulations and empirical measures of rock strength using seismic methods (e.g. Clarke and Burbank, 2010, 2011). This research attempts to answer the question: what effects does variation in lithologic strength have on erosion rate patterns in landscape evolution? Theoretical and empirical development from the Grand Staircase (GSc) of southern Utah and Grand Canyon (GC) in Arizona will allow better interpretation of the effects of lithologic strength on erosion patterns, further yielding when and how canyons have formed in the Colorado Plateau and provide a helpful framework for landscapes with similar substrate patterns.

The stratigraphy of the GSc and the GC can be simplified to a weak rock package over a strong rock package (discussed in detail below). Each of these two generalized rock packages, however, contains significant variation in rock strength among individual stratigraphic units. For instance, the stepped pattern of the GSc represents the interaction between weak and strong layers, where the stronger layer forms a cliff and the weaker layer forms a broad slope. It is worth noting that the topographic expression of alternating strong and weak rock units is much more strongly developed in the GSc with very wide topographic benches separated by short, steep cliff bands, than in the GC, suggesting that erosion rate patterns may likewise be more exaggerate in the GSc. To evaluate erosion patterns (topography and rate) and their relationship to base level fall rates and rock strength variation, we develop predictions from one-dimensional numerical simulations that show river longitudinal profiles through two-layer stacks of rock (Figure 3.2 and 3.3). Each scenario produces knickpoints in the channel, but the erosion rate patterns are diagnostically different. In panel 2a weak rock overlies strong rock and base level fall is constant (3.2a) or increases shortly before exposure of the stronger rock (3.2b; (cf. Darling and Whipple, 2015). Diagnostic differences in erosion rate are produced, allowing distinction between canyons that form purely as a result of lithologic strength contrast (3.2c) or as a result of increased base

level fall rate with a strength contrast (Darling and Whipple, 2015). In Figure 3.3, constant base level fall rate is imposed and the incising base level drives erosion into the strong rock, the channel steepens and produces an upstream-migrating kinematic wave (Rosenbloom and Anderson, 1994; Whipple and Tucker, 1999). Local erosion rate is reduced at the top of the strong rock as the profile above the knickpoint continues eroding, eventually producing a flat, low-erosion-rate bench (pink curve). The kinematic wave of erosion through the upper, weaker rock is faster than that through the lower, harder rock. The erosion waves separate, creating a bench where erosion rate is low. This is often referred to as “stripping off” the weak, overlying rock. In panel 3.3b, strong rock above a weaker rock unit also produces two competing channel geometries. The shallow gradient stream in the weak rock produces a kinematic wave of erosion that migrates upstream faster than the horizontal kinematic wave of the upper section, the opposite pattern seen in 3.2. This wave-speed difference inherently undermines the upper, stronger, rock layer. This produces an upstream-migrating knickpoint that is only due to the change in rock strength: an autogenic response. Further, the erosion rate within the zone of knickpoint retreat is systematically much higher than base level fall rates. For discussions in this paper, note that the relevant implications of the model can be expressed at a variety of scales: the same patterns should result from the interactions of erosion on two different rock beds that are a few tens of meters thick to units (or unit packages) that are kilometers thick.

We address three aspects of the influence of rock strength on erosion: (1) empirical confirmation of these simulated patterns requires techniques that can determine long-term base level fall rates as well as the spatial distribution of erosion rates; (2) inference of relative rock strength from seismic surveys of outcrops throughout the stratigraphic column is needed to justify simulated stratigraphy and inferences about erosion patterns; and (3) for erosion rates determined by detrital samples of in-situ cosmogenic radionuclides (CRNs), the relative contribution of quartz derived from weak and hard layers within the watershed plays a crucial role, especially if they bias erosion rate estimates toward the erosion rate of the cliffs. The variation of quartz concentration in bedrock stratigraphy of the Colorado Plateau is large and complex, requiring detailed exploration and simulations of relative sources of quartz input to sediment

samples that are derived from particular sequences of rock units. Where quartz is uniformly distributed in a landscape, erosion rates calculated from ^{10}Be concentrations in sediment represent spatially averaged erosion rates (Bierman and Steig, 1996; Granger et al., 1996). For complex erosion rate patterns (e.g. Figures 3.2 and 3.3), the presence of non-uniform distributions of quartz present a more complicated meaning for the measured concentrations of CRNs in sediment that are modeled here using a combination of Channel-Hillslope Integrated Landscape Development (CHILD) and Cosmic-Ray-Produced Nuclide Systematics (CRONUS) production rate numerical simulations (Tucker et al., 2001; Balco et al., 2008).

This paper examines the interaction among rate of base-level fall, CRN-derived erosion rate, and rock strength, in the context of landscape evolution of the Colorado Plateau. The data sets are intended to help answer five driving questions, listed with increasing scope:

(1) What is the erosion rate of catchments within the GSc and how does it relate to the rate of base level fall?

(2) What effect does the stratigraphic variation in rock strength have on erosion rates in the GC and GSc?

(3) What is the relationship between the rate of erosion of the GC and that of the GSc?

(4) What is the effect of stratigraphic variation in rock strength and quartz yield on measurements of ^{10}Be concentrations in fluvial sediment?

(5) What expectations about variation in rock type can be applied to erosion-rate patterns in the Colorado Plateau and other landscapes with similar structure and stratigraphy?

Study Area

Two physiographic regions are the focus of this study: the GSc and GC (Figure 3.4). Black Mesa, in northern Arizona, is also considered as an analogous landscape to the GSc, eroding upland Mesozoic rocks with the Little Colorado River as the local base level (Figs 3.1 and 3.3). Erosion rates on the Colorado Plateau have been suggested to represent transient incision due to increased incision rates of the Colorado River (Cook et al., 2009; Darling et al., 2012; Darling and Whipple, 2015), or isostatic rebound of the crust by erosional unloading (Pederson et

al., 2002b; Roy et al., 2004; Lazear et al., 2013); and may reflect modifications due to mantle dynamics (Roy et al., 2009; Crow et al., 2014).

The GSc is aptly named for its display of rows of cliffs supported by relatively strong bands of rocks mixed with packages of weak predominantly shale units (Figures 3.5 and 3.6). The Cenozoic and Mesozoic cliff bands tend to be developed in fluvial or eolian sandstone-rich units, which sometimes contain higher quartz concentrations than weaker shale units. Sporadic Paleogene volcanic activity across the landscape has emplaced lava flows that serve as incision rate markers.

Relief of the GSc landscape is characterized by gentler slopes and lower overall relief than that of the GC (Figure 3.1). The GC displays a suite of variably weak and strong strata but most are generally stronger than strata in the GSc (e.g. Pederson and Tressler, 2012; Bursztyn et al., 2015). Erosion of the GC has been documented using incision-rate and thermochronometric studies (Pederson et al., 2002a; Karlstrom et al., 2007; Polyak et al., 2008; Darling et al., 2012; Flowers and Farley, 2012; Crow et al., 2014; Karlstrom et al., 2014), most of which agree that the majority of incision began 5 to 6 million years ago. The Paleozoic and Proterozoic rock layers of the GC are composed of shales, sandstones, and limestone that are each relatively thin compared to the depth of the canyon (Figures 3.7 and 3.8).

The Colorado Plateau also provides an interesting setting for studies of landscape evolution with renewed debate over the timing and nature of incision of the GC. De-convolving the effects of rock strength on erosion rates helps to clarify the relationships between incision rate of the main-stem Colorado River and will illuminate aspects of the evolutionary progression of the Grand Canyon and its many tributaries.

Methods

Numerical Modeling

We use the CHILD model (Tucker et al., 2001) for quantitative analysis of erosion rate patterns instigated by rock strength variability. In order to implement the CHILD code with variable rock strength for more than two layers, modifications were made to the code, which we

refer to as LithoCHILD (c.f. Forte et al., 2016). The erosion-rate patterns determined from these simulations are used to guide interpretation of spatial patterns of erosion rates in our study areas.

Two 2-dimensional simulations are presented here. First, a simple strong-over-weak scenario is modeled to explore the spatial distribution of erosion rates like figure 3.3 (Figure 3.9 and 3.10). This simple strong-over-weak pattern is similar to that of the highest step of the GSc, where limestone and sandy-silty and local conglomerate beds of the Eocene Claron Formation overly more erodible Cretaceous sandstone and shale units (Figure 3.4, Weimer, 1960; Anderson and Rowley, 1975). The second model simulation groups several relatively thin units (Figure 3.11 and 3.12) to determine relative input of eroded sediment from a catchment that has several weak and several strong units that represent the Paleozoic rocks of the GC.

In addition, MATLAB code developed for CRONUS (Balco et al., 2008) was modified to calculate synthetic ^{10}Be catchment averaged erosion rates directly from CHILD topographic output data using assumed metrics for comparison within model simulations. The simulations are not meant to represent the field areas precisely; rather, they are used to develop quantitative expectations of relationships between erosion rate and rock strength as landscapes erode.

Topographic Analysis

We analyze river profiles in relation to lithology to reach the goals of this study. United States Geological Survey (USGS) 30-m resolution digital elevation models (DEMs) are used for the analyses. River profiles can provide insight into base-level fall history of a river system and can also reveal the relative importance of controls such as rock strength, tectonic uplift and climate (Hack, 1957; Wobus et al., 2006; Kirby and Whipple, 2012; Whittaker, 2012; Lague, 2014).

Flint's Law is an empirical relation between local river gradient (S) and upstream contributing drainage area (A) that reflects the tendency of a river to develop smooth concave-up profiles (Hack, 1957; Flint, 1974):

$$S = k_s A^{-\theta}. \quad (1)$$

In this relation, k_s is the channel steepness index, and θ is the concavity index (ranging from 0.4 and 0.6; Tucker and Whipple, 2002). In order to compare streams with different drainage areas, it is necessary to assume a reference concavity (θ_{ref}), usually 0.45, and use the integral method to calculate a channel steepness index from the integration of cumulative drainage area (Harkins et al., 2007). The variable k_{sn}, relates to slope and area such that:

$$S = k_{sn} A^{-\theta_{ref}}, \quad (2)$$

Maps and single profile regressions of channel steepness index (k_{sn}) can be made from DEMs using the Profiler Toolbar in ArcMap and MATLAB (www.geomorphtools.org) or in-house Matlab scripts to harness functionality in TopoToolbox MATLAB (Schwanghart and Scherler, 2014). For a given catchment, the normalized channel steepness index, k_{sn}, can be calculated for all segments of all streams over a user-specified stream length (usually 0.5 – 2 km).

In landscape evolution theory, topography is a direct result of erosional processes driven by climate and tectonics and modulated by rock strength (Whipple and Tucker, 1999). Our numerical simulations are based on the well-known stream power river incision model:

$$E = KA^m S^n, \quad (3)$$

where *A* is contributing area, *S* is channel gradient, *m* and *n* are exponents related to erosion process, and the proportionality constant, *K, is referred to as* erosional efficiency. In addition, we follow recent studies that have explored the relationship between topography and erosion rate using channel steepness with a power function (Lague et al., 2005; DiBiase and Whipple, 2011), such that:

$$k_{sn} = K' E^a, \quad (4)$$

where the exponent *a, (0<a<1)*, is set by runoff variability and *K'* is erosional efficiency of the landscape, set by climate and rock properties. Note that K and K' are not the same variable.

Incision Rate Determination

The base-level fall rate of a river averaged over time is determined by dividing the height of a fluvial deposit by a numerical estimate of age to determine an incision rate (e.g. Wolkowinsky and Granger, 2004; Pederson et al., 2006; Karlstrom et al., 2007; Darling et al., 2012). For this

study, incision rate is determined from basalt flows that cap river deposits elevated above the modern East Fork of the Virgin River. Two basalt samples astride the Sevier Fault were obtained for $^{40}Ar/^{39}Ar$ dating by Schiefelbein (2002), an additional previously dated flow ($^{40}Ar/^{39}Ar$) north of Grand Staircase (Biek et al., 2012). Several independent studies constrain incision rates in the Grand Canyon (Karlstrom et al., 2007; Karlstrom et al., 2008; Crow et al., 2014). Field surveys using a laser range-finder were conducted to measure the height of the base of the basalt flows and the height of the base of underlying fluvial gravel, both of which were measured relative to the modern stream channel (Table 3.1). From prior research, long term (10^5-10^6 year) records of relative base level fall on the Colorado Plateau were obtained from numerous incision rate studies (e.g. Repka et al., 1997; Pederson et al., 2002a; Schiefelbein, 2002; Wolkowinsky and Granger, 2004; Pederson et al., 2006; Karlstrom et al., 2007; Darling et al., 2012; Karlstrom et al., 2012; Marchetti et al., 2012; Pederson et al., 2013a; Crow et al., 2014; Nelson and Rittenour, 2014).

Erosion Rates from Cosmogenic Isotopes

Concentrations of cosmogenically produced ^{10}Be are routinely measured to determine basin-averaged erosion rates from analysis of modern stream sediment (Bierman and Steig, 1996; Granger et al., 1996; DiBiase et al., 2010; Portenga and Bierman, 2011; Granger et al., 2013; Willenbring et al., 2013). Physical separation of detrital cosmogenic erosion rate samples took place at Arizona State University Wombat Laboratory, and chemical analysis of detrital samples was carried out at the University of Vermont Cosmogenic Nuclide Laboratory using optimized methods described by Corbett et al. (2016). Targets were processed at SUERC and PRIME labs. Grain sizes from 0.5 to 1.0 mm were extracted to avoid likely Quaternary-age eolian grain (which is usually <0.5mm) inclusion before further sample processing. Most samples yielded small fractions of viable quartz, requiring sample volumes of two or three one-gallon containers in order to yield approximately 20-100 grams of clean quartz for dissolution.

The erosion rate is inversely proportional to measured concentration of ^{10}Be in the sediment. We calculate erosion rates using standard values for production rates in the on-line tool

CRONUS (Balco et al., 2008). Traditionally studies of ^{10}Be have focused on simple catchments that have relatively little chance of landslide (Niemi et al., 2005), uniform quartz distribution, and uniform erosion rate inferred from topography within a catchment. Quantification of non-uniform quartz concentration in calculations has yielded differences that are equal to or less than the analytical uncertainty (~10%, e.g. Safran et al., 2005), and we use this observation compared with synthetic ^{10}Be inventories to discuss reliability of catchment average erosion rate calculations (see the Discussion and Numerical Modeling Methods sections below). It is important to note that if the quartz distribution is not uniform, then the erosion rate of the dominant quartz source will bias the CRN rate and it will differ from the actual mean erosion rate. Extensive discussion of this problem, our simulations, and field evidence together provide a framework for working in environments where typical production rate assumptions are not ideal.

Seismic Velocity Measurements

Analysis of the landscape evolution simulations and empirical erosion rate data requires constraints on proxies for relative rock strength in the GSc and GC. Here we utilize seismic refraction surveys to measure P-wave velocities (V_p) through bedrock as a proxy for rock-mass strength and erodibility (Suzuki, 1982; Hack, 2000; Clarke and Burbank, 2010, 2011). Seismic velocities reflect the elastic moduli and material properties of the rock mass and are influenced by the mineralogy, density, and porosity of the rock, as well as by the degree of degradation of the rock-mass by fractures and weathering, which are the same factors believed to influence rock-mass strength (Sjøgren et al., 1979; El-Naqa, 1996; Barton, 2007; Cha et al., 2009; Jaeger et al., 2009). The relationship between impedance (product of V_p and density)) and hillslope gradient shows ability to discriminate slope and cliff formers, showing that V_p variation with strength is greater than the effect of density (Stafleu et al., 1996). Engineering studies of “rippability” (e.g., bulldozer operations as a proxy for erosion), show that rock removal efficiency by excavation increases rapidly as V_p decreases for V_p <3 km/s (MacGregor et al., 1994).

We acquired seismic refraction data and V_p values along seismic surveys spanning 12-100 m in length using two 24-channel Geometrics Geode seismographs and 12-24 4.5 Hz vertical

component geophones spaced 2-5 m apart. The seismic source signal was generated using a sledgehammer and steel plate. Shot points (source locations) were spaced 2-5 m along the survey line.

Seismic velocities were determined based on first-arrival times from the source to each geophone and inversions of the seismic data using standard seismic refraction techniques and SeisImager software (Sheriff and Geldart, 1995; Mussett and Khan, 2000; Forbriger, 2003a, b). We produced 2-D seismic refraction tomography to image spatial V_p variations of subsurface bedrock. The initial velocity model was produced by a simple time-term 2-3 layered inversion, to roughly differentiate bedrock from colluvial cover. This layered model was then used for the tomographic inversion using the shortest ray-path method from each shot (Moser, 1991). The result is a 2D image of the subsurface velocity structure enabling identification of horizontal and vertical variations in V_p and boundaries between colluvium and bedrock. The V_p values used here, as a proxy for rock-mass strength, represent the range of maximum velocities along the survey from the deepest ray-path, which for all surveys is either a distinct colluvium-bedrock boundary or a direct ray along the surface.

Results

Landscape Evolution Simulations

As expected from 1-D river profile evolution theory (Figure 3.2), simulations of landscape evolution in the presence of gently dipping layers with strong rock overlying a weak rock unit produce a migrating scarp where erosion rates are at a maximum along the contact between the two rock units (Figure 3.9 and Appendix B).

The two-dimensional simulation uses parameters similar to empirical constraints on the GSc for comparison to and interpretation of cosmogenic erosion rates and incision rates. The simulation domain is bounded by a base-level fall rate of 90 m/Ma on the south edge and 40 m/Ma on the north edge. The important part of these variables isn't their magnitude, but that the two sides of the ridge have different base-level level histories to produces the erosional bench. The entire model space is uplifting at 90 m/Ma. The model begins with a uniform low-relief,

randomly generated surface, and then erosion progresses through time as the model is run. The key observation occurs when the model has developed to the point where the underlying weak rock is exposed and a scarp of high erosion rate develops (Figures 3.9 and 3.10).

Incision rates on Grand Staircase and in Grand Canyon

For the GSc, several basalt flows provide possible chronologic constraints, but few have been dated with $^{40}Ar/^{39}Ar$ methods. At present, the most applicable basalt flows for incision rate study are along the East Fork of the Virgin (EFV) River (Figs. 3.13 and 3.14). Schiefelbein (2001; 2002) dated the Spencer Bench/Black Mountain flows (Figure 3.14) with two samples yielding a weighted mean date of 0.57 +/-0.02 Ma. Field surveys of exposed outcrops along US Highway 89 (Table 3.2, Figures 3.13 and 3.14) yield minimum height of ~60 m of incision between the base of the basalt flows and the current level of the Virgin River. River gravel underlies the lowest basalt, and is largely obscured by vegetation (Figure 3.13 a-d). One road cut exposes the unconformity between this gravel and bedrock (Figure 3.13a). The basal gravel at this point is ~30 m above the modern EFV. The contact between the Spencer Bench basalt and gravel yields a maximum incision rate (height of basalt base) of 100 m/Ma (60 m/0.57 Ma). The lower elevation strath height and the assumption that the basalt flow closely marks gravel deposition on this strath yield a minimum incision rate of ca. 50 m/Ma (30 m/0.57 Ma). These rates are both maxima for the respective measures because the lowest actual elevation of each contact may be below the observed basal contact. For a long-term bedrock incision rate, the rate of 50 m/Ma rate is preferred the methodology for choosing that value is consistent with recent incision studies elsewhere on the Colorado Plateau (e.g. Karlstrom et al., 2007; Darling et al., 2012; Crow et al., 2014). However, we consider the range 50-100 m/Ma (or 75 +/- 25 m/Ma) to be more robust due to uncertainty in the relationship between the base of the gravel strath and the overlying basalt.

We analyze the profile of the EFV and distinguish the gradient of three reaches based on regressed channel steepness values (Figure 3.14). Upstream of the EFV knickpoint, the relatively shallow gradient stream (k_{sn} = 28 +/-1 $m^{0.9}$) is consistent with the slowly eroding, low-relief landscape surrounding the headwaters of the EFV (Figure 3.1). Along the EFV, at the knickpoint,

the maximum height of the top of the basalts is approximately 25 m above the current river level (black dots, Figure 3.14). We reconstruct the plausible paleo-profile of the river before incision through the basalt flow (purple dashed line, Figure 3.14). This projected profile represents the channel of the EFV before the increase in base-level fall rate, carved the current knickzone.

Downstream of the EFV knickpoint, we regressed channel steepness along the steepest portion of the channel (k_{sn} = 101 +/- 4 $m^{0.9}$, Figure 3.14). Downstream of the remnant basalt flows, a longer, less steep (k_{sn} = 74 +/- 2 $m^{0.9}$) section occurs. Comparison of projected profiles (based on modern drainage area) to paleo-profiles preserved by the basalt matches the relatively low (74) k_{sn} value well. An inferred paleo-profile from the single gravel point and upstream extent of the knickzone (furthest upstream basalt) matches the slightly greater channel steepness gradient. The observed profile of the basalt flow (orange line, Figure 3.14) is more robust than the profile inferred from two data points (blue line, Figure 3.14). Further, the section with higher steepness (k_{sn} = 101 +/-4 $m^{0.9}$) may be a local perturbation expressed by the passing knickpoint (Whipple, 2004; Haviv et al., 2010), and could be over-steepened relative to the equilibrium profile given the more recent, higher erosion rate boundary condition (50-100 m/Ma).

Few regional incision rates have been determined in the vicinity of the GSc, although several lava flows exist. Two recently dated basalt flows along Kanab Creek rest on the modern strath and about 30 m above the strath, and are inferred to be Quaternary in age because they rest within canyons that contain Pleistocene-Holocene arroyo deposits (Nelson and Rittenour, 2014). The face-value dates of these two flows are <211 ka and <276 ka respectively. However, both samples exhibited characteristics of excess argon during step-heating and are considered maximum ages (Nelson and Rittenour, 2014). Because of this analytical uncertainty, we do not rely on these basalts for incision rate estimates, but a loosely constrained incision rate of 75 +/- 25 m/Ma from the higher flow is consistent with relatively slowly eroding channels similar to the nearby EFV. Indeed, the lower flow -implies very slow erosion. The scarp of the next nearest incision point on the plateau north of the GSc, 35 km north of Spencer Bench on the upper Sevier R, yields a net incision rate since 5.45 Ma of <2 m/Ma at Rock Canyon along US Highway 89 (Figs. 1, 8f, age from Biek et al., 2012). This very low incision rate of the plateau is inferred from

topography and used to justify a low base level fall rate in the simulation of GSc, which has a low erosion rate on the northern boundary of the simulation (Figure 3.9).

In the GC, incision rate decreases from ~175 m/Ma in the eastern canyon to ~90 m/Ma in the central canyon (Crow et al., 2014). To simplify, we use an approximate average value of 150 m/Ma for the eastern GC for comparison. We take this incision rate range to be representative of the majority of the GC downstream of the GSc. Lower apparent incision rates in the western GC have been affected by local normal faulting and hanging-wall anticlines (Karlstrom et al., 2007; Crow et al., 2014), and so we focus on the eastern GC as a proxy of base level fall relevant to the relationship between GSc and GC. The best general estimate of incision rates from the GSc and GC landscapes are about 75 +/- 25 m/Ma and about 150 +/- 25 m/Ma, respectively. Approximate uncertainties given are representative of the range of data.

Spatially-averaged Erosion Rates and Topography

Topographic metrics in the study areas are quantified to evaluate the relationships between rock strength and erosion rates. The values of channel steepness (k_{sn}) averaged across individual catchments on the GSc are typically 20-60 $m^{0.9}$, and in the GC k_{sn} values typically range from 80-120 $m^{0.9}$.

Cosmogenic erosion rates from the GSc, GC (including data from Nichols et al., in review), and Black Mesa east of GC show a wide range (18-1261 m/Ma) of measured rates (Table 3.2, Figure 3.15). The apparent erosion rates of the GSc are higher (177-1261 m/Ma) than those of the GC (18-267 m/Ma). This is opposite to constraints from longer term incision rate data (~75 m/Ma in the GSc vs ~150 m/Ma in the GC). Note that the CRN samples in the GSc primarily tap catchments eroding from the upper 'step' of the Staircase, the Pink Cliffs (Figure 3.5), which are formed of the Eocene Claron Formation atop weaker Upper Cretaceous beds. These contrast to GC samples that tap catchments eroding from numerous units in the Paleozoic and Proterozoic strata (Figures 3.7 and 3.8), which include several quartz-bearing units and several cliff-slope alternations, (that are much more closely spaced horizontally than GSc) in the canyon.

Simulated Erosion and Simulated CRN Determination of Erosion Rate

Simulated landscapes were sampled with modified CRONUS scripts to extract the expected ^{10}Be erosion rate (Table 3.3). In this analysis three key rates are compared: the imposed base-level fall rate that drives erosion, the catchment-averaged erosion rate, and the estimate of catchment-averaged erosion rate obtained from ^{10}Be measurements. The simulated landscape has similar boundary conditions to the Pink Cliffs of the GSc (Figures 3.5 and 3.9), and produces "real" catchment-averaged erosion rates calculated directly from the model that are greater than base-level fall rate in any catchment sampling the scarp (Figures 3.10). For most cases tested, the ^{10}Be measured estimate closely matches the calculated average erosion rate, supporting the well-established idea that detrital ^{10}Be concentrations provide a good measure of catchment mean erosion rate despite expected spatial complexity in erosion rate (Bierman and Steig, 1996; Granger et al., 1996).

A critical question for our analysis is whether or not the catchment mean rate measured by detrital ^{10}Be concentrations reflect long-term base-level fall rate. As illustrated in Figure 3.3d, where erosion of weak rocks undermines stronger rock units to form retreating cliff bands, local and even spatially averaged erosion rates can significantly exceed the rate of base-level fall. The degree to which real catchment average erosion rate exceeds base-level fall rate is proportional to the distance from the rapidly eroding scarp (Figure 3.10). Preliminary analyses indicate that variable quartz fertility within the rock layers (Figure 3.10) typically does not cause real and ^{10}Be rates to differ until quartz fertility ratios approach 50 to 100 times greater concentration in one unit than another. The simulation with stratigraphy like that of the GC (Figures 3.7, 3.8, 3.11 and 3.12) yields real catchment averaged erosion rates (calculated directly from adjacent time-steps) that typically do not differ greatly from ^{10}Be averaged rates or imposed base-level fall rate (Figure 3.12). The relationships between modeled catchment averaged erosion rates, modeled ^{10}Be estimates of that erosion rate and base level suggest particular scenarios for which ^{10}Be data will not match base-level fall rates given wide ranges of rock strength and quartz distribution, which are needed for direct assessment of the validity of erosion rate estimates in landscapes affected by quartz disparity and horizontal strata. For instance, the substantial difference between base

level fall rate and cosmogenic erosion rates in the Grand Staircase is likely a result of undermining the cliff bands, which can be viewed as a means of increasing efficiency or as skewing data from expected k_{sn} vs E relationships.

Seismic Velocity Measurements

Seismic-refraction tomography reveals V_p through the near-surface bedrock that can be used as a proxy for rock-mass strength (Sjøgren et al., 1979; El-Naqa, 1996; Barton, 2007; Cha et al., 2009; Jaeger et al., 2009) over geomorphically relevant scales. The bedrock in GC shows generally faster V_p values than those in the GSc (Figs. 3.7 and 3.8). The fastest V_p values, ranging from 4 to 6 km/s, are in un-weathered limestones, granites, and schists exposed within the Paleozoic and Proterozoic rocks of GC. The slowest V_p values are found within the shale units from both regions, ranging from 0.5 to 1.3 km/s, and appear invariant with age. In both regions, the stronger cliff-forming units reveal V_p values greater than 2.7 km/s, whereas the weaker, slope forming, units show consistently slower V_p values around 1 km/s. In a limited number of surveys over shale units, V_p values, unsurprisingly, reflect an unusually strong (fast V_p) bed within a generally weaker shale unit, which we interpret as not representative of the velocity structure or strength of the rock unit as a whole.

The minimum two- to three-fold contrast in V_p values between strong and weak units supports the simulated stratigraphic columns for the models that loosely represent the GC and GSc (Figs. 3.9 and 3.11). However, the measured V_p values are not directly used to calibrate the erosional efficiency of simulated stratigraphy – an important future step that is beyond the scope of this paper. Rather, the data support the classification as groups of ‘strong’ versus ‘weak’ rock units for simplicity, and the models use a factor of 2 difference in rock strength. Further evaluation of the relationships between V_p, measures of intrinsic rock strength, and erosional efficiency are appropriate for a more detailed study of rock strength.

Discussion

Modeled Spatial Patterns of Erosion vs Empirical Erosion Rates

CRN-derived erosion rates in the GC approximately match incision rates within the GC (Nichols et al., 2011; Nichols et al., In Review). Comparing the weak over hard scenario (Figure 3.2) to the GSc (overall weak rock) vs the GC (overall harder rock), long-term incision rates suggest that the morphology of the GC reflects an increase in incision rate. Increased incision rate was perhaps caused by integration of the Colorado River, an idea consistent with recent studies and early thinking (Davis, 1901; Blackwelder, 1934; Longwell, 1946; Karlstrom et al., 2008; Karlstrom et al., 2014; Darling and Whipple, 2015).

However, CRN-derived erosion rates do not match incision rates in the GSc, and indeed significantly exceed local long-term incision rates. This mis-match between short-term, CRN-derived, erosion rate estimates and longer-term incision rates in the Grand Staircase likely reflects two end member possibilities or a combination: 1) the interaction of base-level fall and erosion into the stack of strong-over-weak rocks at the scale of the catchments (Figures 3.3 and 3.9) and 2) potential biasing of our CRN-derived erosion rates toward erosion rate of the cliff-bands rather than true catchment average rates. Calculated erosion rates extracted from our landscape evolution simulations (Figure 3.9) suggest that catchment-averaged cosmogenic samples will mimic real catchment-averaged erosion rate even when quartz distribution is not uniform. However, the more important distinction is whether ^{10}Be derived rates will match base level fall rate. Field evidence and numerical simulations both strongly suggest erosion rates will be derived primarily from the cliff band itself (Figure 3.13e) and will record high erosion rates that exceed base level fall rate (Figures 3.9, 3.10).

In the upper portion of the GSc, the source-rock of the sampled catchments is primarily the relatively strong Claron Fm. (Vp = 2-2.5 km/s), a mixture of fluvial and lacustrine sediments above weaker Cretaceous shale (Vp ~ 1-1.5 km/s) and sandstone layers (Sable and Hereford, 2004). Consistent with Figure 3.3, a hard-over-soft rock geometry will produce a rapidly eroding scarp that will generate the majority of the sediment delivered to the stream channel, which is supported by field observations of Claron-sourced sediment filling a channel despite flowing through Cretaceous shale units (catchment of Muddy Creek, sample AD12-MuC, Figure 3.13e).

Average erosion rate in this scenario is expected to exceed the rate of base level fall due to cliff undermining (Forte et al., 2016).

Fluvial erosion is affected by rock strength in how the channel form attempts to reach equilibrium, and so erosion rate is not in direct correlation with rock strength. The pace and pattern of erosion can be tested by evaluating the degree to which measured erosion rates are correlated with the proportion of the contributing area that is steep, less vegetated and underlain by Claron Formation. In Figure 3.16, an example from Main Canyon, a headwater of the Escalante River, uses the overlap of previous geologic mapping of the Claron Formation (panel A), high hillslope angle (B) and un-vegetated Claron outcrop (C) to estimate spatial area of probable sources of rapidly eroding sediment (D). For all catchments in which we measured ^{10}Be concentrations in sediment within the Pink Cliffs, the fractional area of Steep Claron outcrop is strongly correlated with the estimated erosion rate (Figure 3.17, Table 3.4). If quartz in these two units is uniform, then the measured CRN erosion rate will be the average erosion rate of the catchment that includes the localized high rates (Bierman and Steig, 1996; Granger et al., 1996). If the quartz distribution is not uniform, then the erosion rate of the dominant quartz source will bias the CRN rate and it will differ from the actual mean erosion rate. The correlation of Claron source data with CRN erosion rates is consistent with the Claron Formation as the dominant quartz source and the undermining of this rock unit as a significant control on CRN-derived erosion rate magnitude. If the simulated effect of quartz distribution is an indication, it is likely that the apparent high and highly variable cosmogenic erosion-rate data would exist regardless of the quartz distribution, because of high and highly variable erosion rates in the catchments that are due to the undermining of the harder rock layer by competing kinematic erosion velocity (Figure 3.2 and 3.7). As a consequence, in this and similar landscapes, ^{10}Be-derived erosion rate estimates are not reflective of the rate of base-level fall, potentially ranging from much higher to much lower depending on where samples are taken.

Channel Steepness as a Function of Erosion Rate

Landscape evolution is driven by base-level fall rate but can be modulated by spatial variability in substrate properties that produce local erosion rate anomalies (Figs. 3.2 and 3.7). In Figure 3.18, channel steepness index averaged throughout a catchment is plotted vs erosion rate and incision rate data from the GC, western GC, Black Mesa and the GSc (8). The solid yellow, curve is calculated following DiBiase and Whipple (2011) with a bedrock erodibility parameter (k_e) adjusted to $1.0x10^{-12}$ to achieve a reasonable fit to the GC data. A higher erodibility parameter, consistent with the arbitrary blue dashed curve, represents a landscape with weaker rock,as shown by slow Vp measurements in the shales and weak sandstones, and the relatively low gradient reaches . The data appear to be strongly skewed to rates higher than the independent base-level fall rate estimates (e.g., the Spencer Bench incision rate in Figure 3.14).

Given that numerical simulations show local erosion rates can be strongly altered by rock strength differences, the apparent increase in scatter relative to cosmogenic rate data from other studies (e.g. Ouimet et al., 2009; Cyr et al., 2010; DiBiase et al., 2010; Siame et al., 2011; Kirby and Whipple, 2012; Balco et al., 2013; Godard et al., 2014; Lague, 2014; Scherler et al., 2014; Roux-Mallouf et al., 2015; Adams et al., 2016), and the disagreement between long-term incision rates and the cosmogenic rates in this study, it is probable that the cosmogenic erosion rates of the Grand Staircase simply do not reflect longer term base level fall rates in that area. However, within the GC, incision-rate data broadly match erosion-rate data. Simulations suggest numerous variations in bed strength dilute the response of erosion rates to rock strength differences, mixing sediment eroded at higher and lower rates than base level fall, which allows erosion rates to better track base level fall rate (Figures 11 and 12). Therefore, complex quartz and erosion rate distributions in landscapes like the Grand Canyon and Grand Staircase can be interpreted, with caveats, using numerical models and field data on sediment sourcing.

Conclusion

Rock strength significantly alters how base-level fall rate is transmitted upstream, which in turn affects patterns in erosion rates throughout a landscape. Using numerical simulations of landscape evolution to understand the influence of rock strength variation on erosion rate

patterns (Figure 3.2), we improve on frameworks for interpreting previously elusive topographic patterns like steep-walled canyons cut into relatively hard bedrock. We show that careful consideration of rock strength patterns, base level fall rate and catchment erosion rate patterns can distinguish base level control and autogenic rock-strength-controlled rate patterns that drive landscape change.

Two main conclusions about the topography of the Colorado Plateau can be made: the relatively low incision rate of the Grand Staircase relative to the Grand Canyon suggests that incision of the Grand Canyon is likely a result of increased base level fall rate acting on a landscape where rock strength systematically changes in cross section (Figure 3.2). The apparent result that increased incision rate helped form the canyon topography we see today is consistent with relatively young estimates for the age of the incision of the Grand Canyon (Karlstrom et al., 2008; Karlstrom et al., 2014; Darling and Whipple, 2015).

The discrepancy between longer-term incision rates and shorter-term detrital erosion rates in the Grand Staircase can be explained by the rock strength contrasts within the exposed section. The cosmogenic rates are likely reasonable estimates of real erosion rate within the undermining scarps, but this expected (from simulations) erosion-rate pattern may be further enhanced by significant variations in quartz yield if catchments actually produce quartz at magnitudes that differ by 1-2 orders of magnitude or more. In either case, the scarp of the Grand Staircase is rapidly eroding relative to the base level of the streams of the Grand Staircase. In the Grand Canyon, the relief spans many rocks layers, and so long as quartz is spread across several units ranging from top to bottom, the ^{10}Be are not expected to deviate from base level fall rate when several weak/hard units are sampled, as suggested by simulations and supported by average incision rate (~150 m/Ma). Although our imposed erosional efficiency (*K,* here) varies by a factor of 2 in both simulations, it is plausible that greater or lesser ratios of strength may influence the erosion rate anomaly caused by rock strength contrast.

The topography of the Grand Canyon is more than the result of increased rock strength with stratigraphic depth. The combined erosion rate and rock strength data and their relative patterns described here suggest the steep-walled Grand Canyon cut into the Colorado Plateau is

explained by an increase in base-level fall rate in the last few million years that is superimposed on varied rock strength in the stratigraphy. Particular causes for this base-level fall rate increase may be enhanced erosive capacity as the river system integrated from separate drainage systems and may be modified by tectonic forces and isostatic rebound.

References

Adams, B., Whipple, K., Hodges, K., and Heimsath, A., 2016, In-situ development of high-elevation, low-relief landscapes via duplex deformation in the Eastern Himalayan hinterland, Bhutan: Journal of Geophysical Research: Earth Surface.

Ahnert, F., 1970, Functional relationships between denudation, relief, and uplift in large mid-latitude drainage basins: American Journal of Science, v. 268, p. 243-263.

Anderson, J. J., and Rowley, P. D., 1975, Cenozoic stratigraphy of southwestern High Plateaus of Utah: Geological Society of America Special Papers, v. 160, p. 1-52.

Aslan, A., Hood, W. C., Karlstrom, K. E., Kirby, E., Granger, D. E., Kelley, S., Crow, R., Donahue, M. S., Polyak, V., and Asmerom, Y., 2014, Abandonment of Unaweep Canyon (1.4–0.8 Ma), western Colorado: Effects of stream capture and anomalously rapid Pleistocene river incision: Geosphere, v. 10, no. 3, p. 428-446.

Aslan, A., Karlstrom, K. E., Crossey, L. J., Kelley, S., Cole, R., Lazear, G., and Darling, A., 2010, Late Cenozoic evolution of the Colorado Rockies: Evidence for Neogene uplift and drainage integration: Field Guides, v. 18, p. 21-54.

Balco, G., Finnegan, N., Gendaszek, A., Stone, J. O., and Thompson, N., 2013, Erosional response to northward-propagating crustal thickening in the coastal ranges of the US Pacific Northwest: American Journal of Science, v. 313, no. 8, p. 790-806.

Balco, G., Stone, J. O., Lifton, N. A., and Dunai, T. J., 2008, A complete and easily accessible means of calculating surface exposure ages or erosion rates from 10Be and 26Al measurements: Quaternary Geochronology, v. 3, no. 3, p. 174-195.

Barton, N., 2007, Rock quality, seismic velocity, attenuation and anisotropy, CRC press.

Biek, R., Rowley, P., Anderson, J., Maldonado, F., Moore, D., Eaton, J., Hereford, R., and Matyjasik, B., 2012, Interim geologic map of the Panguitch 30'x 60'quadrangle: Garfield, Iron, and Kane Counties, Utah: Utah Geological Survey Open-File Report, v. 599, no. 3.

Bierman, P., and Steig, E. J., 1996, Estimating rates of denudation using cosmogenic isotope abundances in sediment: Earth Surface Processes and Landforms, v. 21, p. 125-139.

Blackwelder, E., 1934, Origin of the Colorado River: Geological Society of America Bulletin, v. 45, no. 3, p. 551-566.

Bursztyn, N., Pederson, J., Tressler, C., Mackley, R., and Mitchell, K., 2015, Rock strength along a fluvial transect of the Colorado Plateau–quantifying a fundamental control on geomorphology: Earth and Planetary Science Letters, v. 429, p. 90-100.

Cha, M., Cho, G.-C., and Santamarina, J. C., 2009, Long-wavelength P-wave and S-wave propagation in jointed rock masses: Geophysics, v. 74, no. 5, p. E205-E214.

Clarke, B. A., and Burbank, D. W., 2010, Bedrock fracturing, threshold hillslopes, and limits to the magnitude of bedrock landslides: Earth and Planetary Science Letters, v. 297, no. 3, p. 577-586.

-, 2011, Quantifying bedrock-fracture patterns within the shallow subsurface: Implications for rock mass strength, bedrock landslides, and erodibility: Journal of Geophysical Research: Earth Surface, v. 116, no. F4.

Cook, K. L., Whipple, K. X., Heimsath, A. M., and Hanks, T. C., 2009, Rapid incision of the Colorado River in Glen Canyon–insights from channel profiles, local incision rates, and modeling of lithologic controls: Earth Surface Processes and Landforms, v. 34, no. 7, p. 994-1010.

Corbett, L. B., Bierman, P. R., and Rood, D. H., 2016, An approach for optimizing insitu cosmogenic 10 Be sample preparation: Quaternary Geochronology, v. 33, p. 24-34.

Crossey, L., Karlstrom, K., Dorsey, R., Lopez, P., J., Wan, E., Beard, L. S., Asmerom, Y., Polyak, V., Crow, R., Cohen, A., Bright, J., and Pecha, M., 2015, The importance of groundwater in propagating downward integration of the 6-5 Ma Colorado River System: Geochemistry of springs, travertines and lacustrine carbonates of the Grand Canyon region over the past 12 million years.: Geosphere, v. in press.

Crow, R., Karlstrom, K., Darling, A., Crossey, L., Polyak, V., Granger, D., Asmerom, Y., and Schmandt, B., 2014, Steady incision of Grand Canyon at the million year timeframe: A case for mantle-driven differential uplift: Earth and Planetary Science Letters, v. 397, p. 159-173.

Cyr, A. J., Granger, D. E., Olivetti, V., and Molin, P., 2010, Quantifying rock uplift rates using channel steepness and cosmogenic nuclide–determined erosion rates: Examples from northern and southern Italy: Lithosphere, v. 2, no. 3, p. 188-198.

Darling, A., and Whipple, K., 2015, Geomorphic constraints on the age of the western Grand Canyon: Geosphere, v. 11, no. 4, p. 958-976.

Darling, A. L., Karlstrom, K., Granger, D. E., Aslan, A., Kirby, E., Ouimet, W. B., Lazear, G. D., Coblentz, D. D., and Cole, R. D., 2012, New incision rates along the Colorado River system based on cosmogenic burial dating of terraces: implications for regional controls on Quaternary incision: Geosphere, v. 8, no. 5, p. 1020-1041.

Davis, W. M., 1901, An excursion to the Grand Canyon of the Colorado, Cambridge, Massachusetts, Printed for the Museum, 201 p.:

DiBiase, R. A., and Whipple, K. X., 2011, The influence of erosion thresholds and runoff variability on the relationships among topography, climate, and erosion rate: Journal of Geophysical Research, v. 116, no. F4.

DiBiase, R. A., Whipple, K. X., Heimsath, A. M., and Ouimet, W. B., 2010, Landscape form and millennial erosion rates in the San Gabriel Mountains, CA: Earth and Planetary Science Letters, v. 289, no. 1-2, p. 134-144.

Dietrich, W. E., and Smith, J. D., 1983, Influence of the point bar on flow through curved channels: Water Resources Research, v. 19, no. 5, p. 1173-1192.

Donahue, M. S., Karlstrom, K., Aslan, A., Darling, A., Granger, D., Wan, E., Dickinson, R., and Kirby, E., 2013, Incision history of the Black Canyon of Gunnison, Colorado, over the past~ 1 Ma inferred from dating of fluvial gravel deposits: Geosphere, v. 9, no. 4, p. 815-826.

Dorsey, R. J., 2010, Sedimentation and crustal recycling along an active oblique-rift margin: Salton Trough and northern Gulf of California: Geology, v. 38, no. 5, p. 443-446.

Duvall, A., Kirby, E., and Burbank, D., 2004, Tectonic and lithologic controls on bedrock channel profiles and processes in coastal California: J. Geophys. Res, v. 109, no. 10.1029.

El-Naqa, A., 1996, Assessment of geomechanical characterization of a rock mass using a seismic geophysical technique: Geotechnical & Geological Engineering, v. 14, no. 4, p. 291-305.

Flint, J. J., 1974, Stream gradient as a function of order, magnitude, and discharge: Water Resources Research, v. 10, p. 969-973.

Flowers, R., and Farley, K., 2012, Apatite 4He/3He and (U-Th)/He evidence for an ancient Grand Canyon: Science, v. 338, no. 6114, p. 1616-1619.

Flowers, R. M., Wernicke, B. P., and Farley, K. A., 2008, Unroofing, incision, and uplift history of the southwestern Colorado Plateau from apatite (U-Th)/He thermochronometry: Geological Society of America Bulletin, v. 120, no. 5-6, p. 571-587.

Forbriger, T., 2003a, Inversion of shallow-seismic wavefields: I. Wavefield transformation: Geophysical Journal International, v. 153, no. 3, p. 719-734.

-, 2003b, Inversion of shallow-seismic wavefields: II. Inferring subsurface properties from wavefield transforms: Geophysical Journal International, v. 153, no. 3, p. 735-752.

Forte, A. M., Yanites, B. J., and Whipple, K. X., 2016, Complexities of Landscape Evolution During Incision Through Layered Stratigraphy with Contrasts in Rock Strength: Earth Surface Processes and Landforms, v. 41, no. 12, p. 1736-1757.

Godard, V., Bourlès, D. L., Spinabella, F., Burbank, D. W., Bookhagen, B., Fisher, G. B., Moulin, A., and Léanni, L., 2014, Dominance of tectonics over climate in Himalayan denudation: Geology, v. 42, no. 3, p. 243-246.

Grams, P. E., and Schmidt, J. C., 1999, Geomorphology of the Green River in the eastern Uinta Mountains, Dinosaur National Monument, Colorado and Utah: Varieties of fluvial form, p. 81-111.

Granger, D. E., Kirshner, J. W., and Finkel, R., 1996, Spatially averaged long-term erosion rates measured from in situ-produced cosmogenic nuclides in alluvial sediment: Journal of Geology, v. 104, no. 3, p. 249-257.

Granger, D. E., Lifton, N. A., and Willenbring, J. K., 2013, A cosmic trip: 25 years of cosmogenic nuclides in geology: Geological Society of America Bulletin, v. 125, no. 9-10, p. 1379-1402.

Hack, J. T., 1957, Studies of longitudinal stream profiles in Virginia and Maryland: U.S. Geological Survey Professional Paper, v. 294-B, p. 97.

Hack, R., 2000, Geophysics for slope stability: Surveys in geophysics, v. 21, no. 4, p. 423-448.

Harkins, N., Kirby, E., Heimsath, A., Robinson, R., and Reiser, U., 2007, Transient fluvial incision in the headwaters of the Yellow River, northeastern Tibet, China: Journal of Geophysical Research, v. 112, no. F3.

Haviv, I., Enzel, Y., Whipple, K. X., Zilberman, E., Matmon, A., Stone, J., and Fifield, K. L., 2010, Evolution of vertical knickpoints (waterfalls) with resistant caprock: Insights from numerical modeling: Journal of Geophysical Research, v. 115, no. F3.

Jaeger, J. C., Cook, N. G., and Zimmerman, R., 2009, Fundamentals of rock mechanics, John Wiley & Sons.

Karlstrom, K., Coblentz, D., Dueker, K., Ouimet, W., Kirby, E., Van Wijk, J., Schmandt, B., Kelley, S., Lazear, G., and Crossey, L., 2012, Mantle-driven dynamic uplift of the Rocky Mountains and Colorado Plateau and its surface response: Toward a unified hypothesis: Lithosphere, v. 4, no. 1, p. 3-22.

Karlstrom, K. E., Crow, R., Crossey, L. J., Coblentz, D., and Van Wijk, J. W., 2008, Model for tectonically driven incision of the younger than 6 Ma Grand Canyon: Geology, v. 36, no. 11, p. 835.

Karlstrom, K. E., Crow, R. S., Peters, L., McIntosh, W., Raucci, J., Crossey, L. J., Umhoefer, P., and Dunbar, N., 2007, 40Ar/39Ar and field studies of Quaternary basalts in Grand Canyon and model for carving Grand Canyon: Quantifying the interaction of river incision and normal faulting across the western edge of the Colorado Plateau: Geological Society of America Bulletin, v. 119, no. 11-12, p. 1283-1312.

Karlstrom, K. E., Lee, J. P., Kelley, S. A., Crow, R. S., Crossey, L. J., Young, R. A., Lazear, G., Beard, L. S., Ricketts, J. W., and Fox, M., 2014, Formation of the Grand Canyon 5 to 6 million years ago through integration of older palaeocanyons: Nature Geoscience, v. 7, p. 239-244.

Kirby, E., and Whipple, K. X., 2012, Expression of active tectonics in erosional landscapes: Journal of Structural Geology, v. 44, p. 54-75.

Koons, E. D., 1955, Cliff retreat in the southwestern United States: American Journal of Science, v. 253, no. 1, p. 44-52.

Korup, O., and Schlunegger, F., 2009, Rock-type control on erosion-induced uplift, eastern Swiss Alps: Earth and Planetary Science Letters, v. 278, no. 3, p. 278-285.

Lague, D., 2014, The stream power river incision model: evidence, theory and beyond: Earth Surface Processes and Landforms, v. 39, no. 1, p. 38-61.

Lague, D., Hovius, N., and Davy, P., 2005, Discharge, discharge variability, and the bedrock channel profile: Journal of Geophysical Research: Earth Surface (2003–2012), v. 110, no. F4.

Lazear, G., Karlstrom, K., Aslan, A., and Kelley, S., 2013, Denudation and flexural isostatic response of the Colorado Plateau and southern Rocky Mountains region since 10 Ma: Geosphere, v. 9, no. 4, p. 792-814.

Longwell, C. R., 1946, How old is the Colorado River?: American Journal of Science, v. 244, no. 12, p. 817-835.

MacGregor, F., Fell, R., Mostyn, G., Hocking, G., and McNally, G., 1994, The estimation of rock rippability: Quarterly Journal of Engineering Geology and Hydrogeology, v. 27, no. 2, p. 123-144.

Marchetti, D. W., Hynek, S. A., and Cerling, T. E., 2012, Gravel-capped benches above northern tributaries of the Escalante River, south-central Utah: Geosphere, v. 8, no. 4, p. 835-853.

Moser, T., 1991, Shortest path calculation of seismic rays: Geophysics, v. 56, no. 1, p. 59-67.

Mussett, A. E., and Khan, M. A., 2000, Looking into the earth: an introduction to geological geophysics, Cambridge University Press.

Nelson, M. S., and Rittenour, T., 2014, Middle to late Holocene chronostratigraphy of alluvial fill deposits along Kanab Creek in southern Utah: Geology of Utah's Far South: Utah Geological Association, Publication, v. 43, p. 97-116.

Nichols, K. K., Bierman, P., and Rood, D., In Review, Cosmogenic 10-Be and sediment budgets reveal a multi-aged Grand Canyon: Geology.

Nichols, K. K., Webb, R. H., Bierman, P. R., and Rood, D. H., 2011, Measurements of cosmogenic 10 Be reveal rapid response of Grand Canyon tributary hillslopes to Colorado River incision: Geological Society of America - Abstracts with Programs, v. 43, p. 274.

Niemi, N. A., Oskin, M., Burbank, D. W., Heimsath, A. M., and Gabet, E. J., 2005, Effects of bedrock landslides on cosmogenically determined erosion rates: Earth and Planetary Science Letters, v. 237, no. 3-4, p. 480-498.

Ouimet, W. B., Whipple, K. X., and Granger, D. E., 2009, Beyond threshold hillslopes: Channel adjustment to base-level fall in tectonically active mountain ranges: Geology, v. 37, no. 7, p. 579-582.

Pederson, J., Burnside, N., Shipton, Z., and Rittenour, T., 2013a, Rapid river incision across an inactive fault—Implications for patterns of erosion and deformation in the central Colorado Plateau: Lithosphere, v. 5, no. 5, p. 513-520.

Pederson, J., Karlstrom, K., Sharp, W., and McIntosh, W., 2002a, Differential incision of the Grand Canyon related to Quaternary faulting - Constraints from U-series and Ar/Ar dating: Geology, v. 30, no. 8, p. 739-742.

Pederson, J. L., Anders, M. D., Rittenhour, T. M., Sharp, W. D., Gosse, J. C., and Karlstrom, K. E., 2006, Using fill terraces to understand incision rates and evolution of the Colorado River in eastern Grand Canyon, Arizona: Journal of Geophysical Research, v. 111, no. F2.

Pederson, J. L., Cragun, W. S., Hidy, A. J., Rittenour, T. M., and Gosse, J. C., 2013b, Colorado River chronostratigraphy at Lee's Ferry, Arizona, and the Colorado Plateau bull's-eye of incision: Geology, v. 41, no. 4, p. 427-430.

Pederson, J. L., Mackley, R. D., and Eddleman, J. L., 2002b, Colorado Plateau uplift and erosion evaluated using GIS: GSA Today, v. 12, no. 8, p. 4-10.

Pederson, J. L., and Tressler, C., 2012, Colorado River long-profile metrics, knickzones and their meaning: Earth and Planetary Science Letters, v. 345, p. 171-179.

Polyak, V., Hill, C., and Asmerom, Y., 2008, Age and evolution of the Grand Canyon revealed by U-Pb dating of water table-type speleothems: Science, v. 319, no. 5868, p. 1377-1380.

Portenga, E. W., and Bierman, P. R., 2011, Understanding Earth's eroding surface with 10Be: GSA Today, v. 21, no. 8, p. 4-10.

Repka, J. L., Anderson, R. S., and Finkel, R. C., 1997, Cosmogenic dating of fluvial terraces, Fremont River, Utah: Earth and Planetary Science Letters, v. 152, no. 1-4, p. 59-73.

Roberson, P., and Pederson, J., 2001, Rock-strength control in Desolation and Gray canyons of the Green River: a river landscape in dynamic equilibrium: Abstracts with Programs, Geological Society of America, v. 33, p. 14.

Rosenbloom, N. A., and Anderson, R. S., 1994, Hillslope and channel evolution in a marine terraced landscape, Santa Cruz, California: Journal of Geophysical Research, v. 99, no. B7, p. 14,013-014,029.

Rossi, M. W., 2014, Hydroclimatic Controls on Erosional Efficiency in Mountain Landscapes: Arizona State University.

Rossi, M. W., Quigley, M., Fletcher, J., Whipple, K., Diaz-Torres, J., Seiler, C., Fifield, L. K., and Heimsath, A. M., In Review, Along-strike variation in catchment morphology and cosmogenic denudation rates reveal the pattern and history of footwall uplift, Main Gulf Escaprment, Baja California: Geological Society America Bulletin.

Roux-Mallouf, L., Godard, V., Cattin, R., Ferry, M., Gyeltshen, J., Ritz, J. F., Drupka, D., Guillou, V., Arnold, M., and Aumaître, G., 2015, Evidence for a wide and gently dipping Main Himalayan Thrust in western Bhutan: Geophysical Research Letters, v. 42, no. 9, p. 3257-3265.

Roy, M., Jordan, T. H., and Pederson, J., 2009, Colorado Plateau magmatism and uplift by warming of heterogeneous lithosphere: Nature, v. 459, no. 7249, p. 978-982.

Roy, M., Kelley, S., Pazzaglia, F., Cather, S., and House, M., 2004, Middle Tertiary buoyancy modification and its relationship to rock exhumation, cooling, and subsequent extension at the eastern margin of the Colorado Plateau: Geology, v. 32, no. 10, p. 925.

Sable, E., and Hereford, R., 2004, Geologic map of the Kanab 30′× 60′ quadrangle: Utah and Arizona: US Geological Survey, Geologic Investigations Series I-2655, scale, v. 1, no. 100,000.

Safran, E. B., Bierman, P. R., Aalto, R., Dunne, T., Whipple, K. X., and Caffee, M., 2005, Erosion rates driven by channel network incision in the Bolivian Andes: Earth Surface Processes and Landforms, v. 30, no. 8, p. 1007-1024.

Scherler, D., Bookhagen, B., and Strecker, M. R., 2014, Tectonic control on 10Be-derived erosion rates in the Garhwal Himalaya, India: Journal of Geophysical Research: Earth Surface, v. 119, no. 2, p. 83-105.

Schiefelbein, I., 2002, Fault segmentation, fault linkage and hazards along the Sevier fault, southwestern Utah: Las Vegas, University of Nevada at Las Vegas: MS thesis, 134 p., 5 plates.

Schiefelbein, I. M., Fault Segmentation, Linkage, and Earthquake hazards along the Sevier Fault, SW Utah *in* Proceedings GSA Abst. w. Progs.2001, Volume 33, p. 38.

Schwanghart, W., and Scherler, D., 2014, Short Communication: TopoToolbox 2-MATLAB-based software for topographic analysis and modeling in Earth surface sciences: Earth Surface Dynamics, v. 2, no. 1, p. 1.

Sheriff, R. E., and Geldart, L. P., 1995, Exploration seismology, Cambridge university press.

Siame, L., Angelier, J., Chen, R.-F., Godard, V., Derrieux, F., Bourlès, D., Braucher, R., Chang, K.-J., Chu, H.-T., and Lee, J.-C., 2011, Erosion rates in an active orogen (NE-Taiwan): A confrontation of cosmogenic measurements with river suspended loads: Quaternary Geochronology, v. 6, no. 2, p. 246-260.

Sjøgren, B., Øfsthus, A., and Sandberg, J., 1979, Seismic Classification of Rock Mass QUALITIES*: Geophysical Prospecting, v. 27, no. 2, p. 409-442.

Stafleu, J., Schlager, W., Everts, A., J., K., Blommers, G., and A., v., 1996, Outcrop topography as a proxy of acoustic impedance in synthetic seismograms: Geophysics, v. 61, no. 6, p. 1779-1788.

Stock, J. D., and Montgomery, D. R., 1999, Geologic constraints on bedrock river incision using the stream power law: Journal of Geophysical Research, v. 104, no. B3, p. 4983-4993.

Suzuki, T., 1982, Rate of lateral planation by Iwaki River, Japan: Transactions, Japanese Geomorphological Union, v. 3, no. 1, p. 1-24.

Tucker, G., Lancaster, S., Gasparini, N., and Bras, R., 2001, The channel-hillslope integrated landscape development model (CHILD), Landscape erosion and evolution modeling, Springer, p. 349-388.

Tucker, G. E., and Whipple, K., 2002, Topographic outcomes predicted by stream erosion models: Sensitivity analysis and intermodel comparison: Journal of Geophysical Research, v. 107, no. B9.

Ward, D. J., Berlin, M. M., and Anderson, R. S., 2011, Sediment dynamics below retreating cliffs: Earth Surface Processes and Landforms, v. 36, no. 8, p. 1023-1043.

Weimer, R. J., 1960, Upper cretaceous stratigraphy, rocky Mountain area: AAPG Bulletin, v. 44, no. 1, p. 1-20.

Whipple, K., 2001, Fluvial landscape response time: How plausible is steady state denudation?: American Journal of Science, v. 301, p. 313-325.

Whipple, K., Kirby, E., and Brocklehurst, S., 1999, Geomorphic limits to climatically induced increases in topographic relief: Nature, v. 401, p. 39-43.

Whipple, K. X., 2004, Bedrock Rivers and the Geomorphology of Active Orogens: Annual Review of Earth and Planetary Sciences, v. 32, no. 1, p. 151-185.

Whipple, K. X., and Tucker, G. E., 1999, Dynamics of the stream-power river incision model: Implications for height limits of mountain ranges, landscape response timescales, and research needs: Journal of Geophysical Research, v. 104, no. B8, p. 17661-17617,17674.

Whittaker, A. C., 2012, How do landscapes record tectonics and climate?: Lithosphere, v. 4, no. 2, p. 160-164.

Whittaker, A. C., Cowie, P. A., Attal, M., Tucker, G. E., and Roberts, G. P., 2007, Bedrock channel adjustment to tectonic forcing: Implications for predicting river incision rates: Geology, v. 35, no. 2, p. 103.

Willenbring, J. K., Gasparini, N. M., Crosby, B. T., and Brocard, G., 2013, What does a mean mean? The temporal evolution of detrital cosmogenic denudation rates in a transient landscape: Geology, v. 41, no. 12, p. 1215-1218.

Wobus, C. W., Whipple, K. W., Kirby, E., and Snyder, N. P., 2006, Tectonics from topography: Proceedures, promise, and pitfalls, *in* Willett, S. D., Hovius, N., Brandon, M., and Fisher, D. M., eds., Climate, Tectonics and Landscape Evolution: Geological Society of America Special Paper, Volume 398, Penrose Conference Series, p. 55-74.

Wolkowinsky, A. J., and Granger, D. E., 2004, Early Pleistocene incision of the San Juan River, Utah, dated with 26Al and 10Be: Geology, v. 32, no. 9, p. 749.

Figures

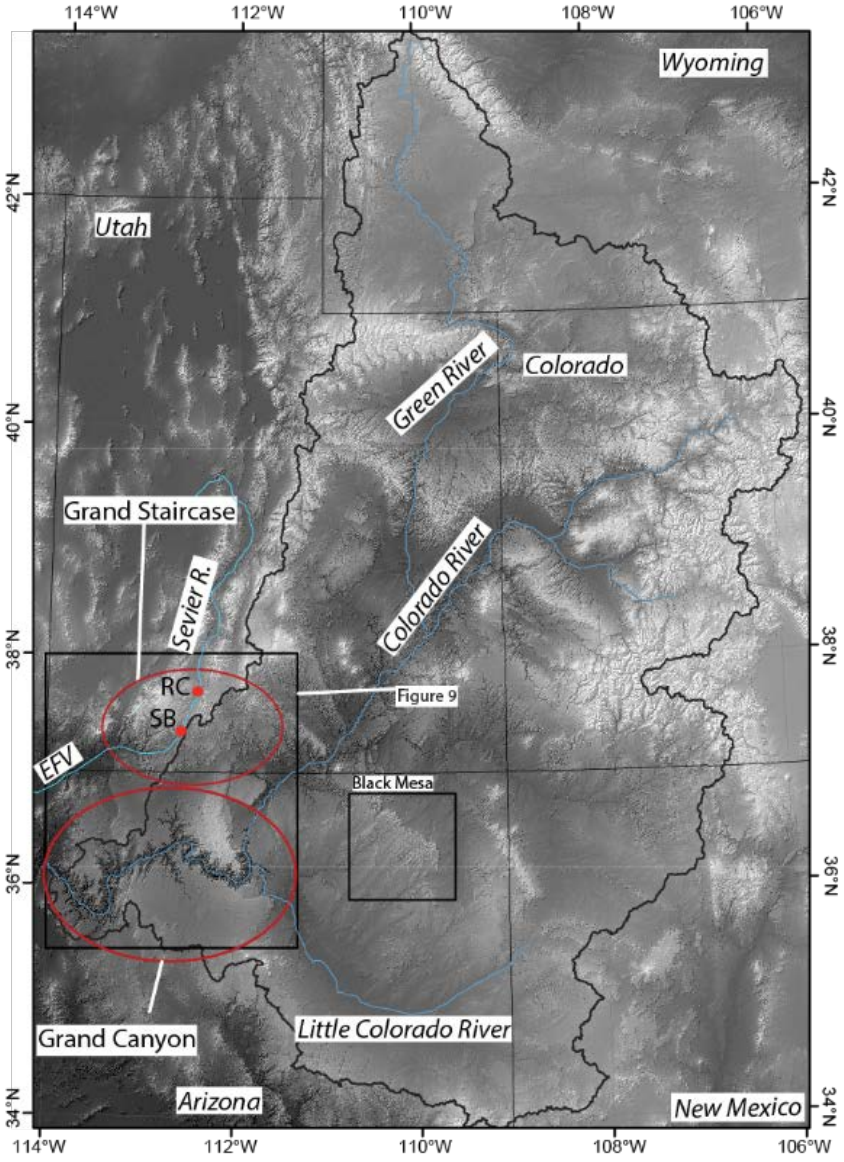

Figure 3.1. Colorado River watershed on DEM over hill-shade showing relationship between Colorado River System and the Grand Staircase and Grand Canyon with insets of map (Figure 3). Colorado River basin outlined in Blue. Abbreviated labels: EFV - East Fork Virgin River; SR - Sevier River, SB – Spencer Bench; RC – Rock Canyon.

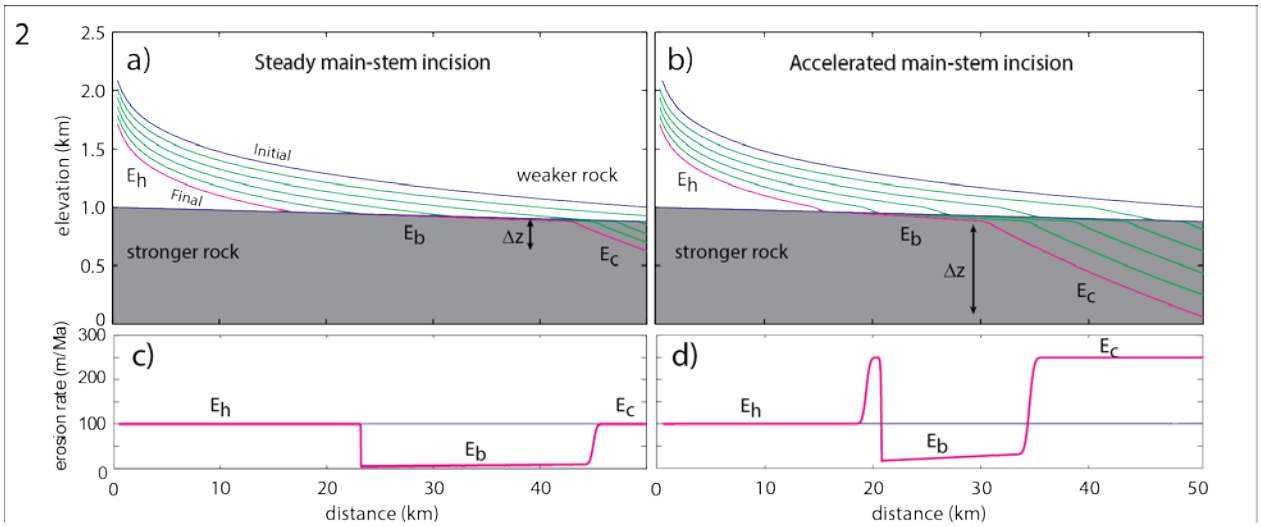

Figure 3.2. Numerical model outputs MATLABfor detachment limited stream power model. In each case, base level fall is input to a predefined stratigraphy. In a), the lithologic sequence is identical (both weak over hard) but a) is constant base level fall rate while b) has an imposed increase in base level fall rate with resulting erosion rate patterns (c) and d), after Darling and Whipple, 2015).

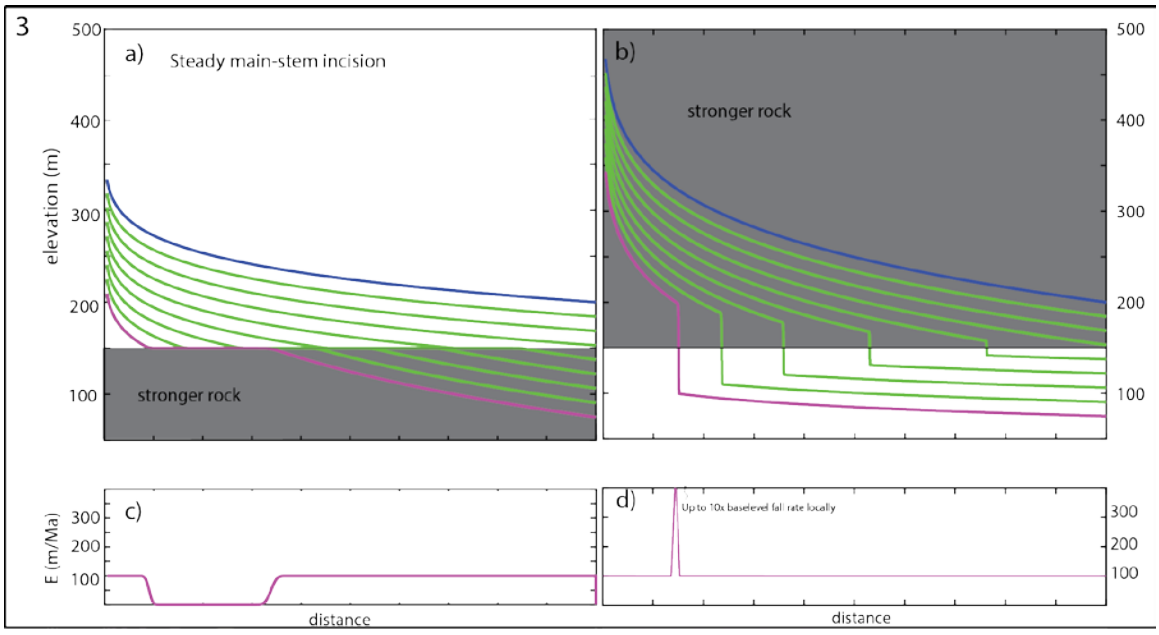

Figure 3.3. Monotonic base level fall rate is imposed on weak-over-hard rock a) and hard-over-weak rock b). Rock strength ratio is 2x, and hard rock is equal in value for both cases in fig. 3. The over-steepened prediction is a result of competing kinematic waves of erosion that undermine the upper layer in the simulation which results in different erosion rate patterns (c and d). See discussion in text.

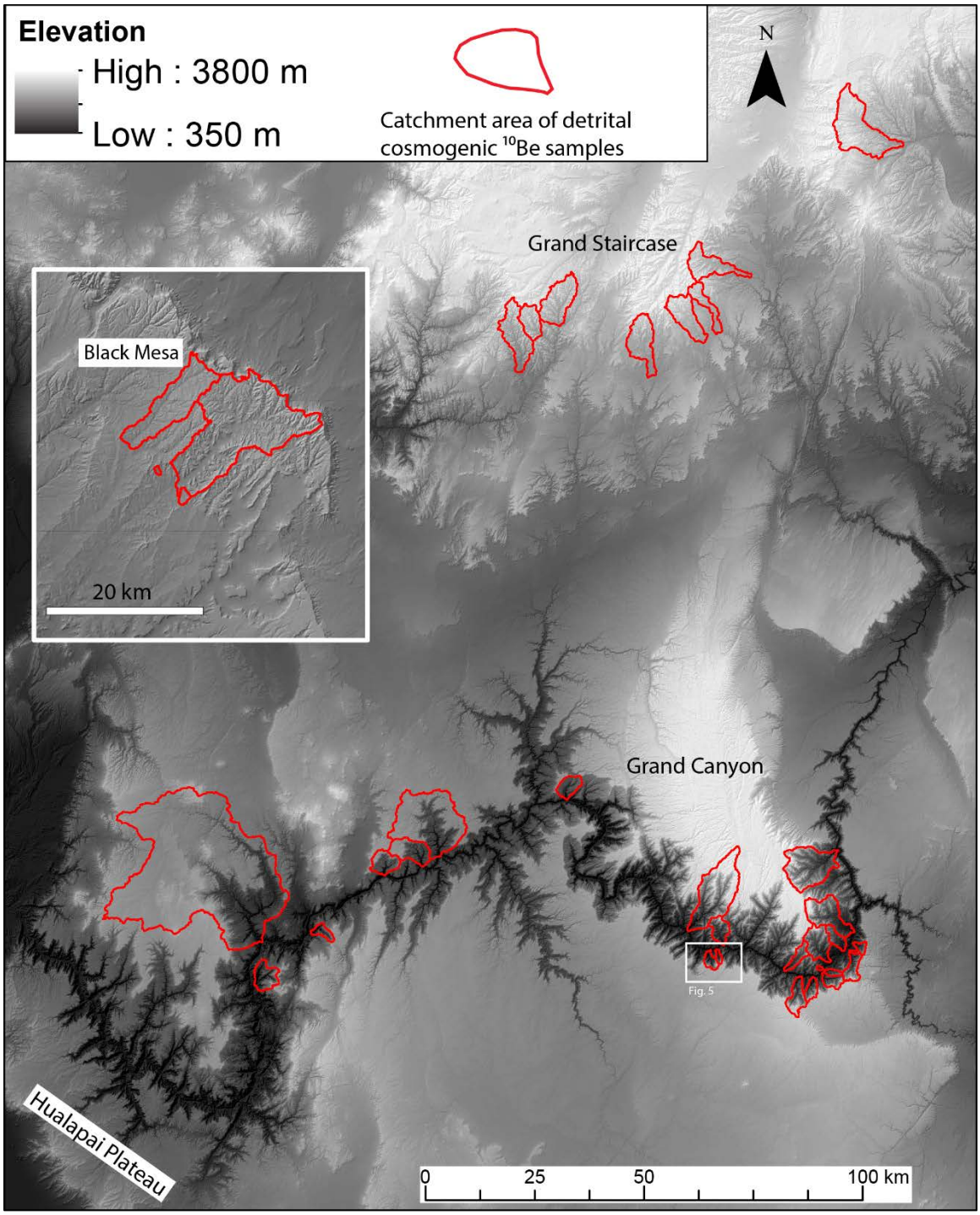

Darling Figure 4

Figure 3.4. Grand Canyon and Grand Staircase sampled catchments on Digital Elevation Model over hillshade. Catchments outlined are from this study and Nichols et al., (In Review).

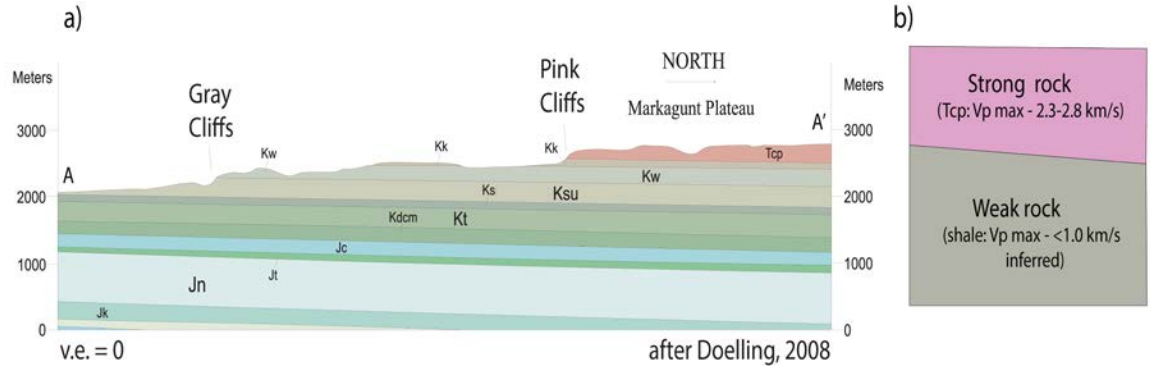

Figure 3.5. a) Geologic -cross section from Kanab 30' x 60' geologic map by Doelling (2008). The sampled catchments are eroding from the Pink Cliffs erosional scarp. Bedrock in the catchments consists of the relatively strong Claron Formation overlying weaker Kaiparowits and Wahweap Formations. b) Stratigraphy of numerical simulation of an eroding scarp. Geologic Units on Cross Section: Tcp - Tertiary Claron Fm., Pink Cliffs Member; Kk - Cretaceous Kaiparowits Fm.; Kw - Cretaceous Wahweap Fm.; Ksu - Straight Cliffs, upper member, Ksl - Straight Cliffs, lower member; Kt - Tropic Shale; Kdcm - Dakota and Cedar Mountain Fm.; Jc – Jurassic Carmel Fm.; Jt – Jurassic Temple Cap Sandstone; Jn – Navajo Sandstone; Jk – Kayenta Fm.

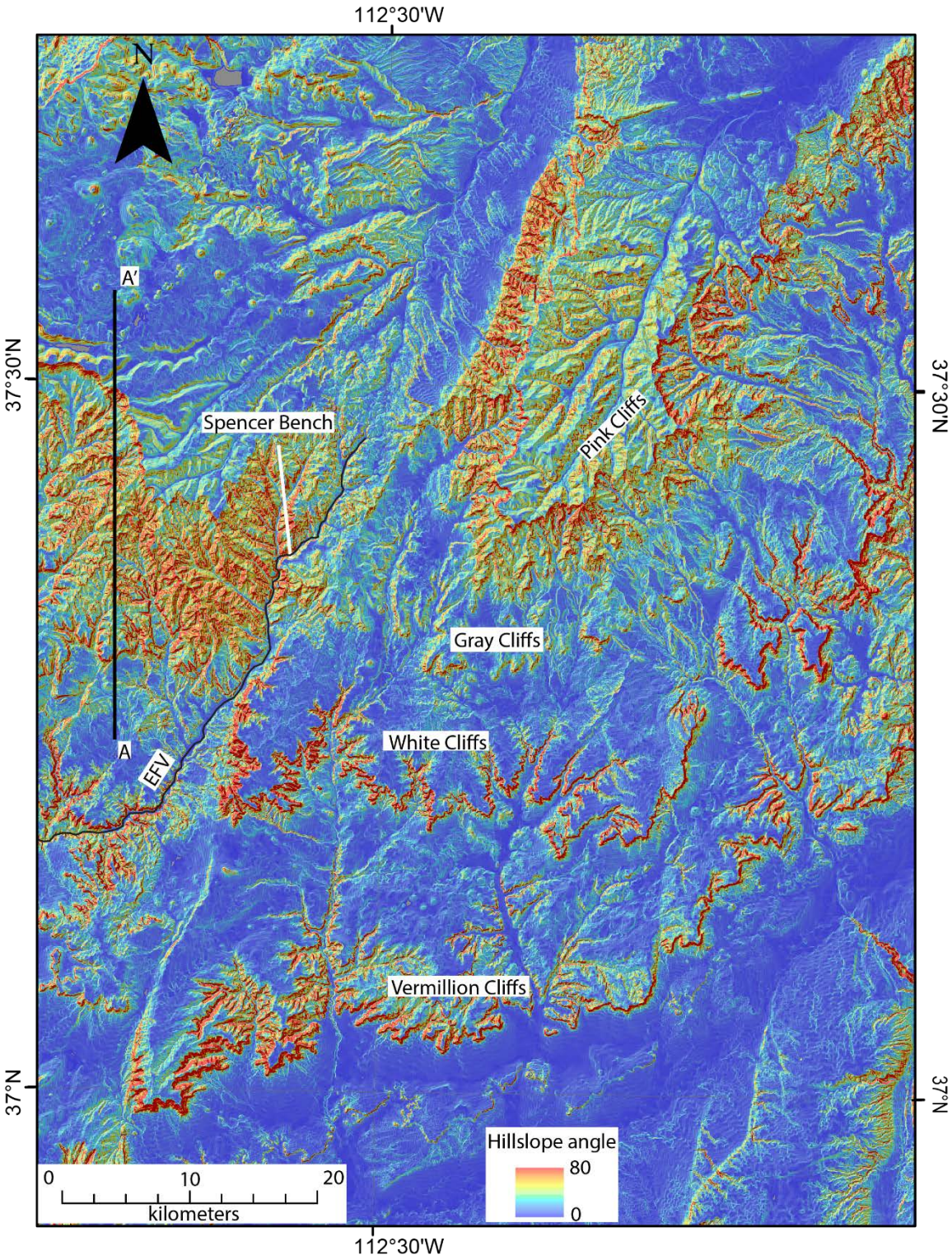

Figure 3.6. Slope map of Grand Staircase over shaded relief and DEM. Cross section line of figure 3.5 is drawn as A-A'.

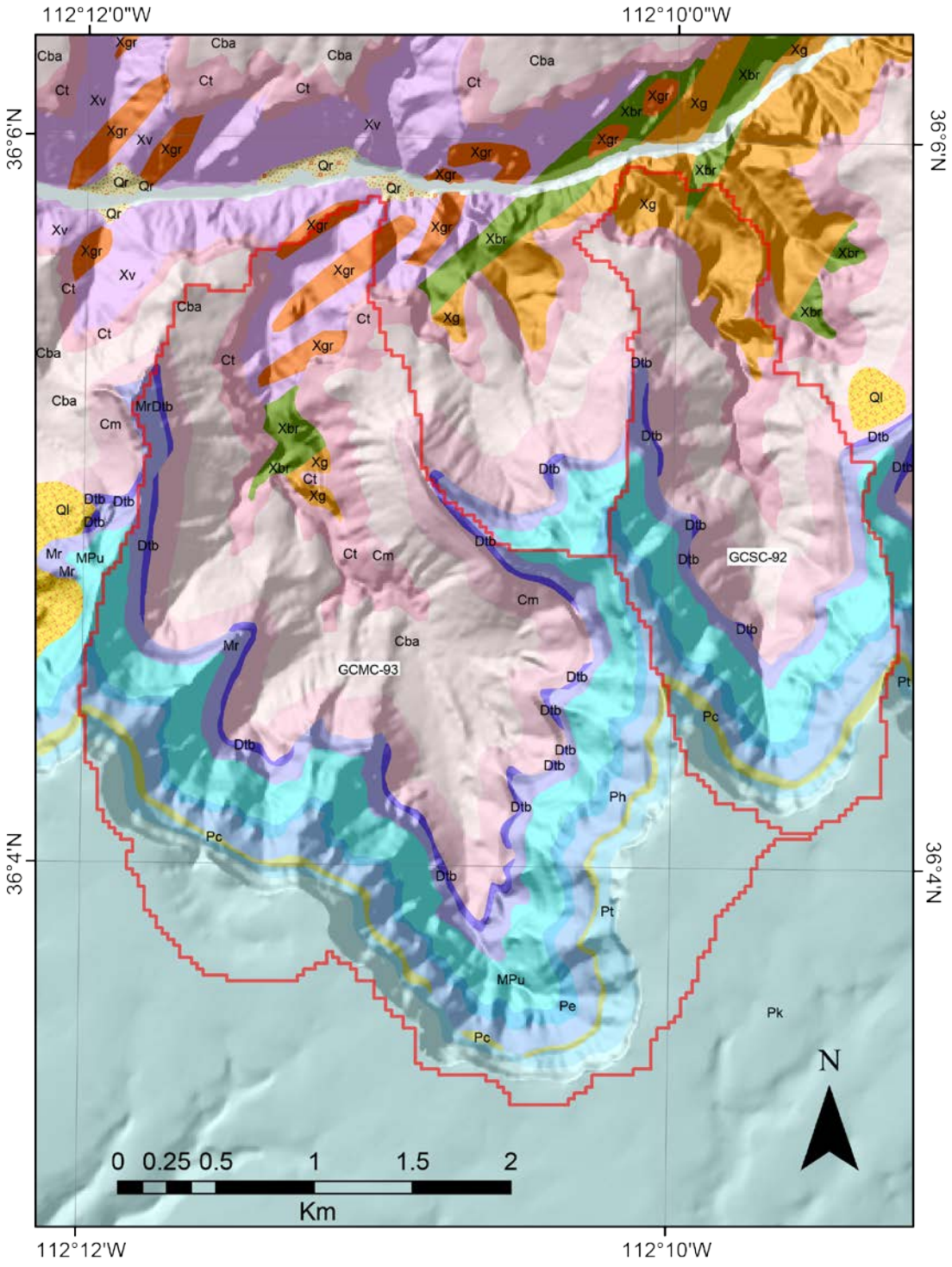

Figure 3.7. Grand Canyon geologic map of two representative catchments (sample numbers on map) that primarily drain Paleozoic stratigraphic units. Xv – Vishnu schist; Xgr – granite; Xbr – Brahma Schist; Xg - , Ct – Tapeats Ss.; Cba – Bright Angel; Cm – Muav Ls., Dtb – Temple Butte; Mr – Redwall Ls.; MPu; Supai Group; Pe – Esplanade Ss.; Pc – Coconino Ss.; Pt – Toroweap Fm.; Pk; Kaibab Fm. Map data from Billingsley (2000).

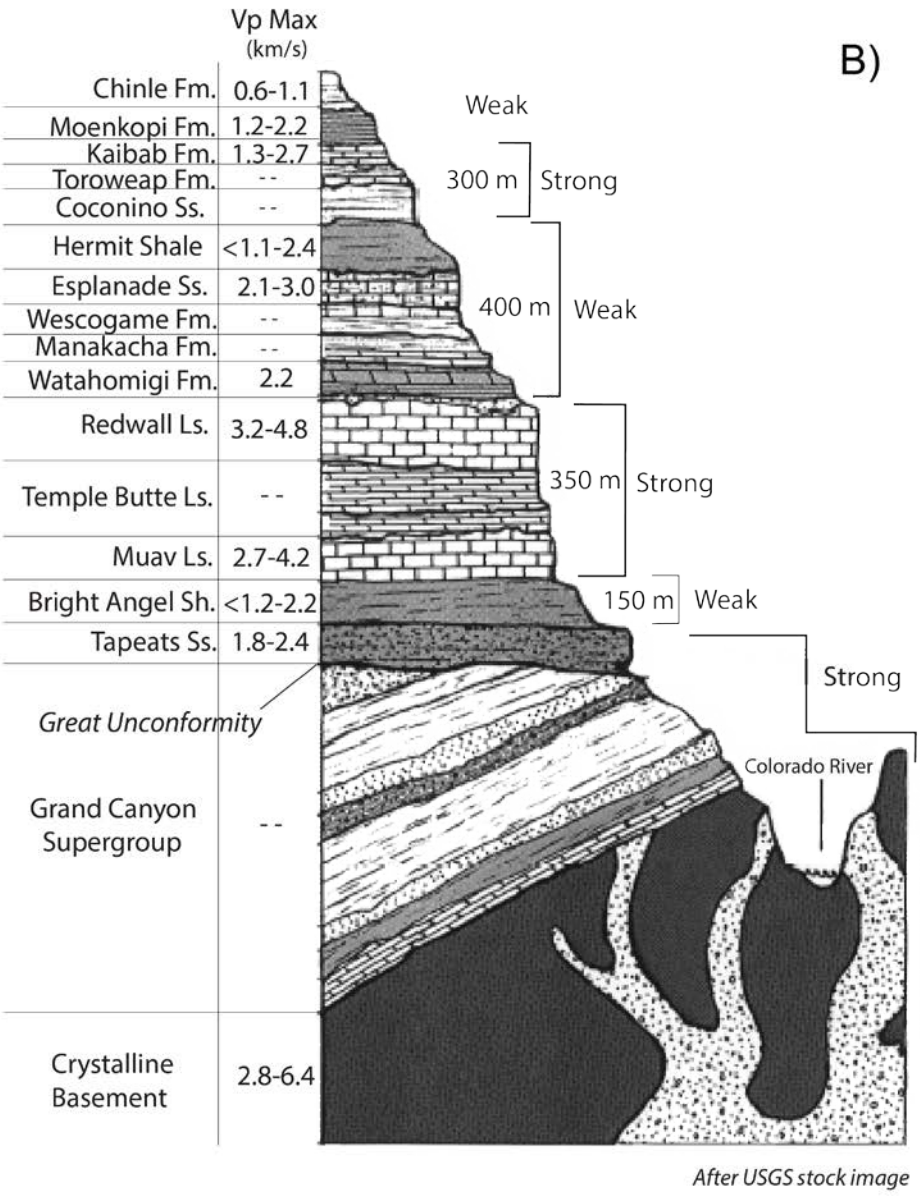

Figure 3.8. Stratigraphic column of Grand Canyon (USGS) and simulated model stratigraphy (this paper) used for second CHILD model. Particular units vary in thickness and facies through the canyon; East to west, most units thicken, Temple Butte is only thin channel beds in eastern canyon. Rock types vary from limestone to shale sandstone and conglomerate. Primary quartz bearing units are near the top (Coconino Ss.), near the middle, middle (Esplanade, Supai) and bottom (Tapeats, Bright Angel) of the section.

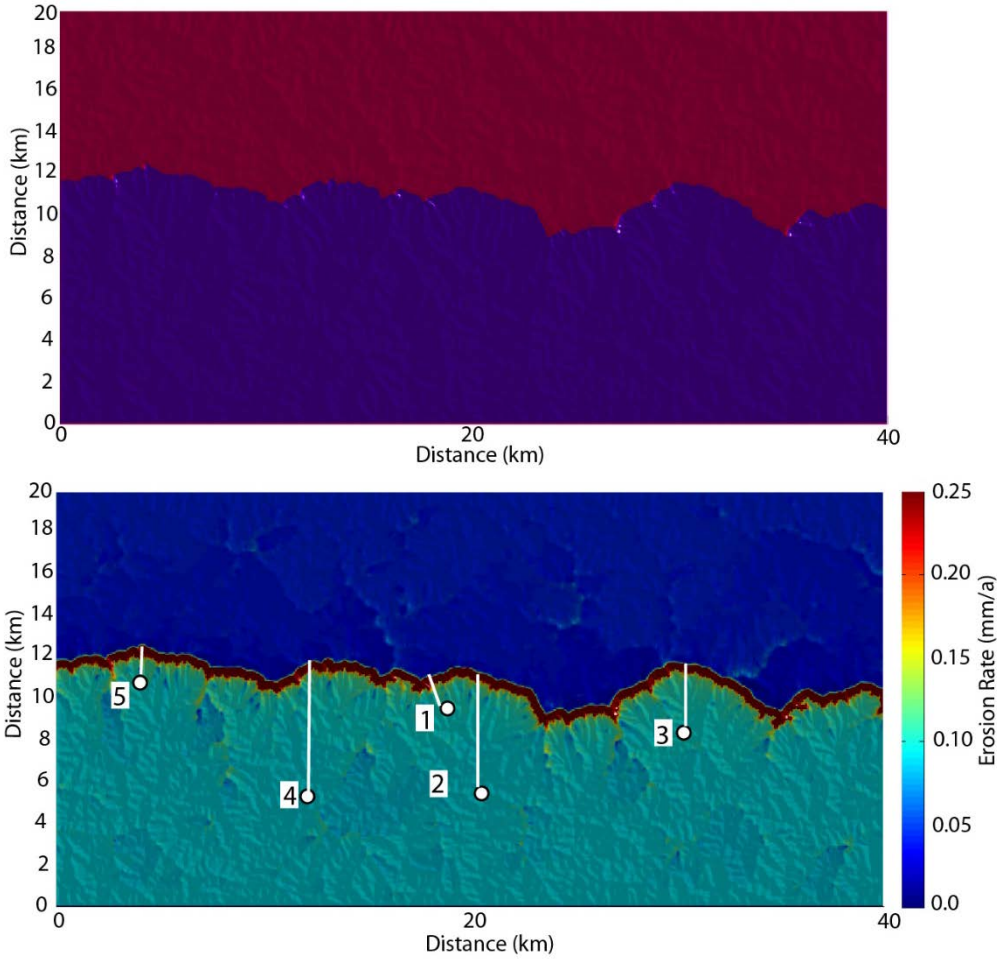

Figure 3.9. Model output from LithoCHILD showing patterns of erosion rate and lithologic strength in strong-over-weak scenario. Parameters for model run are: differential base level fall rate: 40m/Ma along model-"North" edge only, the rest of the model area has uniform steady rock uplift with base level fall rate along the "south" edge set to 90 m/Ma. Strong rock has erodibility of 1e-6 m0.1*10-6 yr and weak rock is 2x higher erodibility. Pixel size is 50 m and the upper hard unit is 800 m thick at simulation start.

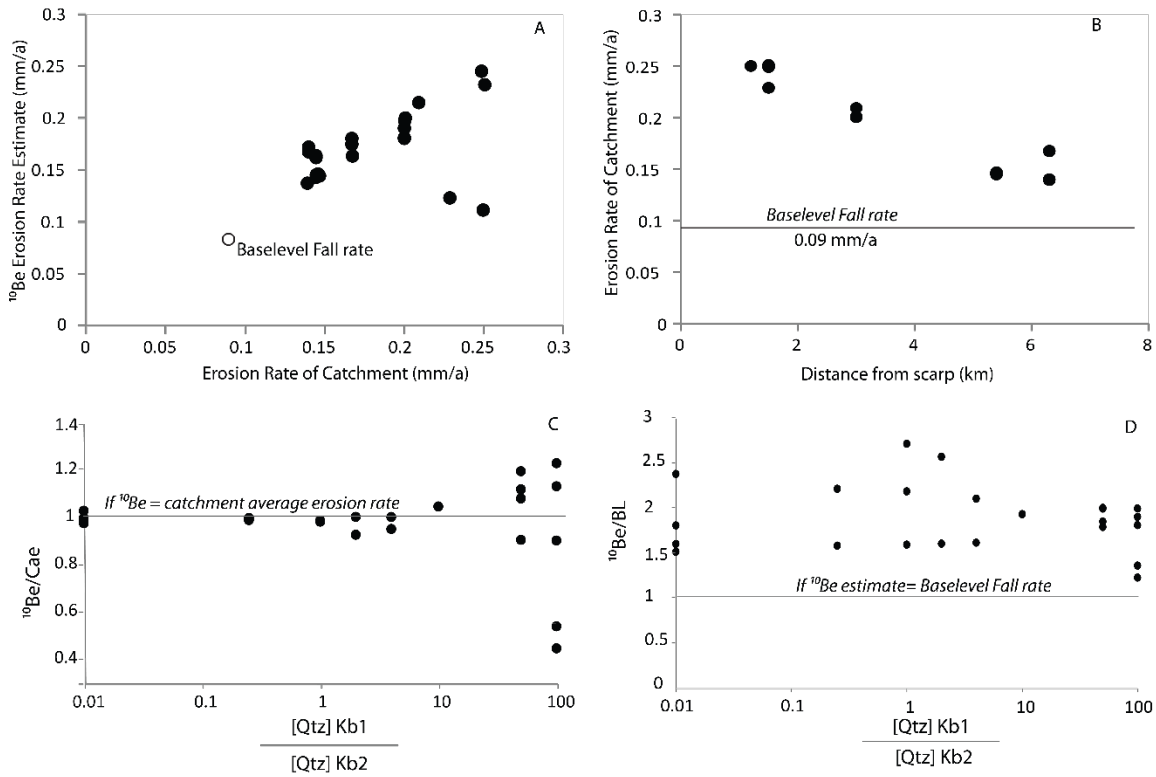

Figure 3.10. Numerically sampling the simulation output (a-d), for erosion rate from the model vs simulated CRN sampling of the synthetic landscape (b), erosion rate as a function of distance from scarp (c) and ratio of 10Be and calculated erosion rates as a function of quartz concentration in the multi-layer simulation (d). Note base level fall rate does not overlap with calculated or 10Be-estimated erosion rates. See also Appendix B.

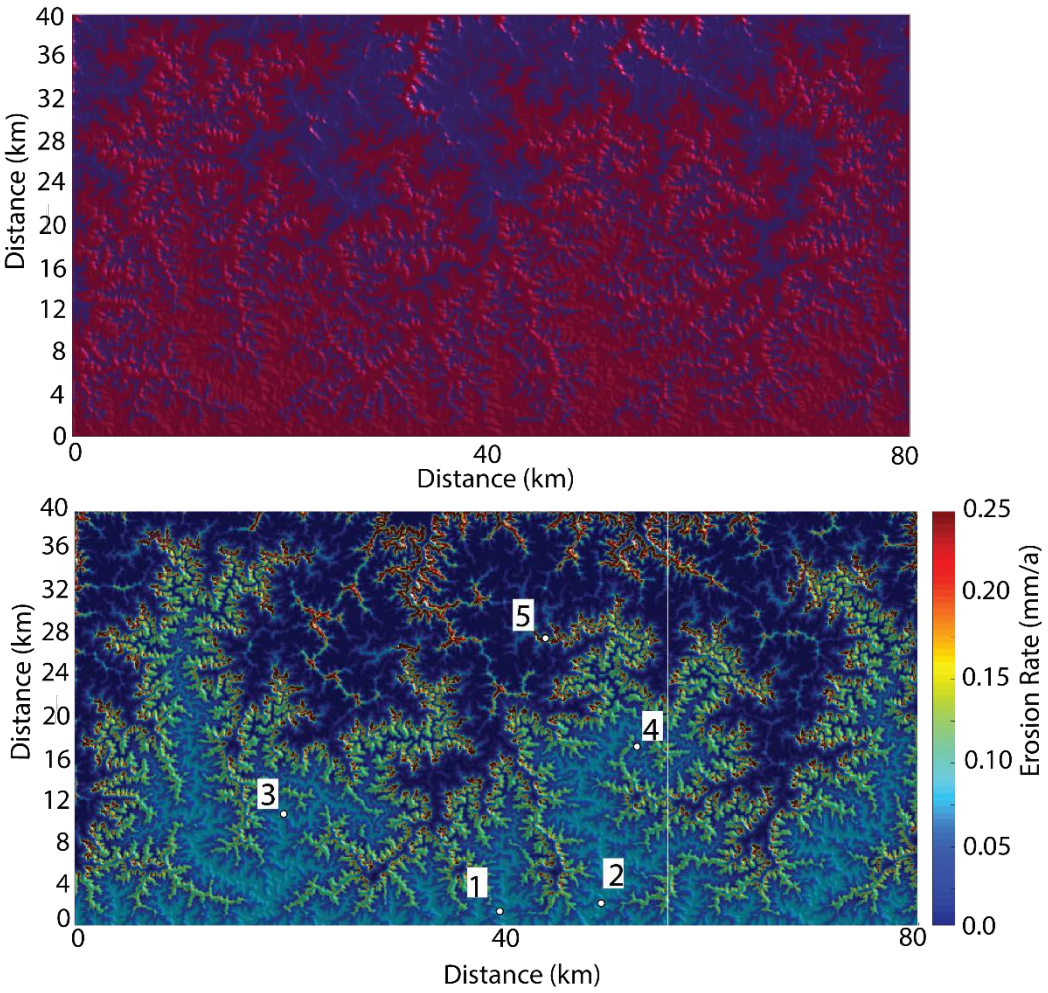

Figure 3.11. Model output from LithoCHILD showing patterns of erosion rate and lithologic strength with several alternating weak-strong rock layers. Uplift is uniform across model area and streams flow out of the southern edge. Strong rock has erodibility of 1e-6 m0.1*10-6 yr and weak rock layers are twice as erodible. Base level fall rate is 170 m/Ma and unit thicknesses are given in Figure 3.8.

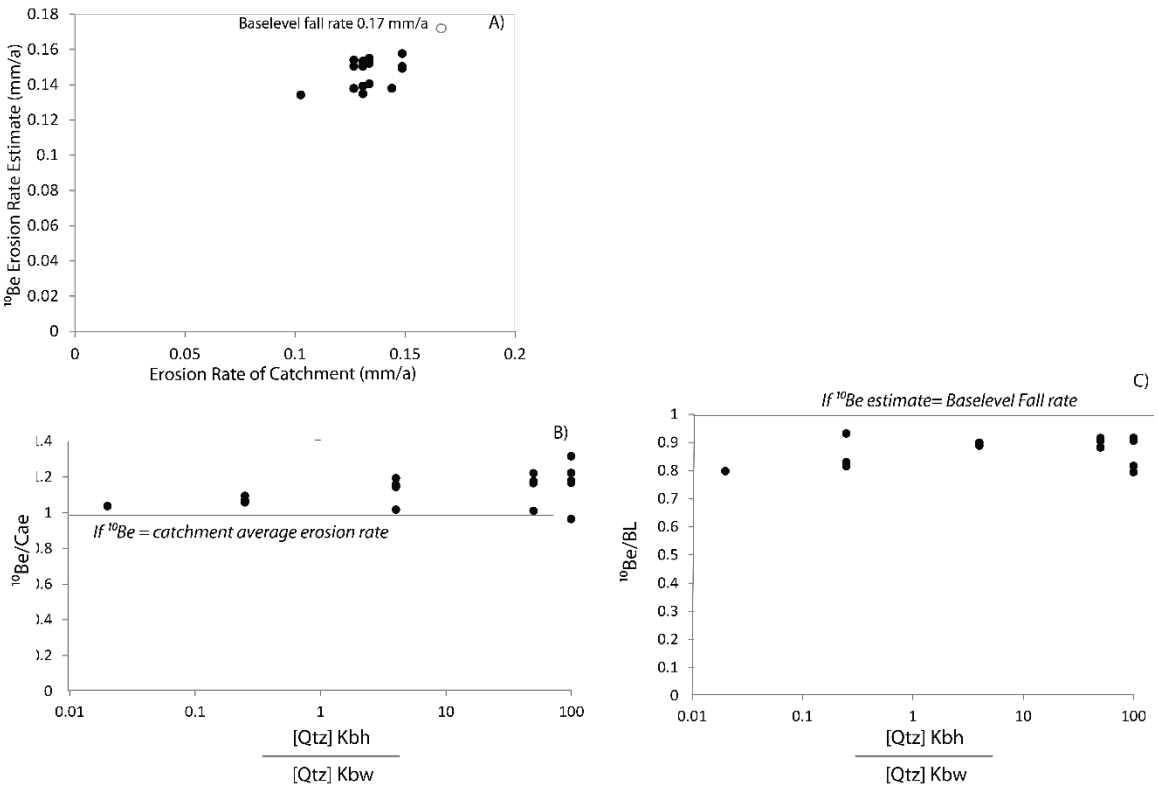

Figure 3.12. Numerically sampling the simulation output (a-d), for erosion rate from the model vs simulated CRN sampling of the synthetic landscape (b), erosion rate as a function of distance from scarp (c) and erosion rate as a function of quartz concentration in the 2-layer simulation (d). See also Appendix 3.6-3.10.

Figure 3.13. A) Road cut along US highway 89 (Photo-survey Site (pss) 8, Figure 3.7) exposing Cretaceous bedrock and Quaternary gravel that underlies Spencer Bench basalt flow. Strath is ~30 m above modern East Fork of Virgin River, Photo: Nari Miller. B) Photo looking approximately west, indurated gravel outcrop along US 89. Photo: Darling, (pss 12) C) North end of Spencer Bench basalt flow (pss 1). D) Basalt flow (Qb) on top of indurated gravels (Qa), over undifferentiated Cretaceous bedrock (Ku). Basalt base height ~104 m, Photo-survey site 11. E) Photo of hillslope sediment (gray) derived from Cretaceous units (Ku) and channel sediments apparently derived from the Claron Fm. (Tcp, pinkish-orange sediment). F) Rock Canyon basalt flow along Sevier River (~35 km North of Spencer Bench), basalt date ~5.45 Ma (see text).

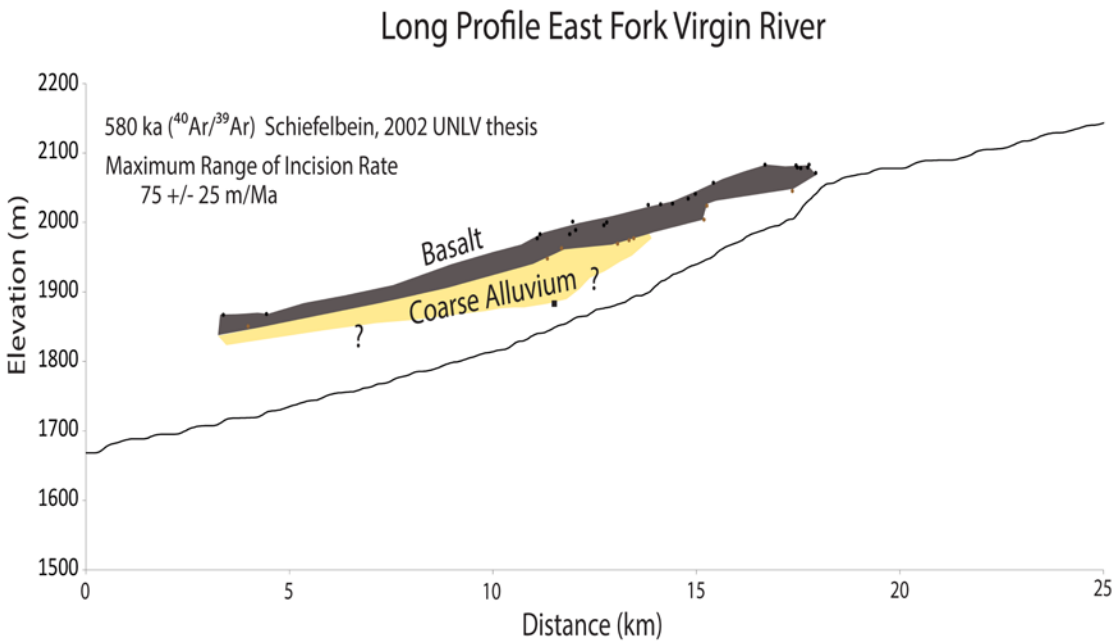

Figure 3.14. A) Long profile, surficial cross-section and geologic map from Sable and Hereford (2004). Spencer basalt flows are along East Fork of the Virgin River, Utah, parallel to US 89. Downstream of Stout canyon, quaternary alluvium is under basalt. Near site 1, coarse gravel alluvium is also present on top of basalt Red dots show position where photos were taken of basalt flows and range finder measurements were taken (Table 3.1). Basalt mapping is modified based on field checking: Qb near photo site 1 is added, noted by different shade of purple. The basalt flow here is partly covered by river gravel (See DR). The previously mapped flow just north of Glendale, Utah does not exist and the geologic map of Sable and Hereford (2004) correctly maps the lack of basalt on this hillside. Lydia's and Stout canyons are streams where cosmogenic erosion rate samples were collected. Geologic Units: Qb – Quaternary basalt flow, Tcp – Tertiary Claron Fm. Pink Member, Kk – Cretaceous Kaiparowits Fm. Kw – Cretaceous Wahweap Fm., Ksu Cretaceous Straight Cliffs Fm., Kt – Tropic Shale, Kdcm – Cretaceous Dakota/Cedar Mountain Fms., Jc(x) – Jurassic Carmel Fm., several members.

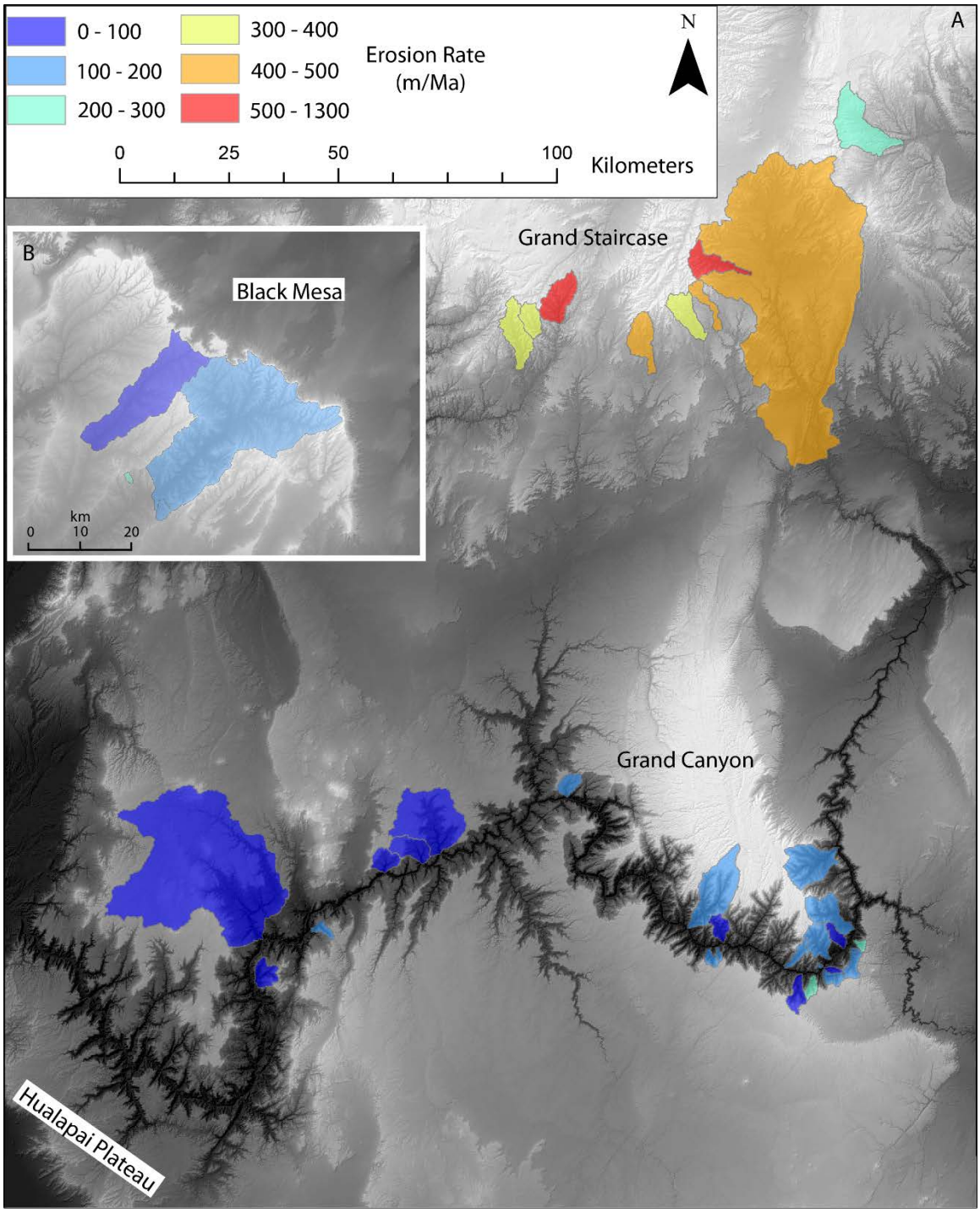

Figure 3.15. Watershed colored as erosion rates mapped on DEM/hill-shade base-map of Grand Canyon and Grand Staircase. Inset B) is Black Mesa, physically located east of Grand Canyon (see Figure 3.3). Tributaries on Black Mesa flow into Little Colorado River before flowing into the Grand Canyon (Figure 3.1).

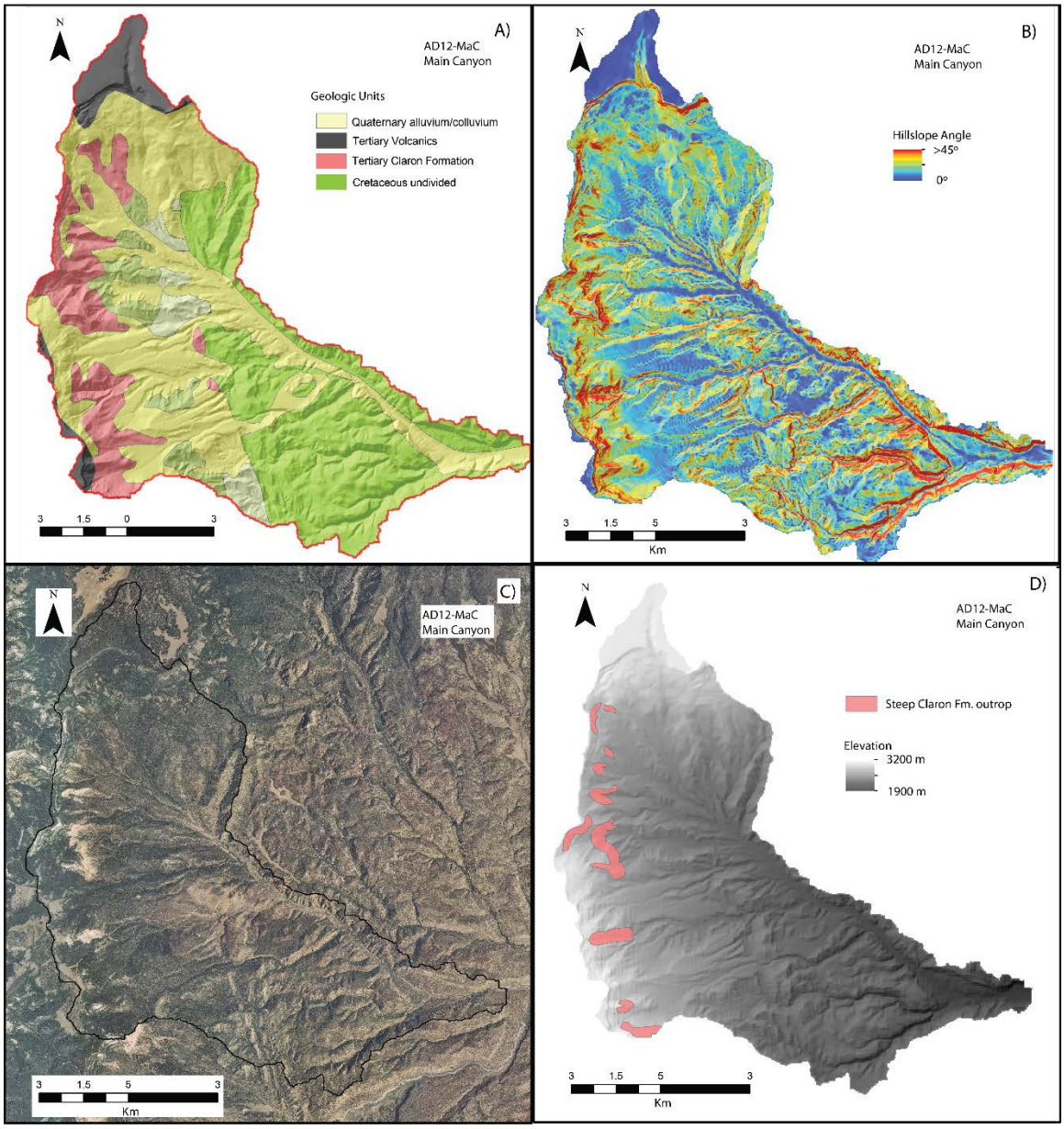

Figure 3.16. Example of determination of the map area of steep-walled, Claron Formation from Grand Staircase catchments. A) Geologic map (Sable and Hereford, 2004), B) slope map created in ArcGIS C) air photo NAIP, D), clipped polygons used to calculate contributing area of predicted dominant 10-Be signal source.

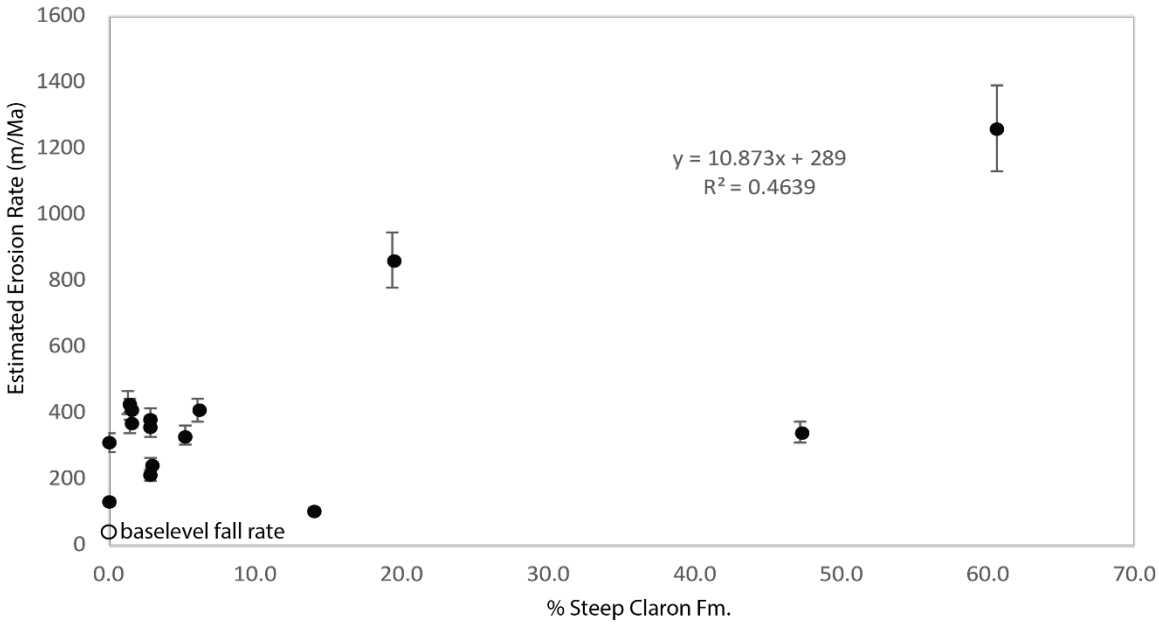

Figure 3.17. Erosion rate vs % of Claron Formation that is exposed in the catchment.

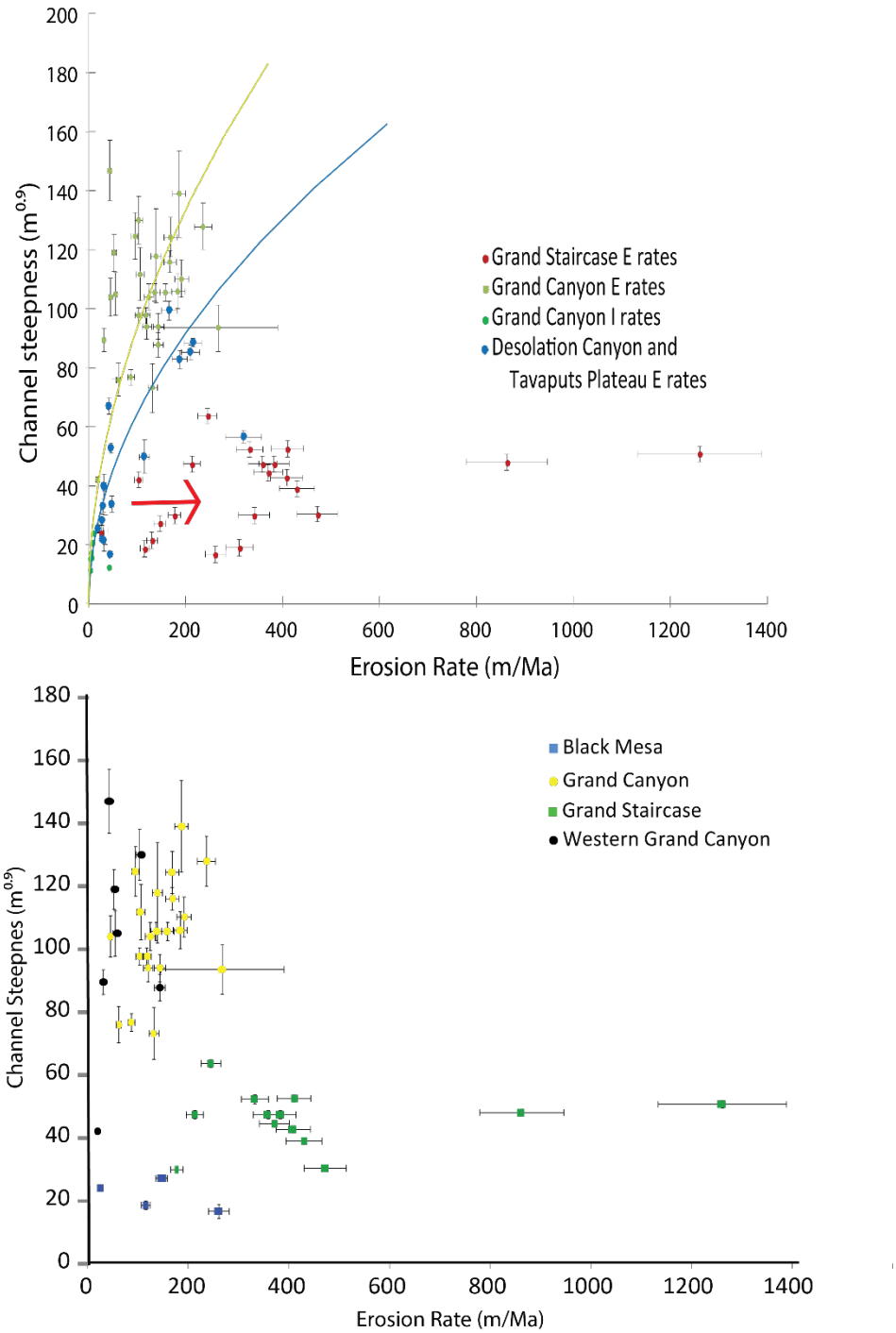

Figure 3.18. Channel steepness plotted as a function of erosion rate data a) colors indicate general source rock age, and incision rates from independent separate regions as in key. Note that data from Hualapai Plateau are incision rates reported in Darling and Whipple, 2015. Uncertainty in erosion rate is the 1-standard deviation analytical uncertainty and the uncertainty in channel steepness is one standard error of catchment average. In upper panel, the curves are theoretical curves (see DiBiase and Whipple, 2011) applicable to these datasets, where the main difference between Desolation and Grand Canyon data is local rock strength. The red dots from Grand Staircase appear skewed to extraordinarily high values by cliff erosion processes, as indicated by the red arrow.

Tables

Table 3.1. Spencer bench latitude, longitude of photo vantage point and height above river of apparent base of basalt flows.

	Figure in Paper	Latitude	Longitude	Height	Target
1	7c	37.39483	112.55779	3	Basalt
2		37.38303	112.57711	97	Basalt
3		37.38104	112.57940	77	Basalt
4		37.38058	112.57977	59	Basalt
5		37.37351	112.59343	84	Basalt
6		37.37280	112.59481	85	Basalt
7		37.37056	112.59500	87	Basalt
8	7a	37.36729	112.59386	30	Gravel/Ku strath
9		37.36312	112.59370	100	Basalt
10		37.36034	112.59818	110	Basalt
11	7d	37.35619	112.59942	104	Basalt
12	7b	37.35265	112.59774	n/a	
13		37.30938	112.59821	116	Basalt

Table 3.2. Table of channel steepness and ^{10}Be isotope data.

Sample Name	Mean Elev. (m)	K_{sn} Mean θ=0.45	std err	Conc. (atm/g)	Unc. (atm/g)	^{10}Be Std	Erosion rate (m/Ma)	error (m/Ma)	Latitude	Longitude
AD14-BM1	2147.9	**24.03**	0.5	557483.77	8256.70	NIST_27900	**25.2**	2	36.405	-110.254
AD14-BM2	2037.8	**16.67**	2.2	53278.17	1610.97	NIST_27900	**261.01**	20.77	36.250	-110.298
AD14-BM3	2009.8	**18.6**	1.4	116019.22	2936.00	NIST_27900	**115.87**	9.08	36.190	-110.225
AD14-BM4	2158.9	**27.17**	0.6	100335.35	2468.05	NIST_27900	**146.62**	11.52	36.344	-110.071
AD12-MePE	2294.7	**47.4**	1.3	44784.31	1469.63	NIST_27900	**358.91**	29.3	37.348	-112.221
AD12-MePE 2	2294.7	**47.4**	1.3	40982.93	1354.60	NIST_27900	**383.01**	31.2	37.348	-112.221
AD12-MuC	2108.2	**52.5**	1.1	34427.26	1201.39	NIST_27900	**410.31**	33.35	37.282	-112.691
AD12-PdC	2212.1	**42.7**	1.1	36498.35	1383.81	NIST_27900	**408.89**	33.99	37.366	-112.189
AD12-StC	2263.6	**50.7**	1.3	12251.51	842.05	NIST_27900	**1261.6**	127.65	37.379	-112.592
AD12-ThC	2121.3	**39.0**	1.1	32901.29	1258.41	NIST_27900	**430.16**	35.61	37.280	-112.346
AD12-UpperParia	1921.2	**30.4**	0.3	26818.82	1388.93	NIST_27900	**472.19**	42.01	37.108	-111.907
AD12-Wic	2269.3	**48.0**	1.1	17860.14	1101.70	NIST_27900	**863.16**	83.29	37.485	-112.100
KN GCPR-0	1874.8	**29.9**	0.4	46807.33	1123.63	07KNSTD	**177.3**	12.56	36.867	-111.593
AD13-Fishtail	1357.2	**87.7**	4.2	62830.89	1798.33	NIST_27900	**143.72**	10.81	36.403	-112.554
AD13-Cove	1505.2	**147.0**	10.1	226650.55	3886.90	NIST_27900	**42.85**	3.22	36.240	-113.015
AD13-Fernglen	1499.8	**105.0**	7.3	178223.54	3840.97	NIST_27900	**54.77**	4.14	36.260	-112.919
AD12-Tuckup	1596.3	**89.5**	3.9	318860.28	6091.63	NIST_27900	**31.24**	2.4	36.281	-112.875
KN GCRC-76	1495.6	**127.9**	8.0	41642.86	1282.61	07KNSTD	**236.27**	18.04	36.044	-111.921
KN GCTR-68	1196.1	**73.2**	8.2	61888.82	1675.01	07KNSTD	**131.87**	9.71	36.098	-111.829
KN GCHC-78	1695.3	**124.7**	7.9	114129.81	2660.23	07KNSTD	**95.1**	7.22	36.045	-111.952
KN GCTC-68	1575.0	**106.0**	5.9	56691.66	1504.59	07KNSTD	**184.27**	13.95	36.100	-111.830
KN GCTL-68	1604.0	**110.2**	6.3	54388.52	1215.66	07KNSTD	**191.73**	14.23	36.098	-111.829
KN GCBC-69	1391.3	**76.7**	2.8	103959.02	2907.13	07KNSTD	**87.34**	6.63	36.099	-111.844
KN GCCC-67	1370.5	**93.5**	7.8	34114.93	3571.25	KNSTD	**267.76**	122.68	36.115	-111.822
KN GCEC-75	1271.7	**76.0**	5.8	135241.95	4173.71	KNSTD	**61.92**	4.77	36.057	-111.895
KN GCL-75	1515.7	**124.4**	6.7	58736.91	2200.54	KNSTD	**168.24**	13.42	36.053	-111.900
KN GCUC-72	1585.5	**104.0**	4.5	82230.68	2491.26	KNSTD	**124.56**	9.64	36.077	-111.877
AD13-Vishnu 1	1531.4	**97.7**	2.7	95373.61	2551.21	NIST_27900	**103.62**	7.87	36.057	-111.995
KN GCMC-93	1418.0	**139**	14.6	50203.01	1089.21	07KNSTD	**186.34**	13.57	36.097	-112.184
KN GCR-75	1173.9	**111.8**	8.8	75568.18	3096.42	07KNSTD	**106.14**	8.5	36.059	-111.898
KN GCCC-99	1960.3	**116.0**	3.6	76039.79	1775.79	07KNSTD	**168.04**	12.89	36.136	-112.243
KN GCSC-92	1364.9	**117.9**	16.0	65069.42	1397.80	07KNSTD	**138.8**	10.1	36.099	-112.169
KN GCVC-81	1531.4	**97.7**	2.7	84031.43	1980.71	07KNSTD	**117.81**	8.8	36.056	-111.996
KN GCTC-91	1457.9	**104.0**	6.5	203483.91	4578.72	07KNSTD	**45.56**	3.46	36.108	-112.152
AD13-Lava/Chuar	1653.3	**94.0**	4.3	76127.39	2416.61	NIST_27900	**143.74**	11.28	36.139	-111.818
AD13-Nanko5	1765.9	**105.7**	2.9	72353.84	1923.36	NIST_27900	**159.1**	12.23	36.304	-111.865
KN GCLC-65	1653.3	**94.0**	4.3	88434.23	2743.88	KNSTD	**120.35**	9.4	36.139	-111.821
KN GCNC-52	1765.9	**105.7**	2.9	83689.35	2705.93	KNSTD	**136.26**	10.78	36.305	-111.862
AD12-Parash	1651.7	**42.1**	0.8	554040.92	8340.98	NIST_27900	**18.04**	1.41	36.097	-113.323
KN GCSC-190	1276.7	**130.0**	8.1	82289.44	1903.84	07KNSTD	**103.48**	7.57	36.122	-113.201
KN GCSC-205	1235.8	**119.0**	6.3	155553.08	4903.23	07KNSTD	**52.47**	4.07	36.008	-113.340

Table 3.3. Values for quartz sourcing and ^{10}Be simulations for Grand Staircase-like simulated landscape.

Table 3.3A	% Area		Quartz Flux %								Distribution of quartz (g/cm^3)		Quartz ratio
Site	Layer 1 (strong)	Layer 2 (weak)	Layer 1	Layer 2	Erosion Rate (mm/a)	^{10}Be E	Erosion rate ratio	^{10}Be / Base level Fall Rate	Distance from divide	BLF Rate (mm/a)	Layer 1	Layer 2	Layer 1/ Layer 2
1	1.028	98.972	0.030	99.970	0.209	0.215	1.026	2.387	3.000	0.090	0.020	2.000	0.010
2	56.890	43.100	0.362	99.638	0.146	0.145	0.995	1.609	5.400	0.090	0.020	2.000	0.010
4	45.856	54.144	0.306	99.694	0.139	0.137	0.983	1.521	6.300	0.090	0.020	2.000	0.010
5	15.577	84.423	0.167	99.833	0.168	0.163	0.973	1.814	6.300	0.090	0.020	2.000	0.010
2	61.000	39.000	9.700	90.300	0.145	0.143	0.986	1.589	5.400	0.090	0.020	0.080	0.250
3	1.160	98.840	2.449	97.551	0.201	0.200	0.995	2.222	3.000	0.090	0.020	0.080	0.250
1	0.000	100.000		100.00	0.249	0.245	0.984	2.722	1.500	0.090	1.000	1.000	1.000
2	59.600	40.400	29.000	71.00	0.147	0.144	0.980	1.600	5.400	0.090	1.000	1.000	1.000
3	4.865	95.135	2.734	97.266	0.201	0.197	0.985	2.193	3.000	0.090	1.000	1.000	1.000
1	0.000	100.000		100.00	0.251	0.232	0.924	2.578	1.500	0.090	2.000	1.000	2.000
2	42.000	58.000	57.000	43.000	0.145	0.145	1.000	1.611	5.400	0.090	2.000	1.000	2.000
2	42.000	58.000	56.000	44.000	0.146	0.146	1.000	1.622	5.400	0.090	0.080	0.020	4.000
3	2.997	97.003	17.273	82.727	0.200	0.190	0.949	2.112	3.000	0.090	0.080	0.020	4.000
5	16.419	83.581	63.660	36.339	0.167	0.175	1.044	1.940	6.300	0.090	0.200	0.020	10.000
1	72.299	27.701	97.003	2.997	0.200	0.181	0.903	2.010	3.000	0.090	0.500	0.010	50.000
2	62.330	32.330	95.900	4.090	0.145	0.162	1.117	1.797	5.400	0.090	0.500	0.010	50.000
4	94.823	5.177	49.595	50.405	0.140	0.167	1.193	1.857	6.300	0.090	0.500	0.010	50.000
5	16.419	83.581	89.754	10.247	0.167	0.180	1.077	2.001	6.300	0.090	0.500	0.010	50.000
1	0.000	100.000	0.000	100.00	0.229	0.123	0.537	1.367	1.500	0.090	2.000	0.020	100.000
2	62.335	37.665	97.911	2.009	0.145	0.164	1.129	1.817	5.400	0.090	2.000	0.020	100.000
3	2.997	97.003	83.923	16.077	0.200	0.180	0.900	2.002	3.000	0.090	2.000	0.020	100.000
4	48.695	51.305	97.310	2.687	0.140	0.172	1.227	1.910	6.300	0.090	2.000	0.020	100.000
6	0.000	100.000	0.000	100.00	0.250	0.111	0.444	1.233	1.200	0.090	2.000	0.020	100.000

Table 3.4. Values for quartz sourcing and ^{10}Be simulations for Grand Canyon-like simulated landscape.

	Proportion of Catchment (%)					Quartz Flux (%)										Quartz (g/cm^3)		Quartz Ratio
Site	Layer 1	Lyr 2	Lyr 3	Lyr 4	Lyr 5	Lyr 1	Lyr 2	Lyr 3	Lyr 4	Lyr 5	E (mm/a)	^{10}Be E	E ratio	^{10}Be/BL	Baselevel Fall Rate (mm/a)	Strong Layers	Weak Layers	Strong/ Weak
1	76.5	23.5	0.0	0.0	0.0	98.9	1.1	0.0	0.0	0.0	0.14	0.14	0.96	0.81	0.17	1.00	0.01	100.00
2	0.7	13.1	39.2	19.2	27.8	2.1	0.1	65.2	0.3	32.2	0.13	0.16	1.16	0.91	0.17	1.00	0.01	100.00
3	0.3	25.2	46.8	15.0	12.7	1.4	0.2	82.7	0.4	15.5	0.13	0.15	1.17	0.90	0.17	1.00	0.01	100.00
4	0.0	3.5	35.2	23.5	37.8	0.0	0.0	58.9	0.7	40.3	0.13	0.15	1.21	0.91	0.17	0.50	0.01	50.00
4	0.0	3.5	35.2	23.5	37.8	0.0	0.0	59.2	0.4	40.5	0.13	0.15	1.22	0.91	0.17	1.00	0.01	100.00
3	0.3	25.2	46.8	15.0	12.8	1.3	0.3	82.2	0.7	15.4	0.13	0.15	1.17	0.90	0.17	0.50	0.01	50.00
1	1.2	69.6	29.1	0.1	0.0	26.7	4.7	68.5	0.2	0.0	0.15	0.15	1.00	0.88	0.17	0.50	0.01	50.00
5	0.0	0.2	29.2	24.4	46.2	0.0	0.0	52.0	0.4	47.7	0.10	0.13	1.31	0.79	0.17	1.00	0.01	100.00
2	0.7	13.1	39.2	19.2	27.8	2.1	0.2	64.9	0.7	32.1	0.13	0.15	1.16	0.91	0.17	0.50	0.01	50.00
3	0.3	25.2	46.8	15.0	12.7	1.2	3.8	73.4	7.8	7.8	0.13	0.15	1.15	0.88	0.17	0.80	0.20	4.00
4	0.0	3.5	35.2	23.5	37.8	0.0	0.2	54.3	8.3	37.2	0.13	0.15	1.19	0.88	0.17	0.80	0.20	4.00
1	1.2	69.6	29.1	0.1	0.0	17.1	37.7	43.8	1.4	0.0	0.15	0.15	1.01	0.88	0.17	0.80	0.20	4.00
2	0.7	13.1	39.2	19.2	27.8	1.9	1.9	59.1	7.9	29.2	0.13	0.15	1.14	0.89	0.17	0.80	0.20	4.00
3	0.3	25.2	46.8	15.0	12.7	0.4	22.3	26.7	45.6	5.0	0.13	0.14	1.06	0.82	0.17	0.20	0.80	0.25
4	0.0	3.5	35.2	23.5	37.8	0.0	1.1	23.9	58.7	16.3	0.13	0.14	1.09	0.81	0.17	0.20	0.80	0.25
1	1.2	69.6	29.1	0.1	0.0	2.5	87.9	6.4	3.3	0.0	0.15	0.16	1.06	0.93	0.17	0.20	0.80	0.25
2	0.7	13.1	39.2	19.2	28.8	0.8	12.4	24.0	51.0	11.9	0.13	0.14	1.05	0.83	0.17	0.20	0.80	0.25
3	0.3	25.2	46.8	15.0	12.7	0.0	31.7	3.0	64.7	0.6	0.13	0.13	1.03	0.79	0.17	0.01	0.50	0.02
4	0.0	3.5	35.2	23.5	37.8	0.0	1.7	3.0	93.2	2.1	0.13	0.13	1.06	0.79	0.17	0.01	0.50	0.02
1	1.2	69.6	29.1	0.1	0.0	0.2	95.7	0.6	3.5	0.0	0.15	0.16	1.09	0.96	0.17	0.01	0.50	0.02
2	0.7	13.1	39.2	19.2	27.8	0.1	18.7	2.9	76.9	1.4	0.13	0.14	1.02	0.80	0.17	0.01	0.50	0.02
3	0.3	25.2	46.8	15.0	12.7	0.0	32.2	1.5	65.9	0.3	0.13	0.13	1.03	0.79	0.17	0.01	1.00	0.01
4	0.0	3.5	35.2	23.5	37.8	0.0	0.2	1.6	95.6	1.0	0.13	0.13	1.05	0.79	0.17	0.01	1.00	0.01
1	1.2	69.6	29.1	0.1	0.0	0.1	96.2	0.3	3.6		0.15	0.16	1.10	0.96	0.17	0.01	1.00	0.01
2	0.7	13.1	39.2	19.2	27.8	0.0	19.1	1.5	78.6	0.7	0.13	0.14	1.01	0.80	0.17	0.01	1.00	0.01
2	0.7	13.1	39.2	19.2	27.8	2.1	0.0	65.4	0.0	32.4	0.13	0.16	1.16	0.91	0.17	1.00	0.00	1000.00
2	0.7	13.1	39.2	19.2	27.8	0.0	19.5	0.2	80.3	0.1	0.13	0.14	1.01	0.80	0.17	0.00	1.00	0.00
3	0.3	25.2	46.8	15.0	12.7	0.0	32.8	0.2	67.0	0.0	0.13	0.13	1.03	0.79	0.17	0.00	1.00	0.00
4	0.0	3.5	35.2	23.5	37.8	0.0	1.8	0.2	97.9	0.1	0.13	0.13	1.05	0.78	0.17	0.00	1.00	0.00

Table 3.5. Erosion rate and Claron area for figures 3.11 and 3.12.

Sample Name	Erosion Rate	Unc.	Claron % Area
AD12-LyC	**332.39**	26.99	5.2
AD12-MaC	**245.09**	19.63	2.9
AD12-MCAF	**370.96**	29.83	1.5
AD12-MeM	**213.16**	16.95	2.8
AD12-MePE	**358.91**	29.3	2.8
AD12-MePE 2	**383.01**	31.2	2.8
AD12-MuC	**410.31**	33.35	1.5
AD12-PdC	**408.89**	33.99	6.1
AD12-StC	**1261.61**	127.65	60.6
AD12-ThC	**430.16**	35.61	1.3
AD12-Wic	**863.16**	83.29	19.4
AD14-MuC1	**341.39**	32.60	47.2
AD14-MuC2	**102.74**	8.46	14.0
AD14-MuC5	**311.02**	27.55	0
AD14-MuC6	**130.81**	11.09	0

CHAPTER 4 TRANSIENT INCISION DUE TO DRAINAGE INTEGRATION IN DESOLATION CANYON, UTAH

Andrew Darling, Kelin Whipple, Paul Bierman, Brian Clarke

Abstract

Desolation Canyon on the Colorado Plateau in Utah connects the Uinta Basin to the deeply exhumed central Colorado Plateau. Despite extensive research on the Colorado River system, unanswered questions persist about the integration history of the Colorado River, including the timing and series of events that led to the Green River's present form. This study uses channel profile analysis, erosion rates, and rock strength measures to evaluate four hypotheses for the formation of Desolation Canyon: (1) Steady base-level fall acting on variable rock strength, (2) isostatically tilted bedrock creating a base level fall gradient, (3) an increase in the rate of base level fall on the Colorado River, and (4) local incision acceleration due to top-down integration of the Green River across the Tavaputs Plateau.

High values of channel steepness on the Green River and tributaries are restricted to within Desolation canyon, implying that incision of the Canyon has been independent of uplift patterns and base level fall history along the Book Cliffs. This finding suggests that regional Colorado River base-level fall rate change or isostatic tilting are not major contributors to channel form in the canyon. Topography also varies without apparent relationship to rock types or units in most of Desolation Canyon. Further, seismic velocity measurements suggest only a factor of ~2 difference in strength from weakest to strongest rocks. Channel steepness differs by a factor of 5 between channels within the canyon and channels outside the canyon, suggesting that rock strength is not a significant control on topography. Erosion rates within the canyon are 5 times higher (220 m/Ma) than erosion rates outside the canyon (40 m/Ma), confirming a local transient response to erosion that is likely due to local, rapid increase in incision after integration of the Green River across the Tavaputs Plateau. Further, channel steepness patterns imply that the Green River integrated across the Tavaputs Plateau after much of the exhumation of Canyonlands in eastern Utah and into western Colorado was completed.

Introduction

Topography in eroding landscapes reflects the competition between the supply of rock through tectonic uplift and isostatic compensation, and the removal of rock by erosion processes, which are mediated by climate and controls on rock strength such as weathering, fracturing and intrinsic strength (Ahnert, 1970; Whipple et al., 1999a; Kirby and Whipple, 2012). The topology of a landscape, distinct from topography, is the spatial position of channels in a network that can change over time as divides migrate (e.g. Willett et al., 2014) and stream capture occurs (Hasbargen and Paola, 2000; Darling et al., 2009; Prince et al., 2011; Aslan et al., 2014) creating local changes in base-level fall rate and thus erosion rates. In Desolation Canyon on the Green River in Utah, USA (Figure 4.1), landscape evolution is influenced by the history of drainage network development, extensive exhumation, isostatic and tectonic rock uplift, and variable rock strength, complicating interpretation (Pederson and Tressler, 2012; Rosenberg et al., 2014). Parsing the effect of each on the topography and geomorphic history on this portion of the Colorado River system provides important information on the development of the Colorado River system including information about the sequence of integration events.

The canyons of the Colorado River system encompass diverse topographic expressions of landscape evolution through varied stratigraphy. Desolation Canyon in Utah has relatively simple stratigraphy, and exhibits a clear topographic expression of canyon erosion driven by base level fall of the Green River (Figure 4.1). The Colorado River and the Green River, its largest tributary, meet in Canyonlands on the central Colorado Plateau. Smaller tributaries respond to base level fall changes of these main-stem rivers, as may be recorded in slope-break knickpoints, though clear interpretation is complicated by variations in rock strength (e.g. Cook et al., 2009). The tributaries in Desolation Canyon have slope-break knickpoints that are sometimes close to unit contacts. The two primary units of interest are the generally slope forming, dominantly shale Green River Formation and the older, generally cliff-forming, dominantly sandstone Wasatch Formation. Desolation Canyon makes an excellent study area for evaluating the roles of rock strength, topographic metrics, and erosion-rate patterns for testing canyon-formation hypotheses where landscape evolution may be affected by several possible influences.

Detailed analysis of regional topography is used to decipher canyon evolution and relate morphometric analyses, erosion rates from cosmogenic methods, and relative rock strength inferred from shallow seismic methods. Independent measures of base-level fall rates, such as incision rates calculated from dating remnant river deposits at higher elevations than modern channels, provide a measure of local base level fall and temporal context to spatial erosion rate measurements (e.g. Anders and Pederson, 2002; Darling et al., 2012; Pederson et al., 2013a; Darling and Whipple, 2015).

Motivation

The canyons of the Colorado River system result from a series of tectonic, climatic and drainage reorganization events acting on a regionally varied substrate (Figure 4.2, Pederson et al., 2002a; Berlin and Anderson, 2007; Karlstrom et al., 2007; Donahue et al., 2013; Pederson et al., 2013a; Pederson et al., 2013b; Aslan et al., 2014; Crow et al., 2014). Contrasting lithologic strength is clearly manifest in the landscapes of the Colorado Plateau, where steep channels and hillslopes in canyons are commonly associated with strong rock units (e.g. Grams and Schmidt, 1999; Cook et al., 2009; Johnson et al., 2009; Pederson and Tressler, 2012; Donahue et al., 2013; Bursztyn et al., 2015).

Regional erosion has exhumed on the order of 2 km of rock along the Colorado River corridor in eastern Utah and western Colorado over the last 11 million years (Kelley and Blackwell, 1990; Pederson et al., 2002b; Hoffman, 2009; Aslan et al., 2010; Lazear et al., 2013). Recently acquired low-temperature thermochronometric data from the Canyonlands region suggest major denudation in Canyonlands <6 million years ago, and, possibly as recently as 2-3 million years ago, with average denudation rates up to 250-700 m/Ma (Murray et al., 2016). Average Colorado River incision in Canyonlands more recently (since 1.5 Ma) is slower (~60 m/Ma), but apparently accelerates again at about ~300 ka in Glen Canyon (Hanks et al., 2001; Garvin et al., 2005; Cook et al., 2009; Darling et al., 2012). Loosely constrained incision pulses recorded by thermochronometers may be related to drainage integration through Grand Canyon ~6 Ma (Karlstrom et al., 2008; Karlstrom et al., 2014; Darling and Whipple, 2015), which may

have produced a complex transient wave of incision (Cook et al., 2009; Darling et al., 2012). The pulse of incision recorded in the cooling ages on the plateau may be related to base level fall on the Green and Colorado rivers, and which could have affected upstream landscapes like Desolation Canyon. Incision rates on the Colorado River east of Desolation canyon show several consistent measurements of ~150 m/Ma from deposits of Lava Creek B ash (640 ka) and basalt flows up to 11 million years old (Willis and Biek, 2001; Darling et al., 2009; Aslan et al., 2010; Darling et al., 2012). The incision rate of the Green River has been estimated in two places near Desolation Canyon (Figure 4.2). Above the Desolation Canyon knickpoint, the incision rate is only ~40 m/Ma since 1.5 Ma (Darling et al., 2012). From below the knickpoint and south of the canyon, terraces and travertine cemented river gravel deposits yield age estimates that suggest high rates of bedrock incision, ~400 m/Ma over the last ~120 ka, suggesting the canyon may be a transient, rapidly evolving landform (Pederson et al., 2013a), but disparate positions of these incision rates in time and space complicate interpretation.

Incision magnitude, incision rate, discharge and topographic metrics like channel steepness and relief of the upper Colorado River system in Colorado have been compared to the same metrics in the Green River. Higher incision magnitude, incision rate, and discharge of the Colorado River is interpreted to suggest that the upper Colorado River and eastern tributaries to the Green River (Yampa, White, Little Snake) may be responding to a modest uplift gradient increasing toward the central Rocky Mountains due to variation in mantle buoyancy under the two regions (e.g. Darling et al., 2012; Karlstrom et al., 2012; Hansen et al., 2013; Rosenberg et al., 2014).

The details and significance of Desolation Canyon were not fully resolved in the scope of these previous studies. I present a detailed analysis of the canyon here based on the following research questions, in order of increasing breadth: (1) What are the erosion rates of tributaries in Desolation Canyon and on the surrounding rim? (2) How has rock strength variation in the canyon affected topography? (3) Do the knickpoints of Desolation Canyon indicate an increase in the rate of incision, and if so, what caused the erosion rate change? (4) When did the Green

integrate with the Colorado? (5) What is the relationship among topography, erosion rates, and rock strength in Desolation Canyon relative to other studies with similar data?

Geologic and Geomorphic Setting

Desolation Canyon is carved in the rocks of the Cretaceous/Paleogene boundary, which represent a transition from Cretaceous shallow-marine shales and sandstones to terrestrial fluvial sandstone (Wasatch Formation, Figure 4.3), conformably grading to and inter-fingering with lacustrine shale and fine sandstone of the Green River Formation (Green River Formation Figure 4.3). The Paleocene Wasatch (also called Colton Fm., Witkind, 1988) and Eocene Green River Fms. filled one of several closed-interior basins between block ranges uplifted in the Laramide orogeny (Dickinson et al., 1988) that continued to fill into the Miocene with sediments from the southwest Colorado Plateau and more local uplands (Davis et al., 2010; Dickinson et al., 2012).

Upstream of Desolation Canyon, the Green River system displays exhumation of 500-1000 meters that began less than 6-9 million years ago, after deposition of the Brown's Park Formation, although significant erosion could be younger (Hansen, 1986; Rosenberg et al., 2014). Hansen proposed an age of Canyon of Lodore, 130 km upstream of Desolation Canyon, of around 5 million years by extrapolating from a Lava Creek B ash bed (~640 ka) in a tributary stream terrace to the height of the modern canyon walls (Hansen, 1986). It is possible that Lodore and Desolation canyons may have integrated at similar times, but the relationship between these canyons is unclear.

Terraces in upper Desolation Canyon represent a firm geomorphic history but limited chronology data are available. Much of the incision of the Uinta basin and uppermost Desolation Canyon had to have been accomplished prior to 1.5 Ma, as incision on the Green River in the upper reach of Desolation Canyon is limited to 60 meters since then (terrace height, Figure 4.2, Darling et al., 2012). Terraces as high as 145 m above the Green River extend this incision record (Darling et al., 2012), but no terrace dates exist at present.

The earliest recognized evidence of a partially connected Colorado River system in western Colorado is a gravel deposit under 11 Ma basalt flows on Grand Mesa in western

Colorado (Figure 4.1) that is inferred to have flowed westward from the Rocky Mountains due to provenance of crystalline basement-derived clasts (Aslan et al., 2010). The destination of this river system, however, is not yet known. Thus far, compiled incision rates from typically Quaternary-age deposits (Dethier, 2001; Willis and Biek, 2001; Darling et al., 2009; Aslan et al., 2010; Darling et al., 2012; Aslan et al., 2014), show a gap of nearly 10 million years with data paucity between around 11 Ma and early Quaternary time.

Thermochronologic studies provide additional but less precise estimates of significant incision along the Colorado River corridor of eastern Utah and western Colorado in the last few million years. Different methods and significant error bounds, in addition to different sample locations, constrain accelerated erosion to have begun between 8 and 2 million years ago, which may reflect actual spatial and temporal variation in acceleration as much as uncertainties in the several applied methods (Kelley and Blackwell, 1990; Hoffman, 2009; Murray et al., 2016). Within the loosely constrained time of denudation of this landscape through the Miocene, tectonic activity may have local (Pederson et al., 2013a) and regional (Karlstrom et al., 2012), effects that also interact with isostatic rebound (Pederson et al., 2002b; Roy et al., 2009; Lazear et al., 2013; Pederson et al., 2013b). By working to understand the evolution of the landscape from intrinsic erosion controls and erosion rate patterns, the integration of the Green River through Desolation Canyon can be incorporated into the landscape evolution history of the Colorado Plateau.

Methods

Topographic Analysis

Channels set the boundary conditions for hillslope and cliff-face erosion, and thus are a key aspect of understanding the driving forces of canyon development. We use two different topographic datasets. For regional figures and calculations the digital elevation model is the 90 m resolution SRTM (Figure 4.4) data retrieved from the United States Geological Survey National Geologic Map Database (USGS_NGMD) collected by the Shuttle Radar Topography Mission (Farr et al., 2007). For figures and calculations focused on Desolation Canyon tributaries, we use

the 10 m USGS DEMs. For more detail than supplied here, see Wobus et al. (2006) on the methods of stream profile analysis.

The gradient of a river decreases downstream as discharge and contributing drainage area increase. An empirical relationship between slope (S) and drainage area (A) is commonly a power function (Hack, 1957; Flint, 1974) such that:

$$S = k_s A^{-\theta}, \quad (1)$$

where k_s and θ are termed channel steepness and concavity. For comparison between streams of different sizes, it is necessary to determine a representative θ value for reference, and recalculate channel steepness such that:

$$S = k_{sn} A^{-\theta_{ref}}, \quad (2)$$

where k_{sn} is the normalized channel steepness index and θ_{ref} is the reference concavity, defined in this paper as the typical value of 0.45 (e.g. Kirby and Whipple, 2012). Each of these parameters is easily obtained from actual stream profile data using the Profiler Toolbar in ArcMap and MATLAB (www.geomorphtools.org) or TopoToolbox in MATLAB (Schwanghart and Scherler, 2014). Channel steepness, k_{sn}, is a normalized channel gradient that allows comparison of different sized catchments. Applying this method to rivers requires using a minimum drainage area that is larger than the drainage area at which hillslope processes transition to channel processes.

For a landscape in steady state, rock upliftrate relative to base level (U) balances erosion rate (E) and the well-known stream power model of river incision can be written as:

$$U = E = KA^m S^n, \quad (3)$$

where *m* and *n* are process dependent, but usually satisfy *m/n* = ~0.5 (Howard, 1994; Whipple and Tucker, 1999). Solving (3) for slope at steady state and rearranging leads to an expression of slope as a function of drainage area, rock uplift (*U)*, and *K*, the erosional efficiency set by climate and rock properties:

$$S = (U/K)^{1/n} A^{-\frac{m}{n}} . \quad (4)$$

By inspection of equations (2) and (4),

$$k_{sn} = (U/K)^{1/n}. \quad (5)$$

In this steady-state formulation, *U* (rock uplift rate) and *E* (erosion rate) are interchangeable. The proportionality, *K*, based on the stream-power model, is referred to as erosional efficiency and is strongly affected by rock strength. High values of channel steepness may reflect either high base level fall rates, high rock uplift rates or a low coefficient of erosion (e.g., strong rock or a weakly-erosive climate). The exponent *n* influences the evolution of the shape of knickpoints (Tucker and Whipple, 2002). As illustrated in figure 4.5, high *n* values lead to more abrupt convex-up knickpoints, (panel c) while lower *n*-values progressively round or "diffuse" convex-up knickpoints. The relative smoothness of knickpoints may also be affected by the degree to which sediment is important to erosion: in a transport limited setting, periodic deposition and armoring of the channel bed can lead to broad, diffuse knickpoints, similar to the *n* > 1 model results (Tucker and Whipple, 2002).

An increase in the rate of base-level fall on a catchment should produce knickpoints that migrate upstream in all tributaries, where the channel segments below the knickpoints have higher channel steepness values (e.g., Darling and Whipple, 2015). Important distinctions about what has caused changes in a landscape among *U*, *E* and/or *K* in some cases can be inferred from the map patterns of channel steepness (e.g., Kirby and Whipple, 2012) to be discussed in this chapter.

In addition, we follow recent studies where channel steepness is related to erosion rate via an empirically determined power function (Lague et al., 2005; DiBiase and Whipple, 2011; Kirby and Whipple, 2012), such that:

$$k_{sn} = K' E^{a}, \quad (6)$$

where the exponent, *a, (*where *0<a<1)*, is theoretically set by runoff variability (Lague et al., 2005) and *K'* is related to erosional efficiency of the landscape (set by climate and rock properties, similar to *K* of equation 3, 4 and 5) as in equations 3-5. As denoted by 0 < *a* < 1, plots of k_{sn} vs E are typically convex-up curves (Figure 4.6). This comparison provides a direct visualization of how much change in topography results from a given change in erosion rate, which varies by how efficiently rock can be removed from a landscape (DiBiase and Whipple, 2011).

Erosion Rates from Cosmogenic Isotopes

The cosmogenic radionuclide (CRN) ^{10}Be is routinely measured to determine basin-averaged erosion rates from samples of modern stream sediment (Bierman and Steig, 1996; Granger et al., 1996; DiBiase et al., 2010; Portenga and Bierman, 2011; Granger et al., 2013; Willenbring et al., 2013). The erosion rate is inversely proportional to measured concentration that accumulates in the upper ~60 cm (determined by an e-folding depth derived from density) of rock during transport to the surface through erosion. Traditionally studies of ^{10}Be concentrations in detrital sediment have focused on catchments that are not dominated by landslides (Niemi et al., 2005), have uniform quartz distribution, and inferred, relatively uniform erosion rate. In this study, my sampling protocol required minimal mixing of rock units, so each sample is predominantly Green River Formation or Wasatch Formation (Figure 4.4). Both sedimentary units contain small amounts of quartz, but the Green River Formation typically contains less quartz, especially in the coarse grain fractions due to fine texture of lake and shallow stream deposits. Large samples were collected (up to ~3 gallons in total) to provide sufficient clean quartz for chemical analysis (20-100 grams) after careful processing to maximize clean quartz yield. Sand samples were sieved to remove grains <500 microns in diameter to reduce impact of potential eolian input, but this may incorporate a bias toward Wasatch Formation derived sediment where the unit is present as Wasatch Fm. is typically coarser-grained, making it more likely to yield quartz through sample processing. To remove this potential bias, catchments were carefully selected to represent only one geologic unit in most cases (Figures 4.4 and 4.3).

In order to preserve a clear relationship between erosion rate and topography, samples were collected in relatively small and relatively well-adjusted equilibrium (uniform k_{sn}) channels. This means that samples collected to represent the rim were taken from streams above major knickpoints (Figure 4.4). Further, sampled catchments within the canyon were chosen to minimize the contributing drainage area above knickpoints and to sample one stratigraphic unit at a time for clarity of interpretation (Figure 4.4 and 4.3).

Seismic Velocity Measurements

Empirical rock strength analysis in Desolation Canyon was conducted with geophysical techniques for comparison to topographic and erosion rate data. Rock mass strength is thought to be primarily controlled by fracture spacing, weathering, elastic moduli, mineralogy, porosity and density (Sjøgren et al., 1979; El-Naqa, 1996; Barton, 2007; Cha et al., 2009; Jaeger et al., 2009). Determining all of these variables at the field scale is not practical, however seismic refraction surveys integrate most of these variables across an outcrop and show value as a proxy for rock-mass strength and even erodibility (Suzuki, 1982; Stafleu et al., 1996; Hack, 2000; Clarke and Burbank, 2010, 2011). The relationship between impedance (V_p*density) and hillslope angle are characteristic for slope and cliff formers, where high impedance correlates to high hillslope angles (Stafleu et al., 1996). Engineering studies of "rippability", i.e., bulldozer operation as an erosion proxy, show that the excavation rate of rock mass increases rapidly as V_p decreases, particularly for rocks with V_p <3 km/s (MacGregor et al., 1994). From our data and supporting data in the literature, a quantifiable relationship between rock strength and V_p can be inferred.

To collect seismic refraction data, seismic source signals were produced by striking a metallic plate with a hammer at even (2-5 m) spacing along a string of geophones. Two 24-channel Geometrics Geode seismographs recorded the signal produced by 12-24 4.5 Hz vertical component geophones.

Seismic velocities were determined based on first-arrival times from the source to each geophone and inversions of the seismic data using standard seismic refraction techniques and SeisImager software (Sheriff and Geldart, 1995; Mussett and Khan, 2000; Forbriger, 2003a, b). We produced 2-D seismic refraction tomography to image spatial V_p variations of subsurface bedrock (Figure 4.7). The initial velocity model was produced by a simple time-term 2-3 layered inversion, to roughly differentiate bedrock from colluvial cover. This layered model was then used for the tomographic inversion using the shortest ray-path method (Moser, 1991) from each shot. The result is a 2-D image of the subsurface velocity structure capable of identifying lateral- and

depth-dependent variations in V_p and boundaries between colluvium and bedrock. The V_p values used here, as a proxy for rock-mass strength, represent the range of maximum velocities along the survey from the deepest ray-path, which for all surveys is either a ray through rock below a distinct colluvium-bedrock boundary or a direct ray along the surface if no carapace of regolith is present.

Results

Topographic Metrics

The gorge of Desolation Canyon is steep, with hillslopes near angle of repose and cliffs of sandstone (Figure 4.8). The gorge emerges from the low relief Uinta Basin (Figure 4.1) along the Green River and continues deepening towards the south (Figure 4.2, 4.3, 4.9). Near the deepest point of the canyon, channel steepness values reach 180 $m^{0.9}$, but are much lower everywhere outside of the canyon. The k_{sn} values of the upland landscape are typically less than 90 $m^{0.9}$. Hillslope angles along tributaries on the rims of the canyon (the Tavaputs Plateau) are also low (Figure 4.10).

A transect of mean k_{sn} of *tributaries* along the Green River yields a gradual increase and then a decrease through the knickzone (Figure 4.2, 4.3, 4.9, 4.11) ranging from ~30 to 180 $m^{0.9}$. Channel steepness characteristics of Desolation Canyon are unique in the region (Figure 4.2). The rest of the Book Cliffs, the north slope of the Tavaputs Plateau, and the northern portion of Canyonlands have channel steepness values (<90 $m^{0.9}$, usually <30 $m^{0.9}$) that are less than those in Desolation Canyon (120-180 $m^{0.9}$).

Cosmogenic Isotope Data

Erosion rates determined from cosmogenically produced ^{10}Be, as calculated with CRONUS using values in Table 4.1 and 4.2, yield 12 samples from the Tavaputs Plateau and upstream of the Green River knickpoint with average rate of 41 +/- 7 m/Ma (n=12, Figure 4.12). Within Desolation Canyon, 5 samples yield a mean erosion rate of 220 +/- 26 m/Ma (see also Tables 4.1 and 4.2). The 12 samples outside of the canyon yield remarkably similar rates given inherent uncertainties in the method. The 5 samples within Desolation Canyon range from 180 to

320 m/Ma, showing erosion within the canyon is occurring at a much higher rate than erosion outside of the canyon.

Figure 4.13 compares k_{sn} to E rates from catchments in Desolation Canyon as well as Grand Canyon and the Grand Staircase shown previously in this dissertation. As discussed below, one of the significant factors regarding the distribution of data on this plot is the inherent rock strength and other factors that affect erodibility.

Rock Strength Data

The rocks of Desolation Canyon display two primary stratigraphic units. There is a conformable inter-fingering transition from the Wasatch Formation to the overlying Green River Formation. Both units contain shale and sandstone beds, with Wasatch Formation dominated by thick, laterally continuous sandstone beds and Green River Formation is a series of mostly shale with thin sandstone beds (e.g. Gualtieri, 1988; Witkind, 1988; Weiss et al., 1990; Sprinkel, 2009).

The schematic stratigraphic column of Figure 4.14 represents positions of rock layers measured relative to their context within the stratigraphy (Figure 4.3). The surveys record ray path velocities with depths that are dependent on the length of the survey line (Figure 4.7) and yield V_p max measurements that range from 1.0-2.5 km/s in Desolation Canyon (Table 4.3). The Green River Formation V_p data range from 1.0 - 2.5 km/s, (n = 5); and the Wasatch Formation has V_p range 1.0 - 2.1 km/s, n=3. For both geologic units, relatively high V_p measurements (2.2-2.5 km/s) are primarily measures of the sandstone in the survey path. The shale layers within each unit have low V_p, 1.0-1.2 km/s.

Discussion

Topographic metrics, erosion rate, and rock strength together can distinguish among causes of transient incision in the history of Desolation Canyon. Channel steepness patterns are strong indicators of events in the history of erosion of Desolation Canyon. Cosmogenic erosion rates quantify base-level fall rate through mean erosion rate response. As posited for this study, the steep topography of the canyon might be the result of 4 testable types of transient landscape erosion: (1) erosionally resistant rock requires steeper channels but constant base-level fall rate,

(2) rock uplift via isostatic rebound, perhaps due to erosional unloading of the Colorado Plateau to the south, (3) base-level fall on the Colorado System driving a kinematic wave of erosion up Desolation Canyon, or (4) local increase in erosion rate (and steep channels) from the integration of the Green River with the Colorado River. In the absence of tectonic influence within the immediate area of the canyon, we turn to the topographic attributes of this unique landscape to decipher its erosional history.

Topographic Analysis

Hypothesis 1: Rock Strength

Regional mapping of channel steepness indicates that elevated k_{sn} values are restricted to the Green River and its small tributaries in the Desolation Canyon corridor (Figure 4.2). The steep-walled inner gorge of Desolation Canyon yields high channel steepness values (up to ~180 $m^{0.9}$) that are surrounded by much lower values on the rim and along the Book Cliffs (<50 $m^{0.9}$, Figures 4.2 and 4.3). Considering the proposed hypotheses for development of this canyon and the bedrock surrounding it, hypothesis (1) suggests that the strength of the Wasatch Formation is sufficient to cause the local steepness in the canyon without a base-level fall rate change. The Wasatch Formation extends east and west of Desolation Canyon (Figure 4.3), however, and the channels that erode Wasatch Formation are only relatively steep in tributaries that drain directly into the Green River within Desolation Canyon. This result implies either that Wasatch Formation rocks are much weaker immediately outside Desolation Canyon, or that rock strength is not the primary influence on the channel steepness pattern. Lateral facies changes do exist in the Wasatch Fm., but channel sands associated with the cliffs in Desolation Canyon persist through much of the unit in the Book Cliffs. Thus, we infer that rock strength variations do not offer a plausible explanation for the formation of Desolation Canyon.

Hypothesis 2: (Isostatic) Uplift Gradient

Regional variation of exhumation supports the possibility of a rock-uplift gradient between the Canyonlands region and the Uinta Basin due to significantly greater depths of exhumation in the Canyonlands region (Pederson et al., 2002b; Roy et al., 2009; Lazear et al., 2013). Isostatic

rebound could provide the rock uplift gradient for hypothesis (2) that may contribute to the gentle tilting of the sedimentary layers of the Tavaputs Plateau (Figure 4.3) and to channel steepness patterns in the Tavaputs Plateau. The expected channel-steepness gradient in response to this uplift gradient would be proportional to uplift and would be imposed on all channels experiencing the uplift gradient, not just the tributaries within the canyon itself. The transect of channel steepness within Desolation Canyon (Figure 4.11) is not a simple response that a rock uplift gradient might predict from erosional isostasy. In addition, streams dissecting the Book Cliffs adjacent to Desolation Canyon have uniformly low steepness values ~50 $m^{0.9}$). Flexural isostasy as a control on topographic form broadly influences topography, and would be expressed beyond the confines of Desolation Canyon (e.g. Lazear et al., 2013). The channel steepness patterns are inconsistent with an ongoing or recent uplift gradient in the immediate area. Thus, isostatic response to exhumation is not likely to exert a primary control on Desolation Canyon topography and erosion rates.

Hypothesis 3: Regional Base-level Fall Rate Change

The Colorado River is the base level for the Green River, and a change in base-level fall rate on the Colorado River would propagate upstream in all tributaries, including the Green River (Hypothesis 3). If Desolation Canyon and its knickpoint on the Green River are a response to a change in base level fall on the Colorado River, all of the surrounding streams connected to the Colorado River should have similar channel steepness patterns, albeit modulated by rock strength variations. Therefore, we would expect to see high channel steepness values in channels throughout the Book Cliffs in response to a recent increase in base level fall rate on the Colorado River. In figures 4.2 and 4.3, the relatively uniform, low channel steepness values of streams draining the Book Cliffs are not consistent with a changed base-level fall response to explain Desolation Canyon.

Hypothesis 4: Integration Across the Tavaputs Plateau

The Uinta Basin is low-relief with low channel steepness and rests at about 1400 m elevation (Figures 4.1 and 4.2). Downstream of Desolation Canyon, the Canyonlands region has

experienced up to ~2 km of erosion in the last ~10 million years (Pederson et al., 2002b; Lazear et al., 2013), and rests at approximately 1000 m elevation (Figure 4.15). The modern drop in elevation between the Uinta Basin and Canyonlands is a topographic step of around 170 m (excluding the elevated Tavaputs Plateau). If the major event driving erosion of Desolation Canyon is the connection of stream flow from the Uinta Basin into Canyonlands along the general path of Desolation Canyon, then the recent, relatively rapid geomorphic response should be localized to the connecting path in the vicinity of the capture or spillover point (Figure 4.15). The channel steepness values downstream of and surrounding the canyon are relatively low and uniform, indicating they are not responding to an increase in base-level fall rate to the extent that Desolation Canyon is. The knickpoints of Desolation Canyon tributaries could be the result of a local increase in base-level fall rate that would be expected from an integration event across a pre-existing Book Cliffs escarpment, connecting to the Colorado River after it had incised to near modern levels (Figure 4.15).

A knickpoint produced by a new connection from the nascent Green River in the Uinta Basin to the Colorado River somewhere around Canyonlands, should have triggered a kinematic wave of erosion that migrated upstream and incised a canyon into the upstream basin, with erosion focused at the spill point and consuming rock both up and downstream of the resulting knickpoint. Because this scenario does not provide a long-term change in overall base-level fall rate, the topographic response will change through time and space. In a given place, the local base-level fall rate will increase as the kinematic wave passes, and then decrease again. In a spatial transect up-canyon, a kinematic wave should be expressed by low, downstream base level fall rate and channel steepness values that increase upstream. These quantities should in reach a maximum and then decrease again upstream of the kinematic wave, particularly where channels are partially transport-limited or the incision process is best described by n less than unity in the stream power river incision model (Figure 4.5). In Desolation Canyon, the channel steepness values of tributary catchments (Figure 4.11) may be consistent with a snapshot of a kinematic wave migrating up Desolation Canyon that we hypothesize began when the Green River integrated across the Book Cliffs.

Eroding scarps like the Book Cliffs typically retreat fastest near large tributaries (e.g. Tucker and Slingerland, 1994; Berlin and Anderson, 2007). The location where Green River cuts through the Book Cliffs is only minimally embayed into a larger promontory, suggesting the canyon incision began after the Book Cliffs began to erode northward. Topographic analysis allows the inference that the Colorado River apparently developed a locally equilibrated network in eastern Utah sub-parallel to the portion of the modern Book Cliffs that are east of the Green River. Then, the Green River integrated across the Tavaputs Plateau, forming what became Desolation Canyon.

Rosenberg et al. (2014) suggest that the incision and integration of streams of the upper Green River system (White, Yampa, Little Snake Rivers) all occurred since about 6-9 Ma. The minimum age of integration is not well known, but certainly occurred before ~1.5 Ma as indicated by terrace ages in Desolation Canyon (Darling et al., 2012). From thermochronometric evidence it may be deduced that exhumation of the Canyonlands began by 6-8 Ma (Hoffman, 2009), and possibly as recently as 2-3 Ma (Murray et al., 2016).

The timing of the Green River integration across the Tavaputs Plateau is not well constrained, but inferences can be made from incision and erosion rate data. Previous terrace mapping in Desolation Canyon from Darling et al., (2012) reveal coarse, well rounded gravel up to 145 m above the Green River The only dated terrace within Desolation canyon is 60 m above the river (1.5 Ma; Darling et al., 2012). The apparent incision rate from this terrace (~40 m/Ma) is consistent with the CRN erosion rates in the surrounding landscape, showing relatively uniform erosion rate above the Desolation knickpoints. This estimate of incision initiation is a minimum due to terraces that are older than 1.5 Ma and higher than 60 m (up to 145 m) above the river in upper Desolation Canyon that have not been dated (See Figure 9 in Darling et al., 2012). Simple extrapolation of 40 m/Ma to 145 m suggests the canyon is ~3.5 million years old, assuming constant incision rate upstream of the knickpoint since canyon cutting began.

Erosion Rate Analysis

The comparison of topography (k_{sn}) and base level fall rate (inferred from CRN concentrations) in landscapes (Figure 4.13) provides useful contextual information about the controls on landscape evolution relative to other landscapes (e.g. DiBiase et al., 2010; Kirby and Whipple, 2012; Lague, 2014; Scherler et al., 2014; Roux-Mallouf et al., 2015; Adams et al., 2016). The high erosion rates show that the canyon is in dynamic readjustment, a landscape in transience as the knickpoints retreat. The Desolation data (blue dots) suggests erosion is slightly more efficient in the Tertiary rocks than the Paleozoic rocks. This is expected, as the Tertiary rocks are generally weaker, as seen from seismic surveys and observed in laboratory measurements of tensile strength (Bursztyn et al.,(2015). The Grand Staircase data record much higher erosion rates for similar mean channel steepness values despite rock properties similar to the substrate exposed in Desolation Canyon, suggesting that our detrital ^{10}Be concentrations are recording the locally high erosion rates associated with undermining of cliff-bands (Chapter 3) rather than the rate of base-level fall that sets mean channel steepness.

Within the Desolation Canyon data, a significant grouping separates the in-canyon, relatively high rates from the lower rate data from the plateau. These two groups approximately fall on a similar erosional efficiency line, which suggests the parameters that control the erosional efficiency, like rock strength, are not significantly different between the Green River and Wasatch Formations to separate significantly theoretical curves that represent the data. However, there is some evidence of secondary lithological effects. For example, one sample, AD15 - Deso 8, from Wire Fence Canyon, mostly samples a weaker member of the Wasatch Formation that resides below the significant cliffs of Wasatch sandstone, yielding lower channel steepness despite exhibiting a high erosion rate.

The Role of Rock Strength

Seismic surveys from the Colorado Plateau yield V_p ranging from 0.5 to >6.0 km/s (Darling et al., Chapter 3 of this dissertation), but rocks in Desolation Canyon all have V_p in the narrow range of 1.0 to 2.5 km/s. This small difference is the maximum range of velocities

between the most erodible shales to the strongest sandstones in the section. This small difference in V_p suggests that the contrast in average rock strength of the Green and Wasatch Fms. is likely insufficient to explain up to a factor of ~6 change in channel steepness (~180 vs ~30). Further evaluation of the relative strength inferred from this velocity contrast requires an estimate of the rock strength from independent data.

Intrinsic rock strength (as tensile strength of cores) and V_p of discs cut from cores are used to help interpret field seismic surveys in which bulk V_p is determined over length scales of 10s of meters and thus incorporates the effects of fractures, joints, bedding, and weathering. Field V_p measurements are thus always expected to be somewhat reduced from V_p measured on fresh rock cores but to be more reflective of effective rock strength. The relationship between rock tensile strength and V_p in cores help inform interpretation of field V_p data in terms of relative rock strength. The laboratory data presented below are for a range of rock types that form a quantitative relationship between tensile strength and V_p (Figure 4.17), and a measure of erodibility, the elastic modulus divided by the square of tensile strength from core data (Table 4.4, Sklar and Dietrich, 2001; Sklar, 2004; Johnson, 2007; Johnson et al., 2009). Comparing the relationship between elastic modulus, tensile strength and V_p from cores, (Figure 4.18), to the field V_p data, leads us to suggest the rock units of Desolation Canyon are both highly erodible, though the Wasatch Fm. is somewhat less so. This result is fully compatible with the topographic analysis presented above that argued that the steep topography of Desolation Canyon is more strongly influenced by erosion rate than by rock strength.

Additional rock strength data for Desolation Canyon in particular are available from Bursztyn et al., (2015) in the form of tensile strength measurements of hand samples of the Green River Formation (13 - 1 MPa, mean=6.72 +/- 1.69 s.d. MPa) and Wasatch Formation (9.35-0.75 MPa, mean= 4.85 +/- 1.27 MPa). These rock-strength estimates are from intact samples that were cored, which biases the tensile strength measurements from a particular rock formation because many weak sandstone and most shale samples within a given formation cannot survive collection and coring to be measured in the lab. Direct inference of the Bursztyn et al. (2015) data suggest that the rare, thin, sandstone layers within the Green River Formation are

stronger than the sandstones that comprise the bulk of the Wasatch Formation, as also indicated by our seismic data in Table 4.3. Because the Green River Formation is mostly shale (Figure 4.10), the measures of tensile strength of the thin sand beds are not representative of the overall erodibility, which must be much lower than the average tensile strength of sandstone cores. In general, the Green River Fm. is only slightly weaker than the Wasatch , which is consistent with the conclusion that rock strength contrast here is not able to influence topography enough to generate the form of Desolation Canyon(Pederson et al., 2013a)

Conclusion

I have used an evaluation of topography, erosion rates, incision rates and rock strength to test hypotheses of formation of Desolation Canyon. The steep inner canyon 180 $m^{0.9}$ and high erosion rates (~220 m/Ma) within indicate the canyon is fundamentally in dynamic adjustment to a significant change in local base level. This transient condition of growing relief indicates geologically recent change. The mechanism inferred from channel steepness patterns, where the canyon itself is adjacent to only lower channel-steepness values, appears best explained by a local increase in incision rate as a paleo-drainage divide on the Tavaputs Plateau was breached. The timing of this event is plausibly after the majority of the Canyonlands region was exhumed and a low, probably slowly eroding base level was established. The upstream migration of the Green River knickpoint has not affected the Green River above the Desolation Canyon knickpoint significantly, given the low erosion rates above the knickpoint. This work strongly suggests the Green River integrated into the Colorado River system after the Colorado River had been established in the Canyonlands region. While the timing of this is uncertain, our result that this integration event is relatively recent is significant to studies of Colorado River history and downstream sedimentation in the Gulf of California that may be affected by large changes in contributing drainage area and accompanying water and sediment from approximately half of the Colorado River system, as represented by the Green River.

References

Adams, B., Whipple, K., Hodges, K., and Heimsath, A., 2016, In-situ development of high-elevation, low-relief landscapes via duplex deformation in the Eastern Himalayan hinterland, Bhutan: Journal of Geophysical Research: Earth Surface.

Ahnert, F., 1970, Functional relationships between denudation, relief, and uplift in large mid-latitude drainage basins: American Journal of Science, v. 268, p. 243-263.

Anders, M. D., and Pederson, J., 2002, Implications of new Quaternary stratigraphic research and age control in eastern Grand Canyon for landscape evolution and lava-dam lakes: Abstracts with Programs, Geological Society of America, v. 34, p. 60.

Aslan, A., Hood, W. C., Karlstrom, K. E., Kirby, E., Granger, D. E., Kelley, S., Crow, R., Donahue, M. S., Polyak, V., and Asmerom, Y., 2014, Abandonment of Unaweep Canyon (1.4–0.8 Ma), western Colorado: Effects of stream capture and anomalously rapid Pleistocene river incision: Geosphere, v. 10, no. 3, p. 428-446.

Aslan, A., Karlstrom, K. E., Crossey, L. J., Kelley, S., Cole, R., Lazear, G., and Darling, A., 2010, Late Cenozoic evolution of the Colorado Rockies: Evidence for Neogene uplift and drainage integration: Field Guides, v. 18, p. 21-54.

Barton, N., 2007, Rock quality, seismic velocity, attenuation and anisotropy, CRC press.

Berlin, M. M., and Anderson, R. S., 2007, Modeling of knickpoint retreat on the Roan Plateau, western Colorado: Journal of Geophysical Research, v. 112, no. F3.

Bierman, P., and Steig, E. J., 1996, Estimating rates of denudation using cosmogenic isotope abundances in sediment: Earth Surface Processes and Landforms, v. 21, p. 125-139.

Bursztyn, N., Pederson, J., Tressler, C., Mackley, R., and Mitchell, K., 2015, Rock strength along a fluvial transect of the Colorado Plateau–quantifying a fundamental control on geomorphology: Earth and Planetary Science Letters, v. 429, p. 90-100.

Cha, M., Cho, G.-C., and Santamarina, J. C., 2009, Long-wavelength P-wave and S-wave propagation in jointed rock masses: Geophysics, v. 74, no. 5, p. E205-E214.

Clarke, B. A., and Burbank, D. W., 2010, Bedrock fracturing, threshold hillslopes, and limits to the magnitude of bedrock landslides: Earth and Planetary Science Letters, v. 297, no. 3, p. 577-586.

-, 2011, Quantifying bedrock-fracture patterns within the shallow subsurface: Implications for rock mass strength, bedrock landslides, and erodibility: Journal of Geophysical Research: Earth Surface, v. 116, no. F4.

Cook, K. L., Whipple, K. X., Heimsath, A. M., and Hanks, T. C., 2009, Rapid incision of the Colorado River in Glen Canyon–insights from channel profiles, local incision rates, and modeling of lithologic controls: Earth Surface Processes and Landforms, v. 34, no. 7, p. 994-1010.

Crow, R., Karlstrom, K., Darling, A., Crossey, L., Polyak, V., Granger, D., Asmerom, Y., and Schmandt, B., 2014, Steady incision of Grand Canyon at the million year timeframe: A case for mantle-driven differential uplift: Earth and Planetary Science Letters, v. 397, p. 159-173.

Darling, A., and Whipple, K., 2015, Geomorphic constraints on the age of the western Grand Canyon: Geosphere, v. 11, no. 4, p. 958-976.

Darling, A. L., Karlstrom, K., Granger, D. E., Aslan, A., Kirby, E., Ouimet, W. B., Lazear, G. D., Coblentz, D. D., and Cole, R. D., 2012, New incision rates along the Colorado River

system based on cosmogenic burial dating of terraces: implications for regional controls on Quaternary incision: Geosphere, v. 8, no. 5, p. 1020-1041.

Darling, A. L., Karlstrom, K. E., Aslan, A., Cole, R., Betton, C., and Wan, E., 2009, Quaternary incision rates and drainage evolution of the Uncompahgre and Gunnison Rivers, western Colorado, as calibrated by the Lava Creek B ash: Rocky Mountain Geology, v. 44, no. 1, p. 71-83.

Davis, S. J., Dickinson, W. R., Gehrels, G. E., Spencer, J. E., Lawton, T. F., and Carroll, A. R., 2010, The Paleogene California River: Evidence of Mojave-Uinta paleodrainage from U-Pb ages of detrital zircons: Geology, v. 38, no. 10, p. 931-934.

Dethier, D. P., 2001, Pleistocene incision rates in the western United States calibrated using Lava Creek B tephra: Geology, v. 29, no. 9, p. 783-786.

DiBiase, R. A., and Whipple, K. X., 2011, The influence of erosion thresholds and runoff variability on the relationships among topography, climate, and erosion rate: Journal of Geophysical Research, v. 116, no. F4.

DiBiase, R. A., Whipple, K. X., Heimsath, A. M., and Ouimet, W. B., 2010, Landscape form and millennial erosion rates in the San Gabriel Mountains, CA: Earth and Planetary Science Letters, v. 289, no. 1-2, p. 134-144.

Dickinson, W. R., Klute, M. A., Hayes, M. J., Janecke, S. U., Lundin, E. R., McKittrick, M. A., and Olivares, M. D., 1988, Paleogeographic and paleotectonic setting of Laramide sedimentary basins in the central Rocky Mountain region: Geological Society of America Bulletin, v. 100, no. 7, p. 1023-1039.

Dickinson, W. R., Lawton, T. F., Pecha, M., Davis, S. J., Gehrels, G. E., and Young, R. A., 2012, Provenance of the Paleogene Colton Formation (Uinta Basin) and Cretaceous–Paleogene provenance evolution in the Utah foreland: Evidence from U-Pb ages of detrital zircons, paleocurrent trends, and sandstone petrofacies: Geosphere, v. 8, no. 4, p. 854-880.

Donahue, M. S., Karlstrom, K., Aslan, A., Darling, A., Granger, D., Wan, E., Dickinson, R., and Kirby, E., 2013, Incision history of the Black Canyon of Gunnison, Colorado, over the past~ 1 Ma inferred from dating of fluvial gravel deposits: Geosphere, v. 9, no. 4, p. 815-826.

El-Naqa, A., 1996, Assessment of geomechanical characterization of a rock mass using a seismic geophysical technique: Geotechnical & Geological Engineering, v. 14, no. 4, p. 291-305.

Farr, T. G., Rosen, P. A., Caro, E., Crippen, R., Duren, R., Hensley, S., Kobrick, M., Paller, M., Rodriguez, E., and Roth, L., 2007, The shuttle radar topography mission: Reviews of Geophysics, v. 45, no. 2.

Flint, J. J., 1974, Stream gradient as a function of order, magnitude, and discharge: Water Resources Research, v. 10, p. 969-973.

Forbriger, T., 2003a, Inversion of shallow-seismic wavefields: I. Wavefield transformation: Geophysical Journal International, v. 153, no. 3, p. 719-734.

-, 2003b, Inversion of shallow-seismic wavefields: II. Inferring subsurface properties from wavefield transforms: Geophysical Journal International, v. 153, no. 3, p. 735-752.

Garvin, C. D., Hanks, T. C., Finkel, R. C., and Heimsath, A. M., 2005, Episodic incision of the Colorado River in Glen Canyon, Utah: Earth Surface Processes and Landforms, v. 30, no. 8, p. 973-984.

Grams, P. E., and Schmidt, J. C., 1999, Geomorphology of the Green River in the eastern Uinta Mountains, Dinosaur National Monument, Colorado and Utah: Varieties of fluvial form, p. 81-111.

Granger, D. E., Kirshner, J. W., and Finkel, R., 1996, Spatially averaged long-term erosion rates measured from in situ-produced cosmogenic nuclides in alluvial sediment: Journal of Geology, v. 104, no. 3, p. 249-257.

Granger, D. E., Lifton, N. A., and Willenbring, J. K., 2013, A cosmic trip: 25 years of cosmogenic nuclides in geology: Geological Society of America Bulletin, v. 125, no. 9-10, p. 1379-1402.

Gualtieri, J. L., 1988, Geologic map of the Westwater 30'x 60'Quadrangle, Grand and Uinta counties, Utah and Garfield and Mesa counties, Colorado.

Hack, J. T., 1957, Studies of longitudinal stream profiles in Virginia and Maryland: U.S. Geological Survey Professional Paper, v. 294-B, p. 97.

Hack, R., 2000, Geophysics for slope stability: Surveys in geophysics, v. 21, no. 4, p. 423-448.

Hanks, T. C., Lucchitta, I., Davis, S. W., Davis, M. E., Finkel, R. C., Lefton, S. A., and Garvin, C. D., 2001, The Colorado River and the age of Glen Canyon: The Colorado River: Origin and Evolution: Grand Canyon, Arizona, Grand Canyon Monograph, v. 12, p. 129-133.

Hansen, S. M., Dueker, K. G., Stachnik, J. C., Aster, R. C., and Karlstrom, K. E., 2013, A rootless rockies—Support and lithospheric structure of the Colorado Rocky Mountains inferred from CREST and TA seismic data: Geochemistry, Geophysics, Geosystems, v. 14, no. 8, p. 2670-2695.

Hansen, W. R., 1986, Neogene tectonics and geomorphology of the eastern Uinta Mountains in Utah, Colorado, and Wyoming: United States Geological Survey, Professional Paper;(USA), v. 75, no. 1356.

Hasbargen, L. E., and Paola, C., 2000, Landscape instability in an experimental drainage basin: Geology, v. 28, no. 12, p. 1067-1070.

Hoffman, M., 2009, Mio-Pliocene erosional exhumation of the central Colorado Plateau, eastern Utah: New insights from apatite (U-Th)/He thermochronometry: University of Kansas.

Howard, A. D., 1994, A detachment-limited model of drainage basin evolution: Water Resources Research, v. 30, no. 7, p. 2261-2285.

Jaeger, J. C., Cook, N. G., and Zimmerman, R., 2009, Fundamentals of rock mechanics, John Wiley & Sons.

Johnson, J. P., 2007, Feedbacks between erosional morphology, sediment transport and abrasion in the transient adjustment of fluvial bedrock channels. [Ph.D. thesis: Massachusetts Institute of Technology.

Johnson, J. P., Whipple, K. X., Sklar, L. S., and Hanks, T. C., 2009, Transport slopes, sediment cover, and bedrock channel incision in the Henry Mountains, Utah: Journal of Geophysical Research: Earth Surface (2003–2012), v. 114, no. F2.

Karlstrom, K., Coblentz, D., Dueker, K., Ouimet, W., Kirby, E., Van Wijk, J., Schmandt, B., Kelley, S., Lazear, G., and Crossey, L., 2012, Mantle-driven dynamic uplift of the Rocky Mountains and Colorado Plateau and its surface response: Toward a unified hypothesis: Lithosphere, v. 4, no. 1, p. 3-22.

Karlstrom, K. E., Crow, R., Crossey, L. J., Coblentz, D., and Van Wijk, J. W., 2008, Model for tectonically driven incision of the younger than 6 Ma Grand Canyon: Geology, v. 36, no. 11, p. 835.

Karlstrom, K. E., Crow, R. S., Peters, L., McIntosh, W., Raucci, J., Crossey, L. J., Umhoefer, P., and Dunbar, N., 2007, 40Ar/39Ar and field studies of Quaternary basalts in Grand Canyon and model for carving Grand Canyon: Quantifying the interaction of river incision and normal faulting across the western edge of the Colorado Plateau: Geological Society of America Bulletin, v. 119, no. 11-12, p. 1283-1312.

Karlstrom, K. E., Lee, J. P., Kelley, S. A., Crow, R. S., Crossey, L. J., Young, R. A., Lazear, G., Beard, L. S., Ricketts, J. W., and Fox, M., 2014, Formation of the Grand Canyon 5 to 6 million years ago through integration of older palaeocanyons: Nature Geoscience, v. 7, p. 239-244.

Kelley, S. A., and Blackwell, D. D., 1990, Thermal history of the multi-well experiment (MWX) site, Piceance Creek Basin Northwestern Colorado, derived from fission-track analysis: International Journal of Radiation Applications and Instrumentation. Part D. Nuclear Tracks and Radiation Measurements, v. 17, no. 3, p. 331-337.

Kirby, E., and Whipple, K. X., 2012, Expression of active tectonics in erosional landscapes: Journal of Structural Geology, v. 44, p. 54-75.

Lague, D., 2014, The stream power river incision model: evidence, theory and beyond: Earth Surface Processes and Landforms, v. 39, no. 1, p. 38-61.

Lague, D., Hovius, N., and Davy, P., 2005, Discharge, discharge variability, and the bedrock channel profile: Journal of Geophysical Research: Earth Surface (2003–2012), v. 110, no. F4.

Lazear, G., Karlstrom, K., Aslan, A., and Kelley, S., 2013, Denudation and flexural isostatic response of the Colorado Plateau and southern Rocky Mountains region since 10 Ma: Geosphere, v. 9, no. 4, p. 792-814.

MacGregor, F., Fell, R., Mostyn, G., Hocking, G., and McNally, G., 1994, The estimation of rock rippability: Quarterly Journal of Engineering Geology and Hydrogeology, v. 27, no. 2, p. 123-144.

Moser, T., 1991, Shortest path calculation of seismic rays: Geophysics, v. 56, no. 1, p. 59-67.

Murray, K., Reiners, P., and Thomson, S., 2016, Rapid Pliocene–Pleistocene erosion of the central Colorado Plateau documented by apatite thermochronology from the Henry Mountains: Geology, v. 44, no. 6, p. 483-486.

Mussett, A. E., and Khan, M. A., 2000, Looking into the earth: an introduction to geological geophysics, Cambridge University Press.

Niemi, N. A., Oskin, M., Burbank, D. W., Heimsath, A. M., and Gabet, E. J., 2005, Effects of bedrock landslides on cosmogenically determined erosion rates: Earth and Planetary Science Letters, v. 237, no. 3-4, p. 480-498.

Pederson, J., Burnside, N., Shipton, Z., and Rittenour, T., 2013a, Rapid river incision across an inactive fault—Implications for patterns of erosion and deformation in the central Colorado Plateau: Lithosphere, v. 5, no. 5, p. 513-520.

Pederson, J., Karlstrom, K., Sharp, W., and McIntosh, W., 2002a, Differential incision of the Grand Canyon related to Quaternary faulting - Constraints from U-series and Ar/Ar dating: Geology, v. 30, no. 8, p. 739-742.

Pederson, J. L., Cragun, W. S., Hidy, A. J., Rittenour, T. M., and Gosse, J. C., 2013b, Colorado River chronostratigraphy at Lee's Ferry, Arizona, and the Colorado Plateau bull's-eye of incision: Geology, v. 41, no. 4, p. 427-430.

Pederson, J. L., Mackley, R. D., and Eddleman, J. L., 2002b, Colorado Plateau uplift and erosion evaluated using GIS: GSA Today, v. 12, no. 8, p. 4-10.

Pederson, J. L., and Tressler, C., 2012, Colorado River long-profile metrics, knickzones and their meaning: Earth and Planetary Science Letters, v. 345, p. 171-179.

Portenga, E. W., and Bierman, P. R., 2011, Understanding Earth's eroding surface with 10Be: GSA Today, v. 21, no. 8, p. 4-10.

Prince, P. S., Spotila, J. A., and Henika, W. S., 2011, Stream capture as driver of transient landscape evolution in a tectonically quiescent setting: Geology, v. 39, no. 9, p. 823-826.

Rosenberg, R., Kirby, E., Aslan, A., Karlstrom, K., Heizler, M., and Ouimet, W., 2014, Late Miocene erosion and evolution of topography along the western slope of the Colorado Rockies: Geosphere, v. 10, no. 4, p. 641-663.

Roux-Mallouf, L., Godard, V., Cattin, R., Ferry, M., Gyeltshen, J., Ritz, J. F., Drupka, D., Guillou, V., Arnold, M., and Aumaître, G., 2015, Evidence for a wide and gently dipping Main Himalayan Thrust in western Bhutan: Geophysical Research Letters, v. 42, no. 9, p. 3257-3265.

Roy, M., Jordan, T. H., and Pederson, J., 2009, Colorado Plateau magmatism and uplift by warming of heterogeneous lithosphere: Nature, v. 459, no. 7249, p. 978-982.

Scherler, D., Bookhagen, B., and Strecker, M. R., 2014, Tectonic control on 10Be-derived erosion rates in the Garhwal Himalaya, India: Journal of Geophysical Research: Earth Surface, v. 119, no. 2, p. 83-105.

Schwanghart, W., and Scherler, D., 2014, Short Communication: TopoToolbox 2-MATLAB-based software for topographic analysis and modeling in Earth surface sciences: Earth Surface Dynamics, v. 2, no. 1, p. 1.

Sheriff, R. E., and Geldart, L. P., 1995, Exploration seismology, Cambridge university press.

Sjøgren, B., Øfsthus, A., and Sandberg, J., 1979, Seismic Classification of Rock Mass QUALITIES*: Geophysical Prospecting, v. 27, no. 2, p. 409-442.

Sklar, L. S., 2004, A mechanistic model for river incision into bedrock by saltating bed load: Water Resources Research, v. 40, no. 6.

Sklar, L. S., and Dietrich, W. E., 2001, Sediment and rock strength controls on river incision into bedrock: Geology, v. 29, no. 12, p. 1087-1090.

Sprinkel, D. A., 2009, Interim Geologic Map of the Seep Ridge 30'X 60'Quadrangle, Uintah, Duchesne, and Carbon counties, Utah, and Rio Blanco and Garfield Counties, Colorado: Utah Geological Survey Open-File Report 549DM.

Stafleu, J., Schlager, W., Everts, A., J., K., Blommers, G., and A., v., 1996, Outcrop topography as a proxy of acoustic impedance in synthetic seismograms: Geophysics, v. 61, no. 6, p. 1779-1788.

Suzuki, T., 1982, Rate of lateral planation by Iwaki River, Japan: Transactions, Japanese Geomorphological Union, v. 3, no. 1, p. 1-24.

Tucker, G. E., and Slingerland, R. L., 1994, Erosional dynamics, flexural isostacy, and long-lived escarpments: a numerical modeling study: Journal of Geophysical Research, v. 99, p. 12,229-212,243.

Tucker, G. E., and Whipple, K., 2002, Topographic outcomes predicted by stream erosion models: Sensitivity analysis and intermodel comparison: Journal of Geophysical Research, v. 107, no. B9.

Weiss, M. P., Witkind, I. J., and Cashion, W. B., 1990, Geologic map of the Price 30'x 60'Quadrangle, Carbon, Duchesne, Uinta, Utah and Wasatch counties, Utah.

Whipple, K., Kirby, E., and Brocklehurst, S., 1999, Geomorphic limits to climatically induced increases in topographic relief: Nature, v. 401, p. 39-43.

Whipple, K. X., and Tucker, G. E., 1999, Dynamics of the stream-power river incision model: Implications for height limits of mountain ranges, landscape response timescales, and research needs: Journal of Geophysical Research, v. 104, no. B8, p. 17661-17617,17674.

Willenbring, J. K., Gasparini, N. M., Crosby, B. T., and Brocard, G., 2013, What does a mean mean? The temporal evolution of detrital cosmogenic denudation rates in a transient landscape: Geology, v. 41, no. 12, p. 1215-1218.

Willett, S. D., McCoy, S. W., Perron, J. T., Goren, L., and Chen, C.-Y., 2014, Dynamic reorganization of river basins: Science, v. 343, no. 6175, p. 1248765.

Willis, G. C., and Biek, R., 2001, Quaternary incision rates of the Colorado River and major tributaries in the Colorado Plateau, Utah: Colorado River: Origin and evolution: Grand Canyon, Arizona, Grand Canyon Association, p. 125-127.

Witkind, I. J., 1988, Geologic Map of the Huntington 30'X 60'Quadrangle, Carbon, Emery, Grand, and Uintah Counties, Utah.

Wobus, C. W., Whipple, K. W., Kirby, E., and Snyder, N. P., 2006, Tectonics from topography: Proceedures, promise, and pitfalls, *in* Willett, S. D., Hovius, N., Brandon, M., and Fisher, D. M., eds., Climate, Tectonics and Landscape Evolution: Geological Society of America Special Paper, Volume 398, Penrose Conference Series, p. 55-74.

Figures

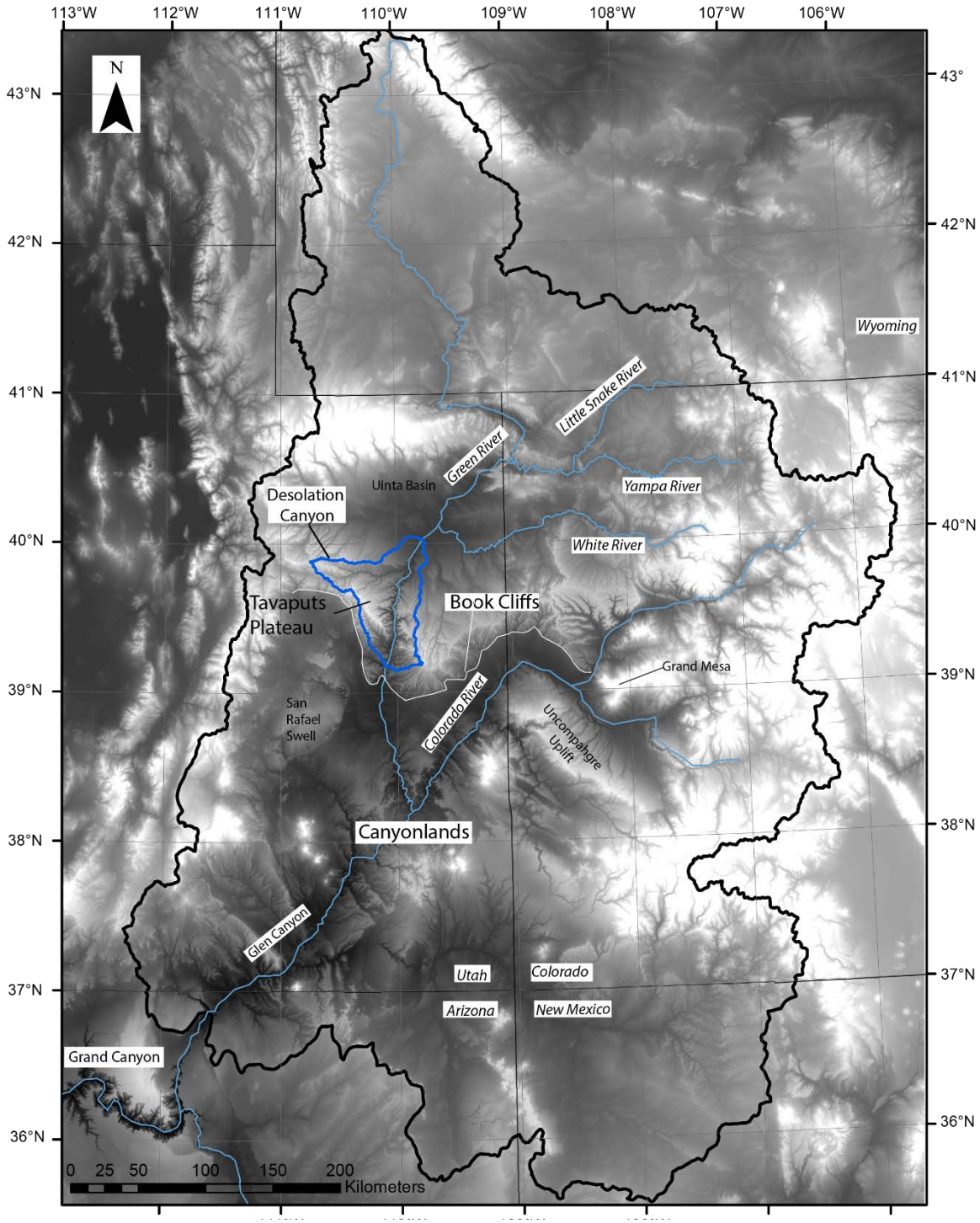

Figure 4.1. Colorado River watershed outlined on digital elevation model over hill-shade with key locations identified. The sub-watershed of tributaries to Desolation Canyon is outlined in blue along the Green River.

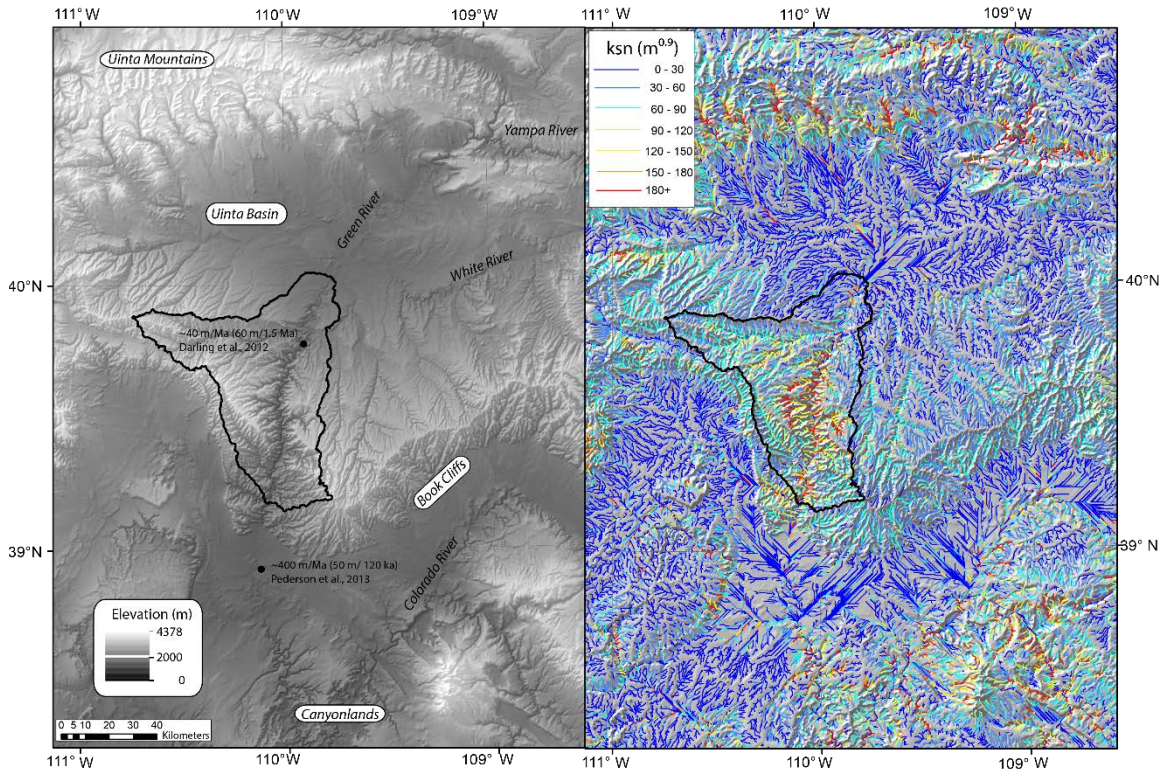

Figure 4.2. Comparison of topography (a) to channel steepness patterns over hill-shade (b) in the region of Desolation Canyon. The watershed for tributaries that flow into Desolation Canyon is outlined in black in both a) and b). In a), black circles indicate location of incision rate markers with rate, date and maximum dated terrace height of the study printed (Darling et al., 2012; Pederson et al., 2013a). Channel steepness is calculated based on $\theta_{ref} = 0.45$ (ksn units = m0.9). DEM is SRTM, 90m pixel-size. Note that unnaturally straight, low steepness channels are the result of DEM pixel-size in low relief areas. These channels, especially in the low portions of the Uinta Basin and below the Book Cliffs, are produced when the TopoToolbox algorithm cannot find a channel and draws a straight line across the flat portion of the DEM. These are not directly interpretable except that the channels and hillslopes are very low gradient.

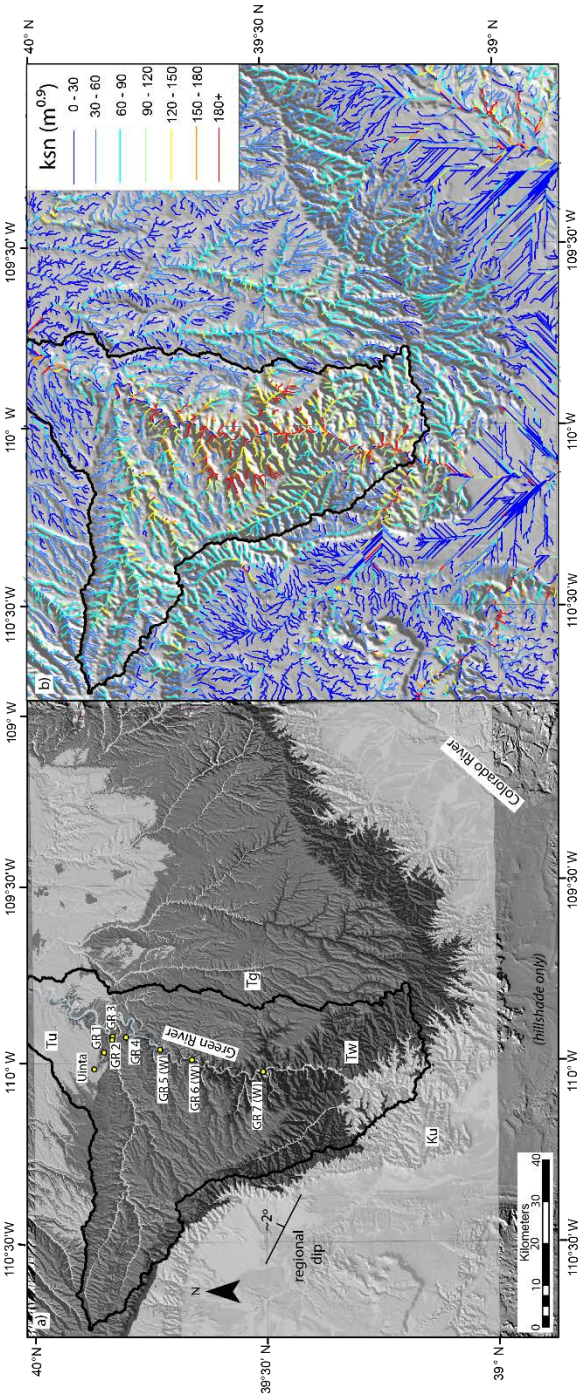

Figure 4.3. Comparison of geology (Tw = Wasatch Formation; Tg = Green River Formation). (a) to channel steepness patterns over hillshade (b) in the region of Desolation Canyon. The watershed for tributaries that flow into Desolation Canyon is outlined in black in both a) and b). In a), yellow circles indicate location of rock strength measurements with seismic surveys. Channel steepness is calculated based on θref = 0.45 (ksn units = m0.9). DEM is SRTM, 90m pixel-size. Note that unnaturally straight, low steepness channels are the result of DEM pixel-size in low relief areas. These channels, especially in the low portions of the Uinta Basin and below the Book Cliffs, are produced when the TopoToolbox algorithm cannot find a channel and draws a straight-line across the flat portion of the DEM. These are not directly interpretable except that the channels and hillslopes are very low gradient.

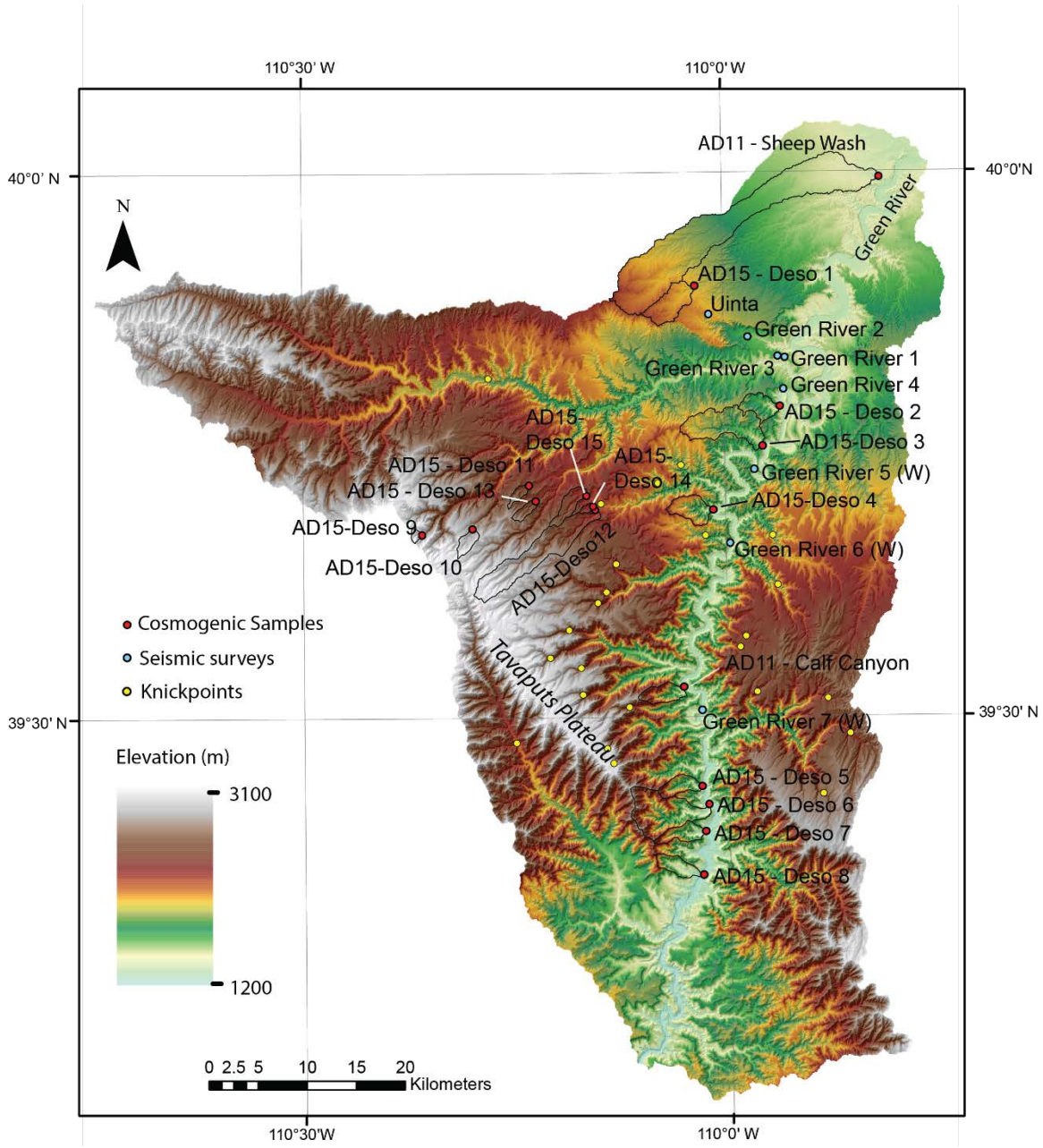

Figure 4.4. Topography of Desolation Canyon in Utah, USA. Survey sites, sample locations and knickpoints of assorted tributaries to the Green River are shown. The knickpoints rise in elevation to the south, approximately parallel to the plateau surface and lithologic lithologic contact (See Figures 4.2 and 4.3).

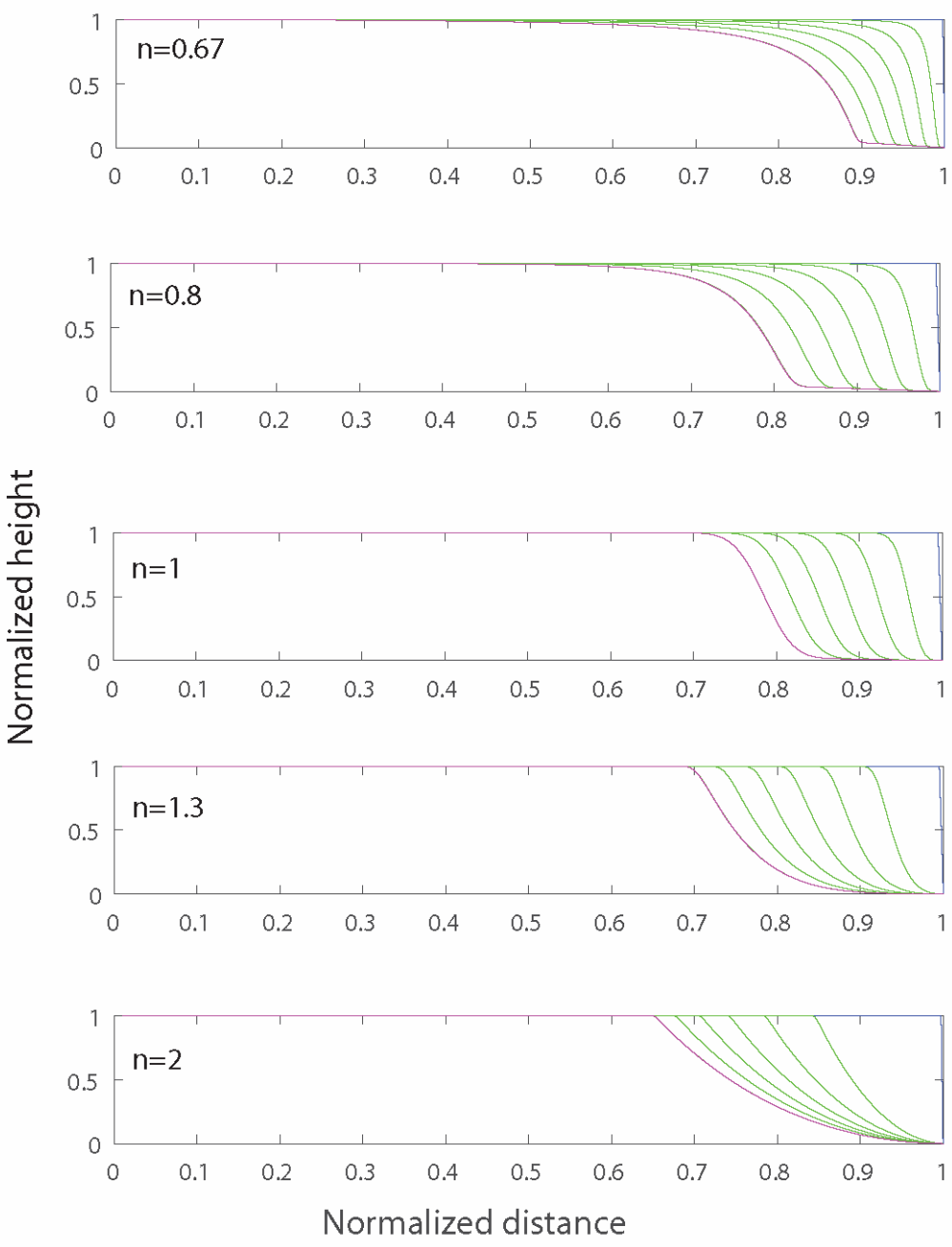

Figure 4.5. Modeled long profiles for given *n*-values evolving from a vertical step, after Tucker and Whipple, (2002). Rivers have different forms because of a variety of process or boundary condition controls that are represented by the value of *n.* Such processes could explain why the Green River knickpoint is smooth compared to its tributaries' respective knickpoints. See text for discussion

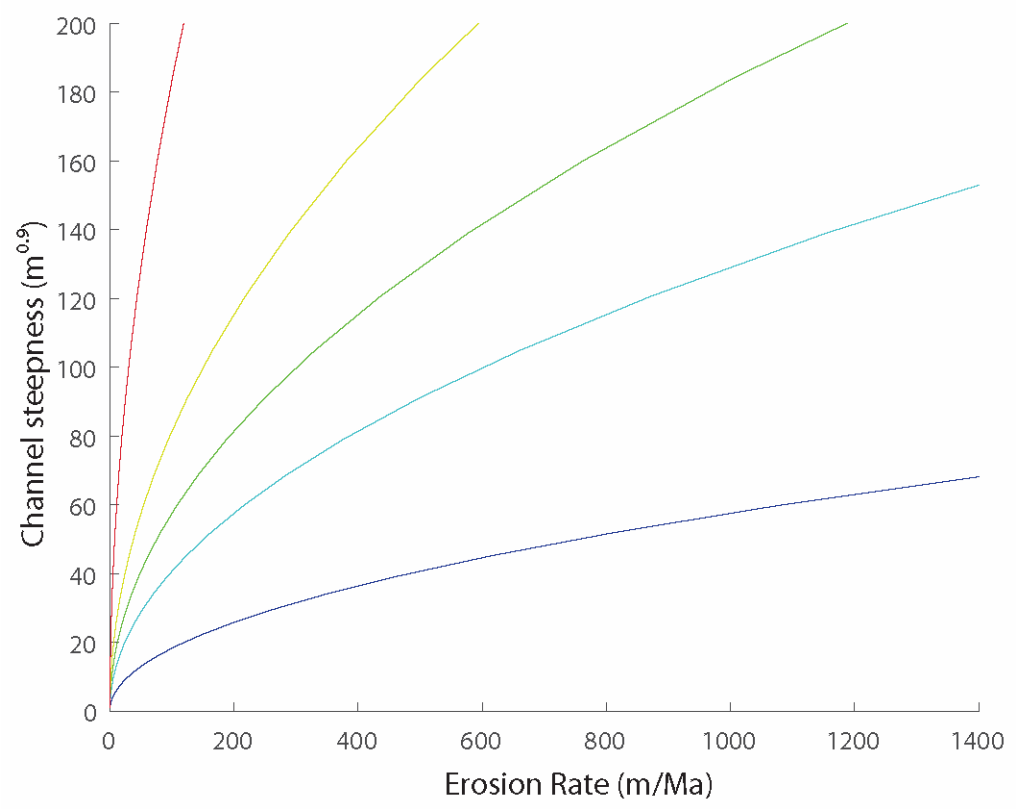

Figure 4.6. Channel steepness and erosion rate theoretical relationship. Colors indicate high erodibility (blue) to lower erodibility (red). Green curve is calibrated from field and cosmogenic data in the San Gabriel Mountains and additional curves differ by up to a factor of 10 change in erodibility (DiBiase et al., 2010).

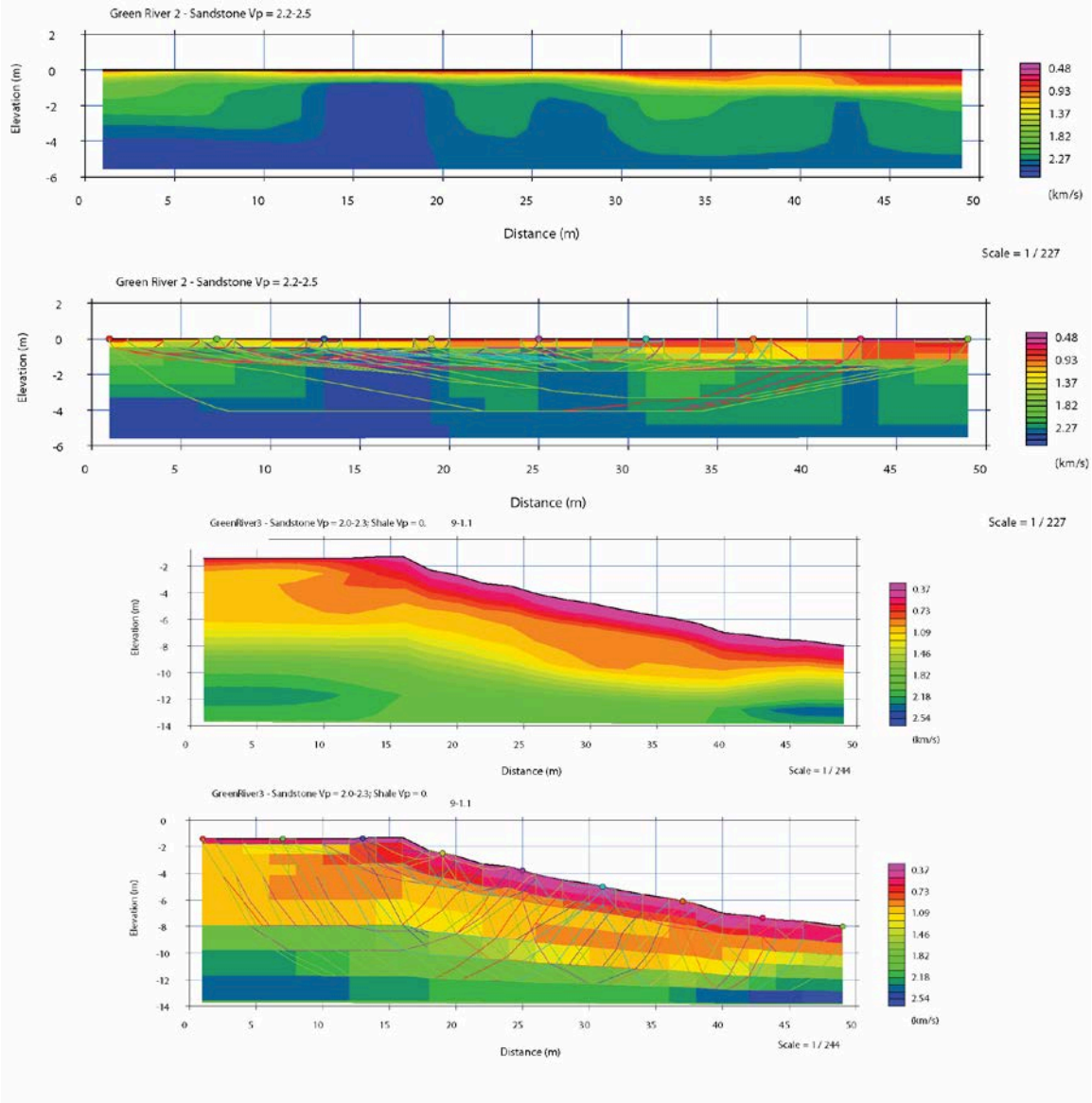

Figure 4.7. Seismic survey tomography for 8 transects through Uinta, Green River and Wasatch Formation outcrops in Desolation Canyon collected May 2015. Additional Vp survey supporting figures available in Appendix C.

Figure 4.8. A) Field photo during collection of survey Green River 5 in the Wasatch Formation. B) and C) Wasatch Formation forming a series of cliffs above the river. D) Collection of survey Green River 6 (W). Photos Nari Miller.

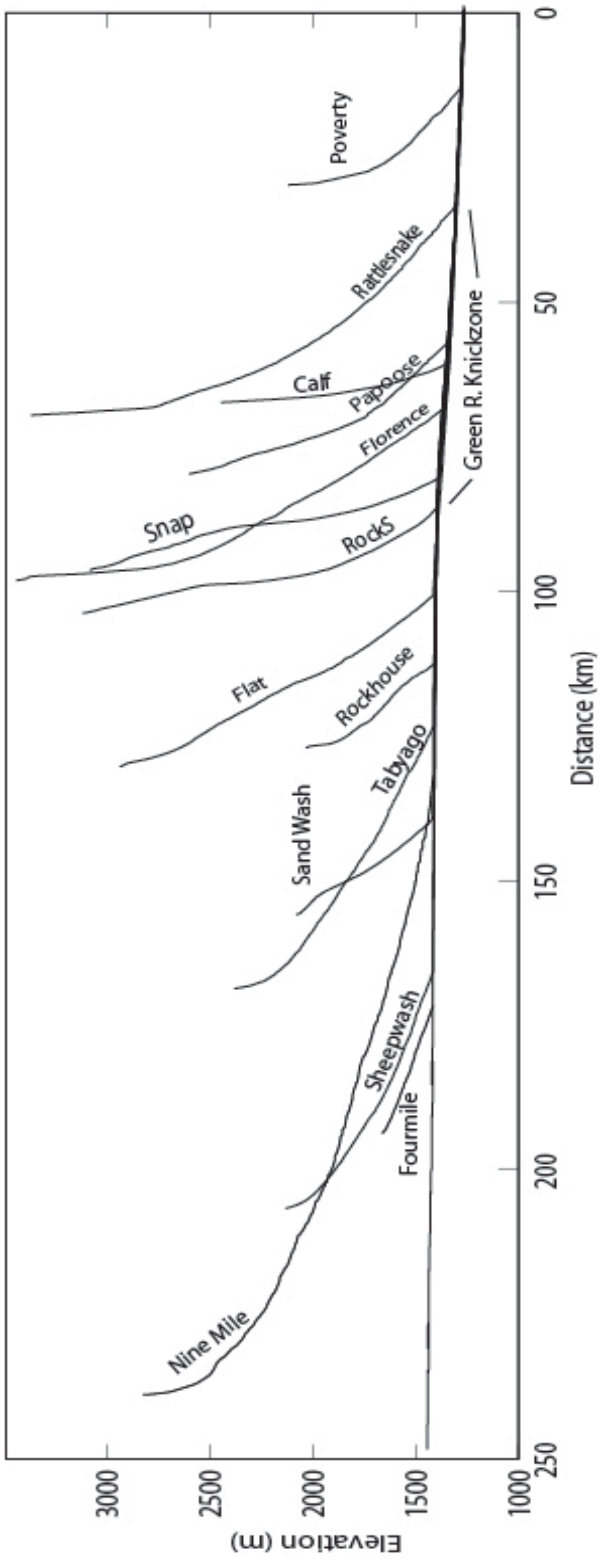

Figure 4.9. Longitudinal profiles from several tributaries and the mainstem Green River in Desolation Canyon with geologic contacts and approximate dip angle. For figure 4.11, channel steepness regressions were determined below any knickpoints in these and similar tributaries.

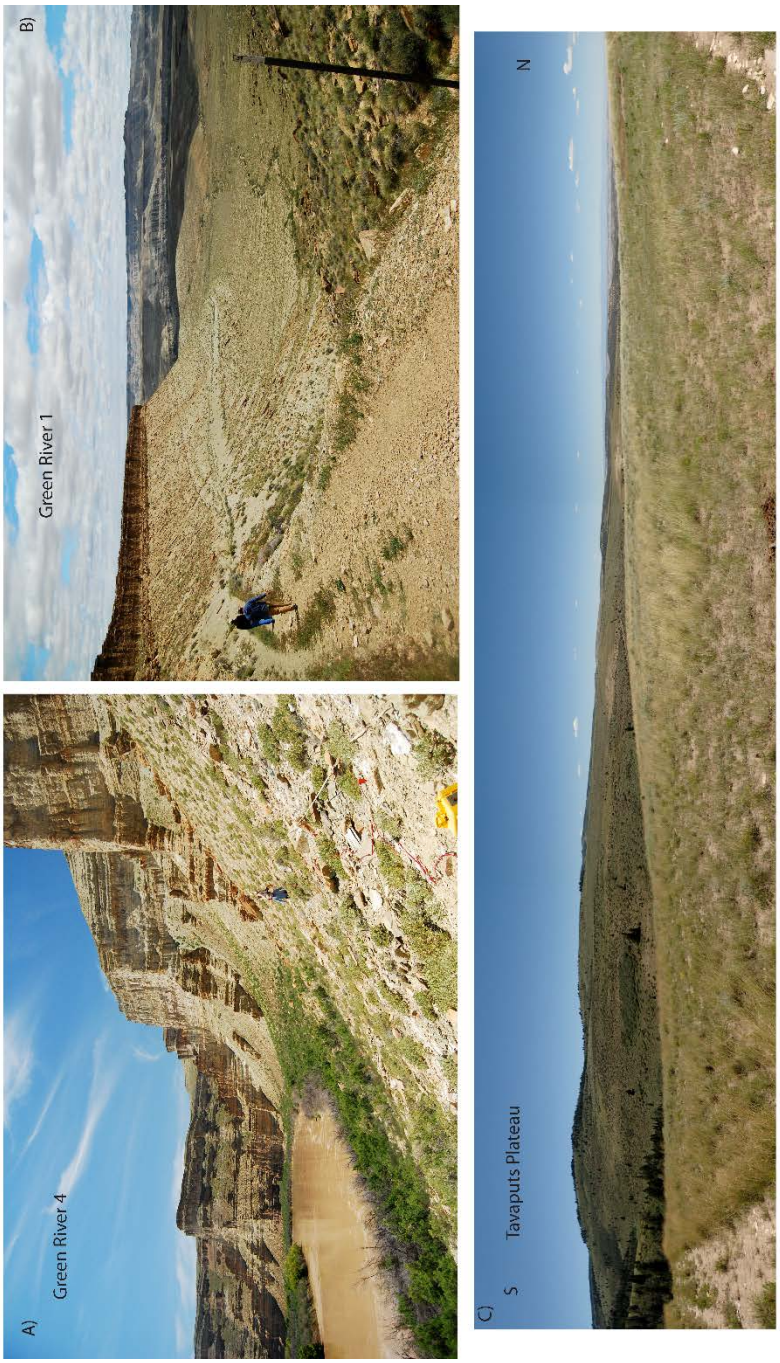

Figure 4.10. A) Field photo during collection of survey Green River 4 (Nari Miller photo). B) Field photo during collection of Green River 1 survey (Nari Miller photo). C) Field photo during collection of cosmogenic samples on Tavaputs Plateau. Panorama views South (left) to North (right side of image). Photo is near sample Deso 10, first author photo.

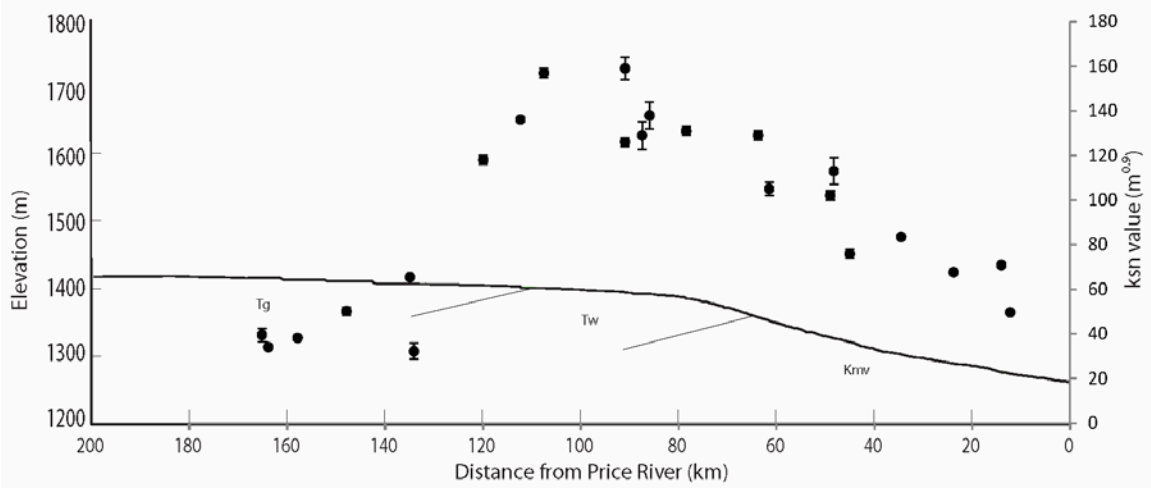

Figure 4.11. Channel steepness values calculated from lower portions of tributary streams, below knickpoints, from 10 m pixel size DEM using the Profiler toolbar. Reference concavity is 0.45. The increase and then decrease of ksn along the profile suggests an ongoing change in base level fall rate across the canyon like a kinematic wave of erosion. See Discussion.

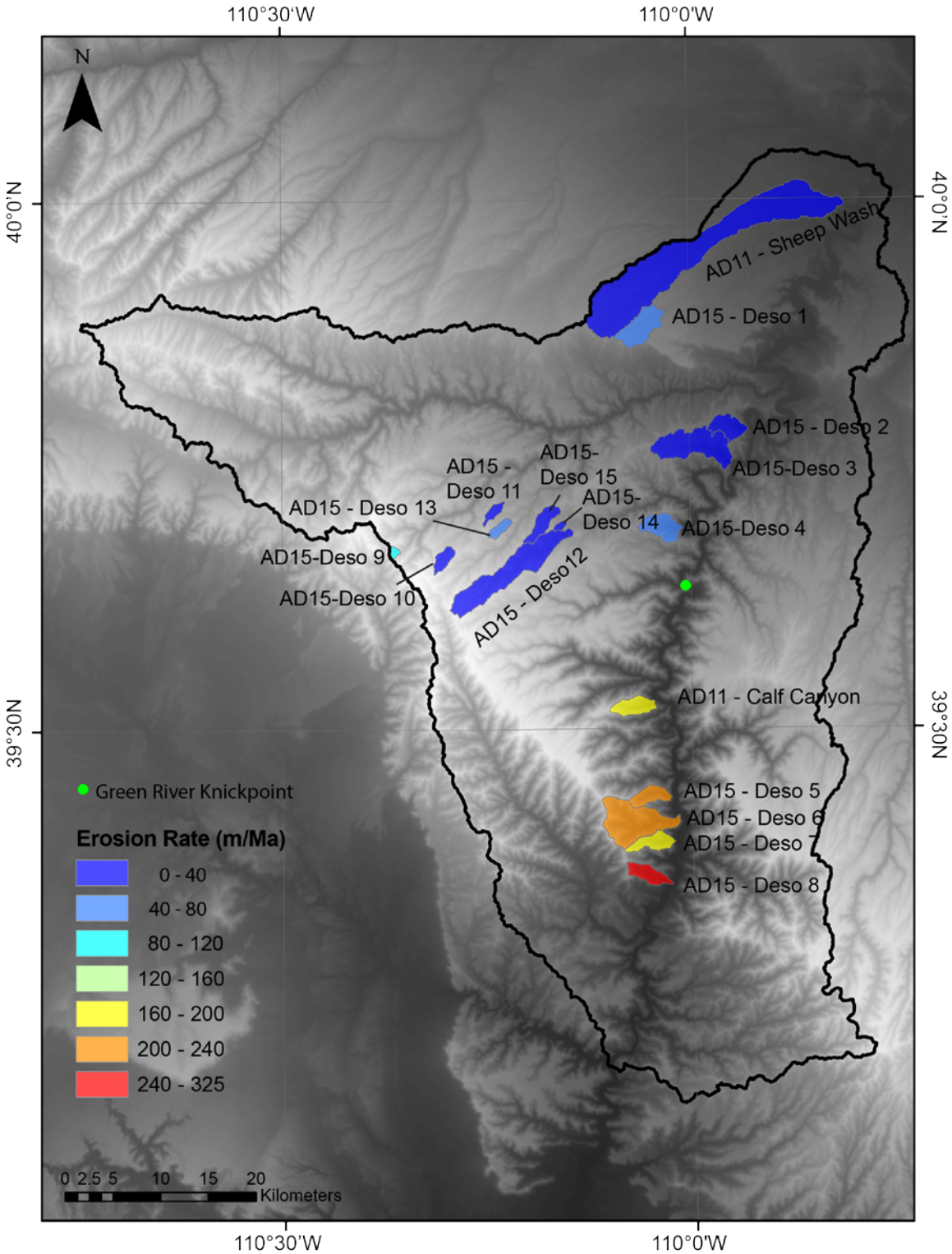

Figure 4.12. Map of catchment-averaged cosmogenic erosion rates in Desolation Canyon. Watersheds are outlined using ArcGIS tools and color coded to match erosion rate value.

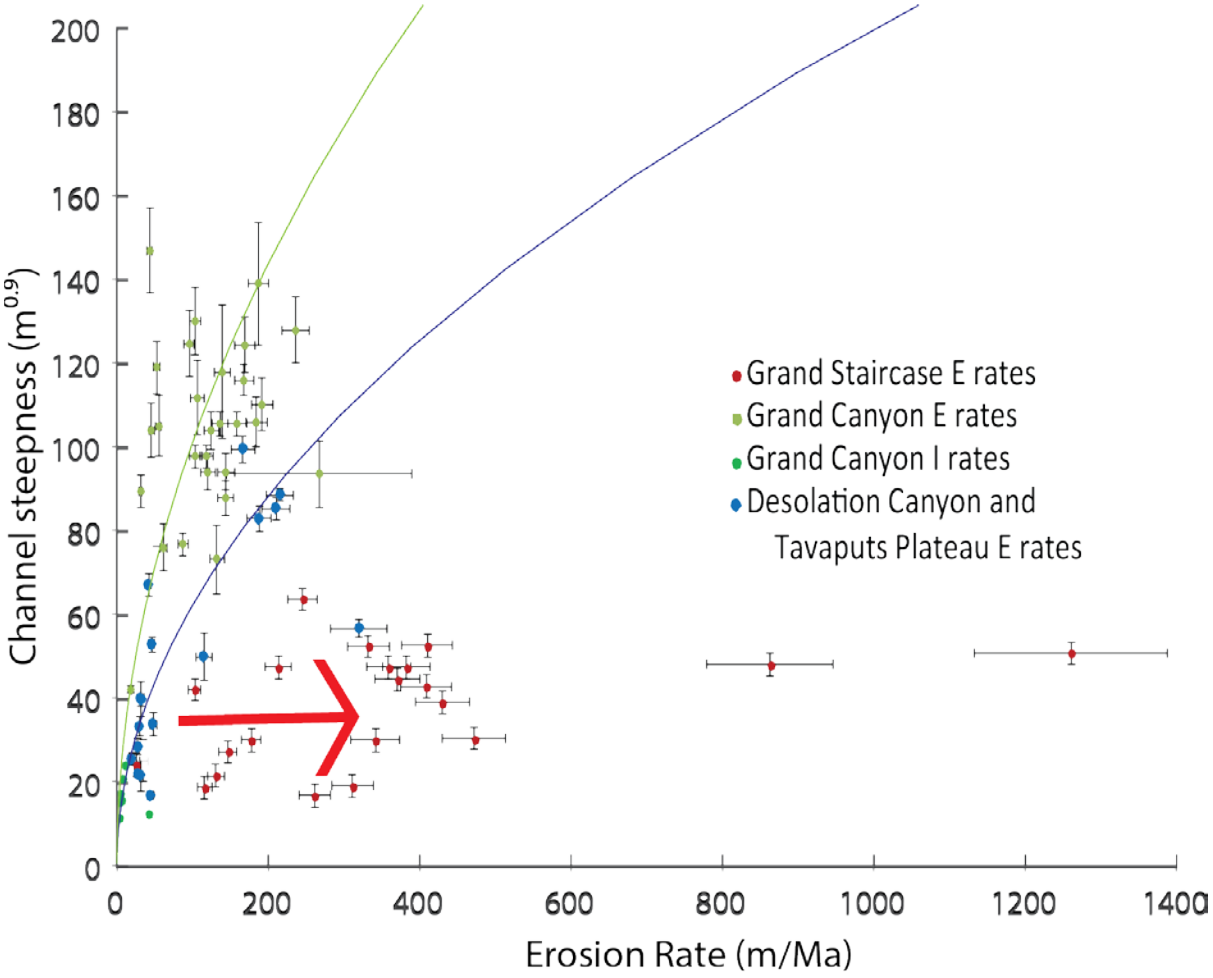

Figure 4.13. Channel steepness as a function of erosion rate for the three major study areas of this dissertation. The curves represent empirical values of K': that differ in the erodibility value, K'. The difference in erosional efficiency is attributed to rock strength differences between Grand Canyon and Desolation Canyon. The red arrow indicates the Grand Staircase sediments are skewed by local cliff retreat erosion and undermining.

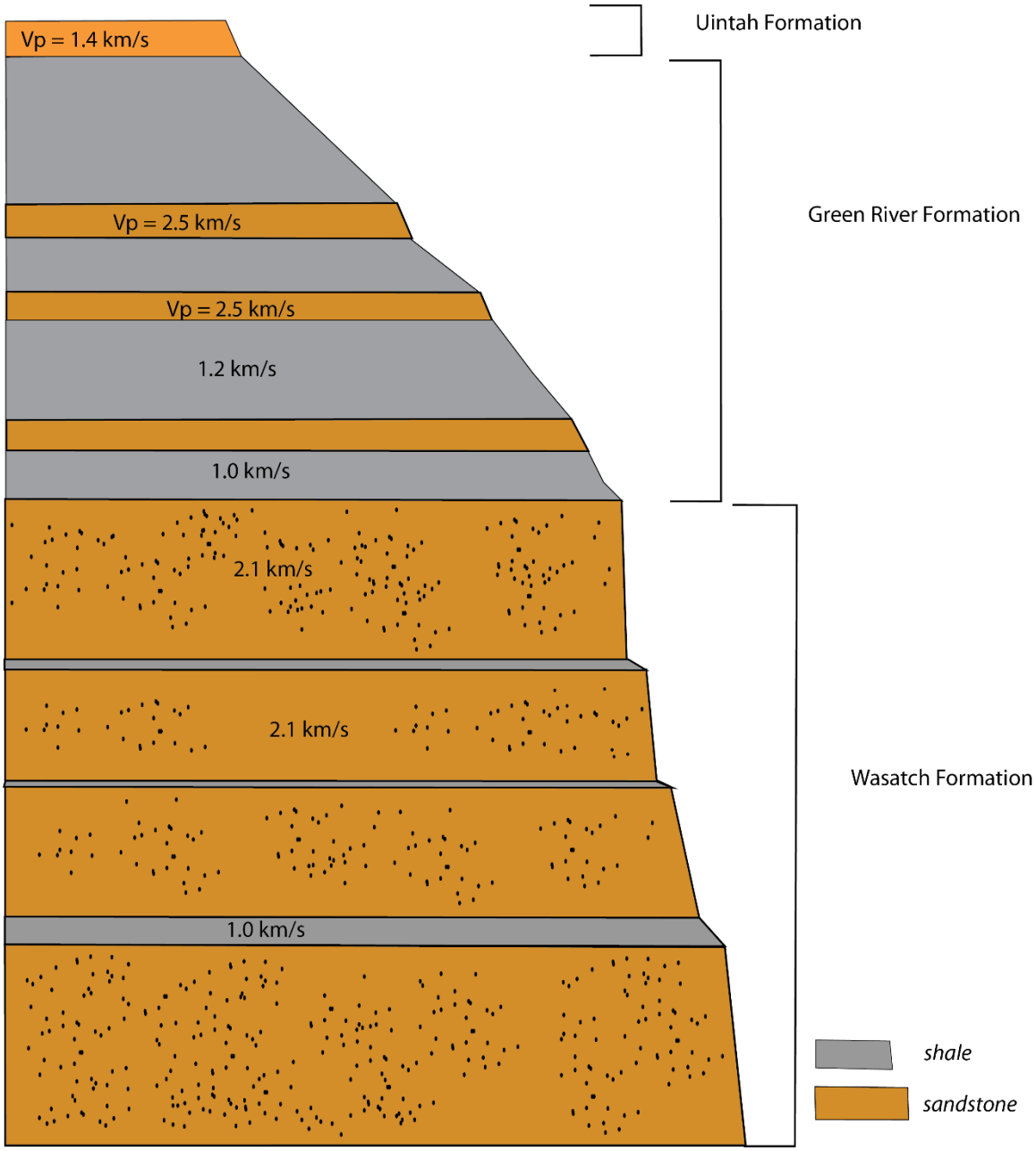

Figure 4.14. Schematic stratigraphic column of Desolation Canyon rock units. Relative positions of units labeled with rock strength measurements are not to scale. Note certain units in Green River Formation are harder than most of the rock in the unit (Figure 10). The Wasatch Formation sandstones dominate outcrops and have relatively high Vp (Figure 4.8).

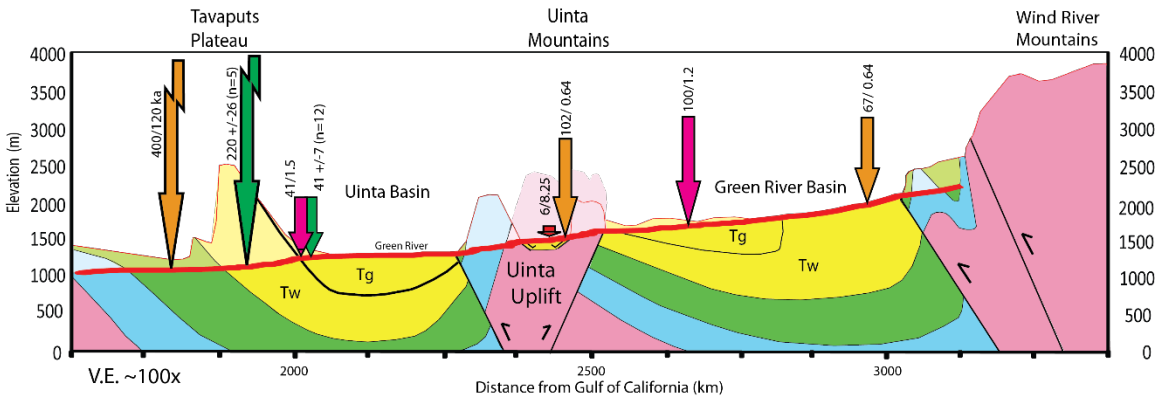

Figure 4.15. Schematic cross-section of geology underlying Green River long profile. Special care is made to ensure unit contacts are accurate, however dip angles and depths are cartooned. Orange arrows represent incision rates from relatively recent deposits and purple arrows are incision rates calculated from older deposits. Green arrows are derived from the mean of detrital cosmogenic erosion rate measurements. In the case of incision rates, numbers indiciate “Rate”/”Age”, from which terrace heights can be calculated.

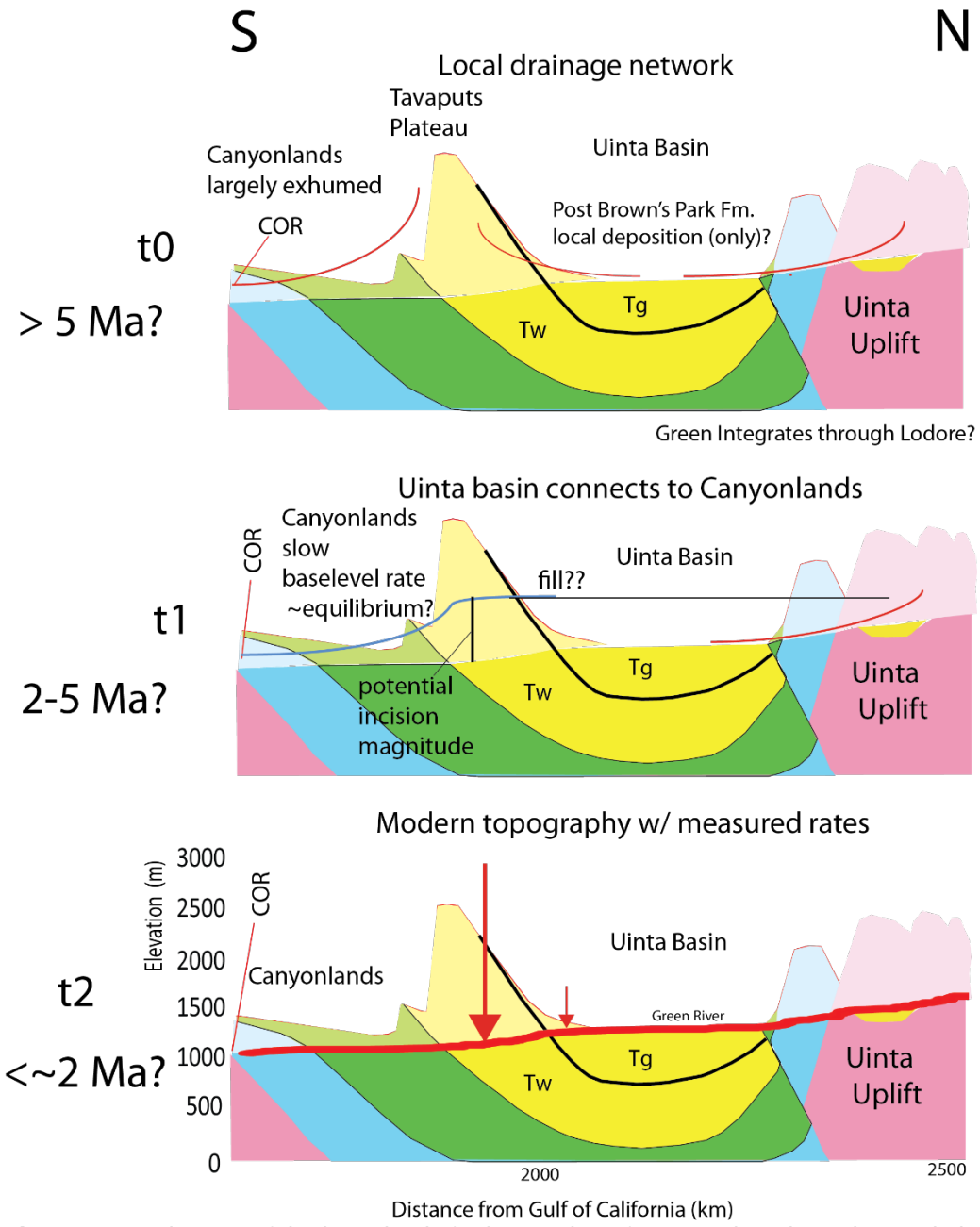

Figure 4.16. Diagram of the hypothesis for integration of Green River through Desolation Canyon. T0, Uinta Basin is a closed basin into the Neogene and Canyonlands is apparently largely exhumed by ~6 million years ago. T1, whether top-down or bottom-up, integration over a topographic step would produce a knickpoints and local fast erosion rates. T2: continued migration of the knickpoints leads to topography we see today with Desolation Canyon and a knickpoints on the Green River.

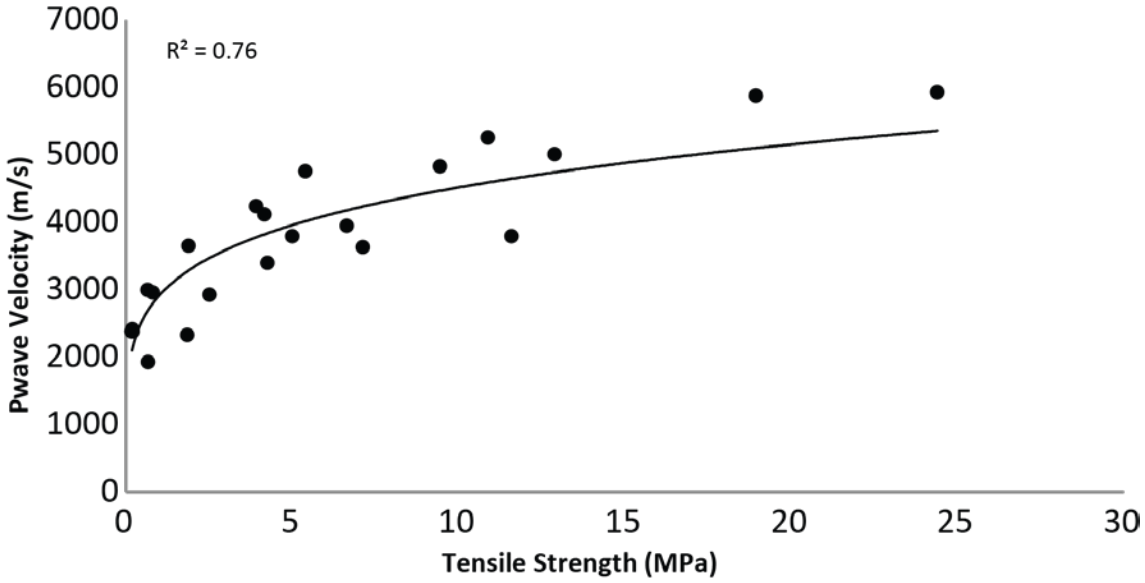

Figure 4.17. Rock strength metrics determined on rock cores from a variety of samples, see Table 4.2 (Johnson, 2007; Johnson et al., 2009; Sklar and Dietrich, 2001)

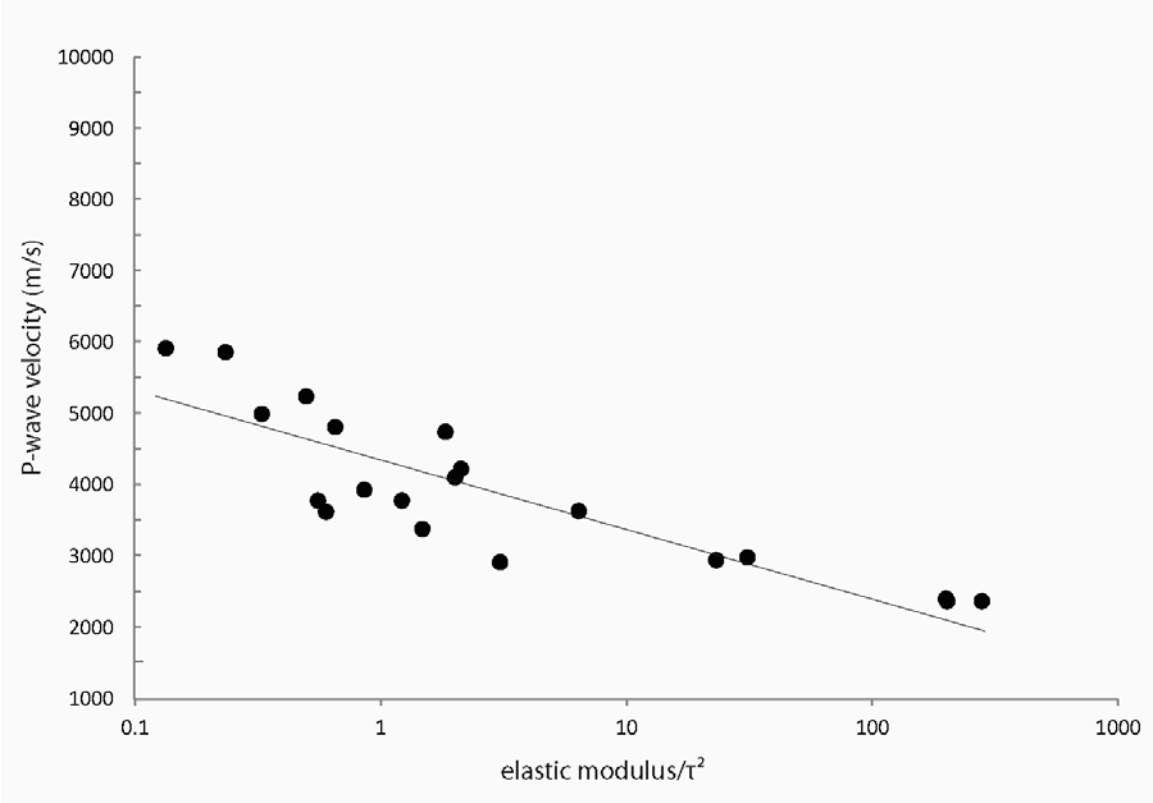

Figure 4.18. Data for Young's (elastic) modulus, tensile strength and Vp determined from core samples by Sklar and Johnson (personal communication). The factor of elastic modulus over tensile strength squared is a useful metric of how easily a material is to erode mechanically (Sklar, 2004).

Table 4.1 Seismic field survey data

Desolation Canyon		UTM E	UTM N	Elev.	Vp min (km/s)	Vp Max (km/s)	Vp Max Range (km/s)	Vp Survey Depth (m)	RMSE (ms)
Uinta	Tu	584450.53	4413763.56	1985.45	0.4	1.4	1.3-1.4	4.8	0.57
Green River1	Tg	592223.41	4409368.04	1608.87	0.3	2.5	2.3-2.5	6.2	0.58
Green River2	Tg	591505.88	4409501.52	1641.40	0.9	2.5	2.2-2.5	4.1	0.44
Green River 3 - Sandstone	Tg	588433.76	4411438.86	1620.09	0.3	2.3	2.0-2.3	10.5	0.77
Green River3 - Shale	Tg	588433.76	4411438.86	1620.09	0.3	1	0.9-1.1	4.6	0.77
Green River4	Tg	592083.68	4406176.04	1411.03	0.4	1.2	1.1-1.2	9.75	1.52
Green River5	Tw	589117.52	4397949.42	1393.77	0.5	2.1	2.0-2.2	2.8	0.95
Green River6	Tw	586685.37	4390437.53	1411.81	0.5	2.1	2.0-2.2	5.2	1.39
Green River7	Tw	583825.01	4373383.82	1353.37	0.4	1	1	6.75	1.9

Table 4.2 Core rock strength data from Johnson (2009).

Rock Type	Tensile Strength (MPa)	Elastic Modulus (GPa)	Vp	E/τ^2
Henry Mtns. Diorite	12.90	54.7	5003	0.328706
Entrada Sandstone	0.68	7.2	1918	
Kayenta Sandstone	2.53	19.6	2918	3.062069
Wingate Sandstone	1.85	10.7	2322	
Navajo Sandstone	0.25	3.7		58.88
'Wafer' Sandstone (PINK SS)	4.26	26.8	3387	1.476779
1:1 (2005)	3.922481	32.7	4230	2.125329
10:1 (2005, SigmaT 2005)	0.181	9.2	2372	279.3871
10:1 (2005, SigmaT 2007)	0.212962	9.2	2372.0	201.8179
2:1 (2005)	4.16951	34.9	4110.0	2.007499
4:1 (2005)	1.892033	22.9	3639.0	6.397028
6:1 (2005)	0.661905	13.6	2985.0	31.04184
8:1 (2005, SigmaT 2005)	0.211	8.9	2408.0	199.9057
Andesite	24.4	79.5	5923.0	0.133533
Basalt (Oz)	11.6	74.8	3786	0.555886
Eel Sandstone	6.65	37.9	3936	0.85703
Freemont Waterfall	0.82	15.6	2949	23.20048
Granite (Granodiorite?)	7.14	30.6	3625.0	0.60024
Lichen Sandstone	5.01	30.6	3786	1.219119
Taroko Marble	5.41	53.7	4748.0	1.834762
Taroko Quartzite	9.45	58.4	4818	0.653957
Welded Tuff	10.9	59.1	5246	0.497433
Yuba Quartzite	18.95	83.9	5868	0.233638

CHAPTER 5 SYNTHESIS

This dissertation outlines a conceptual and empirical basis for evaluating the processes of landscape evolution that form canyons set into low-relief plateau landscapes in the presence of a layered stratigraphy with variable rock strength. The field areas are the Grand Canyon, the Grand Staircase north of the Grand Canyon, and the smaller, but no less interesting, Desolation Canyon of the Green River in Utah. Empirical analysis from these three study areas is developed in each chapter, and each shows how our framework and data can be used together with independent datasets to decipher how complex influences on erosion occur, and are expressed in the topography of the study areas. The use of numerical models to develop intuition about landscapes is helpful in evaluation of the mysteries of the Colorado River systems and its canyons. This approach can be applied to other landscapes. Interpretation of erosion-rate data from cosmogenic nuclides is enhanced by comparing the data to simulated sediment supply from hillslopes that is transported through channels to hypothetical collection points anywhere in the simulation space. These simulations test a variety of rock strength and quartz distributions, tracking ^{10}Be content through transport. Erosion rates in simulations encompassing varied rock strength and quartz concentration may or may not differ from base-level fall even where base-level fall rate and climate are invariant, as explored primarily in Chapter 3. This work highlights how non-uniform quartz and erosion rates can be interpreted, and supports their use in landscapes more complex than ideal, so long as care is taken to thoroughly evaluate *what* the measured erosion rates represent relative to base-level fall and what local erosion rate anomalies are produced in particular non-equilibrium landscapes.

This synthesis highlights advances in each chapter and how they fit into broader contexts and suggests future trajectories in fields of Grand Canyon research, numerical simulations of variable rock strength landscapes, and cosmogenic-nuclide interpretation.

Grand Canyon and the Colorado River System

The origin of the Grand Canyon has been debated for over 100 years, and recent controversial studies have invigorated this debate and helped motivate my research. The

geomorphology and calculated erosion rates of the canyon, supported by theoretical modeling, strongly favor a geologically young canyon. The comparison of cliffs along the Grand Wash Fault to the walls of Grand Canyon provide a powerful natural experiment where rock type and climate are negligibly different although the canyon slopes are much steeper than the fault escarpment slopes, indicating very different erosion rates and thus age of the respective landscapes (Ch. 1). As did other studies before, my study indicates the steep-walled, high-relief landscape of Grand Canyon is youthful, and my analysis strongly suggests incision began <12 million years ago. We further conclude that canyon morphology is not simply a result of the typically stronger rocks found at greater depth in the canyon, which could support steeper slopes and cliffs more easily than weaker rocks could. From the point of view of geomorphology, hypotheses that the topographic form of Grand Canyon has changed little in several tens of millions of years (Wernicke, 2011; Flowers and Farley, 2012) are problematic. Such great antiquity is inconsistent with rates and processes of erosion that have been driven by the Colorado River and the antecedent drainages of the Colorado Plateau (e.g. Darling and Whipple, 2015). Importantly, even in places where the Colorado River is not directly driving erosion, such as the Hualapai Plateau headwaters (Ch. 2), the rates of erosion are high enough (~6 m/Ma) to produce significant change over tens of millions of years even in areas with low relief, relatively flat topography. Cosmogenic data shows that the much steeper portions of the landscape are eroding more quickly, as expected. Therefore, the landscape is dynamic, and steep topography is unstable. Independent data sources support refinement of this estimate to less than 5 or 6 million years ago and is likely closely related to the integration of the Colorado River system (Davis, 1901; Longwell, 1946; Karlstrom et al., 2008; Spencer et al., 2013; Karlstrom et al., 2014; Crossey et al., 2015; Darling and Whipple, 2015).

Current estimates of the time that incision began and the time that the Colorado River began supplying headwater sediment to the Basin and Range are not precise (Karlstrom et al., 2008; Polyak et al., 2008; Karlstrom et al., 2014; Darling and Whipple, 2015). We cannot say beyond speculation that the connection of the Colorado River system to the Gulf of California *caused* an increase in incision rate. This causal relationship is a hypothesis that is consistent with

geomorphic theory and implies a transient landscape (Cook et al., 2009; Darling et al., 2012; Darling and Whipple, 2015). Alternatively, Crow et al., (2014) show temporally steady incision of the Grand Canyon in the last ~1.5 million years from high terrace deposits in the central Grand Canyon, which is inconsistent with a transient incision wave. These concepts may be reconciled by the possibility that the posited transient incision wave passed through Grand Canyon prior to the relaxation to more steady incision recorded by existing terrace dates. One future research trajectory may be to conduct numerical simulations with more detailed datasets of the rock structure and strength, which has been attempted once (Pelletier, 2009). Improvements in understanding of how the landscape responds to various inputs controlled by possible base-level fall changes can improve on the work presented here.

One common method for exploring river systems is to find old river deposits and determine their age. For instance, in the northern end of Desolation Canyon, the terrace that is 60 m above the river is dated, but there are undated river gravels up to 145 m above the river in this area (Chapter 4 and Darling et al., 2012). Sites such as this require improved methods for dating river deposits, such as applying stable *and* radioactive cosmogenic isotopes using the isochron burial dating method. This particular variation of isochron dating (Balco and Rovey, 2008; Darling et al., 2012) requires evaluation of sources of stable isotopes and may not be applicable to deposits that are very thin or do not contain quartz sediment of known provenance. I considered using this enhancement of cosmogenic dating for my second project at ASU, and I still like its potential in the future.

The integration of the Colorado River system appears to be complex. The study of Desolation Canyon on the Green River, the Colorado's biggest tributary, suggests that the Green River integrated with the Colorado River relatively recently. Previous work suggested timing of this integration at somewhere between 8 and 1.5 million years ago (e.g. Darling et al., 2012; Rosenberg et al., 2014), and we can refine that to post-exhumation of the Canyonlands region (Ch. 4). Based on thermochronometric data, rapid exhumation in Canyonlands may have begun just 2-3 million years ago, though <6 million years ago is a more robust estimate (Murray et al., 2016). Our analysis does not distinguish the cause of integration, simply that there is a time

period between exhumation of the Canyonlands and the connection with the Green River. At least two possible scenarios could cause this relationship: head-ward erosion of a stream in the Book Cliffs pierced a low point in the Tavaputs Plateau, or infilling of the Uinta Basin allowed a spill-over and breach of the Tavaputs Plateau at a low point.

Ongoing studies of the upper Colorado River system are intended to date more river terraces and eroded volcanic flows associated with Cenozoic stratigraphy, and measure thermochronometers to study landscape incision and exhumation. The river network is a sensitive response system to possible tectonic and isostatic driving forces that may be operating in concert with processes like the drainage integration suggested in Desolation Canyon. Detailed study of site locations like Desolation Canyon are needed to de-convolve processes that affect broad regions from those processes that affect the landscape more narrowly, and to determine the order of events and their respective timing, making this analysis of Desolation Canyon useful for general research on Colorado Plateau landscape evolution.

Theoretical Exploration Progress

My updates to numerical evaluation of landscape change provide a quantitative framework for thinking about landscapes. My progress is through exploring how landscapes should respond to perturbations in base-level fall and the inherited geologic materials and structures that developed before erosion began and testing those hypotheses with erosion and incision rate data (e.g. Cook et al., 2009; Darling and Whipple, 2015). The complex interaction of bedrock strength with erosion has long been recognized, but not always well understood. Whipple and others developed much of the quantitative framework our models are based on, with the goal of looking at topography and using that to understand what has happened in the past (Ahnert, 1970; Flint, 1974; Kirkby and West, 1979; Whipple et al., 1999b; Whipple and Tucker, 1999; Whipple, 2001b; Tucker and Whipple, 2002; Whipple, 2002; Kirby and Whipple, 2012; Gasparini and Whipple, 2014; Whipple and Gasparini, 2014). A scenario that has long perturbed researchers has been how base-level fall changes would affect a landscape where vertical, stepwise changes in rock strength exist; i.e., layer-cake stratigraphy like the Colorado Plateau.

How could one tell which of these facets of erosion produced the topographic expression of a canyon? From each chapter in this dissertation, I evaluate numerical developments for testing how erosion rates are produced from diverse rock types in comparison to independent data.

One key result is that spatial distributions of erosion rates are diagnostic of landscape evolution history if rock-strength patterns are known. For instance, weak over strong rock provides an empirically supported prediction that erosion rates in the headwaters are indicative of previous (before the base-level change) boundary conditions to erosion in disequilibrium landscapes. Canyons will either have higher, lower or the same erosion rates as the headwaters, which indicate base-level fall rate increased, decreased or remained the same, respectively. While the assumption of constant or only stepwise changes in erosion rate are required to back calculate the timing of an event (from the apparent incision magnitude projected from a knickpoint), it is possible to constrain major geomorphic events, such as the beginning of the carving of Grand Canyon. Independent data that can attest to these inferences are based on geochronology of fluvial deposits which can and have been used in concert with geomorphic theory and modern erosion rate patterns to interpret landscape evolution in this dissertation.

Complex packages of rock produce complex erosion patterns, which I explore with simple numerical simulations that rely on simple erosion functions (especially Ch. 3). One aspect of this complex erosion that is not addressed directly is the observation that landscapes evolve via multiple processes over any given region. For example, in the case of hard rock over strong rock used in the Grand Staircase, the real landscape experiences rock fall, and sometimes, landslides. The model does not change the way that erosion occurs in the simulation, in which “rock fall” does not exist. It is analogous to this process change in that the stochastic, high-erosion-rate events at the scarp in the model are similar in effect to mass wasting; the erosion rate, no matter how it occurs in detail, is high and random. Further, the cosmogenic signature of the model and the real erosion process both provide unusually low doses of cosmic rays by eroding material quickly in some locations.

This type of exploration of erosion rate patterns with simulations based on variable rock strength will be useful in many areas around the world. Further, quartz-bearing rock distribution

patterns can be quantified for more precise determination of simulated erosion rates, used extensively in Chapter 3.

Rock Strength Measures

For many years J. Pederson and his colleagues and students (Grams and Schmidt, 1999; Roberson and Pederson, 2001; Anders et al., 2005; Pederson and Tressler, 2012; Pederson et al., 2013b; Bursztyn et al., 2015) have emphasized the idea that rock strength matters to canyon incision on the Colorado Plateau. I concur, and expand on that notion. My approach follows the ideas of Clarke and Burbank (2010, 2011) and is conducted in collaboration with Clarke. The aim is to collect geomorphically relevant, outcrop-scale data relevant to rock strength that can integrate weathering and rock strength across tens of meters into a single metric as a proxy for relative rock strength. I use near-surface P-wave velocity as this metric. Common measures of and proxies for rock strength sample only intact rock directly (Schmidt hammers, Brazilian tensile strength, P-wave and shear velocities in cores) and do not encompass the influence of weathering or fracture density, which are known to dominate effective rock strength in the field (Selby, 1993). Fracture density especially plays a large role in hillslope and channel erosion (e.g. Whipple et al., 2000; Clarke and Burbank, 2010). The role of rock strength in erosion is important, but determining a useful field metric of erodibility as defined in geomorphic theory (e.g. DiBiase and Whipple, 2011) has been elusive despite decades of research into factors affecting rock mass strength (Selby, 1981, 1982a, b; Moon and Selby, 1983; Augustinus, 1992; Augustinus, 1995; Schmidt and Montgomery, 1995; Schmidt and Montgomery, 1996; Weissel and Seidl, 1997; Clarke and Burbank, 2011). I have approached erodibility from two directions: simulations of assigned erodibility and field geophysical measurements. Simulating landscapes with assigned erodibility values provides an intuition for what the erosion response will look like. The measurement of field V_p allows estimates of tensile strength that can be used to support inferences of erodibility as defined in simulations. This relationship is further supported by rock core data using the ratio of elastic modulus and tensile strength squared as a means for assessing how erodible a rock might be. Although more work is still needed to understand the

relationship between rock strength and erodibility, effective evaluation of erodibility's effect on landscapes can be accomplished with the methods outlined in this dissertation.

Future Interdisciplinary Research

Colorado Plateau Rivers and Canyons

Our research provides improvements on understanding how canyons develop in the presence of stratigraphic variation in rock strength. This progress fundamentally improves ideas and inferences for landscape evolution of the Colorado River system. However, inferences based on recent geomorphic change and landscape evolution theory are not direct evidence of the history of the Colorado River. The integration of the Colorado River system, from a regional river in Colorado 11 million years ago to a continental-scale river by 5 or 6 million years ago and how it has changed since, are still fundamentally not well understood. Where did the river flow between 11 and 6 million years ago? What did intermediate landscapes and canyon systems look like? How were the basins of Wyoming, Utah and Northern Colorado connected to form the Green River? These and other questions can frame future projects as scientific means of testing ideas evolve and intuition for developing testable hypotheses improves.

The history of the upper Green River has been of interest to me for several years. The chapter on Desolation Canyon will frame my thinking for beginning new research into the river history and basin exhumation of this area through whatever means seem useful, including terrace dating (and development of chronological methods) and expanding my working knowledge of volcanic dating methods, especially ^{40}Ar-^{39}Ar dating.

Recent research in thermochronology provides powerful but relatively low precision datasets that bear on changes in heat through time and space that are partially controlled by landscape evolution (e.g. Flowers et al., 2008; Flowers and Farley, 2012; Fox and Shuster, 2014; Karlstrom et al., 2014). Improvements in these techniques will enhance interpretability of landscape change. The connections between thermochronology, geology and geomorphology can also be leveraged to improve on landscape change interpretations if ideas and testability are consistent across techniques. Ultimately, greater potential for improvements in understanding

regions like the Colorado Plateau will come from collaborations across disciplines using diverse techniques to bring more data to bear on key questions.

References

Ahnert, F., 1970, Functional relationships between denudation, relief, and uplift in large mid-latitude drainage basins: American Journal of Science, v. 268, p. 243-263.

Anders, M. D., Pederson, J. L., Rittenour, T. M., Sharp, W. D., Gosse, J. C., Karlstrom, K. E., Crossey, L. J., Goble, R. J., Stockli, L., and Yang, G., 2005, Pleistocene geomorphology and geochronology of eastern Grand Canyon: linkages of landscape components during climate changes: Quaternary Science Reviews, v. 24, no. 23-24, p. 2428-2448.

Augustinus, P., 1995, Rock mass strength and the stability of some glaciated valley slopes: Zeitschrift fur Geomorphologie, v. 39, p. 55-68.

Augustinus, P. C., 1992, The influence of rock mass strength on glacial valley cross-profile morphometry: A case study from the Southern Alps, New Zealand: Earth Surface Processes and Landforms, v. 17, p. 39-51.

Balco, G., and Rovey, C. W., 2008, An isochron method for cosmogenic-nuclide dating of buried soils and sediments: American Journal of Science, v. 308, no. 10, p. 1083-1114.

Bursztyn, N., Pederson, J., Tressler, C., Mackley, R., and Mitchell, K., 2015, Rock strength along a fluvial transect of the Colorado Plateau–quantifying a fundamental control on geomorphology: Earth and Planetary Science Letters, v. 429, p. 90-100.

Clarke, B. A., and Burbank, D. W., 2010, Bedrock fracturing, threshold hillslopes, and limits to the magnitude of bedrock landslides: Earth and Planetary Science Letters, v. 297, no. 3, p. 577-586.

-, 2011, Quantifying bedrock-fracture patterns within the shallow subsurface: Implications for rock mass strength, bedrock landslides, and erodibility: Journal of Geophysical Research: Earth Surface, v. 116, no. F4.

Cook, K. L., Whipple, K. X., Heimsath, A. M., and Hanks, T. C., 2009, Rapid incision of the Colorado River in Glen Canyon–insights from channel profiles, local incision rates, and modeling of lithologic controls: Earth Surface Processes and Landforms, v. 34, no. 7, p. 994-1010.

Crossey, L., Karlstrom, K., Dorsey, R., Lopez, P., J., Wan, E., Beard, L. S., Asmerom, Y., Polyak, V., Crow, R., Cohen, A., Bright, J., and Pecha, M., 2015, The importance of groundwater in propagating downward integration of the 6-5 Ma Colorado River System: Geochemistry of springs, travertines and lacustrine carbonates of the Grand Canyon region over the past 12 million years.: Geosphere, v. in press.

Crow, R., Karlstrom, K., Darling, A., Crossey, L., Polyak, V., Granger, D., Asmerom, Y., and Schmandt, B., 2014, Steady incision of Grand Canyon at the million year timeframe: A case for mantle-driven differential uplift: Earth and Planetary Science Letters, v. 397, p. 159-173.

Darling, A., and Whipple, K., 2015, Geomorphic constraints on the age of the western Grand Canyon: Geosphere, v. 11, no. 4, p. 958-976.

Darling, A. L., Karlstrom, K., Granger, D. E., Aslan, A., Kirby, E., Ouimet, W. B., Lazear, G. D., Coblentz, D. D., and Cole, R. D., 2012, New incision rates along the Colorado River system based on cosmogenic burial dating of terraces: implications for regional controls on Quaternary incision: Geosphere, v. 8, no. 5, p. 1020-1041.

Davis, W. M., 1901, An excursion to the Grand Canyon of the Colorado, Cambridge, Massachusetts, Printed for the Museum, 201 p.

DiBiase, R. A., and Whipple, K. X., 2011, The influence of erosion thresholds and runoff variability on the relationships among topography, climate, and erosion rate: Journal of Geophysical Research, v. 116, no. F4.

Flint, J. J., 1974, Stream gradient as a function of order, magnitude, and discharge: Water Resources Research, v. 10, p. 969-973.

Flowers, R., and Farley, K., 2012, Apatite 4He/3He and (U-Th)/He evidence for an ancient Grand Canyon: Science, v. 338, no. 6114, p. 1616-1619.

Flowers, R. M., Wernicke, B. P., and Farley, K. A., 2008, Unroofing, incision, and uplift history of the southwestern Colorado Plateau from apatite (U-Th)/He thermochronometry: Geological Society of America Bulletin, v. 120, no. 5-6, p. 571-587.

Fox, M., and Shuster, D., 2014, The influence of burial heating on the (U-Th)/He system in apatite: Grand Canyon case study: Earth and Planetary Science Letters, v. 397, p. 174-183.

Gasparini, N. M., and Whipple, K. X., 2014, Diagnosing climatic and tectonic controls on topography: Eastern flank of the northern Bolivian Andes: Lithosphere, v. 6, no. 4, p. 230-250.

Grams, P. E., and Schmidt, J. C., 1999, Geomorphology of the Green River in the eastern Uinta Mountains, Dinosaur National Monument, Colorado and Utah: Varieties of fluvial form, p. 81-111.

Karlstrom, K. E., Crow, R., Crossey, L. J., Coblentz, D., and Van Wijk, J. W., 2008, Model for tectonically driven incision of the younger than 6 Ma Grand Canyon: Geology, v. 36, no. 11, p. 835.

Karlstrom, K. E., Lee, J. P., Kelley, S. A., Crow, R. S., Crossey, L. J., Young, R. A., Lazear, G., Beard, L. S., Ricketts, J. W., and Fox, M., 2014, Formation of the Grand Canyon 5 to 6 million years ago through integration of older palaeocanyons: Nature Geoscience, v. 7, p. 239-244.

Kirby, E., and Whipple, K. X., 2012, Expression of active tectonics in erosional landscapes: Journal of Structural Geology, v. 44, p. 54-75.

Kirkby, M. J. r., and West, E. E., 1979, The equilibrium of natural streams; a new theoretical approach providing a key to the understanding of longer-term fluvial processes: Journal of Hydrology, v. 42, no. 3-4, p. 397.

Longwell, C. R., 1946, How old is the Colorado River?: American Journal of Science, v. 244, no. 12, p. 817-835.

Moon, B. P., and Selby, M. J., 1983, Rock mass strength and scarp forms in southern Africa: Geografiska Annaler. Series A: Physical Geography, v. 65, no. 1-2, p. 135-145.

Murray, K., Reiners, P., and Thomson, S., 2016, Rapid Pliocene–Pleistocene erosion of the central Colorado Plateau documented by apatite thermochronology from the Henry Mountains: Geology, v. 44, no. 6, p. 483-486.

Pederson, J. L., Cragun, W. S., Hidy, A. J., Rittenour, T. M., and Gosse, J. C., 2013, Colorado River chronostratigraphy at Lee's Ferry, Arizona, and the Colorado Plateau bull's-eye of incision: Geology, v. 41, no. 4, p. 427-430.

Pederson, J. L., and Tressler, C., 2012, Colorado River long-profile metrics, knickzones and their meaning: Earth and Planetary Science Letters, v. 345, p. 171-179.

Pelletier, J. D., 2009, Numerical modeling of the late Cenozoic geomorphic evolution of Grand Canyon, Arizona: Geological Society of America Bulletin, v. 122, no. 3-4, p. 595-608.

Polyak, V., Hill, C., and Asmerom, Y., 2008, Age and evolution of the Grand Canyon revealed by U-Pb dating of water table-type speleothems: Science, v. 319, no. 5868, p. 1377-1380.

Roberson, P., and Pederson, J., 2001, Rock-strength control in Desolation and Gray canyons of the Green River: a river landscape in dynamic equilibrium: Abstracts with Programs, Geological Society of America, v. 33, p. 14.

Rosenberg, R., Kirby, E., Aslan, A., Karlstrom, K., Heizler, M., and Ouimet, W., 2014, Late Miocene erosion and evolution of topography along the western slope of the Colorado Rockies: Geosphere, v. 10, no. 4, p. 641-663.

Schmidt, K. M., and Montgomery, D. R., 1995, Limits to relief: Science, v. 270, p. 617-620.

Schmidt, K. M., and Montgomery, D. R., 1996, Rock mass strength assessment for bedrock landsliding: Environmental & Engineering Geoscience, v. 2, no. 3, p. 325-338.

Selby, M. J., 1981, A method of determining rock mass strength; field tested in Antarctica: New Zealand Antarctic Record, v. 3, no. 2, p. 22.

-, 1982a, Controls on the stability and inclinations of hillslopes formed on hard rock: Earth Surfaces Processes and Landforms, v. 7, no. 5, p. 449-467.

-, 1982b, Rock mass strength and the form of some inselbergs in the central Namib Desert: Earth Surfaces Processes and Landforms, v. 7, no. 5, p. 489-497.

-, 1993, Hillslope Materials and Processes, Oxford, Oxford University Press.

Spencer, J. E., Patchett, P. J., Pearthree, P. A., House, P. K., Sarna-Wojcicki, A. M., Wan, E., Roskowski, J. A., and Faulds, J. E., 2013, Review and analysis of the age and origin of the Pliocene Bouse Formation, lower Colorado River Valley, southwestern USA: Geosphere, v. 9, no. 3, p. 444-459.

Tucker, G. E., and Whipple, K., 2002, Topographic outcomes predicted by stream erosion models: Sensitivity analysis and intermodel comparison: Journal of Geophysical Research, v. 107, no. B9.

Weissel, J. K., and Seidl, M. A., 1997, Influence of rock strength properties on escarpment retreat across passive continental margins: Geology (Boulder), v. 25, no. 7, p. 631-634.

Wernicke, B., 2011, The California River and its role in carving Grand Canyon: Geological Society of America Bulletin, v. 123, no. 7-8, p. 1288-1316.

Whipple, K., 2002, GE Tucker: Journal of Geophysical Research, v. 107, no. B9, p. 2179.

Whipple, K. X., 2001, Fluvial landscape response time: How plausible is steady-state denudation?: American Journal of Science, v. 301, no. 4-5, p. 313-325.

Whipple, K. X., and Gasparini, N., 2014, Tectonic control of topography, rainfall patterns, and erosion during rapid post–12 Ma uplift of the Bolivian Andes: Lithosphere, v. 6, no. 4, p. 251-268.

Whipple, K. X., Hancock, G. S., and Anderson, R. S., 2000, River incision into bedrock: Mechanics and relative efficacy of plucking, abrasion, and cavitation: Geological Society of America Bulletin, v. 112, no. 3, p. 490-503.

Whipple, K. X., Kirby, E., and Brocklehurst, S. H., 1999, Geomorphic limits to climate-induced increases in topographic relief: Nature, v. 401, p. 39-43.

Whipple, K. X., and Tucker, G. E., 1999, Dynamics of the stream-power river incision model: Implications for height limits of mountain ranges, landscape response timescales, and research needs: Journal of Geophysical Research, v. 104, no. B8, p. 17661-17617, 17674.

Comprehensive References

Adams, B., Whipple, K., Hodges, K., and Heimsath, A., 2016, In-situ development of high-elevation, low-relief landscapes via duplex deformation in the Eastern Himalayan hinterland, Bhutan: Journal of Geophysical Research: Earth Surface.

Ahnert, F., 1970, Functional relationships between denudation, relief, and uplift in large mid-latitude drainage basins: American Journal of Science, v. 268, p. 243-263.

Anders, M. D., and Pederson, J., 2002, Implications of new Quaternary stratigraphic research and age control in eastern Grand Canyon for landscape evolution and lava-dam lakes: Abstracts with Programs, Geological Society of America, v. 34, p. 60.

Anders, M. D., Pederson, J. L., Rittenour, T. M., Sharp, W. D., Gosse, J. C., Karlstrom, K. E., Crossey, L. J., Goble, R. J., Stockli, L., and Yang, G., 2005, Pleistocene geomorphology and geochronology of eastern Grand Canyon: linkages of landscape components during climate changes: Quaternary Science Reviews, v. 24, no. 23-24, p. 2428-2448.

Anderson, J. J., and Rowley, P. D., 1975, Cenozoic stratigraphy of southwestern High Plateaus of Utah: Geological Society of America Special Papers, v. 160, p. 1-52.

Antinao, J. L., and McDonald, E., 2013a, An enhanced role for the Tropical Pacific on the humid Pleistocene–Holocene transition in southwestern North America: Quaternary Science Reviews, v. 78, p. 319-341.

-, 2013b, A reduced relevance of vegetation change for alluvial aggradation in arid zones: Geology, v. 41, no. 1, p. 11-14.

Armstrong, R. L., 1968, Sevier orogenic belt in Nevada and Utah: Geol. Soc. Amer. Bull., v. 79, p. 429-458.

Aslan, A., Hood, W. C., Karlstrom, K. E., Kirby, E., Granger, D. E., Kelley, S., Crow, R., Donahue, M. S., Polyak, V., and Asmerom, Y., 2014, Abandonment of Unaweep Canyon (1.4–0.8 Ma), western Colorado: Effects of stream capture and anomalously rapid Pleistocene river incision: Geosphere, v. 10, no. 3, p. 428-446.

Aslan, A., Karlstrom, K. E., Crossey, L. J., Kelley, S., Cole, R., Lazear, G., and Darling, A., 2010, Late Cenozoic evolution of the Colorado Rockies: Evidence for Neogene uplift and drainage integration: Field Guides, v. 18, p. 21-54.

Atwater, T., and Stock, J., 1998, Pacific-North America plate tectonics of the Neogene southwestern United States: an update: International Geology Review, v. 40, no. 5, p. 375-402.

Augustinus, P., 1995, Rock mass strength and the stability of some glaciated valley slopes: Zeitschrift fur Geomorphologie, v. 39, p. 55-68.

Augustinus, P. C., 1992, The influence of rock mass strength on glacial valley cross-profile morphometry: A case study from the Southern Alps, New Zealand: Earth Surface Processes and Landforms, v. 17, p. 39-51.

Balco, G., Finnegan, N., Gendaszek, A., Stone, J. O., and Thompson, N., 2013, Erosional response to northward-propagating crustal thickening in the coastal ranges of the US Pacific Northwest: American Journal of Science, v. 313, no. 8, p. 790-806.

Balco, G., and Rovey, C. W., 2008, An isochron method for cosmogenic-nuclide dating of buried soils and sediments: American Journal of Science, v. 308, no. 10, p. 1083-1114.

Balco, G., Stone, J. O., Lifton, N. A., and Dunai, T. J., 2008, A complete and easily accessible means of calculating surface exposure ages or erosion rates from 10Be and 26Al measurements: Quaternary Geochronology, v. 3, no. 3, p. 174-195.

Baldwin, J. A., Whipple, K. X., and Tucker, G. E., 2003, Implications of the shear stress river incision model for the timescale of postorogenic decay of topography: Journal of Geophysical Research-Solid Earth, v. 108, no. B3, p. art. no.-2158.

Barton, N., 2007, Rock quality, seismic velocity, attenuation and anisotropy, CRC press.

Benedict, J. B., 1973, Chronology of cirque glaciation, Colorado front range: Quaternary Research, v. 3, no. 4, p. 584-599.

Berlin, M. M., and Anderson, R. S., 2007, Modeling of knickpoint retreat on the Roan Plateau, western Colorado: Journal of Geophysical Research, v. 112, no. F3.

Biek, R., Rowley, P., Anderson, J., Maldonado, F., Moore, D., Eaton, J., Hereford, R., and Matyjasik, B., 2012, Interim geologic map of the Panguitch 30'x 60'quadrangle: Garfield, Iron, and Kane Counties, Utah: Utah Geological Survey Open-File Report, v. 599, no. 3.

Bierman, P., and Steig, E. J., 1996, Estimating rates of denudation using cosmogenic isotope abundances in sediment: Earth Surface Processes and Landforms, v. 21, p. 125-139.

Bird, P., 1998, Kinematic history of the Laramide orogeny in latitudes 35o-49oN, western United States: Tectonics, v. 17, no. 5, p. 780-801.

Blackwelder, E., 1934, Origin of the Colorado River: Geological Society of America Bulletin, v. 45, no. 3, p. 551-566.

Bohannon, R. G., 1984, Nonmarine sedimentary rocks of Tertiary age in the Lake Mead region, southeastern Nevada and northwestern Arizona: U.S. Geological Survey Professional Paper, v. 1259, p. 72.

Bohannon, R. G., Grow, J. A., Miller, J. J., and BLANK, R. H., 1993, Seismic stratigraphy and tectonic development of Virgin River depression and associated basins, southeastern Nevada and northwestern Arizona: Geological Society of America Bulletin, v. 105, no. 4, p. 501-520.

Bull, W. B., 1991, Geomorphic Responses to Climate Change, New York, Oxford University Press, 326 p.:

Bursztyn, N., Pederson, J., Tressler, C., Mackley, R., and Mitchell, K., 2015, Rock strength along a fluvial transect of the Colorado Plateau–quantifying a fundamental control on geomorphology: Earth and Planetary Science Letters, v. 429, p. 90-100.

Cather, S. M., Connell, S. D., Chamberlin, R. M., McIntosh, W. C., Jones, G. E., Potochnik, A. R., Lucas, S. G., and Johnson, P. S., 2008, The Chuska erg: Paleogeomorphic and paleoclimatic implications of an Oligocene sand sea on the Colorado Plateau: Geological Society of America Bulletin, v. 120, no. 1-2, p. 13-33.

Cha, M., Cho, G.-C., and Santamarina, J. C., 2009, Long-wavelength P-wave and S-wave propagation in jointed rock masses: Geophysics, v. 74, no. 5, p. E205-E214.

Chadwick, O. A., Hall, R. D., and Phillips, F. M., 1997, Chronology of Pleistocene glacial advances in the central Rocky Mountains: Geological Society of America Bulletin, v. 109, no. 11, p. 1443-1452.

Clarke, B. A., and Burbank, D. W., 2010, Bedrock fracturing, threshold hillslopes, and limits to the magnitude of bedrock landslides: Earth and Planetary Science Letters, v. 297, no. 3, p. 577-586.

-, 2011, Quantifying bedrock-fracture patterns within the shallow subsurface: Implications for rock mass strength, bedrock landslides, and erodibility: Journal of Geophysical Research: Earth Surface, v. 116, no. F4.

Cook, K. L., Whipple, K. X., Heimsath, A. M., and Hanks, T. C., 2009, Rapid incision of the Colorado River in Glen Canyon–insights from channel profiles, local incision rates, and modeling of lithologic controls: Earth Surface Processes and Landforms, v. 34, no. 7, p. 994-1010.

Corbett, L. B., Bierman, P. R., and Rood, D. H., 2016, An approach for optimizing insitu cosmogenic 10 Be sample preparation: Quaternary Geochronology, v. 33, p. 24-34.

Crossey, L., Karlstrom, K., Dorsey, R., Lopez, P., J., Wan, E., Beard, L. S., Asmerom, Y., Polyak, V., Crow, R., Cohen, A., Bright, J., and Pecha, M., 2015, The importance of groundwater in propagating downward integration of the 6-5 Ma Colorado River System: Geochemistry of springs, travertines and lacustrine carbonates of the Grand Canyon region over the past 12 million years.: Geosphere, v. in press.

Crossey, L. J., Karlstrom, K. E., Springer, A. E., Newell, D., Hilton, D. R., and Fischer, T., 2009, Degassing of mantle-derived CO2 and He from springs in the southern Colorado Plateau region--Neotectonic connections and implications for groundwater systems: Geological Society of America Bulletin, v. 121, no. 7-8, p. 1034-1053.

Crow, R., Karlstrom, K., Darling, A., Crossey, L., Polyak, V., Granger, D., Asmerom, Y., and Schmandt, B., 2014, Steady incision of Grand Canyon at the million year timeframe: A case for mantle-driven differential uplift: Earth and Planetary Science Letters, v. 397, p. 159-173.

Crow, R., Karlstrom, K. E., McIntosh, W., Peters, L., and Dunbar, N., 2008, History of Quaternary volcanism and lava dams in western Grand Canyon based on lidar analysis, 40Ar/39Ar dating, and field studies: Implications for flow stratigraphy, timing of volcanic events, and lava dams: Geosphere, v. 4, no. 1, p. 183.

Cyr, A. J., Granger, D. E., Olivetti, V., and Molin, P., 2010, Quantifying rock uplift rates using channel steepness and cosmogenic nuclide–determined erosion rates: Examples from northern and southern Italy: Lithosphere, v. 2, no. 3, p. 188-198.

Cyr, A. J., Miller, D. M., and Mahan, S. A., 2015, Paleodischarge of the Mojave River, southwestern United States, investigated with single-pebble measurements of 10Be: Geosphere, v. 11, no. 4, p. 1158-1171.

Dallegge, T. A., Ort, M. H., and McIntosh, W. C., 2003, Mio-Pliocene chronostratigraphy, basin morphology and paleodrainage relations derived from the Bidahochi Formation, Hopi and Navajo Nations, northeastern Arizona: Mountain Geologist, v. 40, no. 3, p. 55-82.

Darling, A., and Whipple, K., 2015, Geomorphic constraints on the age of the western Grand Canyon: Geosphere, v. 11, no. 4, p. 958-976.

Darling, A. L., Karlstrom, K., Granger, D. E., Aslan, A., Kirby, E., Ouimet, W. B., Lazear, G. D., Coblentz, D. D., and Cole, R. D., 2012, New incision rates along the Colorado River system based on cosmogenic burial dating of terraces: implications for regional controls on Quaternary incision: Geosphere, v. 8, no. 5, p. 1020-1041.

Darling, A. L., Karlstrom, K. E., Aslan, A., Cole, R., Betton, C., and Wan, E., 2009, Quaternary incision rates and drainage evolution of the Uncompahgre and Gunnison Rivers, western Colorado, as calibrated by the Lava Creek B ash: Rocky Mountain Geology, v. 44, no. 1, p. 71-83.

Davis, S. J., Dickinson, W. R., Gehrels, G. E., Spencer, J. E., Lawton, T. F., and Carroll, A. R., 2010, The Paleogene California River: Evidence of Mojave-Uinta paleodrainage from U-Pb ages of detrital zircons: Geology, v. 38, no. 10, p. 931-934.

Davis, W. M., 1901, An excursion to the Grand Canyon of the Colorado, Cambridge, Massachusetts, Printed for the Museum, 201 p.:

Dethier, D. P., 2001, Pleistocene incision rates in the western United States calibrated using Lava Creek B tephra: Geology, v. 29, no. 9, p. 783-786.

DiBiase, R. A., and Whipple, K. X., 2011, The influence of erosion thresholds and runoff variability on the relationships among topography, climate, and erosion rate: Journal of Geophysical Research, v. 116, no. F4.

DiBiase, R. A., Whipple, K. X., Heimsath, A. M., and Ouimet, W. B., 2010, Landscape form and millennial erosion rates in the San Gabriel Mountains, CA: Earth and Planetary Science Letters, v. 289, no. 1-2, p. 134-144.

DiBiase, R. A., Whipple, K. X., Lamb, M. P., and Heimsath, A. M., 2014, The role of waterfalls and knickzones in controlling the style and pace of landscape adjustment in the western San Gabriel Mountains, California: Geological Society of America Bulletin, p. B31113. 31111.

Dickinson, W. R., 1976, Sedimentary basins developed during evolution of Mesozoic-Cenozoic arc-trench system in western North America: Canadian Journal of Earth Sciences, v. 13, no. 9, p. 1268-1287.

-, 2013, Rejection of the lake spillover model for initial incision of the Grand Canyon, and discussion of alternatives: Geosphere, v. 9, no. 1, p. 1-20.

Dickinson, W. R., Klute, M. A., Hayes, M. J., Janecke, S. U., Lundin, E. R., McKittrick, M. A., and Olivares, M. D., 1988, Paleogeographic and paleotectonic setting of Laramide sedimentary basins in the central Rocky Mountain region: Geological Society of America Bulletin, v. 100, no. 7, p. 1023-1039.

Dickinson, W. R., Lawton, T. F., Pecha, M., Davis, S. J., Gehrels, G. E., and Young, R. A., 2012, Provenance of the Paleogene Colton Formation (Uinta Basin) and Cretaceous–Paleogene provenance evolution in the Utah foreland: Evidence from U-Pb ages of detrital zircons, paleocurrent trends, and sandstone petrofacies: Geosphere, v. 8, no. 4, p. 854-880.

Dietrich, W. E., and Smith, J. D., 1983, Influence of the point bar on flow through curved channels: Water Resources Research, v. 19, no. 5, p. 1173-1192.

Donahue, M. S., Karlstrom, K., Aslan, A., Darling, A., Granger, D., Wan, E., Dickinson, R., and Kirby, E., 2013, Incision history of the Black Canyon of Gunnison, Colorado, over the past~ 1 Ma inferred from dating of fluvial gravel deposits: Geosphere, v. 9, no. 4, p. 815-826.

Dorsey, R. J., 2010, Sedimentation and crustal recycling along an active oblique-rift margin: Salton Trough and northern Gulf of California: Geology, v. 38, no. 5, p. 443-446.

Duvall, A., Kirby, E., and Burbank, D., 2004, Tectonic and lithologic controls on bedrock channel profiles and processes in coastal California: J. Geophys. Res, v. 109, no. 10.1029.

El-Naqa, A., 1996, Assessment of geomechanical characterization of a rock mass using a seismic geophysical technique: Geotechnical & Geological Engineering, v. 14, no. 4, p. 291-305.

Elston, D. P., and Young, R. A., 1991a, Cretaceous-Eocene (Laramide) Landscape Development and Oligocene-Pliocene Drainage Reorganization of Transition Zone and Colorado Plateau, Arizona: Journal of Geophysical Research-Solid Earth and Planets, v. 96, no. B7, p. 12389-12406.

Elston, D. P., and Young, R. A., 1991b, Cretaceous-Eocene (Laramide) landscape development and Oligocene-Pliocene drainage reorganization of transition zone and Colorado Plateau, Arizona: Journal of Geophysical Research: Solid Earth (1978–2012), v. 96, no. B7, p. 12389-12406.

Farr, T. G., Rosen, P. A., Caro, E., Crippen, R., Duren, R., Hensley, S., Kobrick, M., Paller, M., Rodriguez, E., and Roth, L., 2007, The shuttle radar topography mission: Reviews of Geophysics, v. 45, no. 2.

Faulds, J. E., Price, L. M., and Wallace, M. A., 2001, Pre–Colorado River paleogeography and extension along the Colorado Plateau–Basin and Range boundary, northwestern Arizona: Colorado River: Origin and Evolution. Monograph, v. 12, p. 93-99.

Flint, J. J., 1974, Stream gradient as a function of order, magnitude, and discharge: Water Resources Research, v. 10, p. 969-973.

Flowers, R., and Farley, K., 2012, Apatite 4He/3He and (U-Th)/He evidence for an ancient Grand Canyon: Science, v. 338, no. 6114, p. 1616-1619.

Flowers, R. M., Wernicke, B. P., and Farley, K. A., 2008, Unroofing, incision, and uplift history of the southwestern Colorado Plateau from apatite (U-Th)/He thermochronometry: Geological Society of America Bulletin, v. 120, no. 5-6, p. 571-587.

Forbriger, T., 2003a, Inversion of shallow-seismic wavefields: I. Wavefield transformation: Geophysical Journal International, v. 153, no. 3, p. 719-734.

-, 2003b, Inversion of shallow-seismic wavefields: II. Inferring subsurface properties from wavefield transforms: Geophysical Journal International, v. 153, no. 3, p. 735-752.

Forte, A. M., Yanites, B. J., and Whipple, K. X., 2016, Complexities of Landscape Evolution During Incision Through Layered Stratigraphy with Contrasts in Rock Strength: Earth Surface Processes and Landforms, v. 41, no. 12, p. 1736-1757.

Fox, M., and Shuster, D., 2014, The influence of burial heating on the (U-Th)/He system in apatite: Grand Canyon case study: Earth and Planetary Science Letters, v. 397, p. 174-183.

Gallen, S. F., Wegmann, K. W., and Bohnenstiehl, D., 2013, Miocene rejuvenation of topographic relief in the southern Appalachians: GSA Today, v. 23, no. 2, p. 4-10.

Garvin, C. D., Hanks, T. C., Finkel, R. C., and Heimsath, A. M., 2005, Episodic incision of the Colorado River in Glen Canyon, Utah: Earth Surface Processes and Landforms, v. 30, no. 8, p. 973-984.

Gasparini, N. M., and Whipple, K. X., 2014, Diagnosing climatic and tectonic controls on topography: Eastern flank of the northern Bolivian Andes: Lithosphere, v. 6, no. 4, p. 230-250.

Gehrels, G., Valencia, V., and Pullen, A., 2006, Detrital zircon geochronology by laser-ablation multicollector ICPMS at the Arizona LaserChron Center: Paleontological Society Papers, v. 12, p. 67.

Godard, V., Bourlès, D. L., Spinabella, F., Burbank, D. W., Bookhagen, B., Fisher, G. B., Moulin, A., and Léanni, L., 2014, Dominance of tectonics over climate in Himalayan denudation: Geology, v. 42, no. 3, p. 243-246.

Grams, P. E., and Schmidt, J. C., 1999, Geomorphology of the Green River in the eastern Uinta Mountains, Dinosaur National Monument, Colorado and Utah: Varieties of fluvial form, p. 81-111.

Granger, D. E., Kirshner, J. W., and Finkel, R., 1996, Spatially averaged long-term erosion rates measured from in situ-produced cosmogenic nuclides in alluvial sediment: Journal of Geology, v. 104, no. 3, p. 249-257.

Granger, D. E., Lifton, N. A., and Willenbring, J. K., 2013, A cosmic trip: 25 years of cosmogenic nuclides in geology: Geological Society of America Bulletin, v. 125, no. 9-10, p. 1379-1402.

Gualtieri, J. L., 1988, Geologic map of the Westwater 30'x 60'Quadrangle, Grand and Uinta counties, Utah and Garfield and Mesa counties, Colorado.

Hack, J. T., 1957, Studies of longitudinal stream profiles in Virginia and Maryland: U.S. Geological Survey Professional Paper, v. 294-B, p. 97.

-, 1975, Dynamic equilibrium and landscape evolution, *in* Melhorn, W. N., and Flemal, R. C., eds., Theories of Landform Development: New York, Allen & Unwin, p. 87-102.

Hack, R., 2000, Geophysics for slope stability: Surveys in geophysics, v. 21, no. 4, p. 423-448.

Hancock, G. S., and Anderson, R. S., 2002, Numerical modeling of fluvial strath-terrace formation in response to oscillating climate: Geological Society of America Bulletin, v. 114, no. 9, p. 1131-1142.

Hancock, J. M., and Kauffman, E., 1979, The great transgressions of the Late Cretaceous: Journal of the Geological Society, v. 136, no. 2, p. 175-186.

Hanks, T. C., Lucchitta, I., Davis, S. W., Davis, M. E., Finkel, R. C., Lefton, S. A., and Garvin, C. D., 2001, The Colorado River and the age of Glen Canyon: The Colorado River: Origin and Evolution: Grand Canyon, Arizona, Grand Canyon Monograph, v. 12, p. 129-133.

Hansen, S. M., Dueker, K. G., Stachnik, J. C., Aster, R. C., and Karlstrom, K. E., 2013, A rootless rockies—Support and lithospheric structure of the Colorado Rocky Mountains inferred from CREST and TA seismic data: Geochemistry, Geophysics, Geosystems, v. 14, no. 8, p. 2670-2695.

Hansen, W. R., 1986, Neogene tectonics and geomorphology of the eastern Uinta Mountains in Utah, Colorado, and Wyoming: United States Geological Survey, Professional Paper;(USA), v. 75, no. 1356.

Harkins, N., Kirby, E., Heimsath, A., Robinson, R., and Reiser, U., 2007, Transient fluvial incision in the headwaters of the Yellow River, northeastern Tibet, China: Journal of Geophysical Research, v. 112, no. F3.

Hasbargen, L. E., and Paola, C., 2000, Landscape instability in an experimental drainage basin: Geology, v. 28, no. 12, p. 1067-1070.

Haviv, I., Enzel, Y., Whipple, K. X., Zilberman, E., Matmon, A., Stone, J., and Fifield, K. L., 2010, Evolution of vertical knickpoints (waterfalls) with resistant caprock: Insights from numerical modeling: Journal of Geophysical Research, v. 115, no. F3.

Haviv, I., Enzel, Y., Whipple, K. X., Zilberman, E., Stone, J., Matmon, A., and Fifield, L. K., 2006, Amplified erosion above waterfalls and oversteepened bedrock reaches: Journal of Geophysical Research, v. 111, no. F4.

Heller, P. L., Bowdler, S. S., Chambers, H. P., Coogan, J. C., Hagen, E. S., Shuster, M. W., Winslow, N. S., and Lawton, T. F., 1986, Time of initial thrusting in the Sevier orogenic belt, Idaho-Wyoming and Utah: Geology, v. 14, p. 388-391.

Hoffman, M., 2009, Mio-Pliocene erosional exhumation of the central Colorado Plateau, eastern Utah: New insights from apatite (U-Th)/He thermochronometry: University of Kansas.

House, P. K., Pearthree, P. A., and Perkins, M. E., 2008, Stratigraphic evidence for the role of lake spillover in the inception of the lower Colorado River in southern Nevada and western Arizona: Geological Society of America Special Papers, v. 439, p. 335-353.

Howard, A., and Dolan, R., 1981, Geomorphology of the Colorado River in the Grand Canyon: The Journal of Geology, p. 269-298.

Howard, A. D., 1994, A detachment-limited model of drainage basin evolution: Water Resources Research, v. 30, no. 7, p. 2261-2285.

Huntoon, P., 1988, Late Cenozoic gravity tectonic deformation related to the Paradox salts in the Canyonlands area of Utah: Salt deformation in the Paradox region, Utah: Utah Geological and Mineral Survey Bulletin, v. 122, p. 81-93.

Huntoon, P. W., 1975, The Surprise Valley landslide and widening of the Grand Canyon, Northern Arizona Society of Science and Art.

Ingersoll, R. V., Grove, M., Jacobson, C. E., Kimbrough, D. L., and Hoyt, J. F., 2013, Detrital zircons indicate no drainage link between southern California rivers and the Colorado Plateau from mid-Cretaceous through Pliocene: Geology, v. 41, no. 3, p. 311-314.

Ivory, S. J., McGlue, M. M., Ellis, G. S., Lézine, A.-M., Cohen, A. S., and Vincens, A., 2014, Vegetation controls on weathering intensity during the last deglacial transition in southeast Africa: PloS one, v. 9, no. 11, p. e112855.

Jaeger, J. C., Cook, N. G., and Zimmerman, R., 2009, Fundamentals of rock mechanics, John Wiley & Sons.

Johnson, J. P., 2007, Feedbacks between erosional morphology, sediment transport and abrasion in the transient adjustment of fluvial bedrock channels. [Ph.D. thesis: Massachusetts Institute of Technology.

Johnson, J. P., Whipple, K. X., Sklar, L. S., and Hanks, T. C., 2009, Transport slopes, sediment cover, and bedrock channel incision in the Henry Mountains, Utah: Journal of Geophysical Research: Earth Surface (2003–2012), v. 114, no. F2.

Karlstrom, K., Coblentz, D., Dueker, K., Ouimet, W., Kirby, E., Van Wijk, J., Schmandt, B., Kelley, S., Lazear, G., and Crossey, L., 2012, Mantle-driven dynamic uplift of the Rocky Mountains and Colorado Plateau and its surface response: Toward a unified hypothesis: Lithosphere, v. 4, no. 1, p. 3-22.

Karlstrom, K. E., Crow, R., Crossey, L. J., Coblentz, D., and Van Wijk, J. W., 2008, Model for tectonically driven incision of the younger than 6 Ma Grand Canyon: Geology, v. 36, no. 11, p. 835.

Karlstrom, K. E., Crow, R. S., Peters, L., McIntosh, W., Raucci, J., Crossey, L. J., Umhoefer, P., and Dunbar, N., 2007, 40Ar/39Ar and field studies of Quaternary basalts in Grand Canyon and model for carving Grand Canyon: Quantifying the interaction of river incision and normal faulting across the western edge of the Colorado Plateau: Geological Society of America Bulletin, v. 119, no. 11-12, p. 1283-1312.

Karlstrom, K. E., Heizler, M., and Quigley, M. C., 2010, Structure and 40Ar/39Ar K-feldspar thermal history of the Gold Butte block: Reevaluation of the tilted crustal section model: Geological Society of America Special Papers, v. 463, p. 331-352.

Karlstrom, K. E., Lee, J. P., Kelley, S. A., Crow, R. S., Crossey, L. J., Young, R. A., Lazear, G., Beard, L. S., Ricketts, J. W., and Fox, M., 2014, Formation of the Grand Canyon 5 to 6 million years ago through integration of older palaeocanyons: Nature Geoscience, v. 7, p. 239-244.

Kelley, S. A., and Blackwell, D. D., 1990, Thermal history of the multi-well experiment (MWX) site, Piceance Creek Basin Northwestern Colorado, derived from fission-track analysis: International Journal of Radiation Applications and Instrumentation. Part D. Nuclear Tracks and Radiation Measurements, v. 17, no. 3, p. 331-337.

Kirby, E., and Whipple, K. X., 2012, Expression of active tectonics in erosional landscapes: Journal of Structural Geology, v. 44, p. 54-75.

Kirkby, M. J. r., and West, E. E., 1979, The equilibrium of natural streams; a new theoretical approach providing a key to the understanding of longer-term fluvial processes: Journal of Hydrology, v. 42, no. 3-4, p. 397.

Koons, E. D., 1955, Cliff retreat in the southwestern United States: American Journal of Science, v. 253, no. 1, p. 44-52.

Korup, O., and Schlunegger, F., 2009, Rock-type control on erosion-induced uplift, eastern Swiss Alps: Earth and Planetary Science Letters, v. 278, no. 3, p. 278-285.

Lague, D., 2014, The stream power river incision model: evidence, theory and beyond: Earth Surface Processes and Landforms, v. 39, no. 1, p. 38-61.

Lague, D., Hovius, N., and Davy, P., 2005, Discharge, discharge variability, and the bedrock channel profile: Journal of Geophysical Research: Earth Surface (2003–2012), v. 110, no. F4.

Lazear, G., Karlstrom, K., Aslan, A., and Kelley, S., 2013, Denudation and flexural isostatic response of the Colorado Plateau and southern Rocky Mountains region since 10 Ma: Geosphere, v. 9, no. 4, p. 792-814.

Longwell, C. R., 1946, How old is the Colorado River?: American Journal of Science, v. 244, no. 12, p. 817-835.

Lucchitta, I., 1966, Cenozoic geology of the upper Lake Mead area adjacent to the Grand Wash Cliffs: Arizona [Ph. D. thesis]: Pennsylvania State University, University Park.

Lucchitta, I., 1972, Early history of the Colorado River in the Basin and Range Province: Geological Society of America Bulletin, v. 83, no. 7, p. 1933-1948.

Lucchitta, I., 1979, Late Cenozoic uplift of the southwestern Colorado Plateau and adjacent lower Colorado River region: Tectonophysics, v. 61, no. 1, p. 63-95.

MacGregor, F., Fell, R., Mostyn, G., Hocking, G., and McNally, G., 1994, The estimation of rock rippability: Quarterly Journal of Engineering Geology and Hydrogeology, v. 27, no. 2, p. 123-144.

Marchetti, D. W., Hynek, S. A., and Cerling, T. E., 2012, Gravel-capped benches above northern tributaries of the Escalante River, south-central Utah: Geosphere, v. 8, no. 4, p. 835-853.

Moon, B. P., and Selby, M. J., 1983, Rock mass strength and scarp forms in southern Africa: Geografiska Annaler. Series A: Physical Geography, v. 65, no. 1-2, p. 135-145.

Moser, T., 1991, Shortest path calculation of seismic rays: Geophysics, v. 56, no. 1, p. 59-67.

Murray, K., Reiners, P., and Thomson, S., 2016, Rapid Pliocene–Pleistocene erosion of the central Colorado Plateau documented by apatite thermochronology from the Henry Mountains: Geology, v. 44, no. 6, p. 483-486.

Mussett, A. E., and Khan, M. A., 2000, Looking into the earth: an introduction to geological geophysics, Cambridge University Press.

Nelson, M. S., and Rittenour, T., 2014, Middle to late Holocene chronostratigraphy of alluvial fill deposits along Kanab Creek in southern Utah: Geology of Utah's Far South: Utah Geological Association, Publication, v. 43, p. 97-116.

Nichols, K. K., Bierman, P., and Rood, D., In Review, Cosmogenic 10-Be and sediment budgets reveal a multi-aged Grand Canyon: Geology.

Nichols, K. K., Webb, R. H., Bierman, P. R., and Rood, D. H., 2011, Measurements of cosmogenic 10 Be reveal rapid response of Grand Canyon tributary hillslopes to Colorado River incision: Geological Society of America - Abstracts with Programs, v. 43, p. 274.

Nielson, J. E., Lux, D. R., Dalrymple, G. B., and Glazner, A. F., 1990, Age of the Peach Springs Tuff: Journal of Geophysical Research, v. 95, p. 571-580.

Niemi, N. A., Oskin, M., Burbank, D. W., Heimsath, A. M., and Gabet, E. J., 2005, Effects of bedrock landslides on cosmogenically determined erosion rates: Earth and Planetary Science Letters, v. 237, no. 3-4, p. 480-498.

Ouimet, W. B., Whipple, K. X., and Granger, D. E., 2009, Beyond threshold hillslopes: Channel adjustment to base-level fall in tectonically active mountain ranges: Geology, v. 37, no. 7, p. 579-582.

Pearthree, P. A., Spencer, J. E., Faulds, J. E., and House, P. K., 2008, Comment on "Age and evolution of the Grand Canyon revealed by U-Pb dating of water table-type speleothems": Science, v. 321, no. 5896, p. 1634.

Pederson, J., Burnside, N., Shipton, Z., and Rittenour, T., 2013a, Rapid river incision across an inactive fault—Implications for patterns of erosion and deformation in the central Colorado Plateau: Lithosphere, v. 5, no. 5, p. 513-520.

Pederson, J., Karlstrom, K., Sharp, W., and McIntosh, W., 2002a, Differential incision of the Grand Canyon related to Quaternary faulting - Constraints from U-series and Ar/Ar dating: Geology, v. 30, no. 8, p. 739-742.

Pederson, J., Young, R., Lucchitta, I., Beard, L. S., and Billingsley, G., 2008, Comment on "Age and evolution of the Grand Canyon revealed by U-Pb dating of water table-type speleothems": Science, v. 321, no. 5896, p. 1634; author reply 1634.

Pederson, J. L., 2008, The mystery of the pre-Grand Canyon Colorado River-results from the Muddy Creek formation: GSA Today, v. 18, no. 3, p. 4.

Pederson, J. L., Anders, M. D., Rittenhour, T. M., Sharp, W. D., Gosse, J. C., and Karlstrom, K. E., 2006, Using fill terraces to understand incision rates and evolution of the Colorado River in eastern Grand Canyon, Arizona: Journal of Geophysical Research, v. 111, no. F2.

Pederson, J. L., Cragun, W. S., Hidy, A. J., Rittenour, T. M., and Gosse, J. C., 2013b, Colorado River chronostratigraphy at Lee's Ferry, Arizona, and the Colorado Plateau bull's-eye of incision: Geology, v. 41, no. 4, p. 427-430.

Pederson, J. L., Mackley, R. D., and Eddleman, J. L., 2002b, Colorado Plateau uplift and erosion evaluated using GIS: GSA Today, v. 12, no. 8, p. 4-10.

Pederson, J. L., and Tressler, C., 2012, Colorado River long-profile metrics, knickzones and their meaning: Earth and Planetary Science Letters, v. 345, p. 171-179.

Pelletier, J. D., 2009, Numerical modeling of the late Cenozoic geomorphic evolution of Grand Canyon, Arizona: Geological Society of America Bulletin, v. 122, no. 3-4, p. 595-608.

Perron, J. T., and Royden, L., 2013, An integral approach to bedrock river profile analysis: Earth Surface Processes and Landforms, v. 38, no. 6, p. 570-576.

Polyak, V., Hill, C., and Asmerom, Y., 2008, Age and evolution of the Grand Canyon revealed by U-Pb dating of water table-type speleothems: Science, v. 319, no. 5868, p. 1377-1380.

Portenga, E. W., and Bierman, P. R., 2011, Understanding Earth's eroding surface with 10Be: GSA Today, v. 21, no. 8, p. 4-10.

Potochnik, A. R., 1989, Depositional style and tectonic implications of the Mogollon Rim Formation (Eocene), east-central Arizona: Globe, v. 1, no. 1, p. 0.

Potochnik, A. R., and Faulds, J. E., 1998, A tale of two rivers: Tertiary structural inversion and drainage reversal across the southern boundary of the Colorado Plateau: Geologic excursions in northern and central Arizona: Field trip guidebook: Flagstaff, Arizona, Northern Arizona University, p. 149-173.

Powell, J. W., 1875, Exploration of the Colorado River of the West and its Tributaries.

Prince, P. S., Spotila, J. A., and Henika, W. S., 2011, Stream capture as driver of transient landscape evolution in a tectonically quiescent setting: Geology, v. 39, no. 9, p. 823-826.

Quigley, M. C., Karlstrom, K. E., Kelley, S., and Heizler, M., 2010, Timing and mechanisms of basement uplift and exhumation in the Colorado Plateau-Basin and Range transition zone, Virgin Mountain anticline, Nevada-Arizona: Geological Society of America Special Papers, v. 463, p. 311-329.

Repka, J. L., Anderson, R. S., and Finkel, R. C., 1997, Cosmogenic dating of fluvial terraces, Fremont River, Utah: Earth and Planetary Science Letters, v. 152, no. 1-4, p. 59-73.

Reynolds, R., Belnap, J., Reheis, M., Lamothe, P., and Luiszer, F., 2001, Aeolian dust in Colorado Plateau soils: nutrient inputs and recent change in source: Proceedings of the National Academy of Sciences, v. 98, no. 13, p. 7123-7127.

Roberson, P., and Pederson, J., 2001, Rock-strength control in Desolation and Gray canyons of the Green River: a river landscape in dynamic equilibrium: Abstracts with Programs, Geological Society of America, v. 33, p. 14.

Rosenberg, R., Kirby, E., Aslan, A., Karlstrom, K., Heizler, M., and Ouimet, W., 2014, Late Miocene erosion and evolution of topography along the western slope of the Colorado Rockies: Geosphere, v. 10, no. 4, p. 641-663.

Rosenbloom, N. A., and Anderson, R. S., 1994, Hillslope and channel evolution in a marine terraced landscape, Santa Cruz, California: Journal of Geophysical Research, v. 99, no. B7, p. 14,013-014,029.

Rossi, M. W., 2014, Hydroclimatic Controls on Erosional Efficiency in Mountain Landscapes: Arizona State University.

Rossi, M. W., Quigley, M., Fletcher, J., Whipple, K., Diaz-Torres, J., Seiler, C., Fifield, L. K., and Heimsath, A. M., In Review, Along-strike variation in catchment morphology and cosmogenic denudation rates reveal the pattern and history of footwall uplift, Main Gulf Escaprment, Baja California: Geological Society America Bulletin.

Roux-Mallouf, L., Godard, V., Cattin, R., Ferry, M., Gyeltshen, J., Ritz, J. F., Drupka, D., Guillou, V., Arnold, M., and Aumaître, G., 2015, Evidence for a wide and gently dipping Main Himalayan Thrust in western Bhutan: Geophysical Research Letters, v. 42, no. 9, p. 3257-3265.

Roy, M., Jordan, T. H., and Pederson, J., 2009, Colorado Plateau magmatism and uplift by warming of heterogeneous lithosphere: Nature, v. 459, no. 7249, p. 978-982.

Roy, M., Kelley, S., Pazzaglia, F., Cather, S., and House, M., 2004, Middle Tertiary buoyancy modification and its relationship to rock exhumation, cooling, and subsequent extension at the eastern margin of the Colorado Plateau: Geology, v. 32, no. 10, p. 925.

Sable, E., and Hereford, R., 2004, Geologic map of the Kanab 30′× 60′ quadrangle: Utah and Arizona: US Geological Survey, Geologic Investigations Series I-2655, scale, v. 1, no. 100,000.

Safran, E. B., Bierman, P. R., Aalto, R., Dunne, T., Whipple, K. X., and Caffee, M., 2005, Erosion rates driven by channel network incision in the Bolivian Andes: Earth Surface Processes and Landforms, v. 30, no. 8, p. 1007-1024.

Scherler, D., Bookhagen, B., and Strecker, M. R., 2014, Tectonic control on 10Be-derived erosion rates in the Garhwal Himalaya, India: Journal of Geophysical Research: Earth Surface, v. 119, no. 2, p. 83-105.

Schiefelbein, I., 2002, Fault segmentation, fault linkage and hazards along the Sevier fault, southwestern Utah: Las Vegas, University of Nevada at Las Vegas: MS thesis, 134 p., 5 plates.

Schiefelbein, I. M., Fault Segmentation, Linkage, and Earthquake hazards along the Sevier Fault, SW Utah *in* Proceedings GSA Abst. w. Progs.2001, Volume 33, p. 38.

Schmidt, K. M., and Montgomery, D. R., 1995, Limits to relief: Science, v. 270, p. 617-620.

Schmidt, K. M., and Montgomery, D. R., 1996, Rock mass strength assessment for bedrock landsliding: Environmental & Engineering Geoscience, v. 2, no. 3, p. 325-338.

Schoenbohm, L., Whipple, K., Burchfiel, B., and Chen, L., 2004, Geomorphic constraints on surface uplift, exhumation, and plateau growth in the Red River region, Yunnan Province, China: Geological Society of America Bulletin, v. 116, no. 7-8, p. 895-909.

Schwanghart, W., and Scherler, D., 2014, Short Communication: TopoToolbox 2-MATLAB-based software for topographic analysis and modeling in Earth surface sciences: Earth Surface Dynamics, v. 2, no. 1, p. 1.

Selby, M. J., 1981, A method of determining rock mass strength; field tested in Antarctica: New Zealand Antarctic Record, v. 3, no. 2, p. 22.

-, 1982a, Controls on the stability and inclinations of hillslopes formed on hard rock: Earth Surfaces Processes and Landforms, v. 7, no. 5, p. 449-467.

-, 1982b, Rock mass strength and the form of some inselbergs in the central Namib Desert: Earth Surfaces Processes and Landforms, v. 7, no. 5, p. 489-497.

-, 1993, Hillslope Materials and Processes, Oxford, Oxford University Press.

Sheriff, R. E., and Geldart, L. P., 1995, Exploration seismology, Cambridge university press.

Siame, L., Angelier, J., Chen, R.-F., Godard, V., Derrieux, F., Bourlès, D., Braucher, R., Chang, K.-J., Chu, H.-T., and Lee, J.-C., 2011, Erosion rates in an active orogen (NE-Taiwan): A confrontation of cosmogenic measurements with river suspended loads: Quaternary Geochronology, v. 6, no. 2, p. 246-260.

Sjøgren, B., Øfsthus, A., and Sandberg, J., 1979, Seismic Classification of Rock Mass QUALITIES*: Geophysical Prospecting, v. 27, no. 2, p. 409-442.

Sklar, L. S., 2004, A mechanistic model for river incision into bedrock by saltating bed load: Water Resources Research, v. 40, no. 6.

Sklar, L. S., and Dietrich, W. E., 2001, Sediment and rock strength controls on river incision into bedrock: Geology, v. 29, no. 12, p. 1087-1090.

Spencer, J. E., Patchett, P. J., Pearthree, P. A., House, P. K., Sarna-Wojcicki, A. M., Wan, E., Roskowski, J. A., and Faulds, J. E., 2013, Review and analysis of the age and origin of the Pliocene Bouse Formation, lower Colorado River Valley, southwestern USA: Geosphere, v. 9, no. 3, p. 444-459.

Sprinkel, D. A., 2009, Interim Geologic Map of the Seep Ridge 30'X 60'Quadrangle, Uintah, Duchesne, and Carbon counties, Utah, and Rio Blanco and Garfield Counties, Colorado: Utah Geological Survey Open-File Report 549DM.

Stafleu, J., Schlager, W., Everts, A., J., K., Blommers, G., and A., v., 1996, Outcrop topography as a proxy of acoustic impedance in synthetic seismograms: Geophysics, v. 61, no. 6, p. 1779-1788.

Stock, J. D., and Montgomery, D. R., 1999, Geologic constraints on bedrock river incision using the stream power law: Journal of Geophysical Research, v. 104, no. B3, p. 4983-4993.

Suzuki, T., 1982, Rate of lateral planation by Iwaki River, Japan: Transactions, Japanese Geomorphological Union, v. 3, no. 1, p. 1-24.

Taylor, W. J., Bartley, J. M., Martin, M. W., Geissman, J. W., Walker, J. D., Armstrong, P. A., and Fryxell, J. E., 2000, Relations between hinterland and foreland shortening: Sevier orogeny, central North American Cordillera: Tectonics, v. 19, no. 6, p. 1124-1143.

Tucker, G., Lancaster, S., Gasparini, N., and Bras, R., 2001, The channel-hillslope integrated landscape development model (CHILD), Landscape erosion and evolution modeling, Springer, p. 349-388.

Tucker, G. E., and Slingerland, R. L., 1994, Erosional dynamics, flexural isostacy, and long-lived escarpments: a numerical modeling study: Journal of Geophysical Research, v. 99, p. 12,229-212,243.

Tucker, G. E., and Whipple, K., 2002, Topographic outcomes predicted by stream erosion models: Sensitivity analysis and intermodel comparison: Journal of Geophysical Research, v. 107, no. B9.

Umhoefer, P. J., Duebendorfer, E. M., Blythe, N., Swaney, Z. A., Beard, L. S., and McIntosh, W. C., 2010, Development of Gregg Basin and the southwestern Grand Wash Trough during

late-stage faulting in eastern Lake Mead, Arizona: Geological Society of America Special Papers, v. 463, p. 221-241.

Ward, D. J., Berlin, M. M., and Anderson, R. S., 2011, Sediment dynamics below retreating cliffs: Earth Surface Processes and Landforms, v. 36, no. 8, p. 1023-1043.

Weimer, R. J., 1960, Upper cretaceous stratigraphy, rocky Mountain area: AAPG Bulletin, v. 44, no. 1, p. 1-20.

Weiss, M. P., Witkind, I. J., and Cashion, W. B., 1990, Geologic map of the Price 30'x 60'Quadrangle, Carbon, Duchesne, Uinta, Utah and Wasatch counties, Utah.

Weissel, J. K., and Seidl, M. A., 1997, Influence of rock strength properties on escarpment retreat across passive continental margins: Geology (Boulder), v. 25, no. 7, p. 631-634.

Wenrich, K. J., Billingsley, G. H., and Blackerby, B. A., 1995, Spatial migration and compositional changes of Miocene-Quaternary magmatism in the western Grand Canyon: Journal of Geophysical Research, v. 100, no. B6, p. 10417-10410,10440.

Wernicke, B., 2011, The California River and its role in carving Grand Canyon: Geological Society of America Bulletin, v. 123, no. 7-8, p. 1288-1316.

Whipple, K., 2001a, Fluvial landscape response time: How plausible is steady state denudation?: American Journal of Science, v. 301, p. 313-325.

Whipple, K., 2002, GE Tucker: Journal of Geophysical Research, v. 107, no. B9, p. 2179.

Whipple, K., Kirby, E., and Brocklehurst, S., 1999a, Geomorphic limits to climatically induced increases in topographic relief: Nature, v. 401, p. 39-43.

Whipple, K. X., 2001b, Fluvial landscape response time: How plausible is steady-state denudation?: American Journal of Science, v. 301, no. 4-5, p. 313-325.

Whipple, K. X., 2004, Bedrock Rivers and the Geomorphology of Active Orogens: Annual Review of Earth and Planetary Sciences, v. 32, no. 1, p. 151-185.

Whipple, K. X., and Gasparini, N., 2014, Tectonic control of topography, rainfall patterns, and erosion during rapid post–12 Ma uplift of the Bolivian Andes: Lithosphere, v. 6, no. 4, p. 251-268.

Whipple, K. X., Hancock, G. S., and Anderson, R. S., 2000, River incision into bedrock: Mechanics and relative efficacy of plucking, abrasion, and cavitation: Geological Society of America Bulletin, v. 112, no. 3, p. 490-503.

Whipple, K. X., Kirby, E., and Brocklehurst, S. H., 1999b, Geomorphic limits to climate-induced increases in topographic relief: Nature, v. 401, p. 39-43.

Whipple, K. X., and Tucker, G. E., 1999, Dynamics of the stream-power river incision model: Implications for height limits of mountain ranges, landscape response timescales, and research needs: Journal of Geophysical Research, v. 104, no. B8, p. 17661-17617,17674.

Whittaker, A. C., 2012, How do landscapes record tectonics and climate?: Lithosphere, v. 4, no. 2, p. 160-164.

Whittaker, A. C., Cowie, P. A., Attal, M., Tucker, G. E., and Roberts, G. P., 2007, Bedrock channel adjustment to tectonic forcing: Implications for predicting river incision rates: Geology, v. 35, no. 2, p. 103.

Willenbring, J. K., Gasparini, N. M., Crosby, B. T., and Brocard, G., 2013, What does a mean mean? The temporal evolution of detrital cosmogenic denudation rates in a transient landscape: Geology, v. 41, no. 12, p. 1215-1218.

Willett, S. D., McCoy, S. W., Perron, J. T., Goren, L., and Chen, C.-Y., 2014, Dynamic reorganization of river basins: Science, v. 343, no. 6175, p. 1248765.

Willis, G. C., and Biek, R., 2001, Quaternary incision rates of the Colorado River and major tributaries in the Colorado Plateau, Utah: Colorado River: Origin and evolution: Grand Canyon, Arizona, Grand Canyon Association, p. 125-127.

Witkind, I. J., 1988, Geologic Map of the Huntington 30'X 60'Quadrangle, Carbon, Emery, Grand, and Uintah Counties, Utah.

Wobus, C. W., Whipple, K. W., Kirby, E., and Snyder, N. P., 2006, Tectonics from topography: Proceedures, promise, and pitfalls, *in* Willett, S. D., Hovius, N., Brandon, M., and Fisher, D. M., eds., Climate, Tectonics and Landscape Evolution: Geological Society of America Special Paper, Volume 398, Penrose Conference Series, p. 55-74.

Wolkowinsky, A. J., and Granger, D. E., 2004, Early Pleistocene incision of the San Juan River, Utah, dated with 26Al and 10Be: Geology, v. 32, no. 9, p. 749.

Young, R., 1979, Laramide deformation, erosion and plutonism along the southwestern margin of the Colorado Plateau: Tectonophysics, v. 61, no. 1, p. 25-47.

Young, R. A., 1999, Nomenclature and Ages of Late Cretaceous-Tertiary Strata in the Hualapai Plateau Region, Northwest Arizona, US Government Printing Office.

Young, R. A., 2008, Pre-Colorado River drainage in western Grand Canyon: potential influence on Miocene stratigraphy in Grand Wash trough, *in* Reheis, M. C., Hershley, R., and Miller, D. M., eds., Special Paper - Geological Society of America, Volume 439, p. 319.

Young, R. A., and Brennan, W. J., 1974, Peach Springs Tuff: Its bearing on structural evolution of the Colorado Plateau and development of Cenozoic drainage in Mohave County, Arizona: Geological Society of America Bulletin, v. 85, no. 1, p. 83-90.

Young, R. A., and Crow, R., 2014, Paleogene Grand Canyon incompatible with Tertiary paleogeography and stratigraphy: Geosphere, v. 10, no. 4, p. 664-679.

Young, R. A., and Hartman, J. H., 2014, Paleogene rim gravel of Arizona: Age and significance of the Music Mountain Formation: Geosphere, v. 10, no. 5, p. 870-891.

Young, R. A., and McKee, E. H., 1978, Early and middle Cenozoic drainage and erosion in west-central Arizona: Geological Society of America Bulletin, v. 89, no. 12, p. 1745-1750.

Young, R. A., and Spamer, E. E., 2001, Colorado River: Origin and Evolution: Proceedings of a Symposium Held at Grand Canyon National Park in June, 2000, Grand Canyon Assn, v. 12.

APPENDIX A

SLOPE-AREA DATA AS LOG-LOG PLOTS FOR EACH CATCHMENT STUDIED IN CHAPTER TWO.

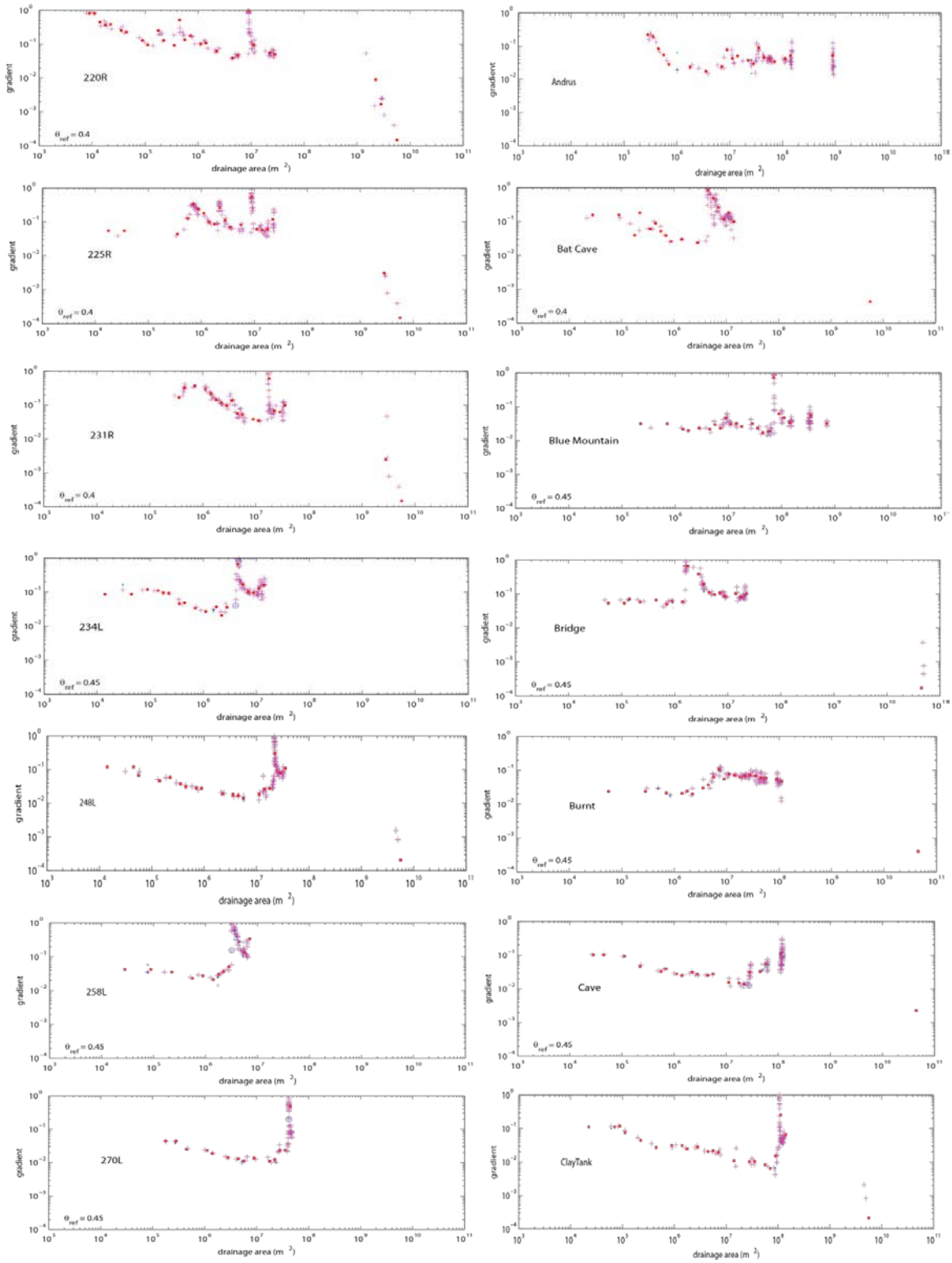
220R
θref = 0.4
Andrus
225R
θref = 0.4
Bat Cave
θref = 0.4
231R
θref = 0.4
Blue Mountain
θref = 0.45
234L
θref = 0.45
Bridge
θref = 0.45
248L
Burnt
θref = 0.45
258L
θref = 0.45
Cave
θref = 0.45
270L
θref = 0.45
ClayTank
gradient
drainage area (m 2)

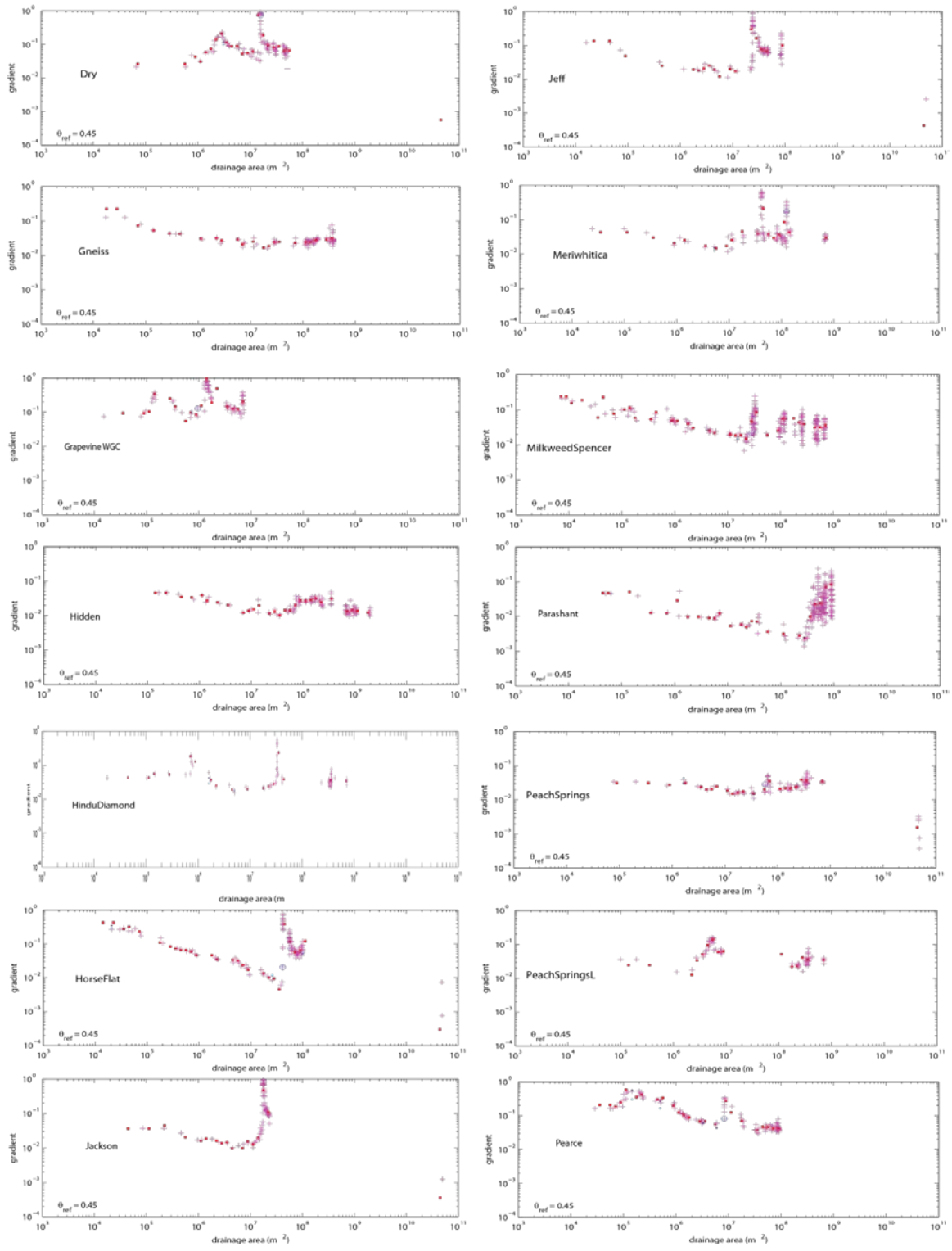
Dry
Jeff
Gneiss
Meriwhitica
Grapevine WGC
MilkweedSpencer
Hidden
Parashant
HinduDiamond
PeachSprings
HorseFlat
PeachSpringsL
Jackson
Pearce
gradient
drainage area (m 2)
θref = 0.45

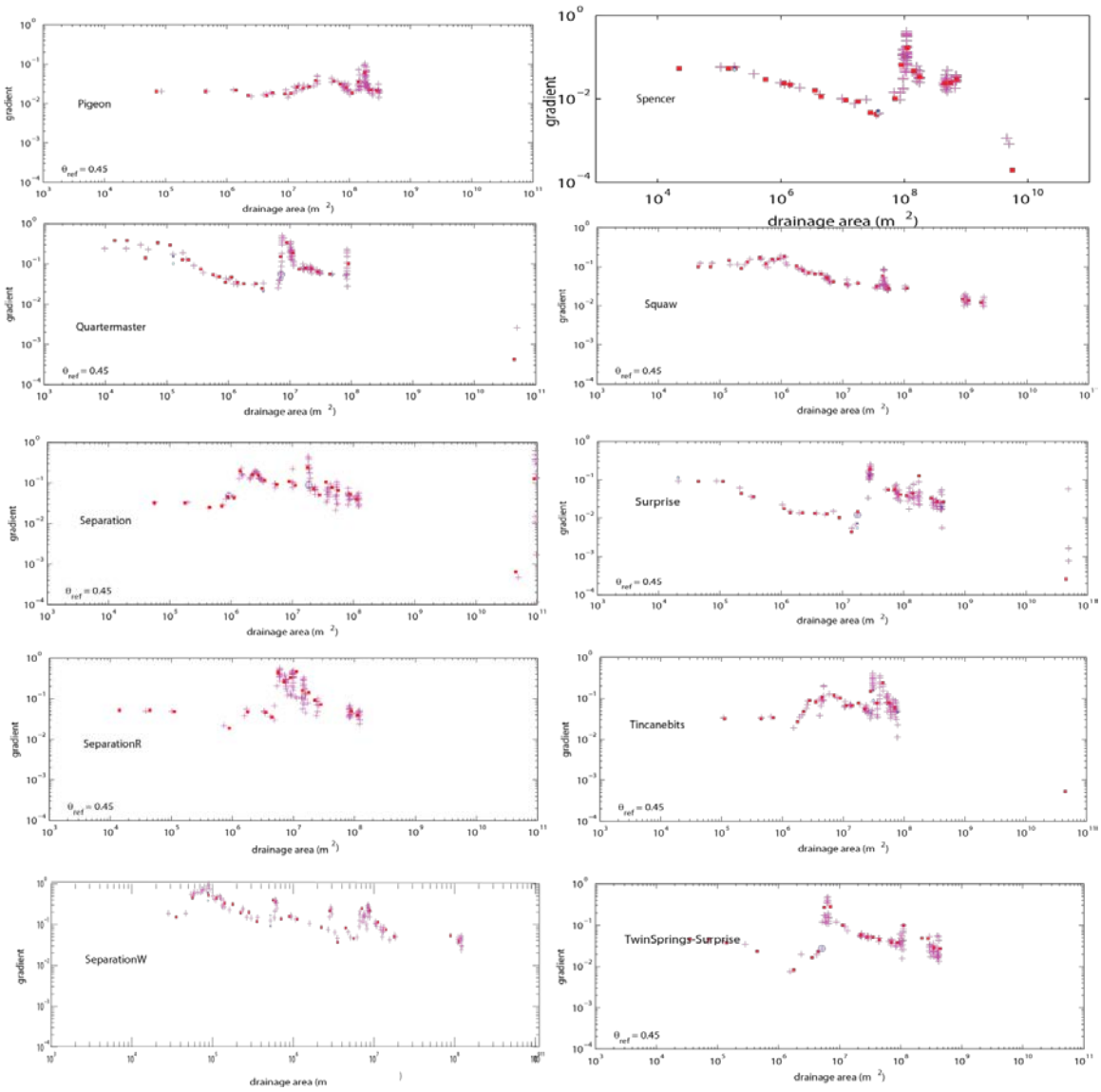

Appendix A: Slope-area plots used for stream profile analysis and, if appropriate, regression of channel steepness and theta for projection. Criteria for selection include geologic, independent observations and a relatively linear section above the knickpoints in these plots.

Appendix A: Chi-distance plots of all streams analyzed in western Grand Canyon, grouped by relative topographic patterns. Purple is Sanup/Shivwits plateax, green is Grand Wash Cliffs and Hualapai Plateau streams are Black and Red.

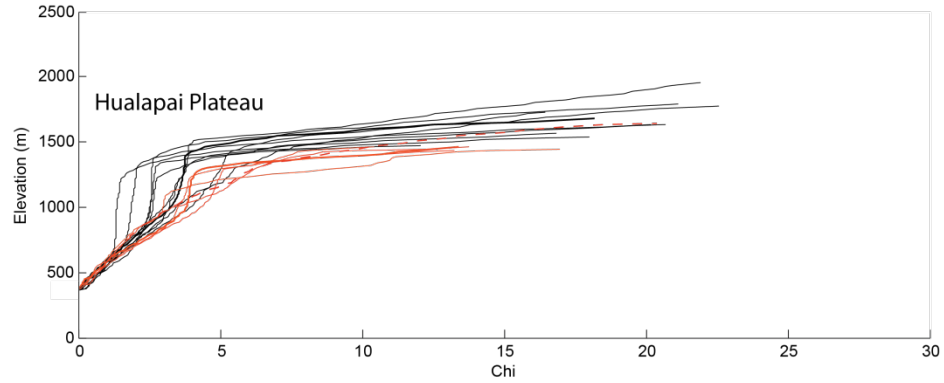

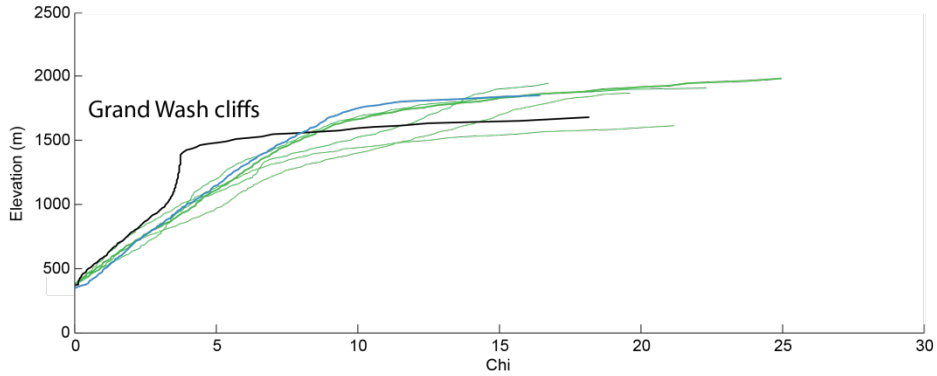

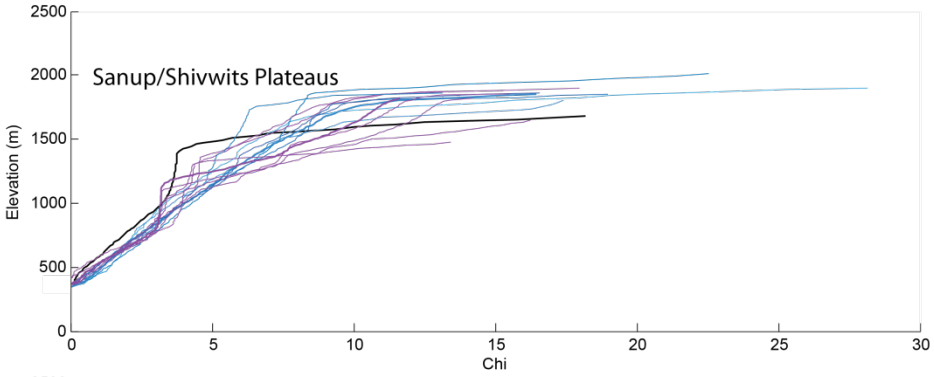

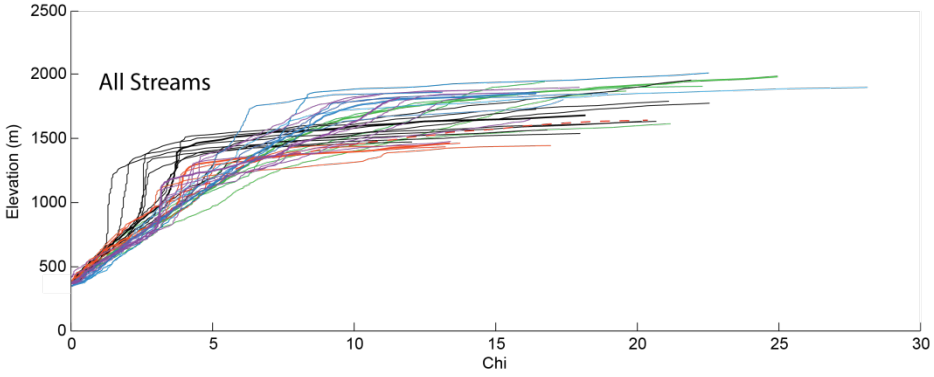

APPENDIX B

GRAND STAIRCASE-LIKE AND GRAND CANYON-LIKE SIMULATIONS

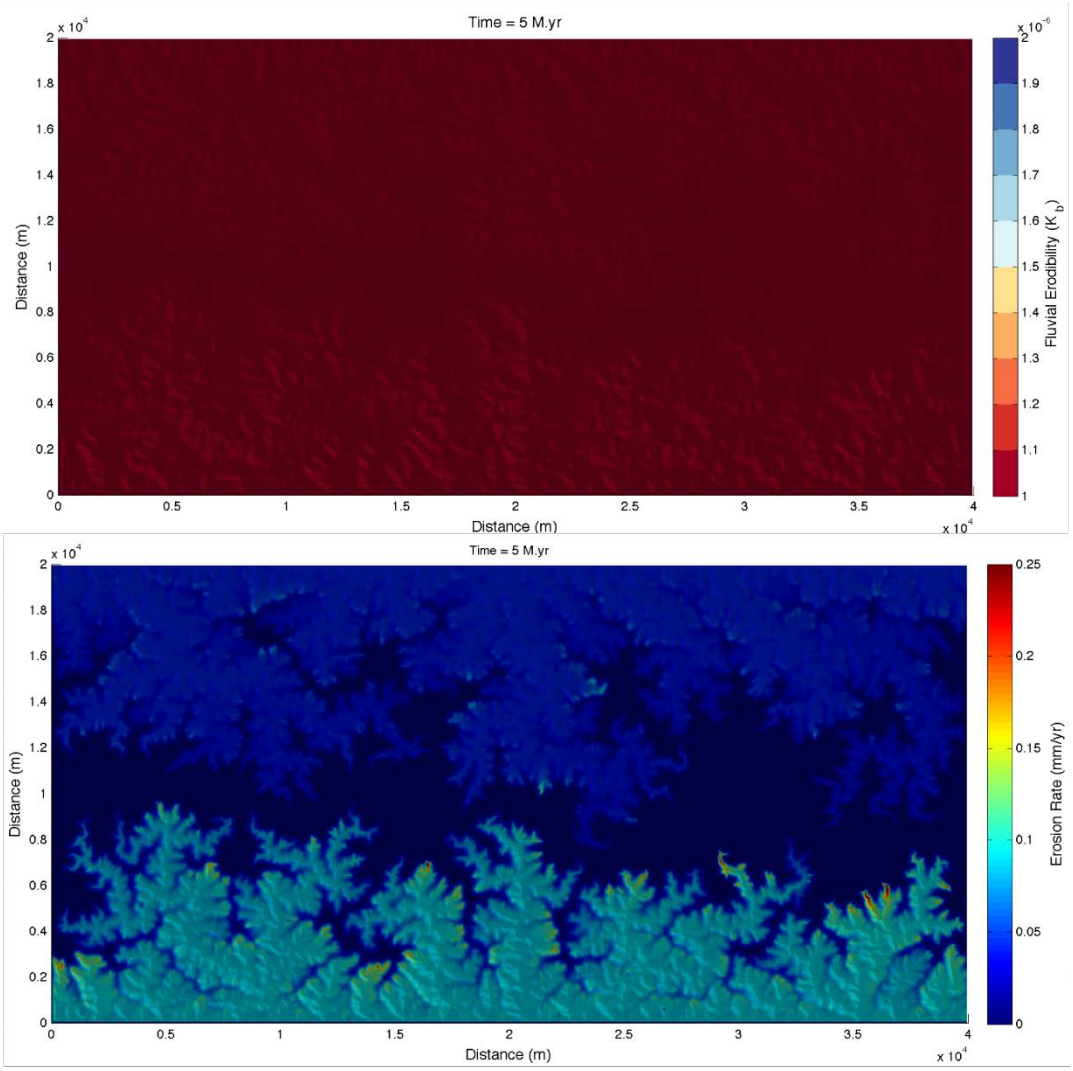

Appendix B.1 Two-dimensional landscape evolution model (CHILD) outputs for a Grand Staircase-like simulation. Figures are mapped by rock type in upper panel; red is stronger rock and blue is weaker rock. Map color is erosion rate in the lower panel.

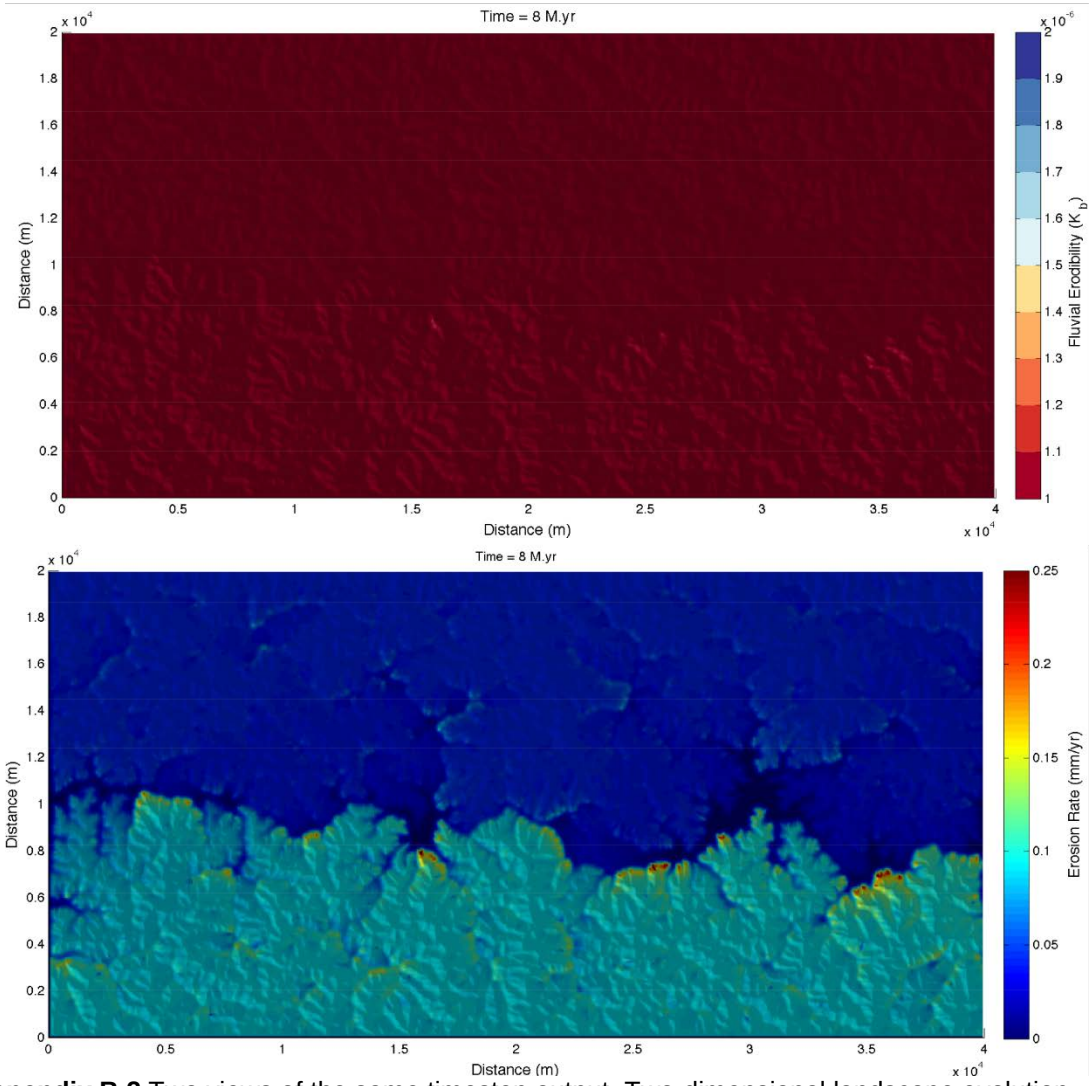

Appendix B.2 Two views of the same timestep output. Two-dimensional landscape evolution model (CHILD) outputs for a Grand Staircase-like simulation. Figures are mapped by rock type in upper panel; red is stronger rock and blue is weaker rock. Map color is erosion rate in the lower panel.

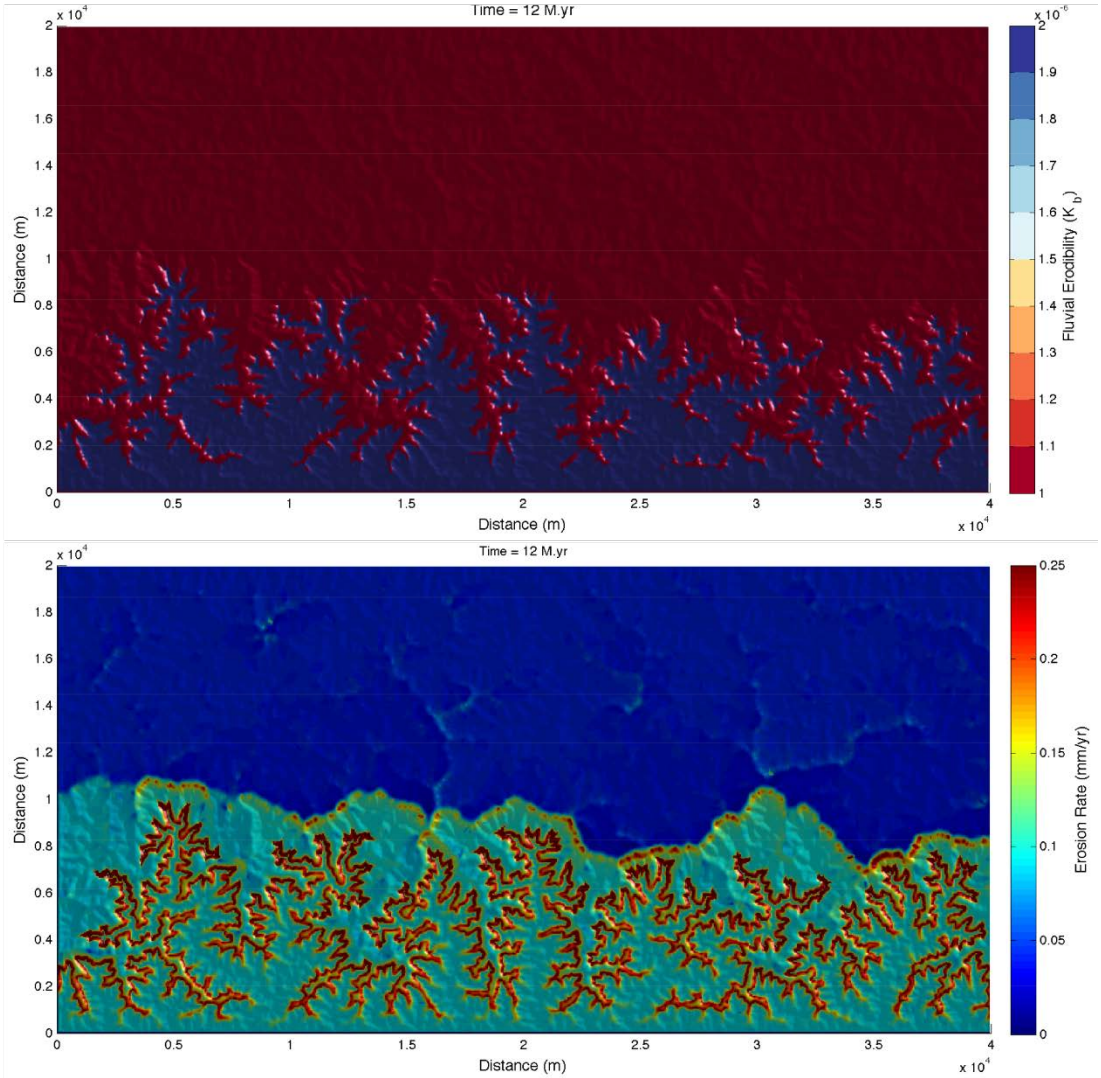

Appendix B.3 Two views of the same timestep output. Two-dimensional landscape evolution model (CHILD) outputs for a Grand Staircase-like simulation. Figures are mapped by rock type in upper panel; red is stronger rock and blue is weaker rock. Map color is erosion rate in the lower panel.

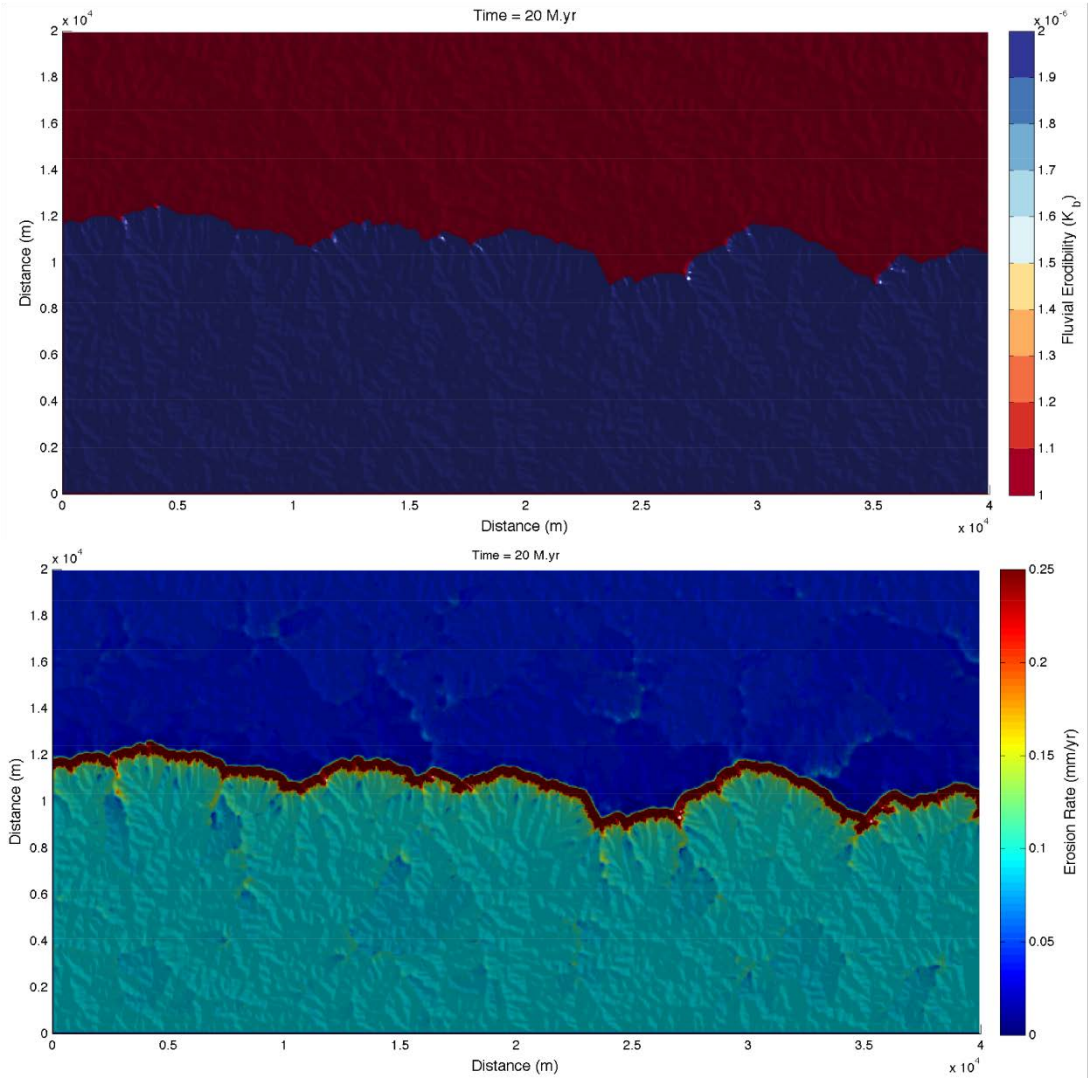

Appendix B.4 Two views of the same timestep output. Two-dimensional landscape evolution model (CHILD) outputs for a Grand Staircase-like simulation. Figures are mapped by rock type in upper panel; red is stronger rock and blue is weaker rock. Map color is erosion rate in the lower panel.

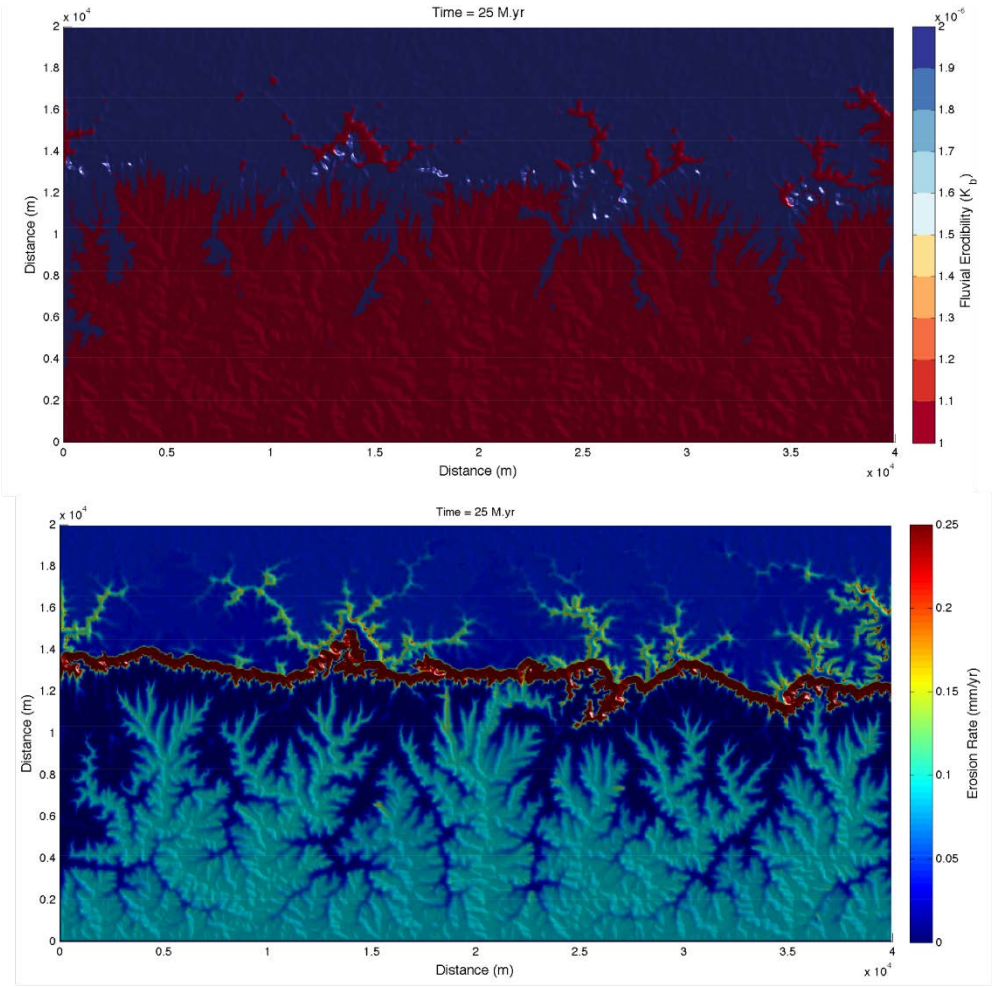

Appendix B.5 Two views of the same timestep output. Two-dimensional landscape evolution model (CHILD) outputs for a Grand Staircase-like simulation. Figures are mapped by rock type in upper panel; red is stronger rock and blue is weaker rock. Map color is erosion rate in the lower panel.

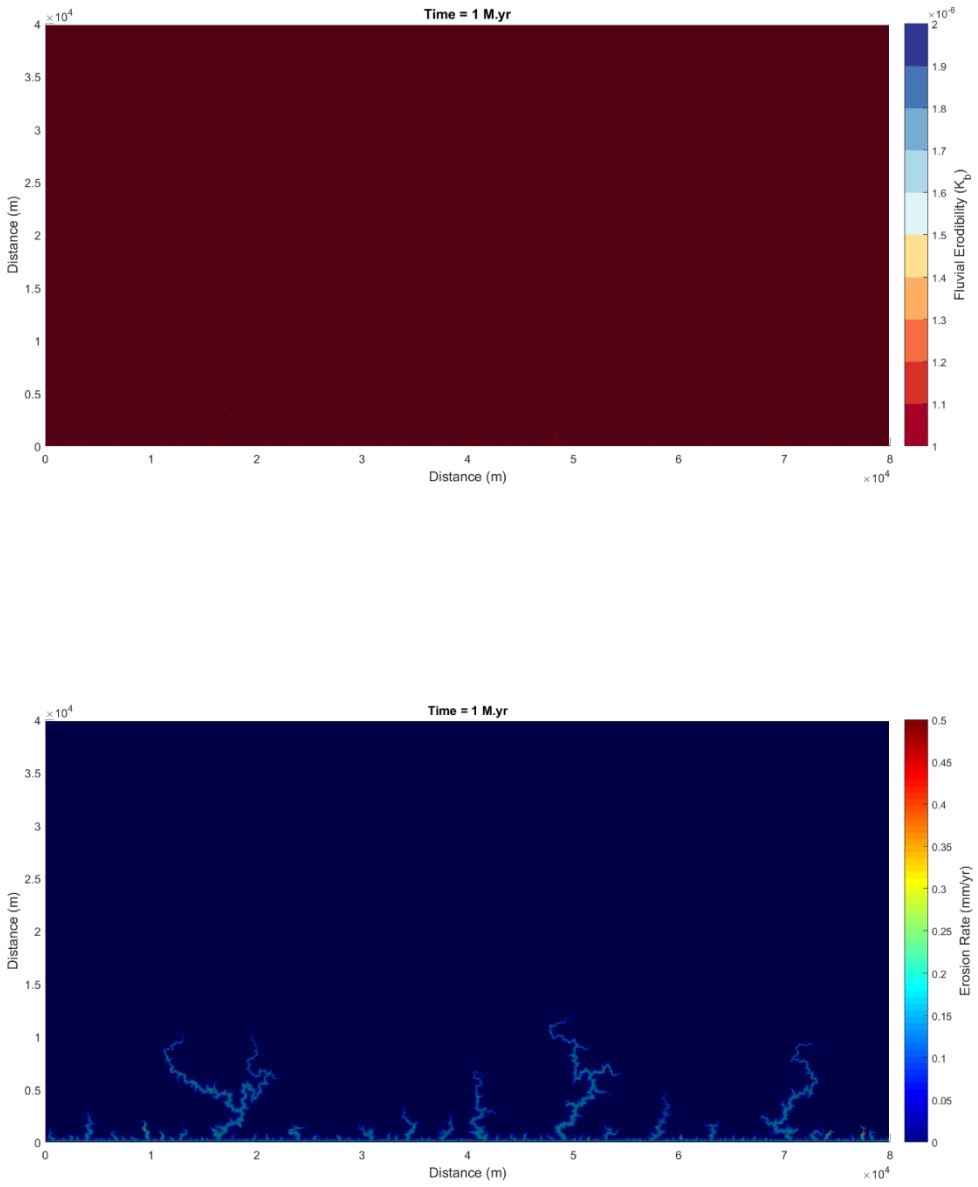

Appendix B.6 Two views of the same timestep output. Two-dimensional landscape evolution model (CHILD) outputs at 2 million year time-steps for a Grand Canyon-like simulation. Figures are mapped by rock type in upper panel; red is stronger rock and blue is weaker rock. Map color is erosion rate in the lower panel.

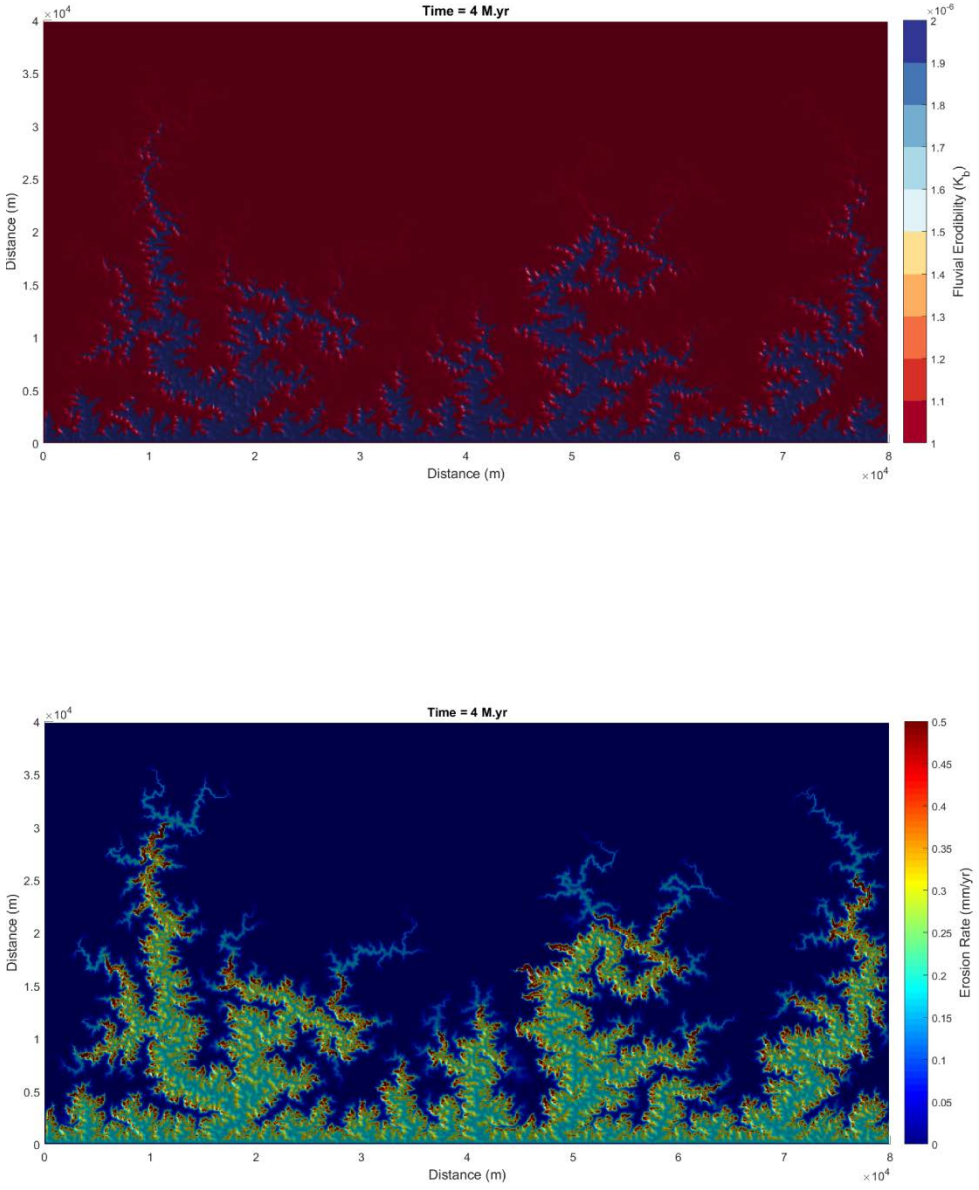

Appendix B.7 Two views of the same timestep output. Two-dimensional landscape evolution model (CHILD) outputs at 2 million year time-steps for a Grand Canyon-like simulation. Figures are mapped by rock type in upper panel; red is stronger rock and blue is weaker rock. Map color is erosion rate in the lower panel.

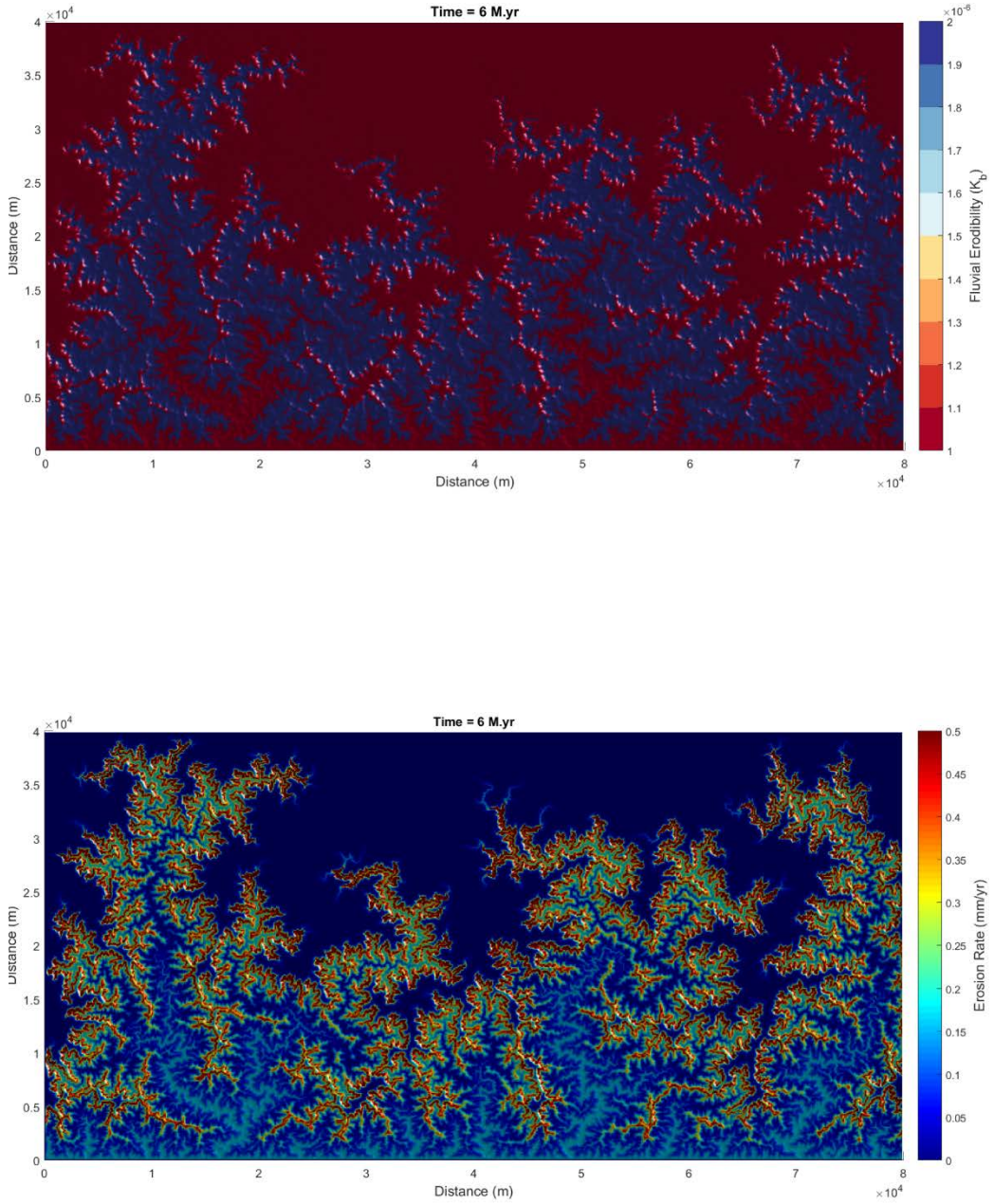

Appendix B.8 Two views of the same timestep output. Two-dimensional landscape evolution model (CHILD) outputs at 2 million year time-steps for a Grand Canyon-like simulation. Figures are mapped by rock type in upper panel; red is stronger rock and blue is weaker rock. Map color is erosion rate in the lower panel.

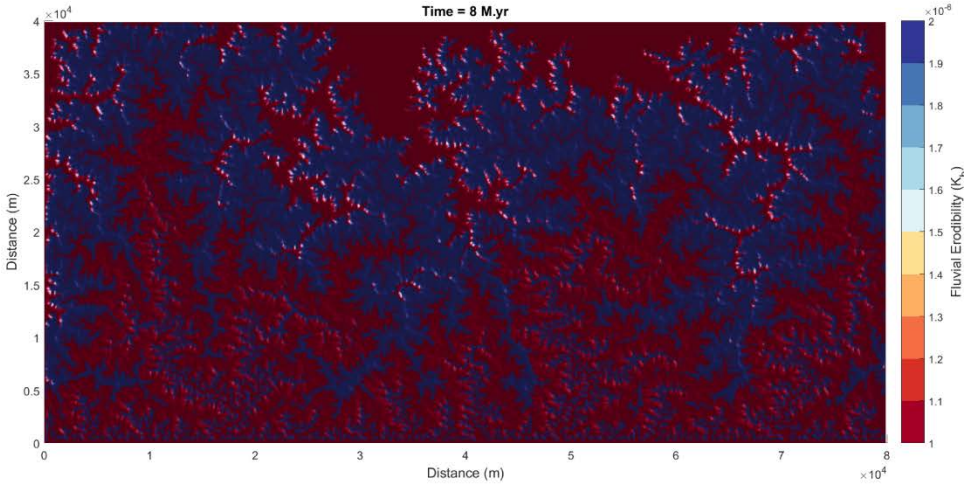

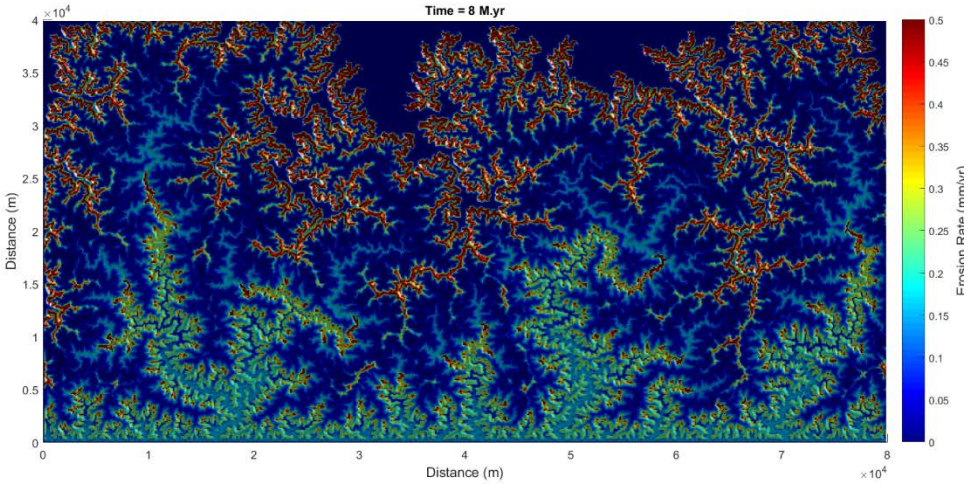

Appendix B.9 Two views of the same timestep output. Two-dimensional landscape evolution model (CHILD) outputs at 2 million year time-steps for a Grand Canyon-like simulation. Figures are mapped by rock type in upper panel; red is stronger rock and blue is weaker rock. Map color is erosion rate in the lower panel.

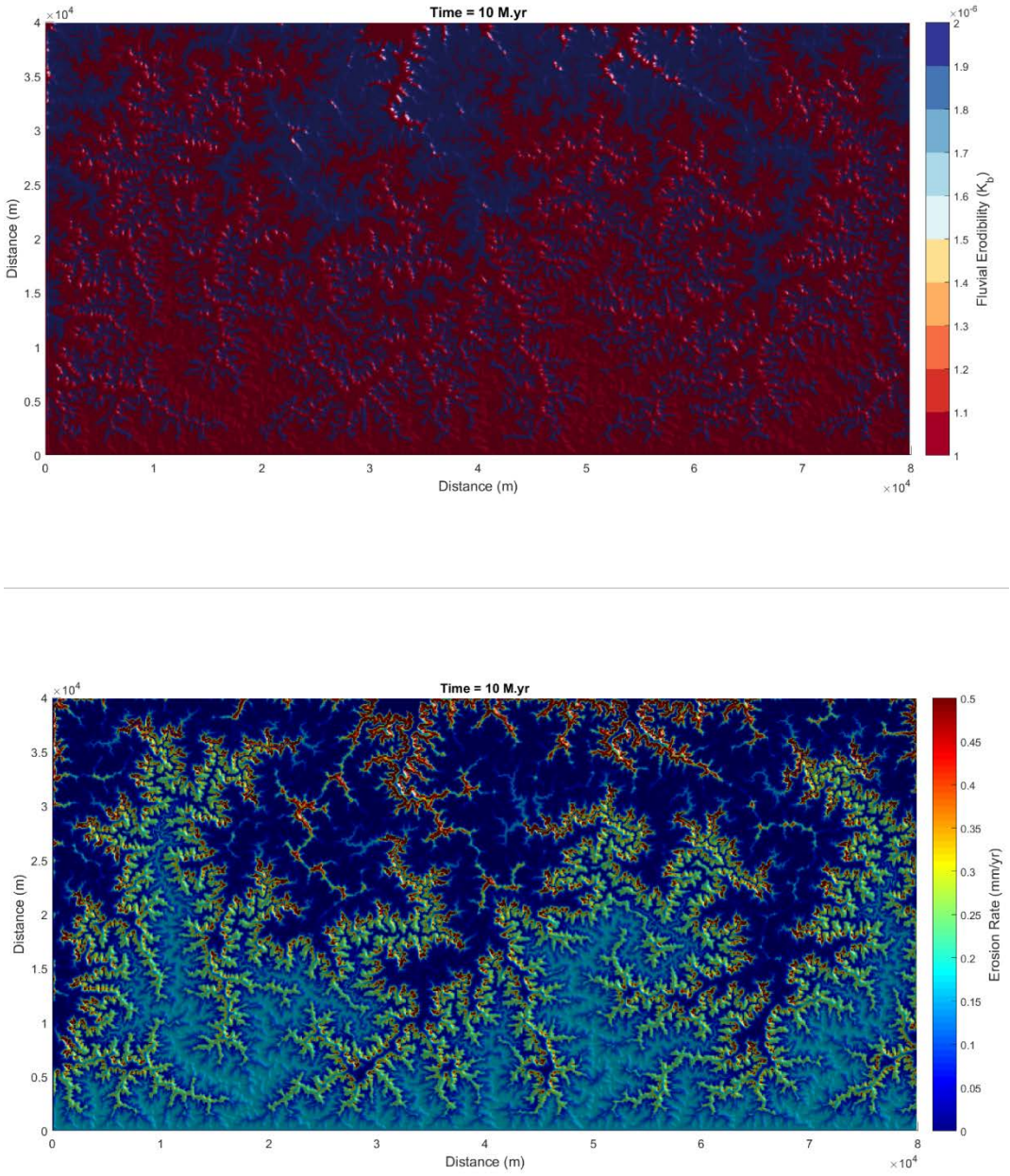

Appendix B.10 Two views of the same timestep output. Two-dimensional landscape evolution model (CHILD) outputs at 2 million year time-steps for a Grand Canyon-like simulation. Figures are mapped by rock type in upper panel; red is stronger rock and blue is weaker rock. Map color is erosion rate in the lower panel.

APPENDIX C

SEISMIC SURVEY FIGURES

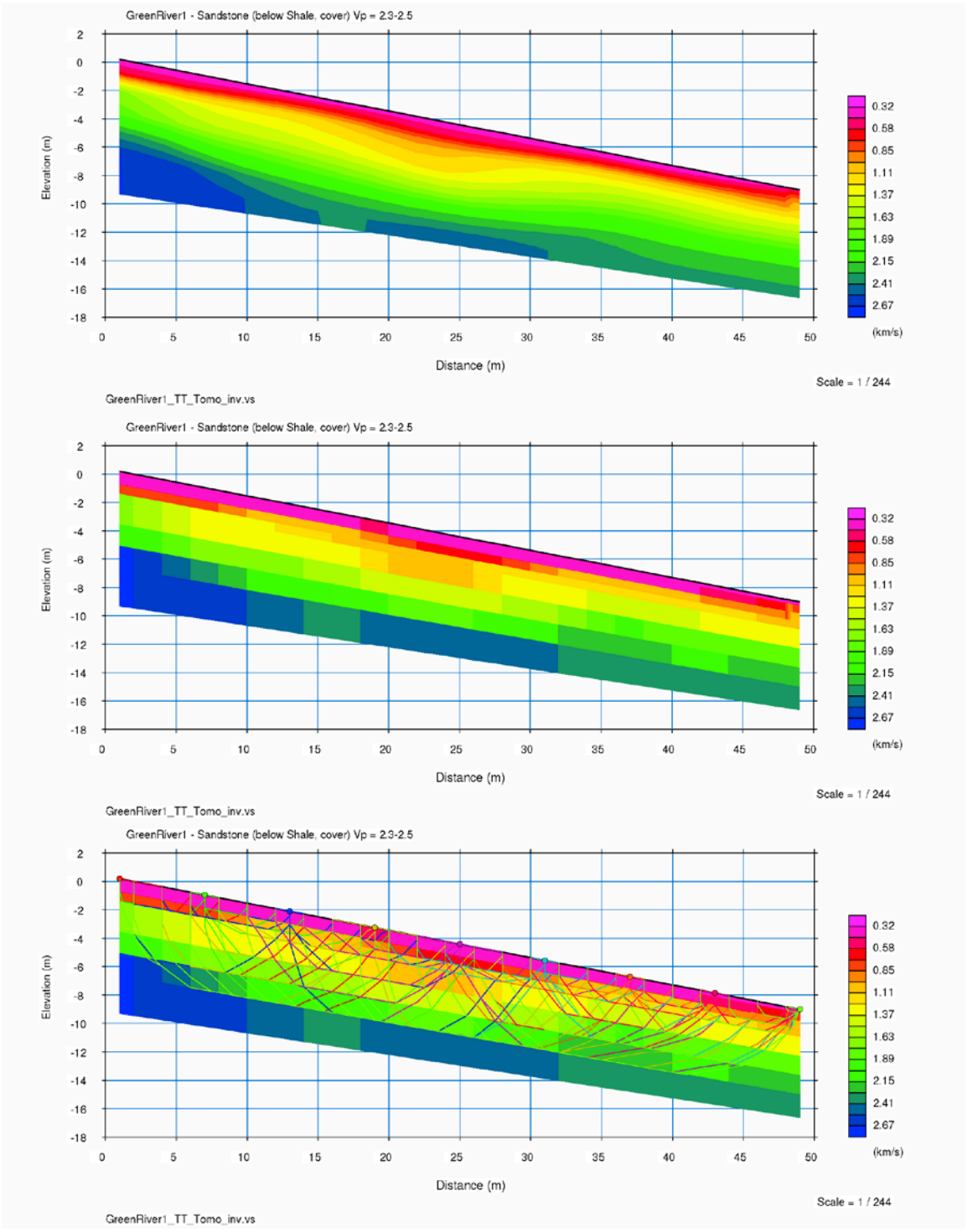
GreenRiver1 - Sandstone (below Shale, cover) Vp = 2.3-2.5
Elevation (m)
Distance (m)
0.32
0.58
0.85
1.11
1.37
1.63
1.89
2.15
2.41
2.67
(km/s)
Scale = 1 / 244
GreenRiver1_TT_Tomo_inv.vs
GreenRiver1 - Sandstone (below Shale, cover) Vp = 2.3-2.5
Elevation (m)
Distance (m)
Scale = 1 / 244
GreenRiver1_TT_Tomo_inv.vs
GreenRiver1 - Sandstone (below Shale, cover) Vp = 2.3-2.5
Elevation (m)
Distance (m)
Scale = 1 / 244
GreenRiver1_TT_Tomo_inv.vs

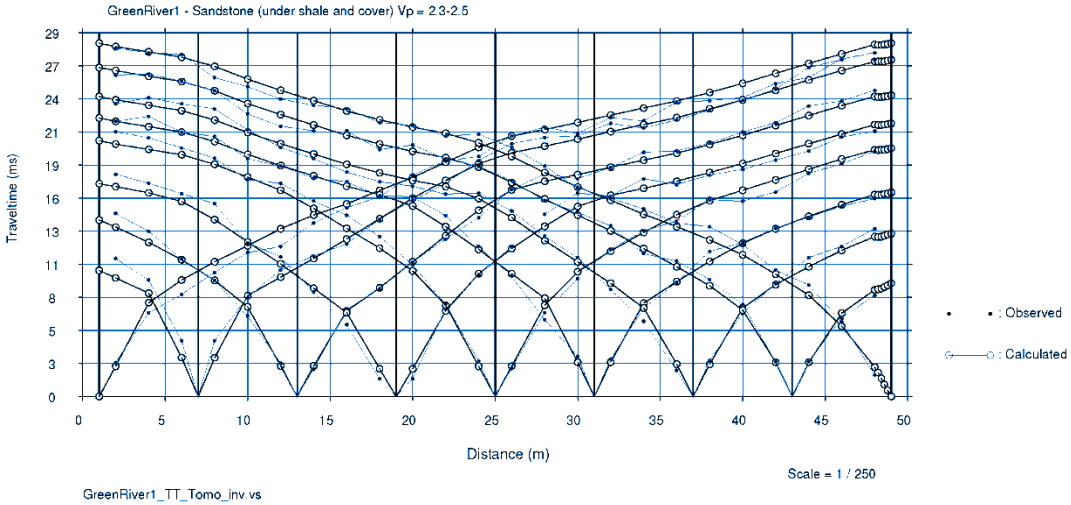
GreenRiver1 - Sandstone (under shale and cover) Vp = 2.3-2.5
Traveltime (ms)
29
27
24
21
19
16
13
11
8
5
3
0
0
5
10
15
20
25
30
35
40
45
50
Distance (m)
: Observed
: Calculated
Scale = 1 / 250
GreenRiver1_TT_Tomo_inv.vs

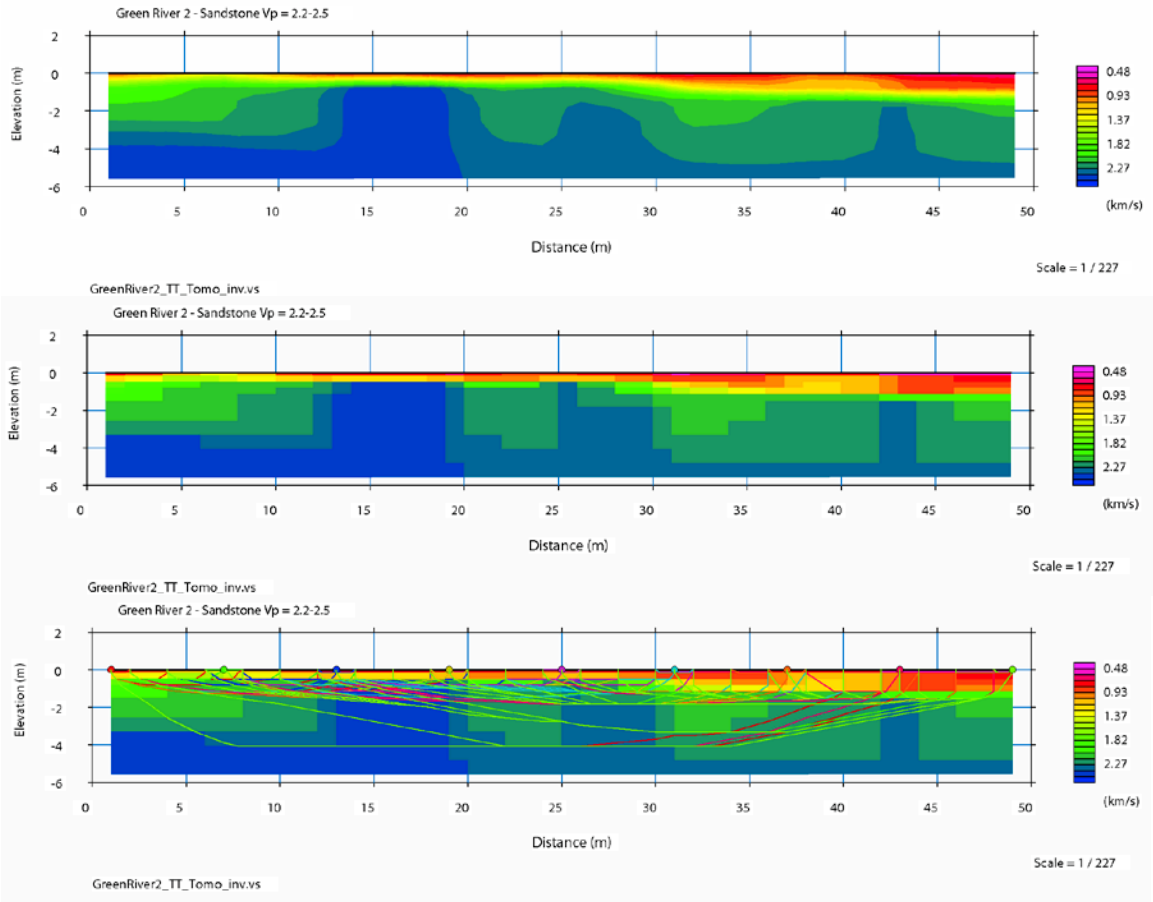
Green River 2 - Sandstone Vp = 2.2-2.5
Elevation (m)
Distance (m)
0.48
0.93
1.37
1.82
2.27
(km/s)
Scale = 1 / 227
GreenRiver2_TT_Tomo_inv.vs
Green River 2 - Sandstone Vp = 2.2-2.5
Elevation (m)
Distance (m)
0.48
0.93
1.37
1.82
2.27
(km/s)
Scale = 1 / 227
GreenRiver2_TT_Tomo_inv.vs
Green River 2 - Sandstone Vp = 2.2-2.5
Elevation (m)
Distance (m)
0.48
0.93
1.37
1.82
2.27
(km/s)
Scale = 1 / 227
GreenRiver2_TT_Tomo_inv.vs

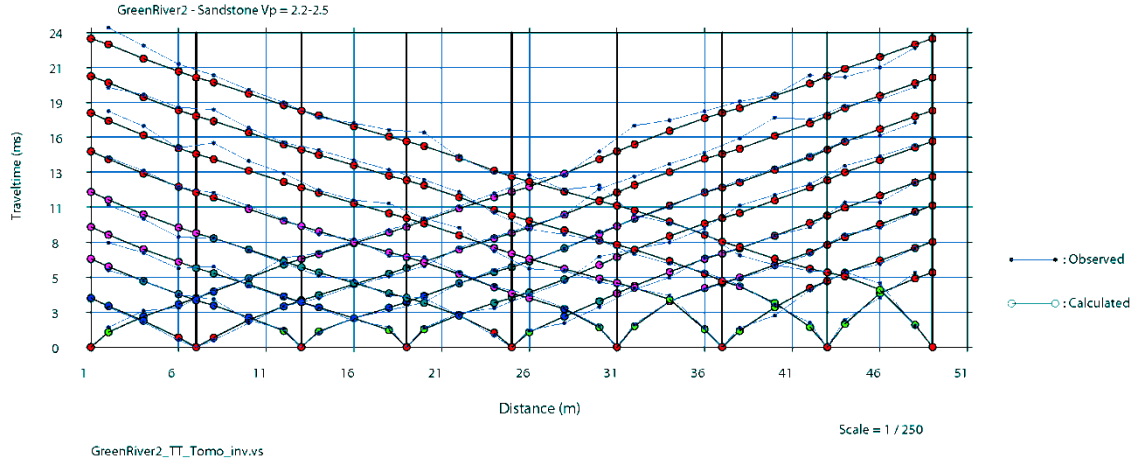
GreenRiver2 - Sandstone Vp = 2.2-2.5
Traveltime (ms)
Distance (m)
: Observed
: Calculated
Scale = 1 / 250
GreenRiver2_TT_Tomo_inv.vs

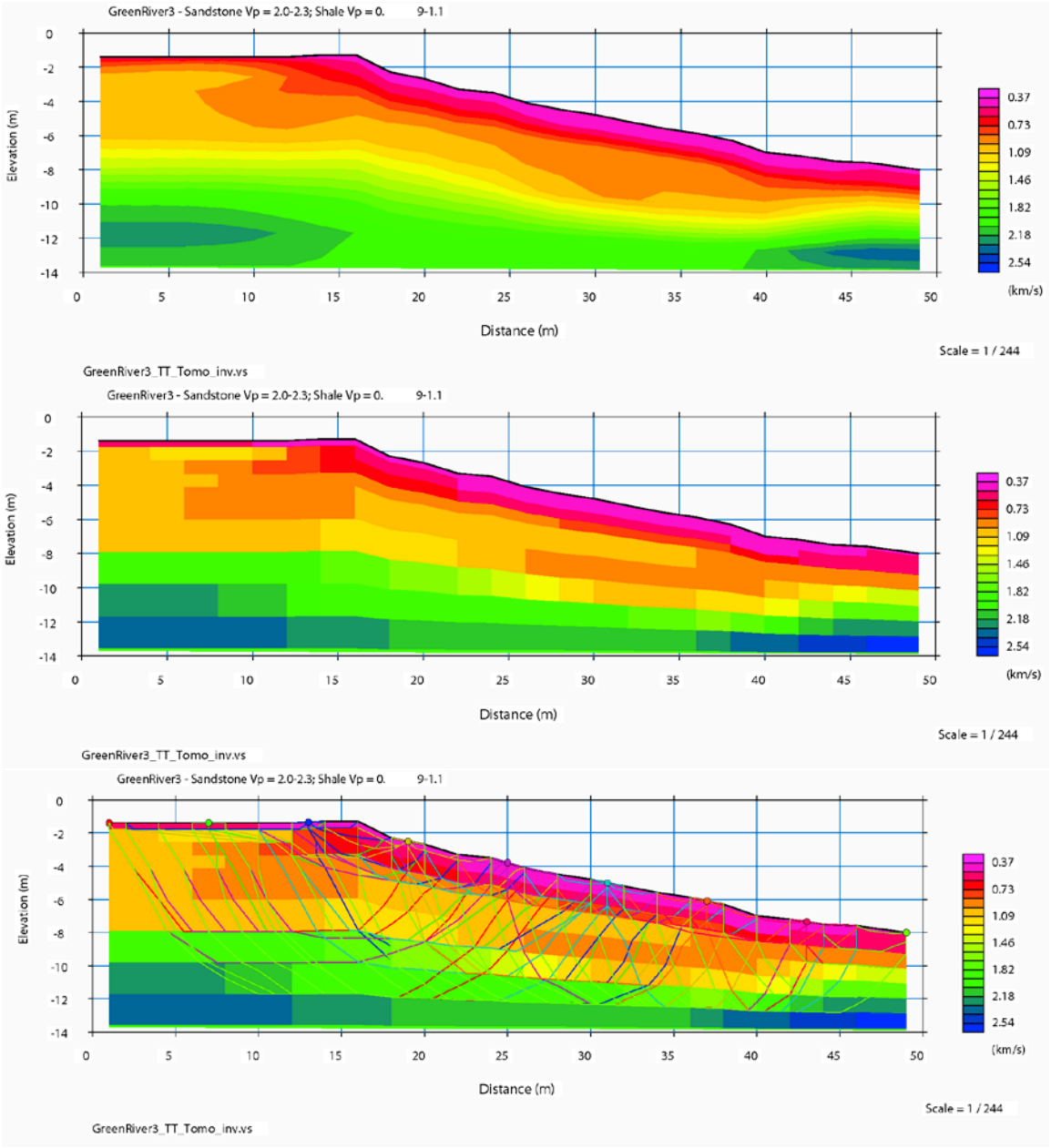
GreenRiver3 - Sandstone Vp = 2.0-2.3; Shale Vp = 0.
9-1.1
Elevation (m)
Distance (m)
0.37
0.73
1.09
1.46
1.82
2.18
2.54
(km/s)
Scale = 1 / 244
GreenRiver3_TT_Tomo_inv.vs
GreenRiver3 - Sandstone Vp = 2.0-2.3; Shale Vp = 0.
9-1.1
Elevation (m)
Distance (m)
Scale = 1 / 244
GreenRiver3_TT_Tomo_inv.vs
GreenRiver3 - Sandstone Vp = 2.0-2.3; Shale Vp = 0.
9-1.1
Elevation (m)
Distance (m)
Scale = 1 / 244
GreenRiver3_TT_Tomo_inv.vs

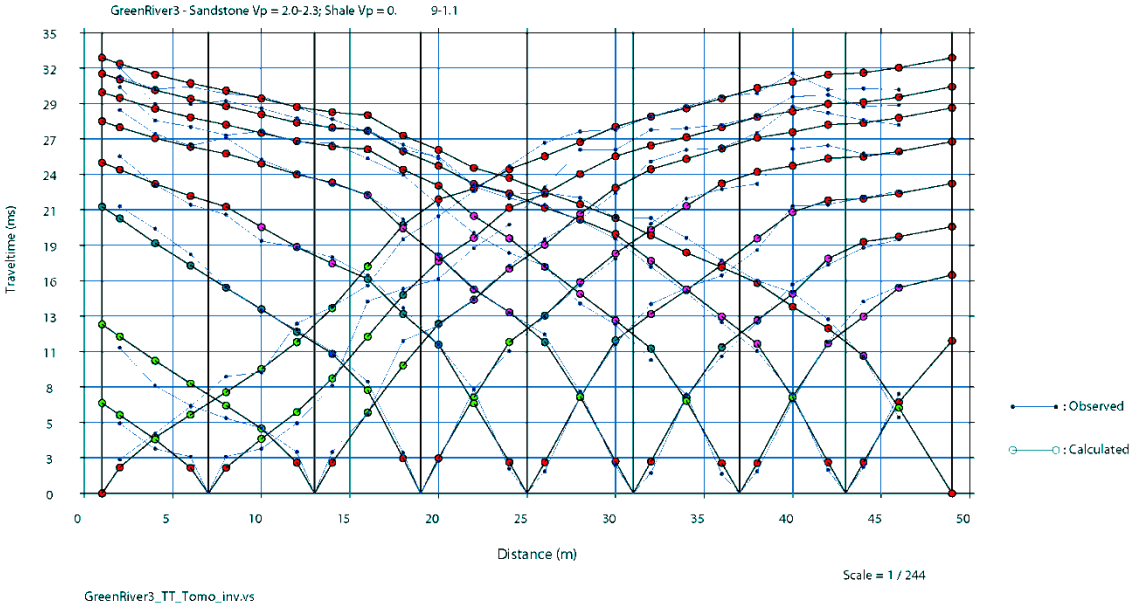
GreenRiver3 - Sandstone Vp = 2.0-2.3; Shale Vp = 0. 9-1.1
Traveltime (ms)
35
32
29
27
24
21
19
16
13
11
8
5
3
0
0
5
10
15
20
25
30
35
40
45
50
Distance (m)
: Observed
: Calculated
Scale = 1 / 244
GreenRiver3_TT_Tomo_inv.vs

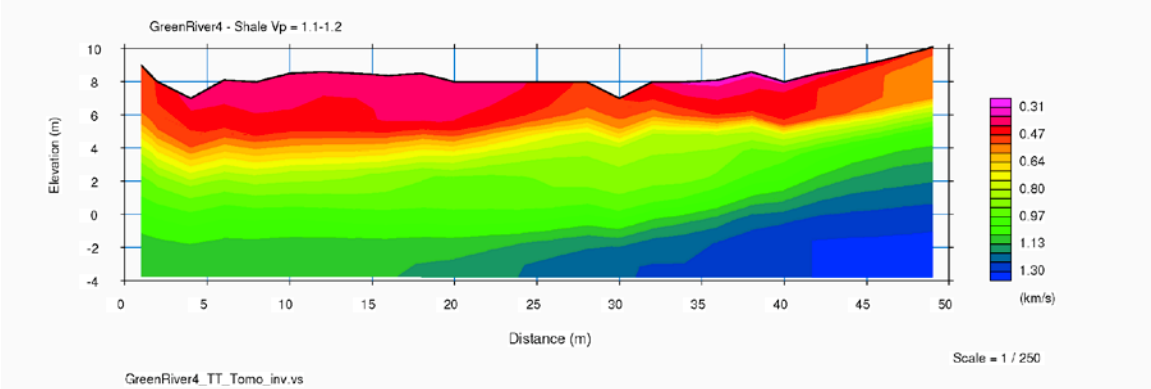
GreenRiver4 - Shale Vp = 1.1-1.2
Elevation (m)
Distance (m)
0.31
0.47
0.64
0.80
0.97
1.13
1.30
(km/s)
Scale = 1 / 250
GreenRiver4_TT_Tomo_inv.vs

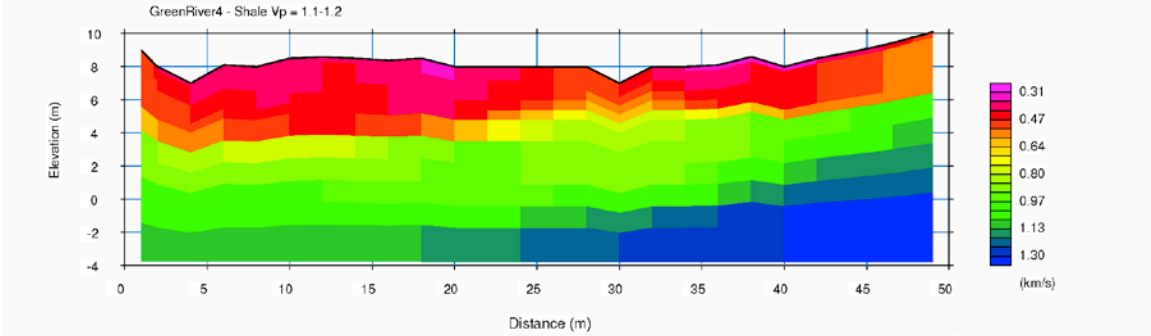
GreenRiver4 - Shale Vp = 1.1-1.2
Elevation (m)
Distance (m)
0.31
0.47
0.64
0.80
0.97
1.13
1.30
(km/s)
Scale = 1 / 250
GreenRiver4_TT_Tomo_inv.vs

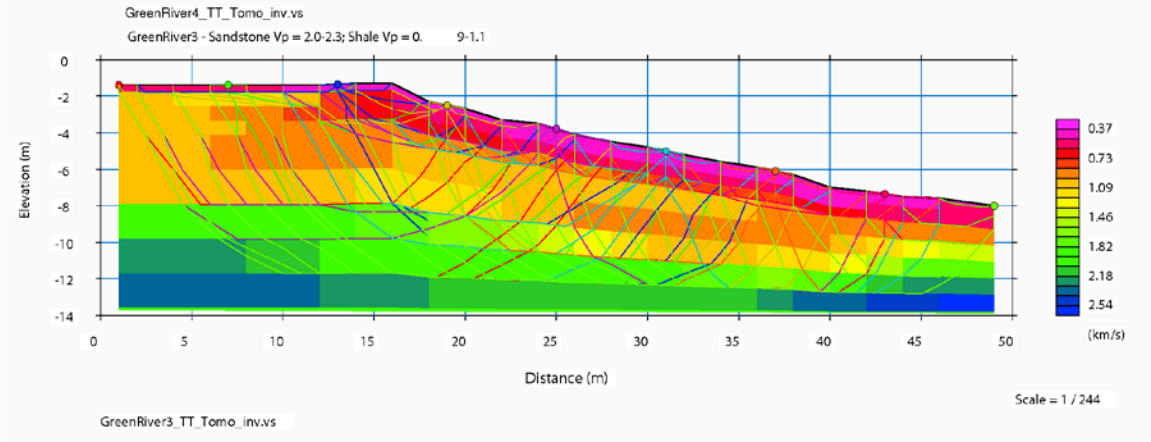
GreenRiver3 - Sandstone Vp = 2.0-2.3; Shale Vp = 0. 9-1.1
Elevation (m)
Distance (m)
0.37
0.73
1.09
1.46
1.82
2.18
2.54
(km/s)
Scale = 1 / 244
GreenRiver3_TT_Tomo_inv.vs

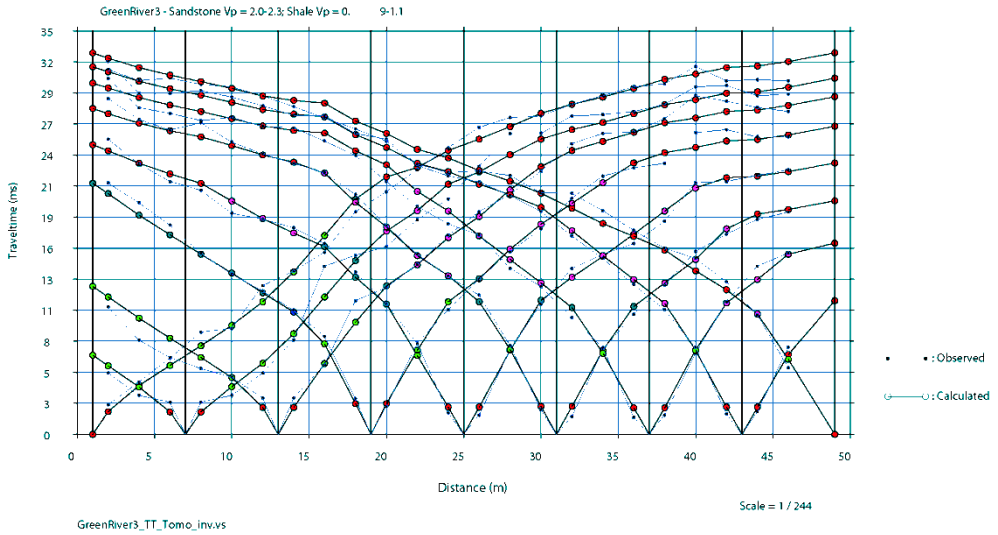
GreenRiver3 - Sandstone Vp = 2.0-2.3; Shale Vp = 0.
9-1.1
Traveltime (ms)
Distance (m)
: Observed
: Calculated
Scale = 1 / 244
GreenRiver3_TT_Tomo_inv.vs

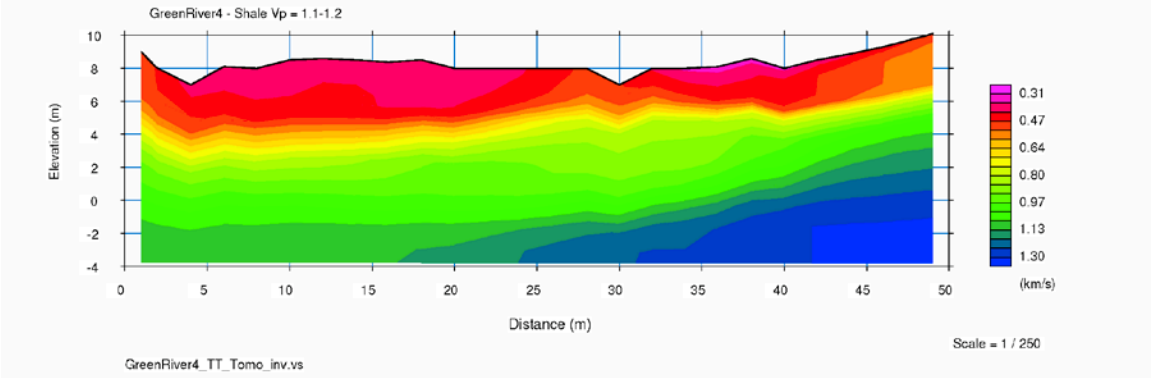
GreenRiver4 - Shale Vp = 1.1-1.2
Elevation (m)
10
8
6
4
2
0
-2
-4
0
5
10
15
20
25
30
35
40
45
50
Distance (m)
0.31
0.47
0.64
0.80
0.97
1.13
1.30
(km/s)
Scale = 1 / 250
GreenRiver4_TT_Tomo_inv.vs

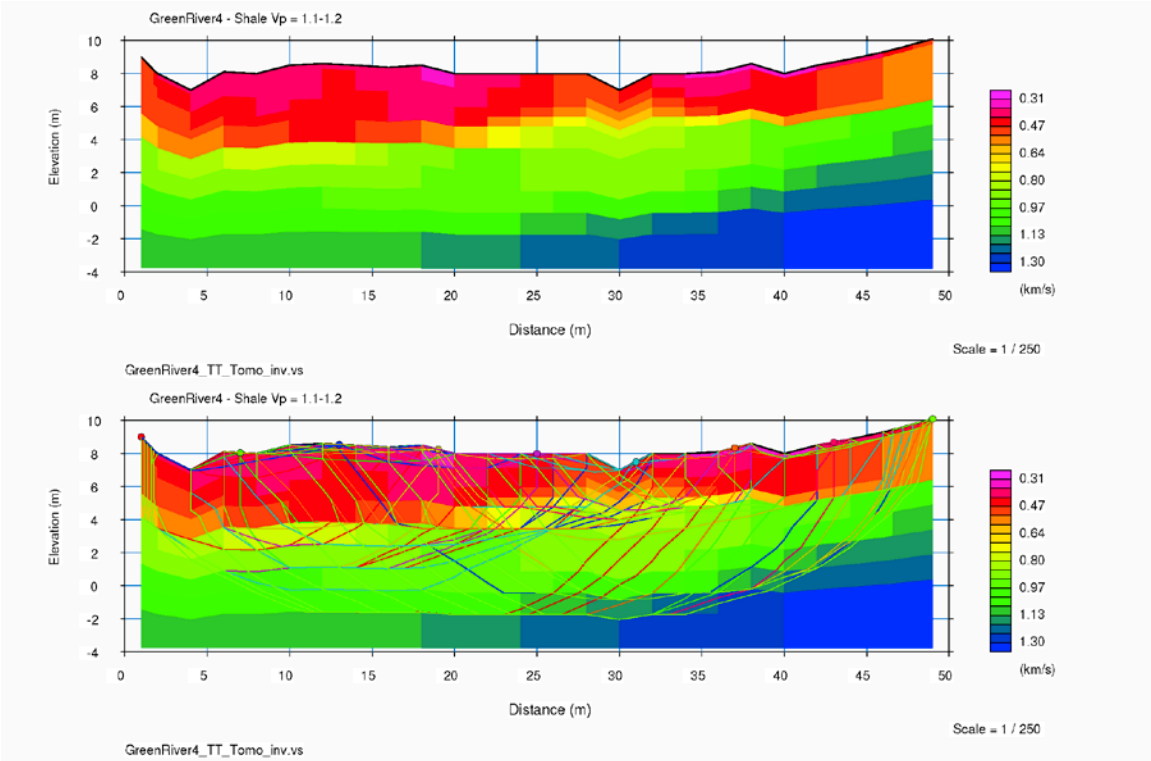
GreenRiver4 - Shale Vp = 1.1-1.2
Elevation (m)
10
8
6
4
2
0
-2
-4
0
5
10
15
20
25
30
35
40
45
50
Distance (m)
0.31
0.47
0.64
0.80
0.97
1.13
1.30
(km/s)
Scale = 1 / 250
GreenRiver4_TT_Tomo_inv.vs
GreenRiver4 - Shale Vp = 1.1-1.2
Elevation (m)
10
8
6
4
2
0
-2
-4
0
5
10
15
20
25
30
35
40
45
50
Distance (m)
0.31
0.47
0.64
0.80
0.97
1.13
1.30
(km/s)
Scale = 1 / 250
GreenRiver4_TT_Tomo_inv.vs

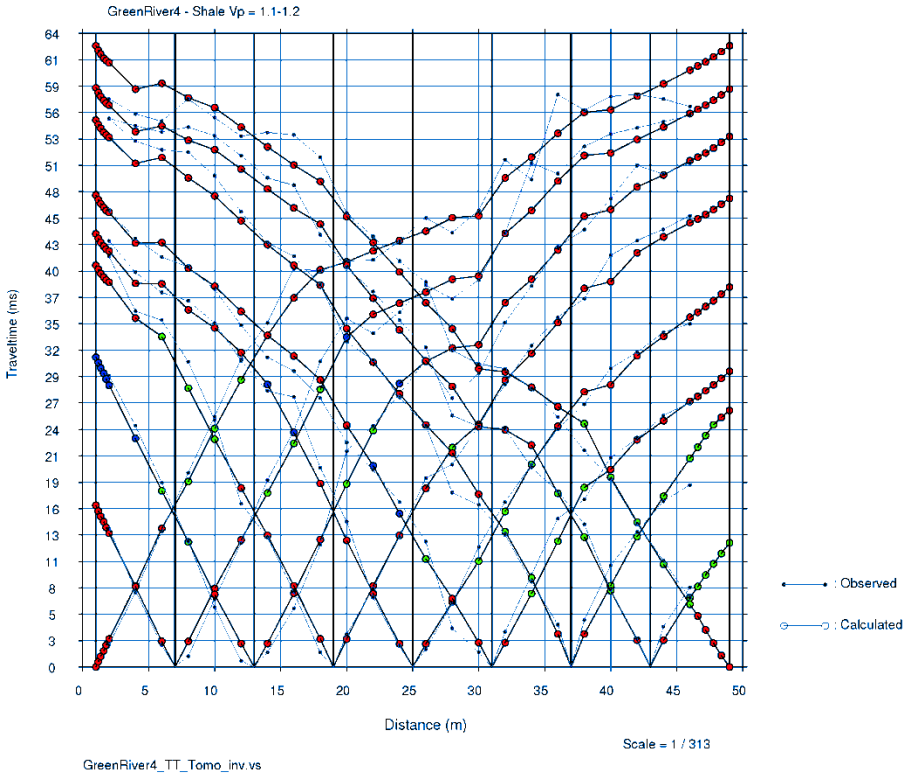
GreenRiver4 - Shale Vp = 1.1-1.2
Traveltime (ms)
64
61
59
56
53
51
48
45
43
40
37
35
32
29
27
24
21
19
16
13
11
8
5
3
0
0
5
10
15
20
25
30
35
40
45
50
Distance (m)
: Observed
: Calculated
Scale = 1 / 313
GreenRiver4_TT_Tomo_inv.vs

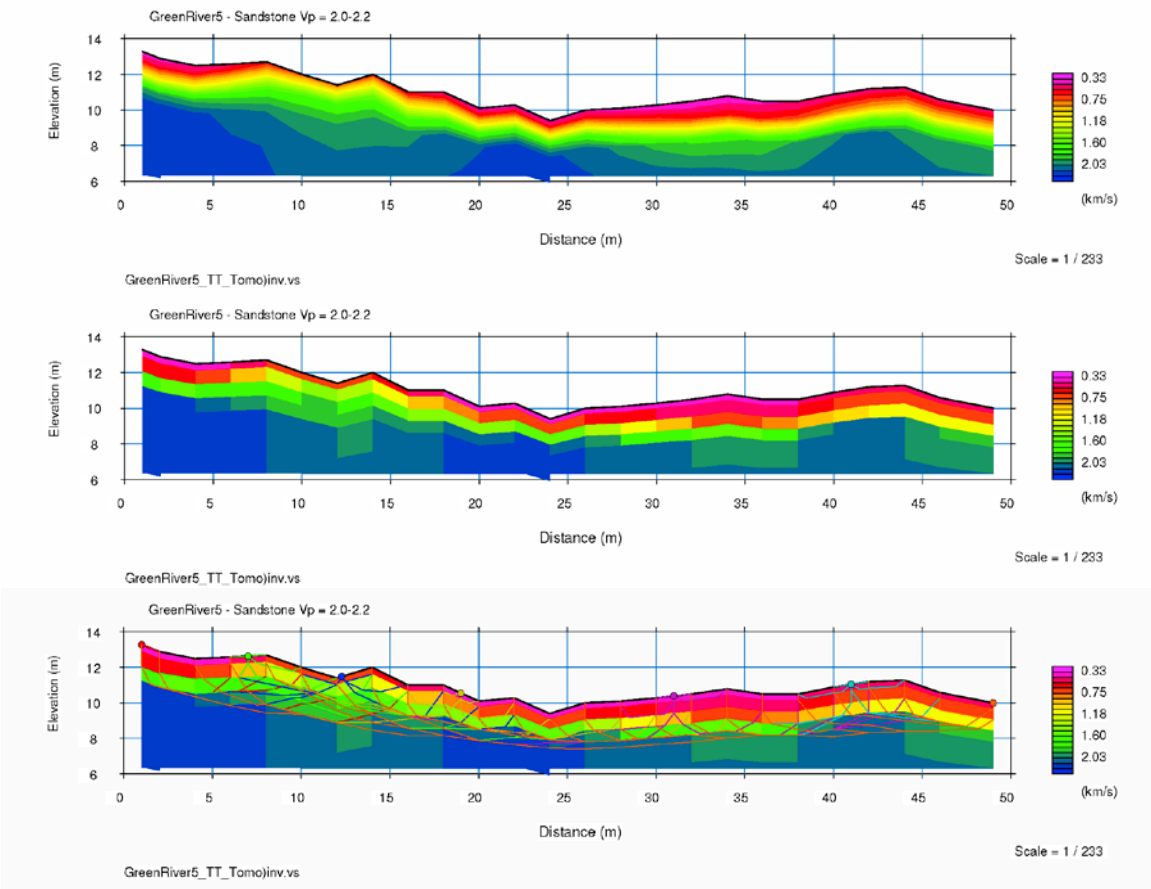
GreenRiver5 - Sandstone Vp = 2.0-2.2
Elevation (m)
14
12
10
8
6
0
5
10
15
20
25
30
35
40
45
50
Distance (m)
0.33
0.75
1.18
1.60
2.03
(km/s)
Scale = 1 / 233
GreenRiver5_TT_Tomo)inv.vs
GreenRiver5 - Sandstone Vp = 2.0-2.2
Elevation (m)
Distance (m)
Scale = 1 / 233
GreenRiver5_TT_Tomo)inv.vs
GreenRiver5 - Sandstone Vp = 2.0-2.2
Elevation (m)
Distance (m)
Scale = 1 / 233
GreenRiver5_TT_Tomo)inv.vs

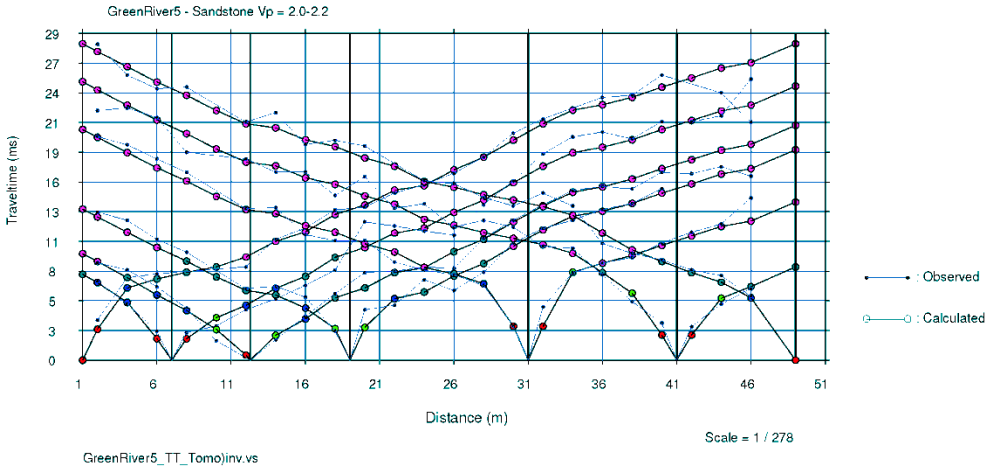
GreenRiver5 - Sandstone Vp = 2.0-2.2
Traveltime (ms)
29
27
24
21
19
16
13
11
8
5
3
0
1
6
11
16
21
26
31
36
41
46
51
Distance (m)
: Observed
: Calculated
Scale = 1 / 278
GreenRiver5_TT_Tomo)inv.vs

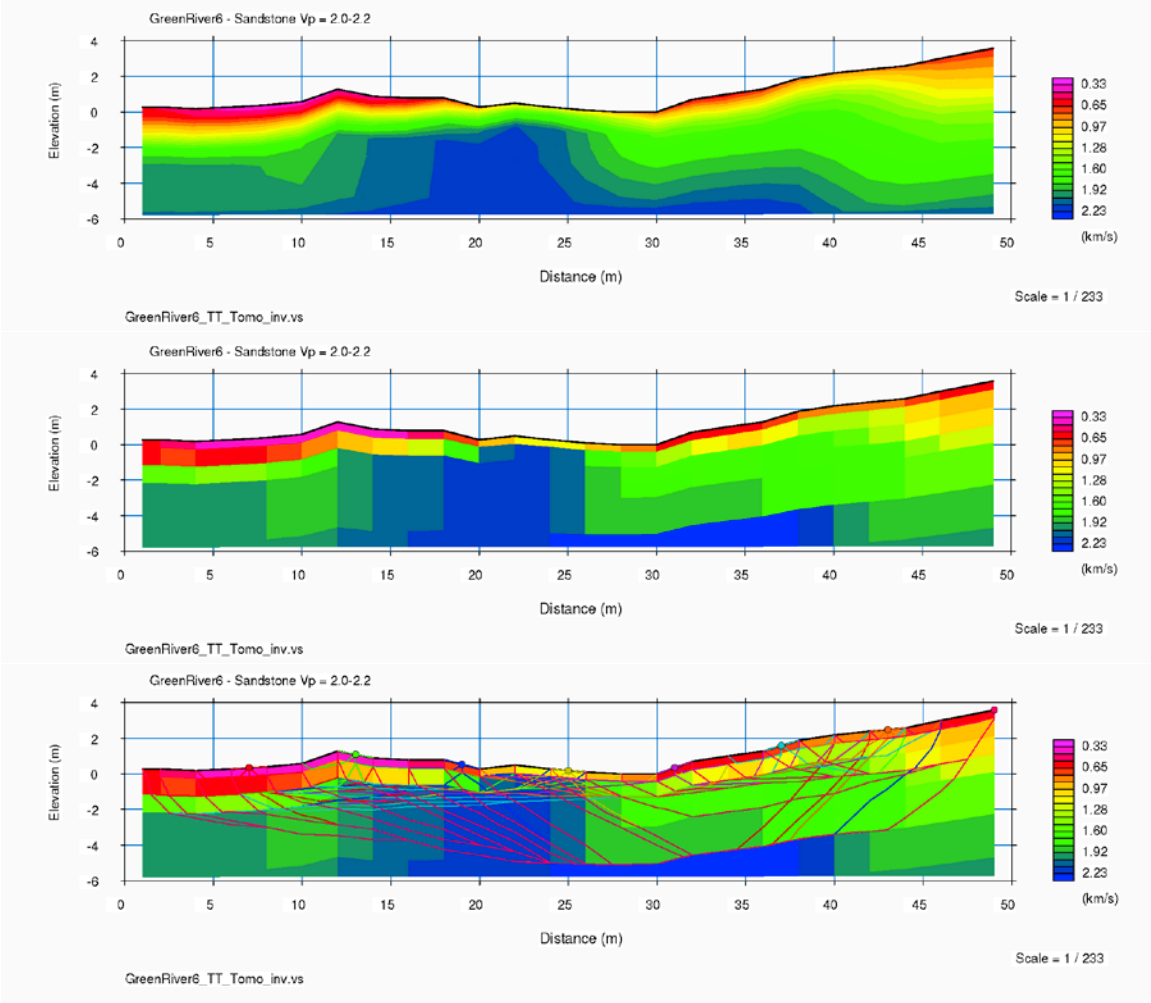
GreenRiver6 - Sandstone Vp = 2.0-2.2
Elevation (m)
Distance (m)
0.33
0.65
0.97
1.28
1.60
1.92
2.23
(km/s)
Scale = 1 / 233
GreenRiver6_TT_Tomo_inv.vs
GreenRiver6 - Sandstone Vp = 2.0-2.2
Elevation (m)
Distance (m)
0.33
0.65
0.97
1.28
1.60
1.92
2.23
(km/s)
Scale = 1 / 233
GreenRiver6_TT_Tomo_inv.vs
GreenRiver6 - Sandstone Vp = 2.0-2.2
Elevation (m)
Distance (m)
0.33
0.65
0.97
1.28
1.60
1.92
2.23
(km/s)
Scale = 1 / 233
GreenRiver6_TT_Tomo_inv.vs

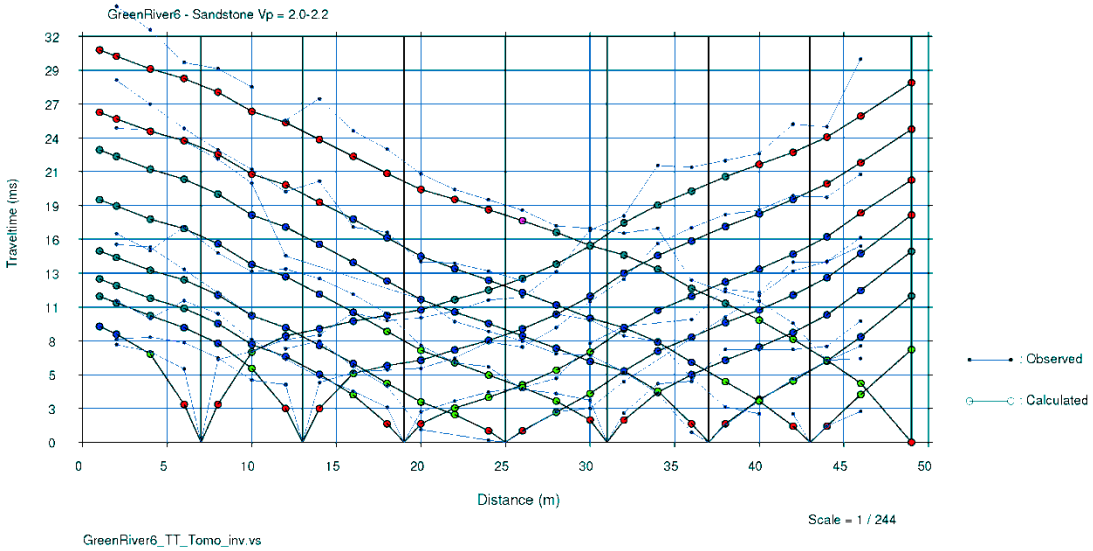
GreenRiver6 - Sandstone Vp = 2.0-2.2
Traveltime (ms)
32
29
27
24
21
19
16
13
11
8
5
3
0
0
5
10
15
20
25
30
35
40
45
50
Distance (m)
: Observed
: Calculated
Scale = 1 / 244
GreenRiver6_TT_Tomo_inv.vs

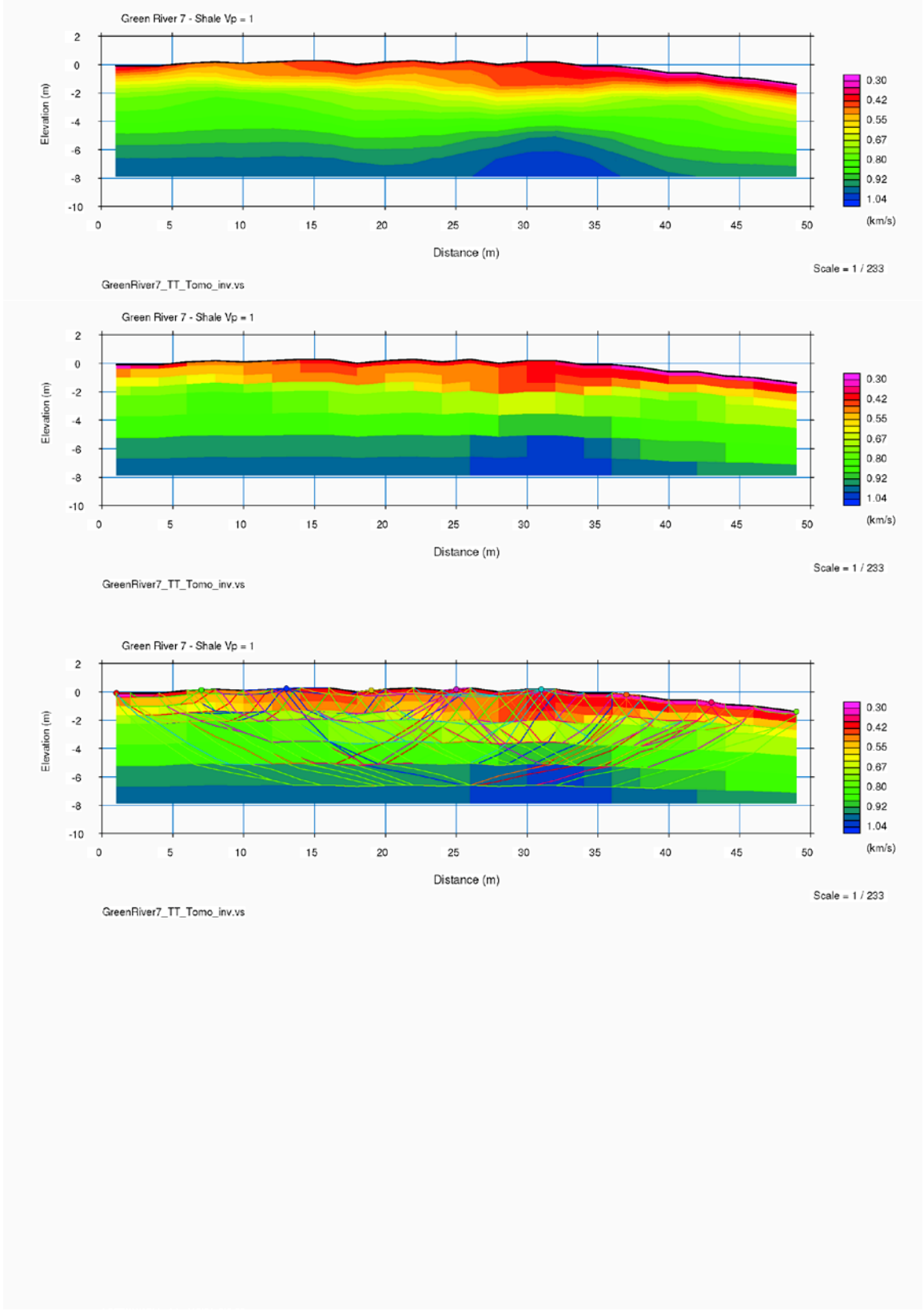
Green River 7 - Shale Vp = 1
Elevation (m)
2
0
-2
-4
-6
-8
-10
0
5
10
15
20
25
30
35
40
45
50
Distance (m)
0.30
0.42
0.55
0.67
0.80
0.92
1.04
(km/s)
Scale = 1 / 233
GreenRiver7_TT_Tomo_inv.vs
Green River 7 - Shale Vp = 1
Elevation (m)
Distance (m)
0.30
0.42
0.55
0.67
0.80
0.92
1.04
(km/s)
Scale = 1 / 233
GreenRiver7_TT_Tomo_inv.vs
Green River 7 - Shale Vp = 1
Elevation (m)
Distance (m)
0.30
0.42
0.55
0.67
0.80
0.92
1.04
(km/s)
Scale = 1 / 233
GreenRiver7_TT_Tomo_inv.vs

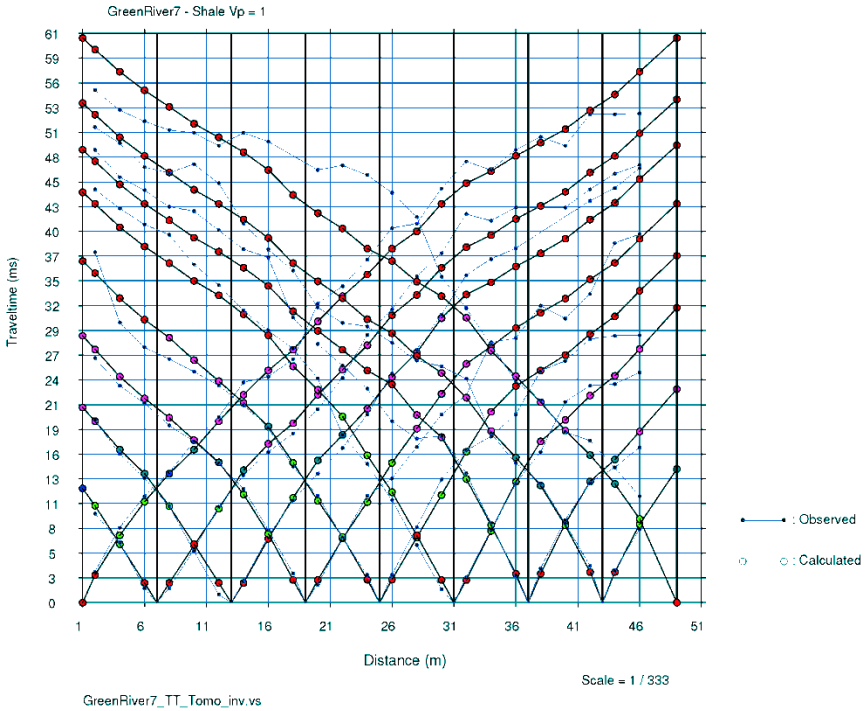
GreenRiver7 - Shale Vp = 1
Traveltime (ms)
61
59
56
53
51
48
45
43
40
37
35
32
29
27
24
21
19
16
13
11
8
5
3
0
1
6
11
16
21
26
31
36
41
46
51
Distance (m)
: Observed
: Calculated
Scale = 1 / 333
GreenRiver7_TT_Tomo_inv.vs

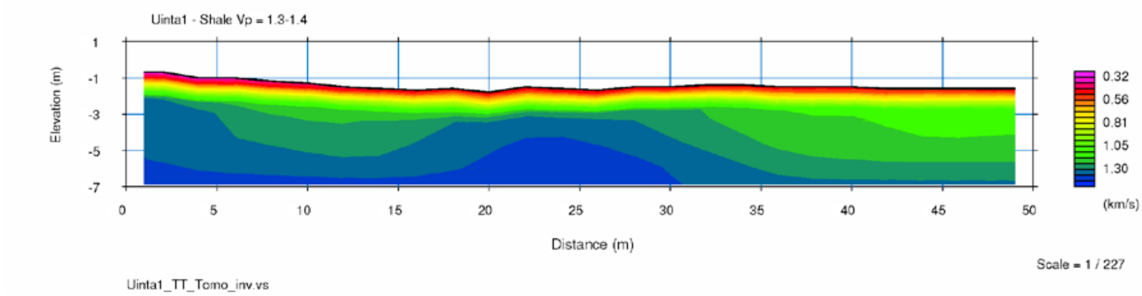
Uinta1 - Shale Vp = 1.3-1.4
Elevation (m)
1
-1
-3
-5
-7
0
5
10
15
20
25
30
35
40
45
50
Distance (m)
0.32
0.56
0.81
1.05
1.30
(km/s)
Scale = 1 / 227
Uinta1_TT_Tomo_inv.vs

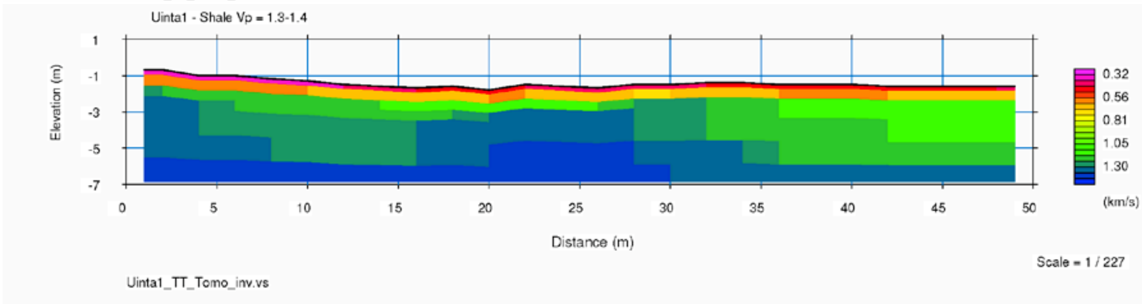
Uinta1 - Shale Vp = 1.3-1.4
Elevation (m)
1
-1
-3
-5
-7
0
5
10
15
20
25
30
35
40
45
50
Distance (m)
0.32
0.56
0.81
1.05
1.30
(km/s)
Scale = 1 / 227
Uinta1_TT_Tomo_inv.vs

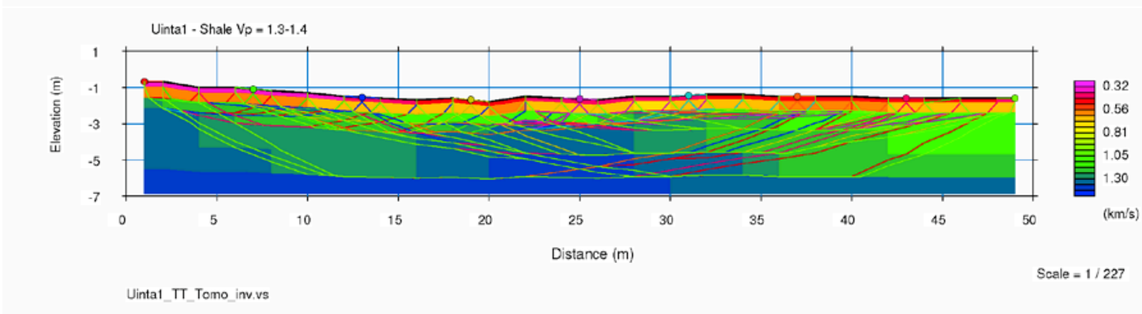
Uinta1 - Shale Vp = 1.3-1.4
Elevation (m)
1
-1
-3
-5
-7
0
5
10
15
20
25
30
35
40
45
50
Distance (m)
0.32
0.56
0.81
1.05
1.30
(km/s)
Scale = 1 / 227
Uinta1_TT_Tomo_inv.vs

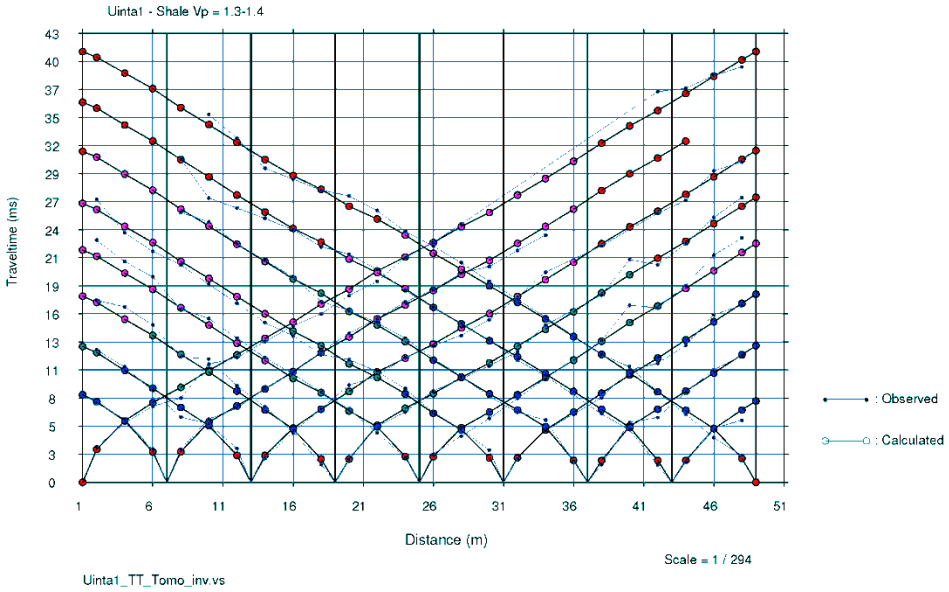
Uinta1 - Shale Vp = 1.3-1.4
Traveltime (ms)
43
40
37
35
32
29
27
24
21
19
16
13
11
8
5
3
0
1
6
11
16
21
26
31
36
41
46
51
Distance (m)
: Observed
: Calculated
Scale = 1 / 294
Uinta1_TT_Tomo_inv.vs